Space Weather

Particle detectors in Solar Physics and Space Weather research

A.Chilingarian

Cosmic Ray Division, Alikhanyan Physics Insitute, Yerevan, Armenia

The use of large area particle detectors which can only be accommodated at Earth surface is vital for measuring the low fluxes of high energy particles accelerated in the vicinity of the Sun. The enigma of particle acceleration in the Universe can not be explored without understanding of solar particle accelerators. The energy spectra of highest energy solar particles, as measured by the surface detectors will shed light on this universal processes of high-energy particles acceleration at numerous galactic and extragalactic sites.

Detected at earth, energetic particles also can provide highly cost-effective information on the key characteristics of the interplanetary disturbances. Because cosmic rays are fast and have large scattering mean free paths in the solar wind, this information travels rapidly and can be useful for space weather forecasting. Taking into account that only very few of a great number of Solar Flares (SF) and Coronal Mass Ejections (CME) produce intensive ion fluxes (so called – Solar Energetic Particle events – SEP), it is not only critical to alert clients about the arrival of the most severe radiation storms, but also to minimize the number of false alarms against events which are not severe enough to cause damage.

Because the flux of high-energy ions is weak and because the most violent particle events are usually highly anisotropic, the network of the large area particle detectors, located at low latitudes and high mountain altitudes is necessary for their reliable detection. The information about primary ion type and energy is mostly smeared during its successive interactions with atmospheric nuclei, therefore, only coherent measurements of all secondary fluxes (neutrons, muons, and electrons), along with their correlations, can help to make unambiguous forecasts and estimations of the energy spectra of upcoming dangerous flux. Particle detectors of Aragats Space Environmental Center (ASEC) in Armenia perform monitoring of various species of secondary cosmic rays with different energy thresholds at altitudes 2000 and 3200 m. a.s.l. We present results on sensitivity of secondary cosmic ray flux to parameters of the incident "beams" of solar particles and – to approaching clouds of the magnetized solar plasma of CME, taking as examples the solar extreme event of 20 January 2005.

Introduction:

The sun influences earth in different ways by emission of radiation, plasma and high energy particles and ions. Although the overall energy fraction of the high energy particles is very small compared with visible light energy, nonetheless, the study of these particles gives clues not only about fundamental and universal processes of particle acceleration, but also provides timely information on the consequences of the huge solar explosions affecting the near-earth environment, space born and surface technologies, i.e. so called Space Weather issues (Lilensten & Bornarel, 2006).

During milliards years of its evolution earth was bombarded by the protons and fully striped ions accelerated in Galaxy in tremendous explosions of the supernovas and by other exotic stellar sources. This flux was changed during the passage of sun through the four galactic arms in its course around the center of Galaxy and, may be, was affected several times by huge explosions of nearby stars. Nonetheless, on the shorter time scales the GeV galactic cosmic ray flux is rather stable. In turn, our nearest star - sun is tremendously variable object, capable to change radiation and particle flux intensities many orders of magnitude during few minutes. Therefore, because of sun's closeness the effects of changing fluxes have major influence on earth, including climate, safety and other issues (see for example, Carslaw et al, 2002, Daglis, 2003).

Influence of sun on the near earth radiation environments can be described as modulation of the stable galactic cosmic ray "background" by the sun activity. The sun "modulates" the low energy Galactic Cosmic Rays (GCR) in several ways. The most energetic in the solar system flaring process releases up to 10^{33} erg of energy during few minutes. Along with broad-band electromagnetic radiation the explosive flaring process results in ejection of huge amounts of solar plasma and in acceleration of the copious electrons and ions. Particles can be generated either directly in the coronal flare site with subsequent escape into interplanetary space, or they can be accelerated in CME associated shocks that propagate through corona and interplanetary space (Aschwanden, 2005). These particles, along with neutrons, produced by protons and ions within the flare, constitute, so called, Solar Cosmic Rays (SCR). Reaching the Earth and, if energetic enough, they initiated secondary elementary particles in the terrestrial atmosphere. Low energy SCR (up to ~1 GeV/nucleon) are effectively registered by the particle spectrometers on board of space stations (SOHO, ACE) and satellites (GOES, CORONAS). Highest energy particles.generate.shower capable to reach Earth surface and be detected by the particle detectors. Only few of SEP events (usually not more than ~10 during solar activity cycle of ~11 years) can be detected by surface monitors. Such events comprise, so called Ground Level Enhancement (GLE). The latitudinal dependence of the strength of earth magnetic field provides possibility to use dispersed world-wide network of the Neutron Monitors (NM, Morall et al, 2000) as a spectrometer registering GCR in the energy range from 0.5 to ~ 10 GeV.

The spectra of GCR can be approximated by the power low - dJ_p/dE (GCR) ~ $E^{-\gamma}$, γ ~ -2.7 . SCR flux at GeV energies usually is very weak, only at some events (like 1956, 20 January 2005), the spectra of SCR is considerably "hard": γ ~ -4 - -5 at highest energies).

The surface particle detectors measure the amount of the secondary particles incident on the usually not very large detector surface of neutron monitors. These measurements (usually not more detailed as one minute time series) are the basic data for the physical inference on the solar modulation effects. There is absolutely no possibility to distinguish SCR and GCR on the event-by-event basis. The solar modulation effects are detected as non-random changes of the time series. And, if at high latitudes, where secondary particles are produced by abundant low energy SCR, modulation effects can reach 1000% and more, at low latitudes the enhancements due to SCR is very small, usually 1-2%, or a fraction of percent. If we take into account that for energies greater than 10 GeV the intensity of the GCR becomes increasingly higher than intensity of biggest known SEP events (see Figure 1), we come to very complicated problem of the detecting small signal of SCR against huge "background" of GCR. Low statistics experiments often demonstrate fake peaks with high significances. Some remedies to avoid erroneous inference on existence of signal are discussed in (Chilingarian et al., 2006).

Existent networks of particle detectors are unable to resolve this problem; therefore we still can not solve the enigma of the maximal energy E_{max} of solar accelerators. The common adopted opinion put E_{max} at ~ 20 GeV, although several underground muon detectors report incident solar ion energies of up to 50 GeV (see review in Miroshnichenko, 2001).

The direct measurement of highest energy cosmic rays by space-born spectrometers or balloons is not feasible yet due to payload and flying time limitations. Therefore, recently some large surface detectors intended to register GCR with energies higher that 10^5 - 10^6 GeV (in the region of the so called all particle energy spectra "knee" region) are used for detecting SCR (Chilingarian et al., 2003, Karpov et al., 2005, Poirier & D'Andrea, 2002)). The experimental technique used for these detectors i.e. registration of the Extensive Air Showers (EAS) is very similar to the techniques used for detection of SCR. The difference is that PeV particles generate millions and millions of secondary particles in the atmosphere, large portion of which is reaching surface (in contrast, only few particles generated by SCR can reach earth surface). To detect and measure energy (and type) of PeV particles hundred square meters of detectors are used. Detectors are triggered by the special condition allowing rejecting low energy particles. By established parallel Data Acquisition System (DAQ) it is possible to simultaneously register time series of the secondary particles incident on each of EAS detectors. In this way, due to large sizes of EAS detectors, the signal-to-noise ratio is significantly enlarged and the unexplored energy region of >10 GeV becomes attainable for research. For example, in (Wang & Wang, 2006) usage of the L3 detector (Adriani et al., 2002), at the CERN electron-positron collider , LEP, was proposed for the measurement of SCR with energies up to 40 GeV.

However, in addition to relevant experimental techniques we need also the particle "beams" from the sun, hard enough to provide sufficient intensities in the GeV region. Solar Extreme Event (SEE), occurring at October 2003, and, especially January 2005, provide such "beams" and the secondary neutrons and muons fortunately were detected by several EAS detectors. Obtained valuable information, still under analysis, notified on the possibility of measuring SCR spectra up to 20-30 GeV (Karpov et al, 2005, Dziomba, 2005, Bostanjyan et al., 2006).

Other solar modulation effects also influence the intensity of the cosmic rays in vicinity of Earth.

The SCRs increase intensity of particles incident on terrestrial atmosphere. The solar wind "blows out" lowest energy GCR from the solar system, thus changing the GCR flux intensity inverse proportionally to the sun activity, well described by the 11 year cycle. Huge magnetized plasma clouds and shocks initiated by Coronal Mass Ejections are traveling in the interplanetary space with velocities up to 2 thousand of kilometer per second (so called interplanetary CME – ICME) and disturb Interplanetary Magnetic Field (IMF). In turn these disturbances introduce anisotropy in the GCR flux in vicinity of Earth, forming depletion and enhancement regions manifested themselves as anisotropic distribution of GeV energies GCR.

Time series of intensities of high energy particles can provide highly cost-effective information on the key characteristics of the interplanetary disturbances (ICMEs). Because cosmic rays are fast and have large scattering mean free paths in the solar wind, this information travels rapidly and may prove useful for space weather forecasting (Leerungnavarat et al., 2003). Size and occurrence of southward B_z in an ICME are correlated with modulation effects ICME poses on the ambient population of the galactic cosmic rays during its propagation till 1 AU. In statistical study (Kudela & Storini, 2006) the relation of CR variability/anisotropy with the geospace disturbance was investigated. It was demonstrated that the parameters of changing CR time series are potentially useful for the geomagnetic activity forecasts. Of course, the direct detection of the Energetic Storm Particles (ESP) by EPAM (Gold, 1998) instrument on board of ACE space station also is alerting hours prior on the approaching interplanetary shock and plasma cloud (ACE news, 2003).

At arrival at Magnetosphere interplanetary shock and plasma cloud triggered overall depletion of the GCR, measured as decrease of the secondary cosmic rays detected by the networks of particle detectors at earth surface (so called Forbush decrease Fd). The relative decrease of the particle monitors count rate is well pronounced at high latitudes. Due to low magnetic cutoff rigidity at high latitudes the primary protons and ions, responsible for the greater part of count rate has considerable low energy 1-2 GeV and are strongly depleted by the disturbances of the IMF. The count rate of the particle monitors at middle and low latitudes is formed by the primaries with energies much higher – 5-7 GeV. The depletion caused by the IMF disturbances is inverse proportional to traversing particle energy. Therefore, the relative depletion of higher energies, and consequently depletion of the count rates of low latitude monitors will be less comparing with high latitude particle monitors.

Visa-verse geomagnetic storms, appears as sudden change of the Earth magnetic field can enlarge count rate of the middle and low latitude particle detectors without any notable alteration of the high latitude detectors count rates. If the magnetic field of ICME is directed southwards it reduces the cutoff rigidity. Therefore, GCRs of lower

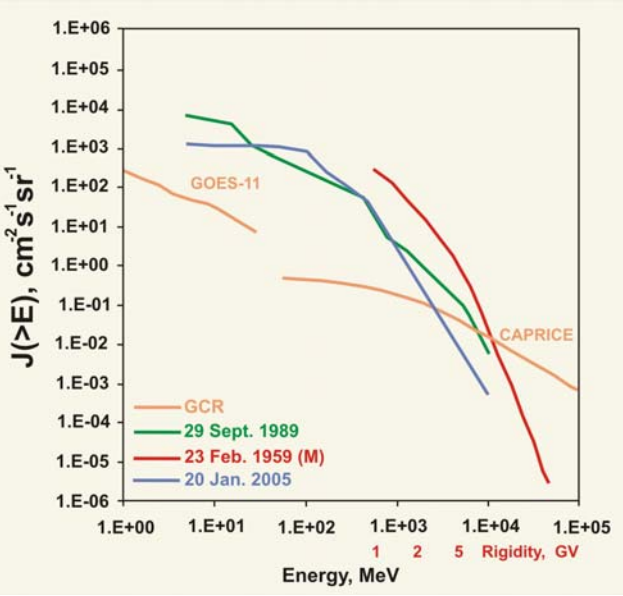

Figure 1 Galactic and Solar Cosmic Rays

energies, usually effectively declined by the magnetosphere are penetrating the atmosphere and generated additional secondary particles, those enlarging the count rate of the monitors located at middle and low latitudes. At high latitudes cutoff rigidity is very low and the count rates of particle detectors are determined mostly by the attenuation of the cascades in the atmosphere and decrease of the cutoff rigidity did not enlarge significantly number of secondary particles reaching detector.

Solar modulation effects in general are not global, i.e. their influences are not uniformly and isotropic affected Earth as whole. Therefore, a network of particle detectors is necessary for providing coverage of as much as possible latitudes and longitudes. The best coverage till now is provided by the network of the neutron monitors; instruments located at ~50 locations, some of which are taking data ~50 years (Shea, Smart 2000).

Charged particles travel and reach the Earth by way of the "best magnetic connection paths", which is not a straight line between their birthplace and the earth. The solar neutrons on the other hand, not influenced by solar and interplanetary magnetic fields, reach earth directly from their place of birth on the solar disc. The special network aimed to detect very rare neutron events from the Sun includes seven particle detectors on high mountains around the world (Tsuchiya et al., 2001).

The muon detector network (Munakata et al., 2000) (Japan, USA, Brazil, Australia) recently was enlarged by adding new facilities located in Kuwait.

All three world-wide networks are intended to measure only one type of secondary particles generated by the primary GCR or SCR. It poses several limitations on the physical inference, especially for the primaries of highest energies.

The large variety of solar modulation effects and the stringent limitations of space and surface based facilities require new ideas for developing experimental techniques for measuring the changing fluxes of the all secondary particles. New type of particle detectors with enhanced flexibility to precisely and simultaneously measure changing fluxes of different secondary particles with different energy thresholds will be a key to better understanding of the sun. Establishing a new world-wide network of such detectors, at low to mid latitudes will give possibility to measure solar proton and ion energy spectra up to 50 GeV, as well as, provide cost-effective possibilities for Space Weather research (Unated Nations, 2006).

The energy distributions of the primary protons which give rise to charged and neutral particles as secondaries in the atmosphere are shifted from each other. Thus, measuring fluxes of different particles with various energy thresholds we can estimate the energy spectra of the highest energy solar ions. To do this we have to understand the detector response function on different particles. For each of the detector channels, we have to determine the efficiency and purity of the detected particles (neutrons, protons, mesons, electrons, muons, gammas). We use the GEANT3 (CERN, 1993) and CORSIKA (Heck & Knapp, 1998) simulation codes for modeling the traversal of particles in the detector and atmosphere respectively.

Hybrid particle detectors of Aragats Space Environmental Center (Chilingarian et al., 2005) measuring both charged and neutral components of secondary cosmic rays provide good coverage of Solar Extremely Events (SEE) of 23-ed solar cycle. First results of the physical analysis of unique event of 20 January 2005 are presented in this paper.

Table 1 Characteristics of the ASEC monitors

Detector	Altitude *m*	Surface m^2	Threshold(s) *MeV*	Operation	Count rate (min^{-1})
NANM (18NM64)	2000	18	50	1996	2.7×10^4
ANM (18NM64)	3200	18	50	2000	6.1×10^4
SNT-4channels + veto	3200	4 (60cm thick) 4 (5cm thick)	120, 200, 300, 500 7	1998	$5.2 \times 10^{4*}$ 1.2×10^5
NAMMM	2000	5 + 5	7 ; 350***	2002	7.0×10^4
AMMM	3200	45	5000	2002	$1.3 \times 10^{5**}$
MAKET-ANI	3200	6	7	1996	1.5×10^5

*Count rate for the first threshold; near vertical charged particles are excluded

**Total count rate of 45 muon detectors from 150 (100 to be put in operation in 2006)

*** First number – energy threshold for the upper detector, second number – bottom detector.

ASEC monitors

The ASEC provides monitoring of different species of secondary cosmic rays and consists of two high altitude research stations on Mt. Aragats in Armenia. Geographic coordinates: 40°30'N, 44°10'E, cutoff rigidity: ~7.6 GV. The characteristics of the main ASEC particle detectors are depicted in the table 1. Data from all ASEC monitors is available on-line from http://crdlx5.yerphi.am/DVIN3/ Data Visualisation Interactive Network for the Aragats Space-environmental Center (DVIN for ASEC) provides wide possibilities for the display physical inference from the multiple time-series of particle fluxes. DVIN enables sending warnings and alerts to users, gives opportunity to remote groups to share the process of analyzing, exchange data analysis methods and schemes, prepare joint publications and maintain networks of particle detectors (Eghikyan & Chilingarian, 2006).

Starting from 1996 we are developing various detectors to measure fluxes of different components of secondary cosmic rays at the Aragats research stations of the Alikhanian Physics Institute in Armenia. In 1996 we restarted our first detector - the Nor Amberd Neutron Monitor 18NM64 (2000m above sea level). A similar detector was commissioned and started to take data at the Aragats research station (3200m above sea level) in 2000. Solar Neutron Telescope (SNT) is in operation at the Aragats station since 1997, as part of the worldwide network coordinated by the Solar-Terrestrial laboratory of the Nagoya University (Tsuchiya et al., 2001). In addition to the primary goal of detecting the direct neutron flux from the Sun, the SNT also has the possibility to detect charged fluxes (mostly muons and electrons) and roughly measure the direction of the incident muons. Another monitoring system is based on the scintillation detectors of the Extensive Air Shower (EAS) surface arrays, MAKET-ANI and GAMMA, located on Mt. Aragats at 3200 m above sea level. Charged component monitoring system on Nor Amberd research station started operation in 2002. Data Acquisition (DAQ) system was modernized in 2005.

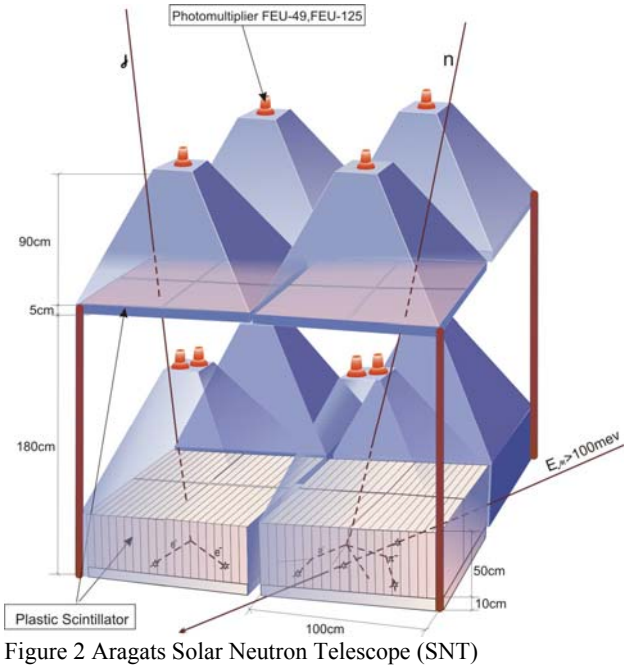

Figure 2 Aragats Solar Neutron Telescope (SNT)

Flexible microcontroller based electronics is designed to support the combined neutron-muon detector system and utilize the correlated information from cosmic ray secondary fluxes, including measurement of the environmental parameters (temperature, pressure, magnetic field). Microcontroller based DAQ systems and high precision time synchronization of the remote installations via Global Positioning System (GPS) receivers are crucial ingredients of the new facilities on Mt. Aragats.

The Aragats SNT is formed from 4 separate identical modules, as shown in Figure 2. Each module consists of standard slabs of 50x50x5 cm^3 plastic scintillators stacked vertically on a 100x100x10 cm^3 horizontal plastic scintillator slab (60 cm total thickness). One meter above the thick lower scintillator slab is another scintillator slab 100 x 100 x 5 cm^3, with the goal to register charged particles. A scintillator light capture cone and Photo Multiplier Tube (PMT) are located on the bottom and top slabs separately to measure the number of events in each of them.

Incoming neutrons undergo nuclear reactions in the thick plastic target and produce protons and other charged particles. The intensity of the scintillation light induced by these charged particles has a dependence on the neutron energy and is measured by the PMT on the scintillators. To get rough information about the incident neutron energy, we discriminate each PMT output signal according to 4 predetermined threshold settings (50, 100, 150, 200 mV) in the data acquisition electronics (4 measurement channels per module, 16 for the entire detector).

The probability for neutron to undergo nuclear reaction in the upper 5 cm scintillator is very small. The thickness of lower 60 cm layer is enough to produce photon emission due to the incident neutron interactions with the scintillator. In contrast charged particles are very effectively registered both by the upper thin 5 cm and the lower thick 60cm scintillators. When a neutral particle traverses the top thin (5cm) scintillator, typically no signal is produced. The absence of signal in the upper scintillators, coinciding with signal in the thick lower scintillators, points to neutral particle detection. When coincidences of the top and bottom scintillators register, it is possible to roughly estimate the direction of the incoming charged particle. Directional information is very useful for registration of the Ground Level Enhancements, when solar ions generate secondaries in the atmosphere with enough energy to reach to and be registered by the SNT. GLEs are usually very anisotropic and the directional information provides additional clues to understanding the origin and spectra of solar ion beams.

The Nor-Amberd Muon Multidirectional Monitor (NAMMM) is an extension of the cubic muon telescope, first described in the (Sandstrom et al., 1965), to the hybrid detector measuring neutral and charged particles with inherent correlations (Beglaryan et al., 1989). NAMMM consists of two layers of plastic scintillators above and below 2 sections (6 counters BP28) of the Nor Amberd NM (see in Figure 3 one of 2 units of NAMMM). Detector consists of 6 up and 6 bottom scintillators, each having the area of 0.81 m^2. The distance between layers is ~ 1 m., and the mean angular accuracy is ~ 25º. 10 cm. of NM lead producer filtered electrons and low energy muons; only

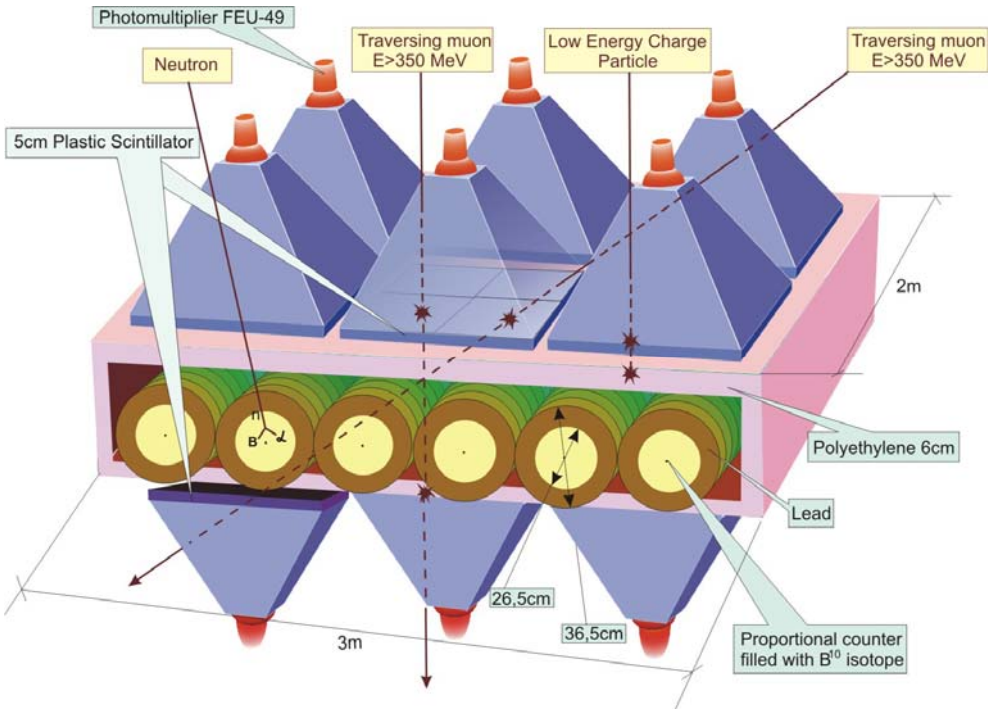

Figure 3. Nor-Amberd Multidirectional Muon Monitor (NAMMM)

muons with energy >350 MeV can reach bottom scintillators.

The data acquisition system of the NAMMM register all coincidences of detector signals from the upper and lower layers, thus, enabling measurements of the angles of incidence of the muons. Detector triggers at hit of at least one from 12 scintillators. The signals ranging from 0.5 mV to 5 V, from each of 12 photomultipliers, are passed to the programmable threshold discriminators. The discriminator output signals are fed in parallel to the 12-channel OR gate triggering device and to a buffer.

Two 6 bit length words are stored in the buffer, reflecting the hits (fires) in 12 channels. The code "1" in the 6 bit word corresponds to "fired" scintillator and "0" to "empty" one. Gate duration is selecting within the range of 100-1000 nsec. Taking into account that the gate width of the OR circuit is less than 1 μsec and the data arrival rate does not exceed 1.5 KHz, we can conclude, that the rate of random coincidences (uncorrelated signals in the upper and lower layers due to more than one near-horizontal muon traversing each layer) is insignificant. The output signal from the OR gate (duration ~1 μsec) interrupts the microcontroller and triggers the data transfer from the buffer to the microcontroller RAM for on-chip data analysis. The duration of the entire data readout and signal processing procedure is less than 10 μsec. Therefore, detector dead time is negligible.

There are 43 different possibilities of so called "basic states" of detector triggers. 36 of them carry information about the direction of the incident muon. For example, trigger word configuration "001000" for the upper layer and "001000" for the lower layer corresponds to the muon traversal through third upper and third lower scintillators (zenith angle between 0 and 45º), as demonstrated in Figure 3. The "basic state" of "001000" and "100000" respectively corresponds to the traversal through the third upper and the first lower scintillator (zenith angle between 45 and 65º). The other 7 possibilities as: more than one hit in upper and bottom layers such as "111100" and 110000", or one in the upper layer and many in the bottom layer, can be analyzed in terms of the various physical processes, such as the extensive air shower hitting the detector setup, or particle generation in the lead, neutron bursts (Stenkin, 2001), etc.

Coherent changes of the count rate in the scintillators due to changing geophysical conditions will result in rising correlation coefficients between all (or vast majority) of the detecting channels. Enhanced channel-means and correlations are pointed on the geoeffective event and after comparisons with other monitor data will be used as inputs for alert generating program.

All electronics are of original design, according to modern compact and high reliable technologies. To minimize data transmission rate, the raw data is partially processed in microcontroller before sending it to the main computer. Taking into account the slow data rates, and to minimize the cost, a serial data transmission is used, instead of much more expensive parallel data transmission standards like CAMAC, VME, etc.

A newly designed readout is based on the concept of a full software control of the detector parameters. Each photomultiplier has its own local programmable high voltage (HV) power supply and buffer preamplifier to condition the pulses in preparation for sending them via long coaxial cables without degrading the dynamic range and signal-to-noise ratio. Counting modules are located in the counter room. They have buffer preamplifiers and programmable threshold comparators (discriminators) at

the inputs. The threshold of the counter module input comparators can be programmed by voltage and polarity in the range from -0.5V to 0.5V. Besides the comparators, preamplifier output signals can be transferred to other data processing devices such as Amplitude-to-Digit-Converters (ADC). All electronics modules are based on using modern 8-bit and 32-bit microcontrollers, for the detector control system (HV programming and measurement) and for the main data acquisition respectively. Currently the Atmel 8-bit and Fujitsu FR 32-bit controllers are used. The microcontroller based electronics units (HV power supply and counting modules) have optional environmental sensors.

The main pressure sensor of the whole system is placed in a special pressure-tight box with possibility of periodic calibration using a standards Hg barometer. It consists of Motorola MPXA6115 Integrated Silicon Pressure Sensor and ATMEL 8-bit microcontroller and has frequency modulated output for direct coupling with counter modules and serial asynchronous interface to connect to the PC.

Two surface arrays measuring the Extensive Air Showers (EAS) are in operation at the Aragats research station. The main goal of the GAMMA (Garyaka edt. Al., 2002) and MAKET-ANI(Avakayn et al., 1986, Chilingarian et al., 1999) installations are to investigate the energy spectra of protons and heavier nuclei of Galactic Cosmic Rays. Both detectors use the same particle density detection techniques to determine the number of electrons hitting the scintillator slab. EAS detectors are triggered by the GCR with energies greater than 1000 GeV (producing tens of thousand of secondary particles at detector location), but each detector continuously counts incident secondary particle flux originated from the much less energetic primaries (primaries with energies starting from 7.6 GeV can produce single charged or neutral particles reaching ASEC detectors location). The count rates of the charged particles at altitude 3200 a.s.l. are ~420 counts/m^2/sec for >10 MeV electrons and ~50counts/m^2/sec for >5 GeV muons. These large high count-rates are very attractive for establishing a monitoring facility to investigate the correlations between variations of electron and muon count rates with solar modulation effects.

The MAKET-ANI surface array, see Figure 4, consists of 92 detectors formed from 5 cm thick plastic scintillators to measure density of the EAS particles. ADC) and Constant Fraction Discriminators are placed in light-tight iron boxes with photomultiplier PM-49. The dynamic range of the registered particle number is ~ 5 x 10^3.

During multiyear measurements the detecting channels were continuously monitored. Data on background cosmic ray spectra was collected for each detector. The slope of the spectra was used for detector calibration. The changing fluxes of muons and electrons incident on the MAKET-ANI detector are available from DVIN section of CRD Internet home page.

150 plastic scintillators with area of 1 m^2 each are located in the underground hall of the ANI 2experiment (Danilova et.al., 1992), to measure the muon content of the EAS. The 6 m thick concrete blocks plus the 7 m soil filter the electrons and the low energy muons. Thus, only muons with energies > 5GeV reach the detectors.

The Aragats Multidirectional Muon Monitor (AMMM) consists of 15 m^2 scintillation detectors, located on top of the ANI concrete calorimeter and 90 m^2 array same type of detectors 14 m below, as shown in Figure 5 (Avakyan

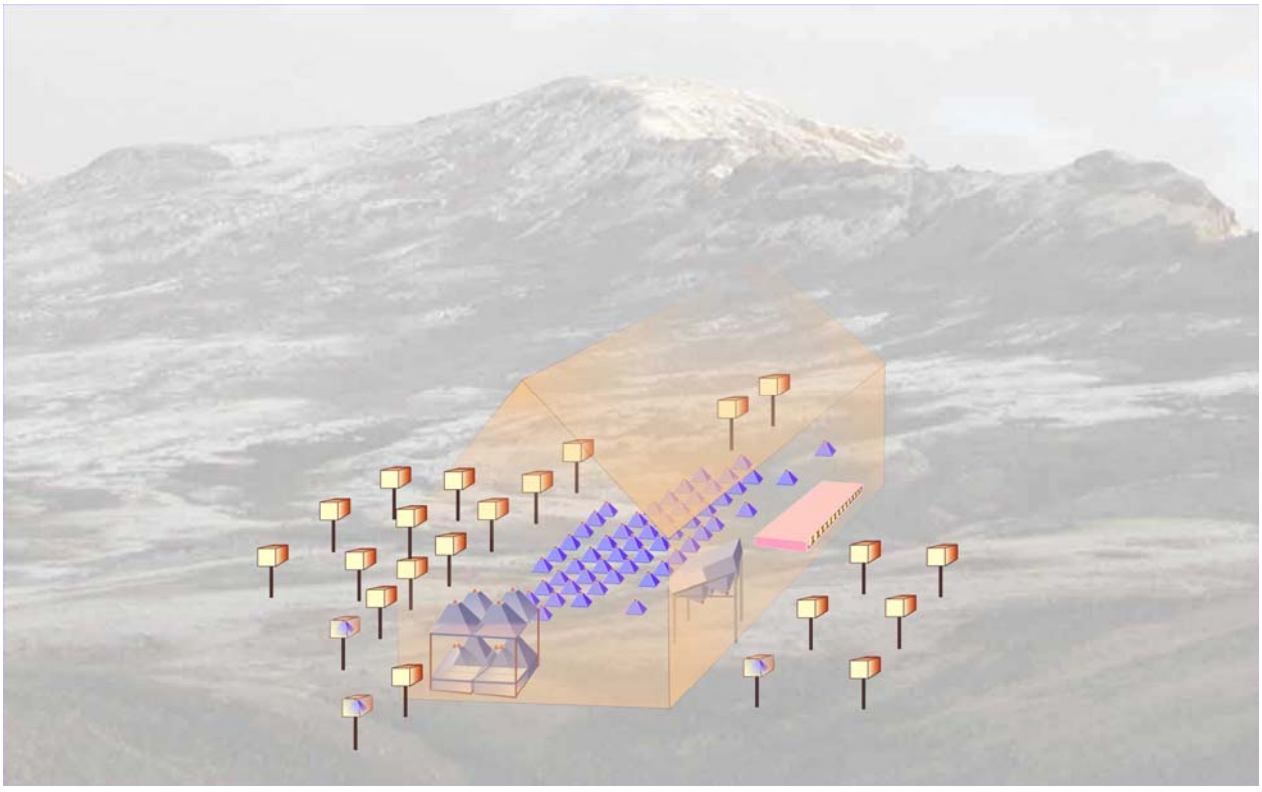

Figure 4 MAKET-ANI Extensive Air Shower Detector

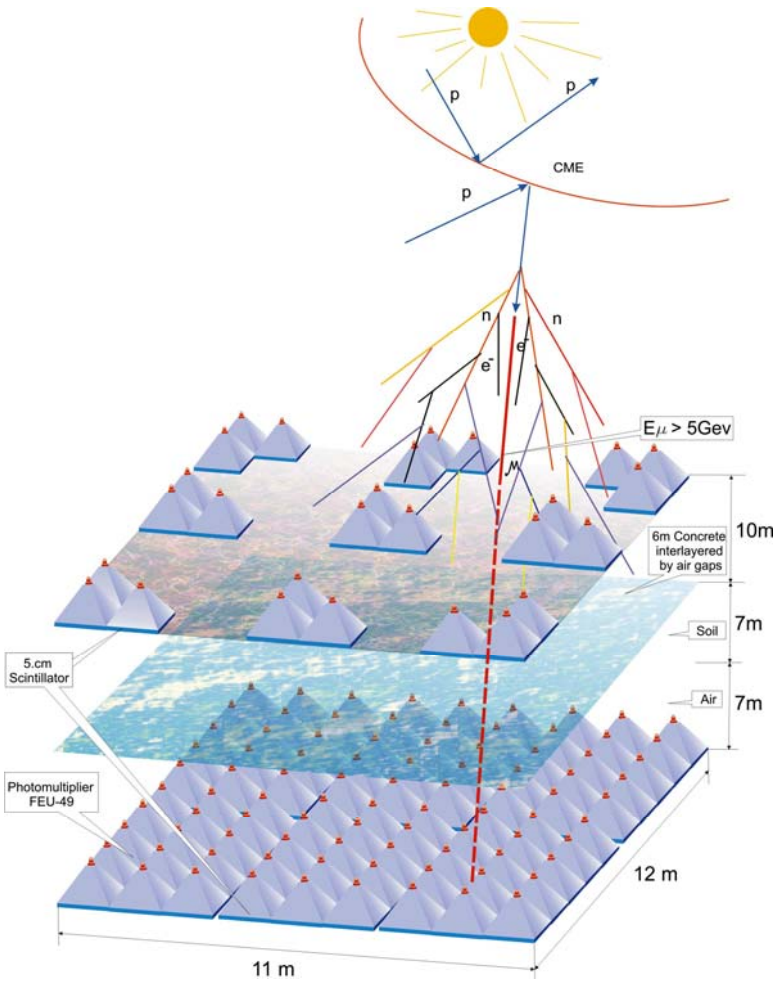

Figure 5 Aragats Multidirectional Muon Monitor (AMMM)

et.al., 1986). Also in the Figure 5 we can see the modulation effects of the solar activity on the isotropic and uniform galactic cosmic rays filling interplanetary space. Protons hitting the shock from the back are reflecting those forming the "depletion" region behind the shock. Protons hitting the approaching shock front, visa –verse, can enhance flux of particles in the definite directions. Both effects can form "precursors" of upcoming geomagnetic storm and can be detected by the ground base monitors far before start of the storm (Kuwabara et al., 2004). From the same Figure we can see the production of the secondary particles in interactions of the primary proton with earth's atmosphere. If energy of primary proton in enough, numerous secondary particles are born and, some of them can reach the mountain altitudes and be registered by the surface monitors.

Using the coincidence technique, we can monitor changing count rates from numerous space directions. Detectors on the top are grouped in 3, while those in the underground hall are grouped in 8 to provide significant amount of coincidences. The geometry of the detector arrangement will allow us to detect particles arriving from the range of directions from vertical to 60º declination, with the accuracy of ~ 5º.

By measuring the intensity deficit of the galactic cosmic rays, it will be possible to determine the loss cone direction and perform "screening" of the approaching magnetized plasma cloud. The world-wide network of muon monitors, covering as many incident directions as possible, could be used for the early forecasting of the upcoming severe geomagnetic storm (K.Munakata et al, 2000).

The lower layer of the AMMM constitutes a very sensitive high energy muon monitor, robust to local atmospheric conditions because of the rather high energy threshold. The total count rate of the monitor is approximately ~130,000 per minute. Thus, the sensitivity of this monitor reaches record value of ~0.3% for one minute count rates, 3 times better than the Aragats NM.

Simultaneous detection of variations in low energy charged particles, neutron, and high energy muon fluxes by the ASEC monitors will provide new possibilities for investigating the transient solar events and will allow us to classify Geoeffective events according to their physical nature and magnitude.

Highest energy Solar Cosmic Rays

The world-wide network of Neutron Monitors located at different latitudes act as a distributed magnetic spectrometer, measuring primary rigidities from 1 to ~10 GV (Ryan et. al., 2000). The current knowledge about solar particles of highest energies is limited by the maximum detectable momentum of this "spectrometer" and by the scarcity of data from solar cosmic rays of highest energies. Furthermore, due to very weak fluxes of GeV particles and vast background of GCR, the energy region of 5-10 GeV is also very poorly investigated by the low latitude NM and there are not many attempts to obtain

energy spectra of SCR above 5 GeV in any detail. Usually the energy spectra well above satellite energies are shown by shaded area or extrapolated dotted line.

Thus, it is vitally important to acquire data on the SCR above 5 GeV. The network of muon monitors is not yet well developed, and moreover very rare GLE events initiated by SCR with energies above 5 GeV are also extremely anisotropic. Therefore, for the estimating of the energy spectra of SCR above 5 GeV, it is crucial to perform multiple measurements at same location. ASEC monitors provide excellent possibilities for research of highest energy SCR measuring muon and neutron content of secondary cosmic rays at same latitude and 2 altitudes (in 2007 we will add additional particle detectors located at 1000 m a.s.l. along with research stations at 2000 and 3200 m a.s.l.).

To understand which primary energies are "selected" by the ASEC monitors, we perform simulation of the particle traversal through atmosphere and detectors by CORSIKA (Heck & Knapp, 1998) and GEANT3 (CERN, 1993) codes. The details of simulations are available from (Zazyan & Chilingarian, 2005).

In Figures 6 the energy spectra of proton flux of GCR incident the terrestrial atmosphere (from M. Boezio et al., 2003) is compared with energy spectra giving rise to different secondary particles. And if protons just above rigidity cutoff of 7.6 GV effectively generate neutrons detected at 3200 m., the most probable energy of the low energy charged particles "parents" is above 10 GeV. 5 GeV muons are effectively generated by the primary protons with energies of 25-30 GeV.

For the SCR, we have to consider much softer energy spectra of primaries. In Figure 7 we assume power index γ= -5 and, as we can expect, the most probable energies of the "parents" of secondary particles are shifted to the lower values. Most probable energy of charged low energy component is ~ 8-9GeV and of 5 GeV muons 15-25 GeV. Nonetheless we have 5 independent measurements for investigation of the energy spectra above 6.7 GeV. We measure neutrons and low energy charged components with Neutron Monitors and scintillators at 2000 and 3200 m a.s.l. and 5 GeV by scintillators located in the underground hall of the ANI experiment.

The highest energy detector is, of course, AMMM, with likely primary energy of ~20-25 GeV for the SCR and rather large detecting surface (45 m^2, to be enlarged to 120 m^2 in 2007). At 20 January 2005 AMMM detects significant excess of count rate at 7:02 – 7:04 UT (Bostanjyan et al., 2006). This short enhancement coincides with signals from other ASEC monitors and with peaks from Tibet NM (Miyasaka et al., 2005), SNT (Zhu et. al., 2005) and Baksan array (Karpov et al., 2005). In Figure 8 we present the preliminary differential energy spectra of the SCR protons at 7:00 – 7:04 UT measured by the space born spectrometers and surface particle detectors. For the comparison we plot also SEP events from 15 and 17 January limited by ~100MeV energies.

Small SEP event from 15 January at ~50 MeV is almost attenuated. At greater energies the GOES 11 count rates are due to background GCR flux. For reference we depict also spectra measured at "calm" Space Weather conditions (same day, 0:00 – 3:00 UT) and shown by yellow rectangles in the Figure 8.

Energy spectrum of 17 January at MeV energies is an order of magnitude larger comparing with 20 January spectra, but after spectral knee (turnover) at ~50 MeV, its spectra becomes 2 orders of magnitude smaller and vanished fast after 100 MeV. The 20 January energy spectra although is much less intensive at MeV energies, remain very hard till ~ 1 CeV (with power index ~ -1) and prolongs till tens of GeV with power index ~ -4 - -5. This signify that acceleration at GeV energies have probably another nature than at MeV energies.

ASEC Neutron Monitors (ANM and NANM) and low energy charged particles (e+μ) correspond to the primary protons with energies slightly greater than cutoff rigidity

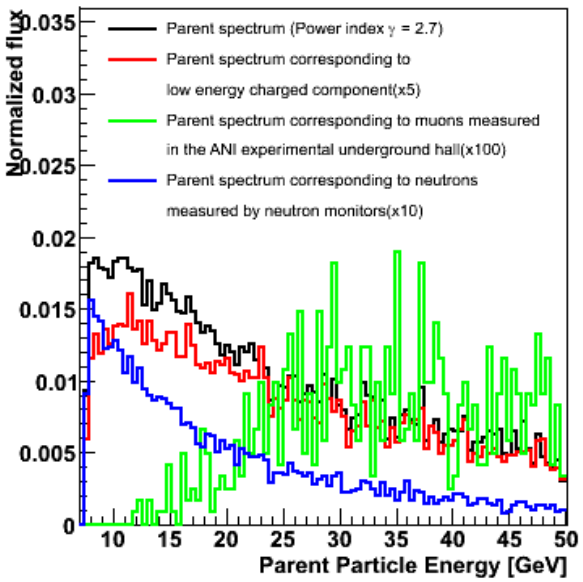

Figure 6. Simulated energy spectra of the Primary GCR protons and and corresponding "parent" spectra of secondary particles detected by the ASEC monitors at 3200 m. a.s.l.

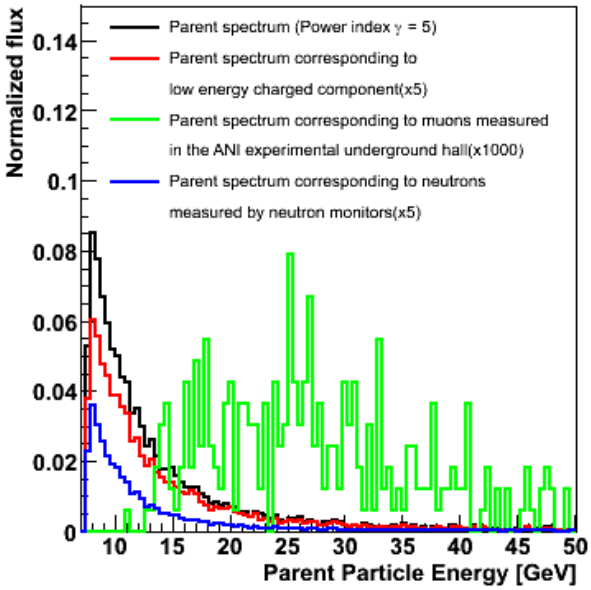

Figure 7. Simulated energy spectra of the Primary SCR protons corresponding "parent" spectra of secondary particles detected by the ASEC monitors at 3200 m. a.s.l.

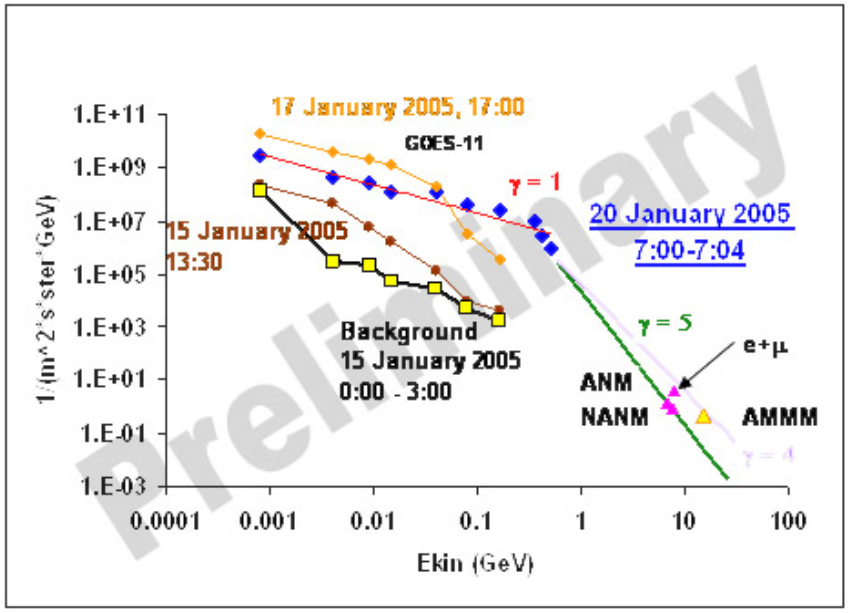

Figure 8 Differential energy spectra of the SCR protons 20 January 2005

threshold (see Figure 7). The most probable proton energy corresponding to the measured 5 GeV muon flux, as we can see from same Figure 7 is in the region 20-25 GeV. Note that the reconstructed differential spectra of AMMM is between the lines correspondent to the index of $\gamma = -4$ and -5. It is consistent with most of spectra estimates reported at 29th ICRC at Puna, India (Miysaka et al., 2005, Vashenuyok et.al., 2005). This uncertainty reflects the methodical difficulties of estimation of differential spectrum at such energies.

The estimated energy spectra index of $\gamma = -4$ - -5 at highest energies is very well indicator of upcoming abundant SCR protons and ions with energies ~50 GeV, extremely dangerous for the astronauts and high over-polar flights, as well as for satellite electronics.

In (Chilingarian et al, 2003, see also ACE news, 2005) based on the four GLE events from of 23-rd cycle we claimed that relativistic solar ions with energies above Neutron Monitor (NM) cutoff rigidity arrive well before 50 MeV protons, thus providing possibility of alerting on upcoming radiation storm. As we can see from Table 2 (updated from Gevorgyan et al., 2005), where arrival times of 4 GLE events of 23-rd cycle are compared, GeV particles are coming usually well before abundant fluxes of middle energy particles reach earth and pose danger to human in space and satellites.

The characteristics of 4 largest GLEs of 23-rd solar cycle are summarized in table 2. In column 5 the time of the first large peak is depicted. Relative standard deviation of the ANM equals: $\sigma \sim 0.7\%$; NAMM ~ 0.9%. For all 4 events the significance of the peak is greater than 3σ, thus the probability that the peak is due to random fluctuation only is very small. The last column shows the time of onset of the S2 type radiation storm according to the **NOAA** Space Weather Scales.

With the exception of the event at 20 January, when due to very good magnetically connection of the flare site with earth all relativistic particles seem to come simultaneously, the enhancements of GeV SCR detected by the Neutron Monitors can alert on upcoming severe radiation storm. The alerts from middle and low latitude monitors are even more important comparing with high latitude network, because of lower probability of false alarms. If an enhancement occurs at monitors with large cutoff rigidity it indicates that spectral knee occurs at large enough energy and energy spectra index is not too small. Enhancements in the AMMM count rates alert on the higher solar ions energies, and, consequently on hard spectra of the GLE in progress. Of course, not all GLEs will have ions with energies of tens GeV, but ones having such energies are of utmost hazard and should be reported as soon as possible to

Table 2 GLE of 23-rd cycle detected by the Aragats Neutron Monitor

Date	Monitors	X-Ray Flare	Onset	First Max	σ	Second Max	σ	I(E>10Mev) >100/cm^2 * s*ster
4/15/2001	ArNM	X14.4	13:55	14:05	4.5	14:30	3.0	14:25
GLE 60	NaNM		13:55	14:05	5.9	14:30	5.9	
4/18/2001	ArNM	C2/2	2:35	3:05	4.5	4:15	5.2	05:15
GLE 61	NaNM		2:35	3:05	3.2	4:15	5.8	
10/28/2003	ArNM	X17	11:25	11:45	6.7	12:10	6.5	12:35
GLE 65	NaNM		11:30	11:35	5.0	12:10	5.2	
1/20/2005	ArNM	X7	6:55	7:10	4.4			6:55
GLE 69	NaNM		6:55	7:00	4.5			

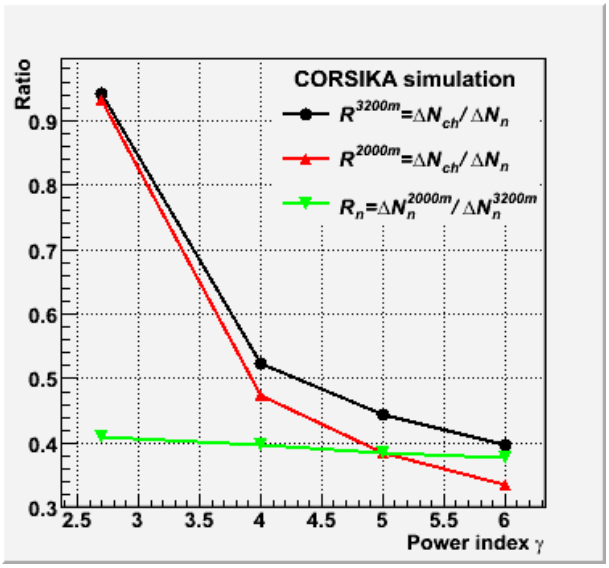

Figure 9 Estimation of the energy Spectra index by the comparing different secondary fluxes measured at same location

satellite operators. To detect very weak fluxes of highest energy solar ions we plan to enlarge the surface of 5 GeV muon detector at Aragats up to 120 m^2, to achieve the relative accuracy of signal detection of 0.16% (for 1 minute time series).

Estimation of the energy spectra index using data from NM located at same latitude, but different altitudes was suggested by (Lockwood et all, 2002). Recently (Lantos, 2006) same methodology was used for the determinations of the radiation dozes received on-board of airplanes during solar particle events. We use this technique for estimation of the spectral index of the 20 January GLE by data of Aragats and Nor Amberd NM (Zazyan & Chilingarian, 2005). Proceeding from big variety of ASEC monitors we check if using ratio of the enhancements of different secondaries, for example, neutrons and low energy charged particles, it is possible to estimate the power law index. As one can see from the Figure 9, indeed the ratio of neutral-to-charge is more sensitive to the changing power index compared with neutron flux ratio, measured at different altitudes.

Conclusions

Investigations of the highest energy solar cosmic rays are very difficult problem, requiring large surfaces of the particle detectors located at middle and low latitudes. For the estimation of the energy spectra detection of the neutral and charged secondary particles are necessary.

Measurements of the energy spectra of primary particles up to several tens of GeV will significantly enlarge the basic knowledge on the universal processes of particle acceleration at Sun and in the Universe and will allow timely warnings on the Space Weather severe conditions. The second is of huge importance taking into account planned manned flights to Moon and Mars and overall enhancement of space activity of our civilization. In 2006 sun reaches the minimum of activity and new solar cycle started. Results of the newest model of migration of solar spots (Dikpati, 2006) shows that we can expect ~50% enhancement of solar activity in the new 24-th cycle comparing with 22 and 23 cycles. Therefore, we need timely and reliable information on the state of radiation environments in the interplanetary space and correct models of the major solar energetic events in progress. The information about highest energies is necessary to test such models and to obtain overall knowledge on the particle acceleration in flares and by fast chock waves.

Acknowledgment

The author is grateful to the staff of Cosmic Ray division, Alikhanyan Physics Institute for multiyear collaboration and uninterrupted operation of the ASEC monitors. Colleges from Space Weather Analysis Group – N. Bostanjyan, V.Babayan, G. Karapetyan, M.Zazyan, H.Martirosyan and A. Reimers helped to prepare this paper and author thank them for useful discussions and fruitful collaboration.

Reference

[1] Adriani, M. van der Akker, et al (2002), The L3 +C detector, as unique tool-set to study cosmic rays, NIM **A 488**, 209-255
[2] ACE News #87 – February 23, 2005
[3] Avakian V.V., Bazarov E.B., et. al., (1986), VANT, ser. Tech.Phys. Exp., **5(31)**, p.1.
[4] M.J. Aschwanden, (2005) AGU Monograph of AGU Chapman Conference "Solar Energetic Plasmas and Particles", Turku, Finland, 2-6 August 2004, (eds.N. Gopalswamy et al.).
[5] Beglaryan A.S., Bujukyan S.P., et al.(1989), scientific publication of YerPhI, 1197 (74)
[6] J.W. Bieber, Clem J. Et al., (2005)Geophys. Res.Lett., **32**, L03S02
[7] M.Boezio, V.Bonvicini, P.Schiavon, A.Vacchi et al., (2003) The Cosmic-Ray
[8] Proton and Helium Spectra measured with the CAPRICE98 balloon experiment, Astropart.Phys. **19**, 583-604
[9] N. Bostanjyan, A.Chilingarian, V. Eganov, G. Karapetyan, (2006), On the Highest Energies of Proton Acceleration at the Sun on January, 20, 2005, in Proceedings of the Solar Extreme Events Conference, Nor Amberd, Armenia, 2005.
[10] K.S. Carslaw, R.G.Harrison, J.Kirkby, (2002), Cosmic Rays, Clouds, and Climate, Science, **289**, 1732-1737
[11] CERN 1993 GEANT3.21 Detector Description and Simulation Tool, CERN Progarm Library Long Writeups W5015[GEANT3, 1993
[12] Chilingarian A A *et al,* 1999 *Proc. 24th Int. Cosmic Ray Conf. (Salt Lake City),* **1**, p 240
[13] Chilingarian, K.Avagyan, et al., (2003) "Monitoring and Forecasting of the Geomagnetic and Radiation Storms During the 23RD Solar Cycle: Aragats Regional Space Wheather Center, Adv. Space Res., **31**, 861-865
[14] Chilingarian, K.Avagyan et al., (2003)J.Phys. G:Nucl.Part.Phys. **29**, 939-951
[15] Chilingarian, K.Arakelyan et al., (2005) NIM, **A543**, 483-496
[16] Chilingarian, G. Gharagyozyan, G.Hovsepyan, G.Karapetyan,(2006) Astroparticle physics, **25**, pp. 269-276
[17] Daglis, editor (2004), Effects of Space Weather on Technology Infrastructure, NATO Science Series II, v. 176, Kluwer, Dordrecht, Boston, London
[18] T.V.Danilova, et al., (1992), NIM, A323, 104-107
[19] M. Dikpati et al., (2006), Predicting the strength of solar cycle 24 using a flux-transport dynamo-based tool, Geophysical research letters, vol. 33, L05102
[20] M.Dziomba (2005), A new method of analyzing solar flares using secondary muons 2005 REU/NSF Program, Physics Department, University of Notre Dame, http://physics.nd.edu/Pdf/2005%20REU%20Papers/Dziomba.pdf
[21] Eghikyan & Chilingarian (2006), in Proceedings of the Solar Extreme Events Conference, Nor Amberd, Armenia, 2005..
[22] D. Heck and J. Knapp (1998), Forschungszentrum Karlsryhe, FZKA Report 6019
[23] A.P.Garyaka, R.M. Martirosov, et.al.(2002), J.Phys.G, **28**, 2317
[24] N.Gevorgyan for the ASEC team, (2005) Test Alert Service Against Very Large SEP Events, Advances in Space Research (ASR), Vol. 36, issue 12, pp 2351-2356

[25] Gold, R. E., S. M. Krimigis, et al., (1998), Electron, Proton and Alpha Monitor on the Advanced Composition Explorer Spacecraft, *Space Sci. Rev.,* **86**, 541.
[26] S.N. Karpov, Z.M. Karpova, Yu.V. Balabin and E.V. Vashenyuk (2005), Study of the GLE events with use of the EAS-arrays data, Official CD of 29th I.C.R.C., Pune, India
[27] Kuwabara T., Munakata K., et al, (2004), GRL **31**, L19803
[28] K. Leerungnavarat , D. Ruffolo, J. W. Bieber, (2003)The Astrophysical Journal, **593**:587–596
[29] K.Kudela, M.Storini (2006), Advances in Space Research, in press.
[30] P.Lantos, Radiation dozes potentially received on-board airplane during recent solar particle events, Radiation Protection Dosimetry, in press.
[31] J.Lilensten, J.Bornarel (2006) Space Weather, Environment and Societies, Springer ferlag
[32] J.A. Lockwood, H. Debrunner, E.O. Flukiger and J.M. Ryan. (2002), "Solar proton rigidity spectra from 1 to 10 GV of selected flare event since 1960." Solar Physics, 208 (1), pp 113-140
[33] Miroshnichenko L.I., *Solar Cosmic Rays,* Kluwer Academic Publishers, 2001
[34] H. Miyasaka, E. Takahashi, et al., The Solar Event on 20 January 2005 observed with the Tibet YBJ Neutron monitor observatory, Official CD of 29th I.C.R.C., Pune, India
[35] H.Morall, A.Belov, J.M.Clem (2000), Design and Co-ordination of Multi-station International Neutron Monitor Networks, Space Science Reviews **93**: 285-3003
[36] K. Munakata, K., J.W. Bieber, S. Yasue, et al.(2000), *J. Geophys. Res*., 105, 27,457-27,468
[37] J. Poirier and C. D'Andrea, (2002), Ground level muons in coincidence with the solar flare of April 15, 2001, J. Geophys. Res., Space Physics, Vol. 107(A11) 1376-1384.
[38] H. Miyasaka, E. Takahashi et al., (2005), 29th ICRC, Pune, India, **1**, 241-244
[39] A.E. Sandstrom, E. Dyring et al.(1965), Cosmic Ray meson monitors with plastic scintillators, Arkiv Fyz. 29, No 26, 329-341
[40] M.A.Shea, D.F.Smart (2000), Space Science Reviews 93: 229-262.
[41] J.M.Rayan J.A.Lockwood, H. Debrunner (2000), Space Science Reviews **93**: 35-54
[42] Yu.V. Stenkin, J.F.,Valdes-Galicia, et. al., (2001), Asroparticle Physics **16**, 157.
[43] Tsuchiya et al., (2001) Detection efficiency of a new type of solar neutron detector calibrated by an accelerator neutron beam. Nuclear Instruments and Methods in Physics Research **A 463**, 183 – 193.
[44] M. Zazyan, A. Chilingarian, (2006) On the possibility to deduce solar proton energy spectrum of the 20 January 2005 GLE using Aragats and Nor-Amber neutron monitors data, in Proceedings of the Solar Extreme Events Conference, Nor Amberd, Armenia, 2005.
[45] United Nations (2006), Comprehensive overview on the worldwide organization of the International Heliophysical Year 2007, Office for Outer Space affairs, UN office at Vienna, p.44;
[46] Seminars of the United Nations Programme on Space Applications, UN publication E.06.1.5, ISBN 92-1 100987-1, p.61
[47] E.V. Vashenyuk, Yu.V.Balabin et. al., (2005), 29th ICRC, Pune, India, **1**,209-212.
[48] F.R. Zhu, Y.Q. Tang et. al., (2005), 29th ICRC, Pune, India, **1**, 185-188.

Cosmic Ray Variations during Extreme Events in November 2004

A.V. Belov[1], E.A. Eroshenko[1],H. Mavromichalaki [2],G. Mariatos [2], V.G. Yanke [1]

[1] Pushkov Institute of Terrestrial Magnetism, Ionosphere and Radio Wave Propagation RAS (IZMIRAN), RUSSIA

[2] Nuclear and Particle Physics Section, Physics Department, Athens University, GREECE.

As it follows from the observations during the last several years the Sun reserved its main surprises in the current cycle for a descending phase. Solar activity burst in November 2004 led again to the significant sporadic variations in cosmic rays, although less in amplitude when compared to the events in October-November 2003 or in March-April 2001. Permanent releases of the solar matter, mainly from vicinity of the AR10696, occurred almost every day creating interplanetary disturbances followed shocks that caused significant short time variations in the galactic cosmic rays. Cosmic ray density and anisotropy for each hour throughout the period 6-12 November 2004 were derived from the neutron monitor network data by the global survey method. The most significant Forbush effects with a magnitude of CR density decrease of 7.3% and 8.1% turn out to be the events after 3-rd and 4-th shocks. During these events the CR anisotropy revealed sharp and fast changes by the amplitude and direction. It might be explained by the quick changes in the solar wind and IMF during the disturbed period and complicated structures in the interplanetary space which is reflected in the behavior of CR with energies recorded by neutron monitors. The behavior of these parameters during Forbush effect and geomagnetic storm were analyzed in relation to the interplanetary and magnetosphere condition.

The cut off rigidity variations were evaluated for different stations (~ 40) during geomagnetic storms in this period. Maximum changes of the cut off rigidity (dRc~0.7 GV) occurred at the latitudes corresponded to the Rc=5-6 GV, that confirms more weak perturbation of the magnetosphere in this time as compared to the storm in November 2003.

Introduction

Due to the events in autumn 2003 and 2004 the descending phase of solar cycle 23 appears to be one of the most active over 23rd solar cycle the history of the multisided study of the solar-terrestrial connections. The events in 2003 became to be not the last in the cycle. One of the next bursts of the solar activity occurred almost exactly in a year after the events in October-November 2003 [1].

We should remind that n October-November 2003 the effects were observed in the cosmic rays (CR) which are worthy to be called as the most outstanding in the cycle 23 [2, 3, 4, 5]. In this time we recorded the most long series of the ground level enhancements (GLE) of solar cosmic rays, the most significant series of the Forbush effects (FE), the lowest in the cycle intensity of the galactic CR, the greatest amplitude of the Forbush effect , the greatest magnetospheric effect in cosmic rays [6, 7]. The Forbush effect on 29 October and magnetospheric effect in CR on 20 November 2003 are the biggest ones not only in the current cycle, but over the history of CR observations. It would seem after such a stormy activity in a phase toward the minimum of solar cycle that Sun has to become quiescent. But directly in a year the new burst of activity occurred in November 2004.

The activity in November 2004 was mainly related to the fast developing region AO 10696. By the data presented in Preliminary Report and Forecast of Solar Geophysical Data (http://www.sel.noaa.gov/weekly/pdf/prf1523.pdf and 1524.pdf) during the period from the 1-st (heliolongitude E63) to 6-th (W08) November the spot square in this region increased from 60 to 910 (millionth parts of solar hemisphere), the spot number growth from 6 to 48 on the 8 November, and magnetic configuration was complicated from relatively simple (β) one up to the complex and flare productive (βγδ). This fast evolution was followed by the high flare activity: along the time of this region passing the disk the 13 flares of X-ray ball M and 2 flares of the X importance were occurred. This activity was going in a combination with significant eruptive activity. The SOHO/LASCO coronograph recorded a big amount of CMEs including 9 CMEs with full halo and of global large scale character. Although this period yields to October –November 2003 by the strength of disturbance on the Sun, in the solar wind and magnetosphere, unexpectedly big variations in cosmic rays were observed as reflection of highly disturbed solar and heliospheric environment in November 2004. Cosmic ray density and anisotropy for each hour throughout the period 6-12 November 2004 were derived from the neutron monitor network data and were analyzed together with relevant data on the solar and geomagnetic activity.

Data and method

Hourly data from 46 neutron monitors (NMs) of the worldwide network have been used in the analysis: 19 high latitude (Rc<1.2 GV), 22 mid and low latitude, and 5 equatorial (Rc>10 GV) stations. The Dst index was taken from: http://swdcwww.kugi.kyoto-u.ac.jp/dstdir/ (WDC-C2). The global survey method (GSM) described in [8, 9] has been utilized to calculate a set of parameters defining the near-Earth galactic CR density and anisotropy from the ground level neutron monitor network data, and then, for evaluation of the cut off rigidity variation (dRc). The method takes into account cosmic ray propagation in the magnetosphere and atmosphere and uses trajectory calculations in the Earth's magnetic field and the neutron monitor response functions [10, 11].

Results and discussion

Solar activity burst in November 2004 led again to the significant sporadic variations in cosmic rays, although less in amplitude as compared to the events in October-November 2003 or in March-April 2001. In Fig. 1 a behavior of the IMF , solar wind velocity, CR variations and geomagnetic activity indices are presented for the period 6-12 November 2004. By the NOAA data (ftp://ares.nrl.navy.mil/pub/lasco/halo) the releases of solar substation (CME), mainly associated with the AR10696, occurred almost every day at that time creating interplanetary disturbances followed by shocks, so that in the interplanetary space permanently existed 2-3 disturbances at

once. As one can see from Fig. 1 (middle panel), five shocks came to the Earth during the 5 days from 7 to 11 November. The afterwards disturbances were followed by sharp increase of the solar wind velocity (up to 700-800km/s) and by the IMF strengthening (up to 40-45 nT) and resulted significant variations of geomagnetic activity (low panel): Dst index went down to -373 and 289 nT, Kp-index reached 9_ during the storms on 8 and 10 November.

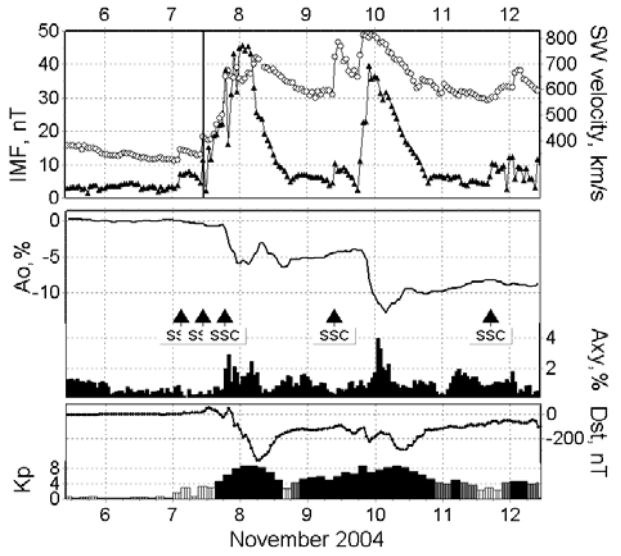

***Fig. 1**. Variation of the parameters of interplanetary space, cosmic ray (CR) and geomagnetic activity in a disturbed period on November 2004: A0-density of 10GV CR derived from the NM network data, Axy-ecliptic component of the first harmonic of CR anisotropy, Kp and Dst-indices of geomagnetic activity.*

This situation was evidently reflected in behavior of the galactic cosmic rays as a series of Forbush effects (FE). In Fig.1 on the mid panel the parameters of CR variation derived from the 46 neutron monitors by the global survey method are plotted for every hour of this disturbed period. The maximum amplitudes of Forbush decreases and equatorial component of CR anisotropy as well are entered in Table 1 together with parameters of interplanetary space and geomagnetic activity for 5 Forbush effects throughout 7-11 November 2004.

There is A0 - of 10 GV CR density variations, Axy-equatorial component of the CR anisotropy, Vsw, IMF, Kp and Dst are the parameters of interplanetary medium and geomagnetic activity, VH is a special index (product of the maximum V and H) characterized the interplanetary space conditions [12]), A_{FE} - the amplitude of the Forbush decrease evaluated from a dependence A on VH. There is a good agreement between calculated and obtained from the observation amplitudes of FE.

These events are not such a giant as in October 2003, but they evidence the level of disturbance to be rather high for the solar cycle phase close to minimum.The most significant, with a decrease depth of 7.3% and 8.1% turned out the FEs after the 3-rd and 4-th shocks (number 3 and 4 in Table 1). The same events in CR are plotted in Fig. 2 by some other way, where CR anisotropy is presented as vectors.

It is noticeable that anisotropy changes essentially even during the small Forbush effects (number 1 and 2 in the Table) with the amplitude <1%: after several quiet days vector Axy began sharply to change its direction from usual ~18 to 12, 0, 6 hours after arrival of the first two shocks. In the third event (number 3) and after this the strong increase of the anisotropy amplitude (both ecliptic and north-south components) was followed by the sharp changes in its direction. Especially large deviations from the behavior in the quiescent period the anisotropy revealed during the events 3 and 4. Fast changes of the solar wind and IMF in a disturbed period create the complicated structures which passing the Earth, influence a behavior of the CR even with the energy by neutron monitor recorded. Estimations of larmor radii ρ for 10GV CR give ~8 10^{10} cm (for 1 GV ~ 8 10^{9} cm). Under SW velocity 730 km/s a disturbance will cross this distance for about 20 min. In the hourly observations the CR changes will be present from a distance about 3-4 ρ. So, it is not surprising to see such sharp changes in CR anisotropy from hour to hour.

Table 1. The main parameters during the series of Forbush effects in November 2006

NN	Day	SSC, UT	A0, %	Axy,%	Vsw, km/s	IMF, nT	VH	A_{FE}, %	Kp	Dst, nT
1	07.11	02:57	0.6	0.86	366	7.2	1.32	0.5	3	-5
2	07.11	10:52	0.4	0.74	414	11.3	2.34	0.7	5_	10
3	07-08.11	18:27	7.3	2.91	726	45.7	16.58	7.5	9_	-373
4	09-10.11	09:30	8.1	3.98	813	39.7	16.13	7.3	9-	-289
5	11.11	17:10	1.1	1.93	673	12.2	4.11	1.5	5	-113

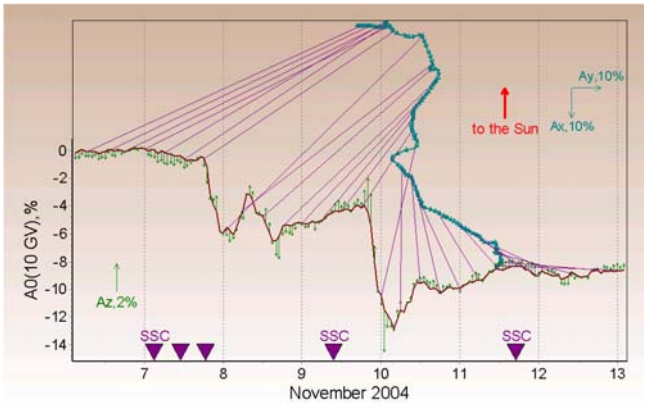

Fig. 2. Behavior of the CR density (A0) and anisotropy (Ax, Ay, Az) in the series of FEs in November 2004. Vector diagram gives an ecliptic component of the first harmonic of CR anisotropy (Axy), and vertical lines correspond to the north-south component. Triangles show the moments of the shock arrival to the Earth. Thin lines

connect the points from the vector diagram with the same moments on the time behavior (UT) of the CR density in every 6 hours.

Unusual peculiarity revealed in the CR density (A0) variation after arrival of the 4-th shock on 9 November at 9:30 UT. During ~10 hours after this there was no density decrease although a response in the anisotropy behavior is noticeable. The absence of significant CR modulation during ~10 hours after the SSC may inform about unclosed structure passing near the Earth. A large FE as well as a strong magnetic storm started only 10 hours later just after the next jump in the SW velocity and IMF (were not followed by SSC).

We emphasize also some unusual behavior of the CR density on 8 November in the minimum of Forbush effect (FE) when during almost 12 hours a density increase of about 2% was observed. Its peak coincides both with the jump of solar wind velocity and with a Dst minimum (-373 nT). This seemingly should be attributed to a magnetosphere effect in cosmic ray. However, additional analysis doesn't allow accept this simple explanation. Magnetosphere effect as a rule reveals at mid- and low latitude stations and is not seen at the stations with cut off rigidity less than 2-2.5 GV. In this case a CR density increase was recorded also at high latitude neutron monitors (except of the very eastern) and even at polar stations (South pole, McMurdo). Excluding from the processing the stations with Rc>1.2 where the magnetospheric effect is more expectable, did not change a situation. Thus, this enhancement of CR density in the minimum of FE at least partly, may be a result of the galactic CR modulation by certain structures in the interplanetary space. At that time a succeeding part of a disturbance propagated with higher velocity than preceding one, and as result of interaction of the solar wind streams a compressed region was created , with higher CR density and rather complicated structure, which manifested in the sharp, although short duration, changes of CR anisotropy (Fig. 2). A somewhat similar effect in the time profiles of NM data during the 1991 March 24 FE has been investigated by Hofer and Flückiger [13]. They attributed the effect to a large-scale interplanetary disturbance passing the Earth, probably a magnetic cloud.

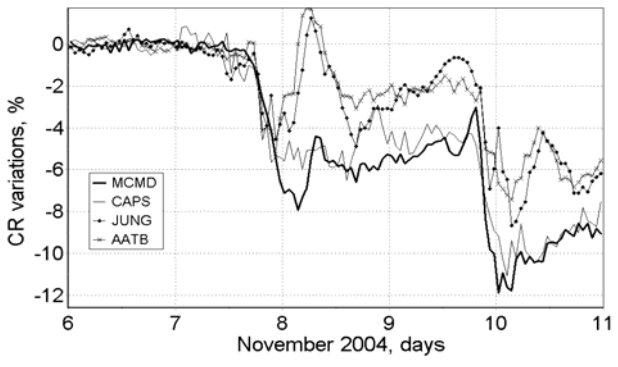

Fig. 3. Cosmic ray variations relatively to basic day November 6 at neutron monitors from the stations: NcMurdo (MCMD), Rc=0.01 ГВ; Cape Shmidt (CAPS), Rc=0.52; Jungfraujoch (JUNG), Rc=4.48 ГВ; Alma-AtaB 3300м (AATB), Rc=6.69 ГВ in November 2004.

Nevertheless, as one may see from Figure 3, during this specific time period the counting rate variation at middle and low latitude NMs (JUNG, AATB) shows a much bigger enhancement than at high latitudes, that may be really related to magnetospheric effect at these stations. The residual dispersion in the calculations by GSM method, is large during these hours that indicates unaccounted magnetospheric effect. Thus, in this event the effects both of interplanetary and geomagnetic origin were present simultaneously.

The variations of the cut off rigidities (DRc) at different stations were calculated by the method described in [14, 15, 9] during the effects in November 2004. A distribution of rigidity variations dRc during the maximum of the magnetic storm on 8 November versus cut off rigidities for the quiescent magnetosphere [16] is presented in Fig 4 for the moment with the minimum Dst. As one can see, the maximum changes of Rc (nearly 0.7 GV) occurred at latitude corresponded to Rc= 5-6 GV, that confirms more weak disturbance of the magnetosphere in this period as compared to the storm in November 2003 [9, 17, 18].

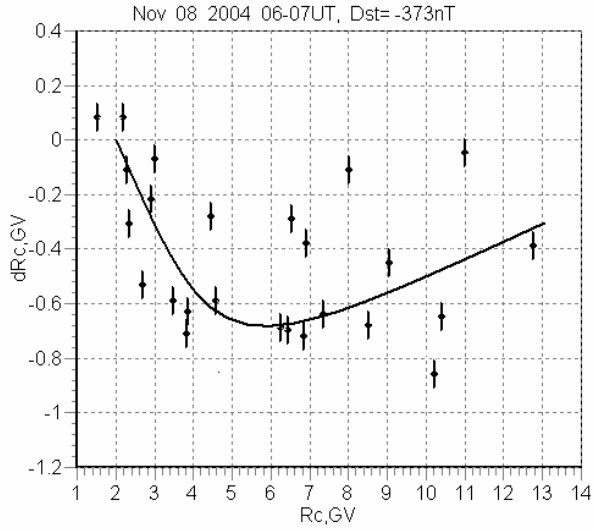

Fig. 4. Latitudinal distribution of the cut off rigidity variations in the maximum of the magnetic storm on November, 8, 2004.

In a whole, by the level of perturbation, by the number and magnitude effects in cosmic rays the situation in November 2004 gives a way only to the events in October-November 2003 and in March-April 2001 during the current solar cycle.

Summary

There was no such giant events in November 2004 as those occurred in November 2003. Nevertheless, the series of Forbush effects and SSC is an evidence of the level of interplanetary and geomagnetic perturbations rather high for a descending the solar cycle phase nearly the minimum;

The FEs on 7 and 9 November 2004 were the most significant in this series with a decrease magnitude 7.3% and 8.1%. This is in a good agreement with the FE amplitudes estimated from the parameter of solar wind disturbances;

During these events the fast changes of SW and IMF created complicated structure which caused especially sharp changes in amplitude and direction of the CR anisotropy.

A good correlation between cut off rigidity variation dRc and Dst indices is obtained due to applying GSM method that

allows a quantitative relation to be defined during the great magnetic storms

Maximum dRc in Nov. 2004 reached -0.7 GV at Rc ~5-6 GV that confirms a weaker disturbance of magnetosphere as compared to the November 2003.

Acknowledgements

This work in operating of the Russian CR stations is partly supported by Russian FBR Grants 04-02-16763 and 03-07-90389; for USA stations - NSF Grant ATM-0000315. The authors thank the collaborators from all CR stations which data were taken for analysis: Alma-Ata, Apatity, Barenzburg, Beijing, Calgary, Cape Shmidt, Climax, Erevan, Erevan3, ESOI, Fort Smith, Haleakala, Hermanus, Irkutsk, Irkutsk2, Irkutsk3, Inuvik, Jungfraujoch, Kergelen, Kiel, Kingston, Larc, Lomnicky Stit, Magadan, Mawson, McMurdo, Mexico, Moscow, Nain, Newark, Norilsk, Novosibirsk, Oulu, Peawanuck, Potchefstrom, Rome, Sanae, Santiago, South Pole, Tbilisi, Terre Adelie, Thule, Tixie Bay, Tsumeb, Yakutsk. This work is also partly supported by HRAKLITOS project of the Greek Ministry of Education

REFERENCES

[1] Ermolaev, Yu. I., L. M. Zeleny and 47 coauthors, Year after: Solar, heliospheric and magnetosphere disturbances in November 2004. Geomagnetism and Aeronom., 45, N6, 723-763, 2005

[2] Belov, A. V., E. A. Eroshenko, V. G. Yanke. The events in October-November 2003 by the ground level cosmic ray observations. Geomagnetism and Aeronomy, V. 45, 1, 51-57, 2005.

[3] Veselovsky I.S., M.I. Panasyuk, et al., ~60 coauthors. Solar and heliospheric phenomena in October-November 2003: reasons and consequences. Kosmicheskie Issledovaniya, V. 42, 5, p. 453-508, 2004

[4] Panasyuk M. I., Kuznetsov S. N., …Belov A. V., Bengin V. V. et al., ~58 coauthors. Solar extreme events in 2003. Kosmicheskie Issledovaniya, V. 42, №5, pp. 509 – 554, 2004.

[5] Eroshenko, E., A. Belov, H. Mavromichalaki, G. Mariatos, V. Oleneva, C. Plainaki, V. Yanke. "Cosmic ray variations during two greatest bursts of solar activity in the 23-rd solar cycle", Solar. Phys., V. 224, N1-2, pp 345 - 358, 2004.

[6] Belov A. V., L. M. Baisultanova, E. A. Eroshenko, H. Mavromichalaki, V. V. Pchelkin, Unusually great magnetospheric effect in cosmic rays on 20 November 2003, Izvestiya RAN, ser. Phys., **69**, № 6, 857-860, 2005.

[7] Ermolaev, Yu. I.; Zelenyi, L. M.; Zastenker, G. N.; Petrukovich, A. A.; Mitrofanov, I. G.; Litvak, M. L.; Veselovsky, I. S.; Panasyuk, M. I.; Lazutin, L. L.; Dmitriev, A. V.; and 41 coauthors, Solar and Heliospheric Disturbances that Resulted in the Strongest Magnetic Storm of November 20, 2003, Geomagnetism and Aeronomy, V. 45, p. 20, 2005.

[8] Belov, A. V., E. A. Eroshenko, and V. G. Yanke, Cosmic ray effects caused by the great disturbances of the interplanetary medium in 1990-1996, *Proc. 26-th ICRC, 6*, 431-434, 1999.

[9] Belov A., Baisultanova L., Eroshenko E., Mavromichalaki H., Yanke V, Pchelkin V, Plainaki C., Mariatos G. Magnetospheric effects in cosmic rays during the unique magnetic storm on November 2003", JGR, VOL. 110, A09S20, doi:10.1029/2005JA011067, 2005

[10] S. Yasue et al., Coupling coefficients of Cosmic Ray Daily Variations for Neutron Monitor Stations, Report of Cosmic Ray Research Laboratory, N7,1982.

[11] Clem, J., and L. I. Dorman, Neutron monitor response functions. *Space Sci. Rev., 93*, 1, 335-359, 2000.

[12] Belov A.V., E.A.Eroshenko, V.A. Oleneva, A.B., A.B. Struminsky, and V.G. Yanke. What determines the magnitude of Forbush decreases? Adv. Space Res. Vol.27, No. 3, pp 625-630, 2001.

[13] M.Y. Hofer and E. O. Flueckiger, J. Geophys. Res., 105 (A10), 23,085-23,097, 2000.

[14] Baisultanova L., A. Belov, L. Dorman, V.Yanke. Magnetospheric effects in cosmic rays during Forbush decrease. Proc. 20-th ICRC, Moscow, **4**, 231, 1987.

[15] Baisultanova L., A.Belov, V.Yanke. Magnetospheric effect of cosmic rays within the different phases of magnetic storms. Proc 24-th ICRC. **4,**1090-1094, 1995.

[16] Shea, M.A., and D. F. Smart, Vertical Cutoff Rigidities for Cosmic Ray Stations since 1955. ICRC27*, Contributed Papers,* 10, 4063-4066, 2001.

[17] Plainaki, C., Belov, A., Eroshenko, E., Kurt, V., Mavromichalaki, H., Yanke, V. "Unexpected burst of solar activity recorded by neutron monitors during October-November 2003" Adv. Space Res. 35, 4, 691, 2005.

[18] Belov, L. Baisultanova, R. Buetikofer, E. Eroshenko, E. O.Fueckiger, G. Mariatos, H. Mavromichalaki, V. Pchelkin, V.Yanke. Geomagnetic effects on cosmic rays during the very strong magnetic storms in November 2003 and November 2004, Proc. ICRC29, Puna, 2005

The Extreme Solar Cosmic Ray Event of January 20, 2005

A.V. Belov[1], E.A. Eroshenko[1], H. Mavromichalaki[2], Ch. Plainaki[2], V.G. Yanke[1]

[1] *Institute of Terrestrial Magnetism, Ionosphere and Radio Wave Propagation RAS (IZMIRAN), RUSSIA abelov@izmiran.ru*
[2] *Nuclear and Particle Physics Section, Physics Department, Athens University, Greece, emavromi@phys.uoa.gr*

Towards the end of the 23rd solar cycle an extreme giant ground level enhancement (GLE) was recorded by the worldwide network of neutron monitors (NMs). The flux of relativistic protons reached the Earth at ~ 6:49 UT on 20 January 2005. The fact that southern polar NM stations recorded increases of the order of 10^3 ranges this event among the greatest ones in history of NM observations, being comparable to that on 23 February 1956. The parameters of the cosmic ray energy spectrum, anisotropy, differential and integral fluxes were derived after applying anisotropic and compound models of solar cosmic ray variations to the data from about forty neutron monitors. Simultaneous maximum in broad energy range in differential fluxes of solar CR testifies the arrival of all energies at the same time in the first minutes. In the first 5-minute interval high energy particles dominated in the flux whereas just before 7:00 UT the number of low energy particles essentially enhanced. Only in the first minutes of the event our compound model selects sufficiently high upper energy E_u reflecting this way a small contribution of the higher energy particles (>3GeV) during this GLE.

Introduction

In rare occasions a solar flare accelerates protons to sufficiently high energies for these particles to propagate along the heliomagnetic field to the Earth and to be detected as a sharp increase in the counting rate of a ground based cosmic ray detectors, causing a ground level enhancement event (GLE).

The greatest GLE was recorded by neutron monitors until January 2005 took place on 23 February 1956. The characteristics of this event have been analyzed by many researchers [1-6]. Since that time 64 GLEs have been registered, but all of them rank below this one by one order of magnitude or more. However, an extreme GLE recorded on 20 January 2005, appearing to exceed all previous enhancements including that of 1956, on the basis of one-minute data. It was associated with the flare X7.1 on 20 January in AR720 (N12 W58) started at 6:36 UT. This ground level event (GLE69) took place in a recovery phase of the Forbush effect, on the background of relatively quiet geomagnetic activity (Kp changed from 2 to 4). It is remarkable that this event occurred in a descending phase of the 23 cycle, very close to the minimum of solar activity.

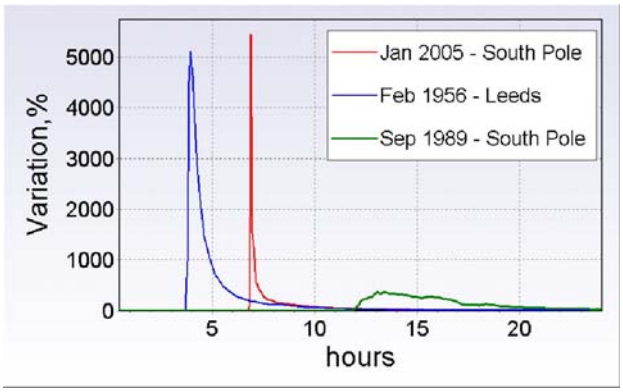

Fig. 1. Three biggest GLE as if they occurred on one day.

In Fig. 1 the profiles of three biggest GLEs are plotted by the data from neutron monitors recorded the maximum effect. It is seen that the last event shows even higher amplitude than the famous GLE05 on 23 February 1956 [5, 6] by one minute data. At the same time in GLE69 there was much less high energy particles than in 1956 or in 1989 and majority of high latitude stations recorded effect an order less (~100-300%) and at mid- latitude stations with cut off rigidity more than 6GV it was very small or absent at all. The most outstanding feature of these both proton enhancements seems to be an extremely high anisotropy and narrow and intensive beam of ultra relativistic particles arriving at Earth during the first minutes after the onset. Several researchers have already analyzed the GLE69 attempting to give explanations on its various features and peculiarities [7-12]. This GLE has been studied by [11] using a transport model based on numerical solutions of the Boltzmann equation, revealing also that the event was enormously anisotropic. An analysis based on the use of solar, geomagnetic and cosmic ray data was carried out by [12], using a simulations with recently developed GEAN4 code for the evaluation of the asymptotic directions and cut off rigidities during this event.

In this work cosmic ray intensity data from almost 40 neutron monitors during the time period of this extreme event has been analyzed and processed in order to interpret the behavior of solar cosmic rays, on the framework of a compound GLE-model, including anisotropic and isotropic components.

GLE model description

Cosmic ray variations recorded by a ground level detector during a GLE may be written as follows [5, 6, 13]:

$$\frac{\Delta N}{N_0}(t,t_0) = \frac{\int_{E_c}^{E_u} W(E,t_0,h)\frac{\Delta I}{I_0}(t,E)dE}{\int_{E_c}^{E_u} W(E,t_0,h)dE} \qquad (1)$$

where N_0 is the basic background counting rate resulted by galactic cosmic ray flux I_0 and measured at the moment t_0 , h is atmospheric depth at the point of observation in b, Ec is the threshold kinetic energy of the primary protons that cause the secondary flux recorded by a specific detector, and Eu is the upper energy limit for the solar particle registered during the event. Coupling coefficients $W(E, t_0, h)$ were calculated analytically for each station separately on the basis of the relation given in [14], taking into consideration, however, the different neutron monitor response in the lower energy range

[15, 5]. A power law spectra as E^{γ} was considered for the primary CR intensity variations $I(t, E)$ which were supposed to consist of an isotropic part and an anisotropic one, characterized by an angular distribution function taken as:

$$\Psi = e^{-n_a^2 \sin^2(x - x_0)} \qquad (2)$$

where x is the angular parameter of the solar CR anisotropy, n_a is a parameter controlling the spatial extension of the anisotropy region and x_0 corresponds to the direction in which Ψ equals to its maximal value 1. In case of a compound model, consisting of an isotropic and an anisotropic component, equation (1) becomes:

$$\Delta I(t, E) = \Delta I_0 + \Delta I_1 = b_0 f_0(E) + b_1 f_0(E) \Psi(\chi, E) \qquad (3)$$

where f_0 is the differential energy spectrum and b_0 and b_1 are the relative contributions of the isotropic and anisotropic comonents, respectively.

Five-minute data from 37 neutron monitors have been processed and analyzed in order to fit the main equation (3) of the GLE model, in the basis of a least square method.

Results- Discussion

Our analysis showed that the event of 20 January 2005 was extremely anisotropic. This fact is testified by the time profiles of cosmic ray variations registered in two neutron monitors of the same cut-off rigidity, located at different longitudes and hemispheres. The results of our exact calculations for the NM stations of Thule and McMurdo, demonstrated in Fig.2, are in good agreement with [8, 11]. Anisotropy contribution dominates during the first 15-20 minutes from the asymptotic direction ~50S, 40W and quickly decreases with time changing sharply its direction (Fig. 3). However the anisotropy remains at a significant high level not less than 11 hours after the onset. The first particles came from the Sun by the narrow beam (big values of n_a) and had very hard spectrum with an index -0.65.

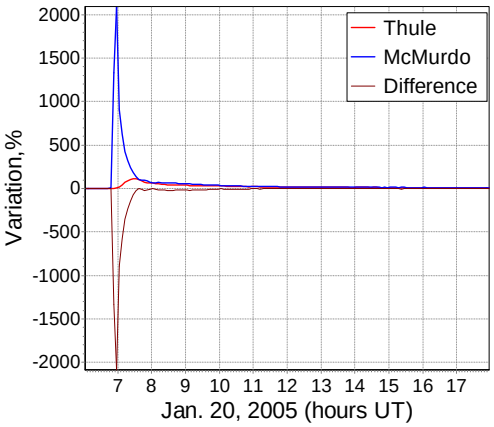

Fig. 2. North-south anisotropy is evident as the great one during the first 40 minutes, but in fact The enhancement at McMurdo significantly exceeds that at Thule even in 10 hrs after the onset.

The anisotropy index na, in equation (2), was calculated as 4.7±0.2, meaning that the first particles have come from the Sun in the form of a narrow beam. In the first 5-minute interval high energy particles dominated in the flux whereas just before the 7:00 UT the number of low energy particles essentially enhanced.

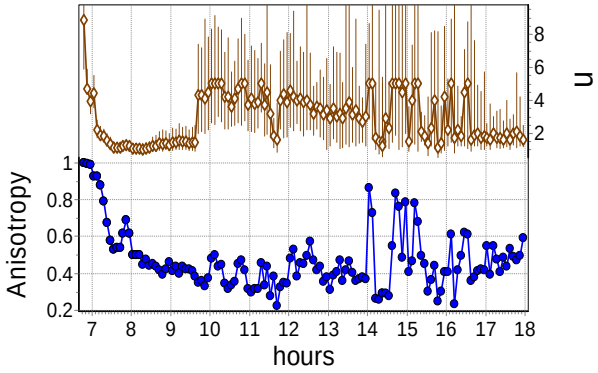

Fig. 3. Behavior of the solar CR anisotropy and coefficient ***n,*** *characterizing gA width of angular distribution of anisotropic flux.*

The flux along the IMF force line started to dominate only some time later. The time evolution of the anisotropic flux source position shows that there were significant fluxes of solar particles coming form southern locations, as it is demonstrated in Fig. 4. This result is in agreement with [8, 10]. The big enhancements observed by the polar stations of South Pole, Terra Adelie and McMurdo, already in a very early phase of the event, occurred as a consequence of the specific beam direction of the anisotropic primary proton flux. In the same time the effect was observed quite ordinary at the other high latitude stations. There was much less high energy particles than in 1956 or in September 1989 events, and majority of high latitude stations recorded effect an order less (~100-300%), and at mid-latitude stations with cut off rigidity more than 6 GV the solar CR flux was very small or absent at all. In some minutes after the onset a spectrum of the solar CR became significantly softer and during the next 5 hours its index varied only within the -3.0 - 4.0 range. The spectrum of solar cosmic rays is presented in Fig. 5. It can be clearly seen that there is a significant softening taking place from the second time interval of the event.

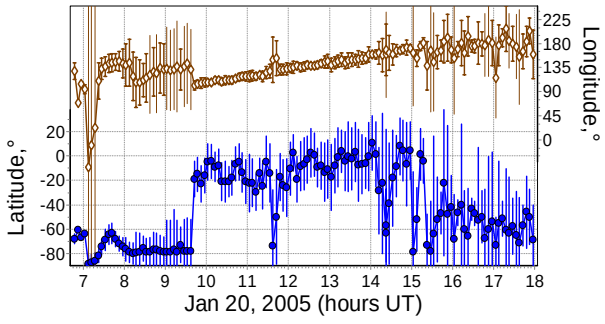

Fig. 4. Behavior of latitude and longitude of the anisotropic solar particle flux.

Only in the first minutes our model selects sufficiently high upper energy. In the later phase Eu seems to be small enough and underestimated. This is a real reflection of the small contribution of the higher energy particles (>3GeV) in the observed GLE. The behavior of the upper energy Eu, obtained by model (circles) and observed by neutron monitors (triangles) is presented in Fig. 6.

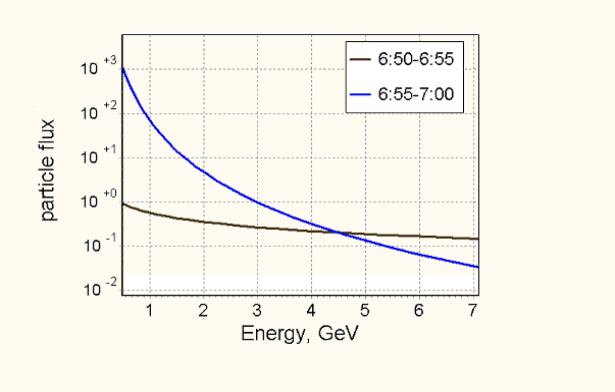

Fig. 5: Spectrum of solar cosmic rays during the first and the second time-interval after the onset of the event

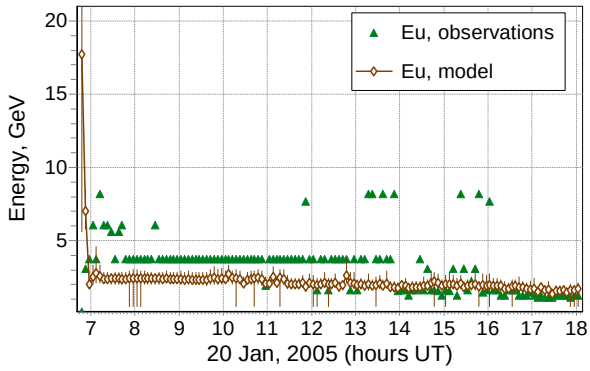

Fig. 6. Time evolution of the upper energy parameter Eu.

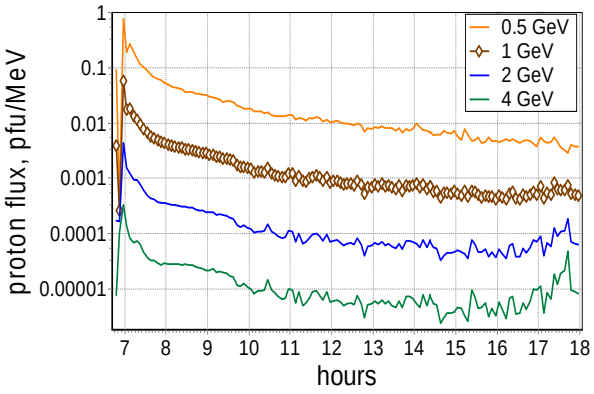

Fig. 7. Behavior of the differential fluxes

Calculation of the differential fluxes of solar cosmic rays with different energies shows a simultaneous maximum in broad energy range testifying the arrival of different energy particles at the same time in the first minutes of the event (Fig. 7).

All parameters changed essentially during the evolution of the event. In particular, the spectral index γ became more negative, the position of the anisotropy source moved southwest, and the beam of solar particle arriving in an anisotropic way widened. A complicated behaviour of the anisotropy lasted at least 11 hrs after the onset that partly reflects significant variations of the IMF in this period [10].

In Fig. 8 the integral fluxes for different energy solar protons are presented. Upper panel shows the fluxes measured onboard GOES, and low panel demonstrates the fluxes calculated from the neutron monitor data using the GLE model.Of course, the fluxes of >300 and especially, >100MeV are the extrapolation, but there is a good agreement for maximal flux >100 MeV with the satellite observations. In the later phase the model gives underestimated fluxes.

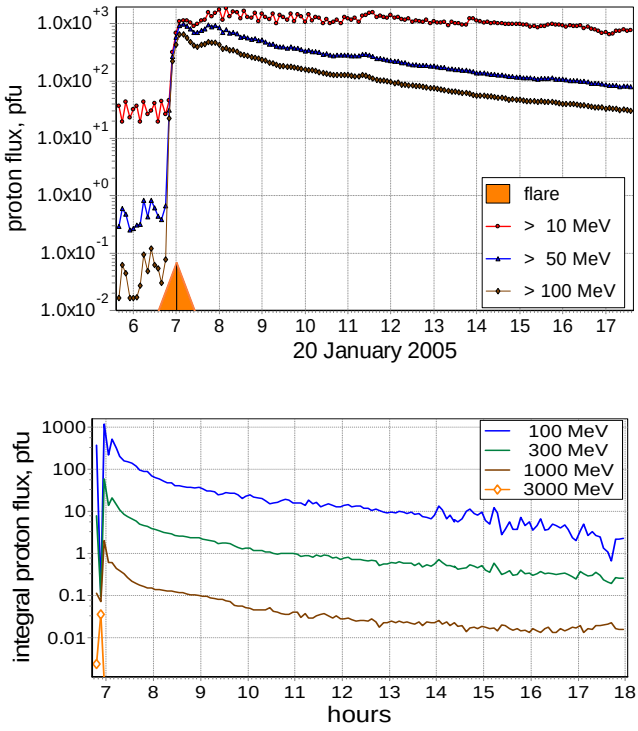

Fig. 8. The integral fluxes of solar protons by different energies: upper panel –plotted by GOES observations; low panel-estimated from NM observations by means of extrapolation.

The event of 20 January has a complex structure with two (or, even three [8]) maxima. For the majority of stations the first peak occurred between 7:00 UT and 7:20 UT, depending on the orientation of the station's asymptotic cone in relation with the anisotropy source. The second peak in neutron monitor fluxes during the GLE event of 20 January occurred at about 7:55 UT – 8:00 UT and it was observed clearly by those stations that had cut-off rigidity in the 2 GV-4 GV range. This second maximum in the GLE data is probably related to SCR density maximum and it is more prolonged than the first one. It is actually the main maximum of the event, observed by almost all neutron monitor stations. The bigger the cut-off rigidity of the station, the later this maximum is registered. The first (additional) peak is observed only by several best-located stations and it is related with the anisotropic beam of solar particles. If the anisotropy wasn't so big during the first time intervals in the event of 20 January 2005, only one maximum would be observed by the majority of the stations (such were the events of "classical" profiles on 15 June, 1991 or on 2 November, 2003).

Conclusions

Our conclusions derived by the analysis presented in this paper can be summarized as follows:

1) The GLE on 20 January 2005 seems to be one of the most extraordinary cases in the history of solar cosmic rays. Nevertheless, high energy particles (>3 GeV) turned out to be of less amount than in 1956 and 1989 events.

2) The first particles came from the Sun forming a narrow beam The asymptotic cones of South Pole, Mc Murdo and Terre Adelie fall into the narrow beam of solar particle arrival observing enhancements of thousands of percentages.

3) The solar cosmic rays energy spectrum was very hard in the beginning with index -0.65. Already in some minutes after the onset the spectrum became soft keeping its form for several hours, with index -3.0-4.0.

4) Anisotropy dominates during the first minutes of the event, and it remains during several hours after, but having the usual form like the first spherical harmonic.

5) The solar CR flux was anisotropic for a period of at least 11 hours. Changes of anisotropy parameters along time seem to be related to the variability of the interplanetary magnetic field.

6) Calculation of the differential fluxes of solar CR with different energies shows a simultaneous maximum in broad energy range testifying the arrival of different energy particles at one time in the first minutes.

7) Our results obtained form the application of a compound GLE model are consistent with the preliminary results of other researchers [10, 11, 12]. A further analysis of the GLE on 20 January 2005 will give a more complete and detailed picture of the evolution of this outstanding event.

Acknowledgements

This work is partly supported by the Russian FBR grants 03-07-90389 and 04-02-16763, by Program BR of the Presidium RAS "Neutrino Physics", and Greece HRAKLEITOS Project (grant 70/3/7218). This project is co-financed within Op. Education by the ESF and National Resources. We thank all responders of neutron monitor data available for this period. We are grateful to the providers of real time sources of solar and interplanetary data in the internet.

REFERENCES

[1] Meyer, P., Parker, E.N., and J.A Simpson. Solar cosmic rays of February 1956 and their propagation through interplanetary space, v.104, No.3, 768-783, 1956.

[2] Pfotzer, G. On the separation of direct and indirect fractions of solar cosmic radiation on February 23, 1956 and on difference in steepness of momentum spectrum of these two components. *Nuovo Cimento Suppl*., v. 8, Series 10, No.2, 180-187, 1958.

[3] Miroshnichenko, L.I.: 1970, On the absolute fluxes of particles accelerated at the Sun on February 23, 1956, *Geomagn. and Aeronomy*, v.10, No.5, 898-900, 1970.

[4] Smart, D.F. and Shea, M.A. Probable pitch angle distribution and spectra of the 23 February 1956 solar cosmic ray event, *Proc. 21st Int. Cosmic Ray Conf.*, Adelaide, Australia, v.5, 257-260, 1990.

[5] Belov, A., Eroshenko E., Mavromichalaki, H., Plainaki, C., Yanke, V.: Solar cosmic rays during the extremely high ground level enhancement of February 23, 1956, Annal. of Geophys. 23, 1-11, 2005a

[6] Belov, Á., Eroshenko, E., Mavromichalaki, H., Plainaki, C., Yanke, V. "A study of Great Ground Level Enhancement on 23 February, 1956" Adv. Space Res. 35, 4, 697-702, 2005

[7] Timofeev, V.E., Krivoshapkin, P.A., Grigoryev, V.G., Prihodko, A.N., Migunov, V.M. Filippov, A.T.: Increase of the Solar Energetic Particle Flux on January 20, 2005, 29th Intern. Cosmic Ray Conf., Pune, 2005

[8] Moraal, H., McCracken, K.G., Schoeman, C.C., Stoker, P.H: The Ground Level Enhancements of 20 January 2005 and 28 October 2003, 29th Intern. Cosmic Ray Conf., Pune, 2005

[9] Belov, A., Eroshenko E., Mavromichalaki, H., Plainaki, C., Yanke, V. Ground level enhancements of the solar cosmic rays on January 20, 2005, 29th Intern. Cosmic Ray Conf., Pune, 2005b

[10] Vashenyuk, E. V., Yu.V. Balabin , B.B. Gvozdevsky , S.N. Karpov,.V.G.Yanke, E.A. Eroshenko, A.V. Belov, R.T. Gushchina. Relativistic solar cosmic rays in January 20, 2005 event on the ground based observations. ICRC29, Pune, 2005.

[11] Bieber, J.W. Extreme Ground Level Enhancements Observed by *Spaceship Earth*, Solar Extreme Events 2005, Armenia, 2005

[12] Fluckiger, E.O., Butikofer, R.B., Moser, M.R., Desorgher, L.- The Cosmic Ray Ground Level Enhancement during the Forbush Decrease in January 2005, 29th Intern. Cosmic Ray Conf., Pune, 2005.

[13] Plainaki, C., Belov, A., Eroshenko, E., Kurt, V., Mavromichalaki, H., Yanke, V.: Unexpected burst of solar activity recorded by neutron monitors during October November 2003, Adv. In Space Res., 35, 4, p. 691-696, 2005

[14] Clem J. and L. I. Dorman. Neutron monitor response functions. *Space Sci. Rev*., 93, 1, 335-359, 2000.

[15] Belov, A. V., and Struminsky A. B. Neutron monitor sensitivity to primary protons below 3 GeV derived from data of ground level events. *Proc. 25-th ICRC*, 1, 201-204, 1997.

Correlation between Variations of Cosmic Ray Spectrum and Interplanetary Medium Parameters

V.M. Dvornikov, M.V. Kravtsova, V.E. Sdobnov

Institute of Solar-Terrestrial Physics Russian Academy of Sciences, Siberian Branch, Irkutsk, Russia
dvornikov@iszf.irk.ru; rina@iszf.irk.ru; sdobnov@iszf.irk.ru

Within the context of the model of cosmic ray (CR) modulation by regular electromagnetic fields of heliosphere under the data about rigidity spectrum of CR variations are determined changes of energy of particles depending on their rigidity. The analytical expression for the description of this relation is obtained on the basis of the solution of an equation of motion of particles in a drift approaching and expression for rigidity spectrum of CR in broad range of energies. The expression for a spectrum contains five parameters describing change of CR energy at the expense of potential, rotational and polarization components of an electrical field of the heliosphere, and also size of areas with non-steady electromagnetic fields. With allowance for of obtained expression the instantaneous values of parameters rigidity spectrum of protons under the data of ground-based and satellite measurements of their intensity in October–November 2003 are determined.

Taking into consideration to obtained momentary values the parameters of the rigidity spectrum of protons using the data of ground-based and satellite measurements of the CR intensity in October–November, 2003 and on the base obtained the information. We have estimated the characteristics of electromagnetic fields of the heliosphere for investigated period.

Introduction

The mathematical formulation of the variations of cosmic ray (CR) intensity during sporadic events in heliosphere is realized mainly in the context of convection-diffusion model [1] according to which the particle intensity decrease during the periods of Forbush effects take place due to density decrease of CR caused by their carrying-out by shock waves and turbulized magnetic fields of high-velocity fluxes of solar wind (SW). It is assumed that the the increases of the CR intensity at this approach are caused by the particle density increase due to solar sources (solar cosmic rays – SCR).

In this study there is considered the alternative approach to the problem of CRs modulation in interplanetary space due to their energy change in heliosphere electromagnetic fields under the assumption of constant particle density in phase space.

We investigate variations of the CR rigidity spectrum in the period of October–November 2003 which is characterized by a series of strong solar proton events, Forbush decreases, and intensive geomagnetic storms.

Data and method

When analyzing the variations of CR rigidity spectrum we have used the data of observations of the proton intensity in the energy ranges 15–40, 40–80, 80–165 and 165–500 MeV onboard the GOES-10 satellite [2] and the data on the global CR intensity obtained by the method of global spectrographic survey using ground-based measurements of the world network of stations of neutron monitors.

In this case, when the CR rigidity spectrum in the Galaxy is described by a power law function of particle rigidity, and their intensity in the heliosphere vary in accordance with the Liouville theorem (i.e., under condition of constant density of particles along their trajectory of motion in the phase space), the differential rigidity spectrum of CRs has the following form [3]:

$$J(R) = A\left[\frac{(\varepsilon^2-\varepsilon_0^2)}{(\varepsilon+\Delta\varepsilon)^2-\varepsilon_0^2}\right]^{3/2}\frac{\varepsilon+\Delta\varepsilon}{\varepsilon}\left[\frac{2\sqrt{(\varepsilon+\Delta\varepsilon)^2-\varepsilon_0^2}-\sqrt{(\varepsilon^2-\varepsilon_0^2)}}{\sqrt{(\varepsilon^2-\varepsilon_0^2)}}\right]^{-\gamma} \quad (1)$$

where ε is the total energy of particles; Δε is the change in the electromagnetic fields of heliosphere; ε_0 is the rest energy; A and γ are the spectral indices of the galactic spectrum.

The expression (1) has been obtained under assumption that the CR intensity with the rigidity R varies proportionally to variations of the product of the particle velocity v and the squared module of its impulse p, that is in accordance with Liouville theorem.

$$\frac{J(R)}{vp^2} = const \quad (2)$$

This assumption is valid if we can neglect effects of particle scattering on magnetic inhomogeneities with no SCR within the considered energy range.

Inserting the observable intensities of different rigidity particles into the left side of equation (1) the values of Δε can be obtained depend upon the particle rigidity, that is Δε(R).

The results of calculation of Δε(R) for different moments of observations under extreme heliospheric events in October–November 2003 are shown in Fig. 1 as curves.

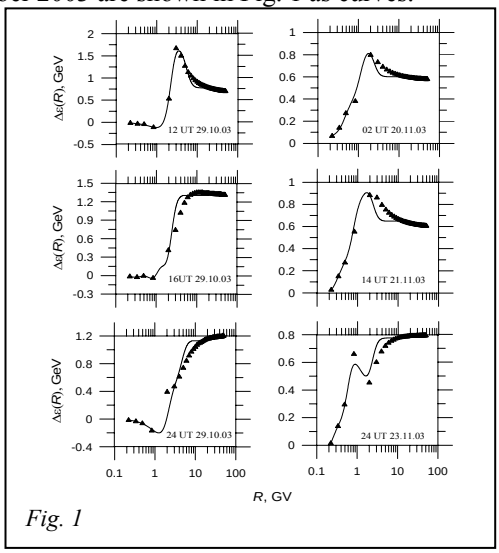

Fig. 1

The value of $\Delta\varepsilon(R)$ shows how the energy of rigidity R particle varies along its trajectory in heliosphere during its moving from the Galaxy to the observation point.

The main peculiarity of the presented results is that energy losses of relativistic particles ($R > 2$ GV) are much more than that for particles of less energies. At some moments the maximum energy losses ($\Delta\varepsilon(R) \sim 1.6$ GeV) are observed for particles of the rigidity of a few GV. At low energies along with energy losses of particles the effects of their acceleration is often observed ($\Delta\varepsilon(R) < 0$).

To interpret the obtained results let us consider the effects of particle energy change based on the solution of the equation of motion in heliosphere electromagnetic field. Within the limits of drift approximation the particle energy change can be obtained by the integration of the equation [4]:

$$\frac{d\varepsilon}{dt} = \vec{E}\left\{\frac{mcv_\perp^2}{2B^3}\vec{B}\times\nabla\vec{B} - \frac{mc}{B^2}\left[\frac{\partial\vec{V}}{\partial t} + (\vec{V}\nabla)\vec{V}, \vec{B}\right]\right\} + \frac{mcv_\perp^2}{2B}\frac{\partial B}{\partial t} \quad (3)$$

Here $\varepsilon = \frac{m}{2}(v_C^2 + v_\perp^2 + v_E^2)$; $\vec{V} = v_C\frac{\vec{B}}{B} + \vec{v}_E$; m is particle mass; $v_\perp$ and $v_\parallel$ are transverse and longitudinal velocity components relative to $\vec{B}$ of interplanetary magnetic field (IMF); B is the IMF intensity; $\vec{E}$ is electric field intensity; $\vec{v}_E = \frac{c}{B^2}\vec{E}\times\vec{B}$; c is the light velocity.

With the purposes of clearness the equation (3) is used in simplified form and describes the energy changes of low-energy ($\frac{v}{c}$ p p 1) particles of large pitch angle ($v_\parallel$ is small value). The first member in the equation (3) characterizes the energy change due to particle magnetic drift along or transversely (depending on IMF gradient) to electric field; the second member describes particle acceleration due to drift under the action of inertial force $-m\left[\frac{\partial\vec{V}}{\partial t} + (\vec{V}\nabla)\vec{V}\right]$ along electric field with its increasing in time; the third member describes the same due to variability of magnetic fields in time.

For the spiral IMF and induced electric field $\vec{E} = -\frac{1}{c}\vec{u}\times\vec{B}$ of homogeneous stationary SW, and from the equation (3) solution the expression (4) is obtained:

$$\Delta\varepsilon_{pt} = \frac{z_e\Omega B_0 r_0^2}{c}(1 - \cos\lambda_E) \quad (4)$$

where Ω is the angular velocity of Sun's rotation; B_0 is the intensity of radial IMF component at the distance of r_0, and λ_E is the Earth's heliolatitude.

As follows from the equation (4) the particle energy losses under potential electric field do not depend on particle rigidity, and are of ~200 MeV at typical IMF intensity.

If the electromagnetic fields of heliosphere are not stationary the particle energy changes should be taken into accounts which are described by second and third members of the equation (3). The corresponding energy changes are determined by the following expressions:

$$\Delta\varepsilon_{p1} = \varepsilon(1 - e^{-\alpha/2}) \quad (5)$$

where $\alpha = \frac{E_{p1}^2}{B^2}$, E_{p1} is the polarized electric field [5] and

$$\Delta\varepsilon_{rot} = \varepsilon - \sqrt{\beta(\varepsilon^2 - \varepsilon_0^2) + \varepsilon_0^2} \quad (6)$$

where $\beta = \frac{B}{\langle B\rangle}$, $\langle B\rangle$ is the background field intensity, and B is the variable magnetic field intensity.

To describe the obtained dependence $\Delta\varepsilon(R)$ (see Fig. 1) it should be assumed that the mentioned mechanisms are of different efficiency for particles of different rigidities. The energy changes of high-energy particles take place in accordance with the equation (4) and depend on large-scale IMF intensity. If the Earth enters the "magnetic cloud" the CR intensity changes are determined by superposition of the background IMF and the magnetic cloud field, as well as by the SW velocity [3]. This effect should be observed for particles the Larmor radius of which is less than magnetic cloud sizes (a few GV). At lower energies the effects dominate which are described by the expressions (5), (6) because the magnetic drift velocity of these particles is considerably less than that for high-energy CR.

We can obtain the expression for particle energy change from the solution of the motion equation in general form:

$$\Delta\varepsilon(R) = \Delta\varepsilon_0 + \Delta\varepsilon_1\left[1 - f(R,\ bR_0)\right] + \Delta\varepsilon_2\left[1 - f(R,\ bR_0)\right]f(R,\ R_0) + \\ + \left[\varepsilon(1 - e^{\alpha/2}) + \varepsilon - \sqrt{\beta(\varepsilon^2 - \varepsilon_0^2) + \varepsilon_0^2}\right]f(R,\ R_0) \quad (7)$$

where $\Delta\varepsilon_0 = 0.1$ GeV; R_0 is the parameter, characterizing the scale of the structural formations in heliosphere with nonstationary electromagnetic fields; $f(R,\ R_0) = \left[\exp\left(\frac{R - R_0}{aR_0}\right) + 1\right]^{-1}$ is quasi-step function which approach 1 at $R < R_0$ and 0 at $R > R_0$ (a<1); $\Delta\varepsilon_1$, $\Delta\varepsilon_2$ are the parameters characterizing the energy changes of the high-energy particles ($\Delta\varepsilon_1$ at $R > bR_0$, $b = 2.5$, and $\Delta\varepsilon_2$ in rigid interval $[R_0, bR_0]$ when the Earth gets into "magnetic cloud").

The rigidity spectrum parameters R_0, $\Delta\varepsilon_1$, $\Delta\varepsilon_2$, α, and β were determined for every hour of observation throughout the entire period under study with used expression (1) taking into accountc (7).

Results of analysis

Figure 2 presents by curves the intensity of particles with R = 0.24, 0.342, 5, and 20 GV calculated according to formulas (1) and (7) using the found spectral parameters and points give the data of observations.

Figure 3 shows (top-down) the module of interplanetary magnetic field (IMF), the angles ψ and λ, characterizing IMF vector orientation, D_{st}-index and the parameters of cosmic ray rigid spectrum R_0, $\Delta\varepsilon_1$, $\Delta\varepsilon_2$, α, β. The values of solar wind (SW) velocity are shown additionally on the β parameter plot (the heavy curve) and the bidirectional anisotropy amplitudes are given on the $\Delta\varepsilon_2$ plot (the heavy curve also).

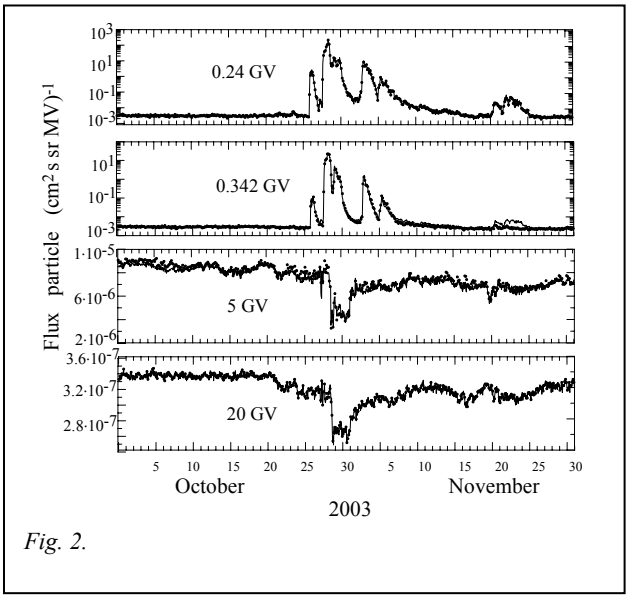

Fig. 2.

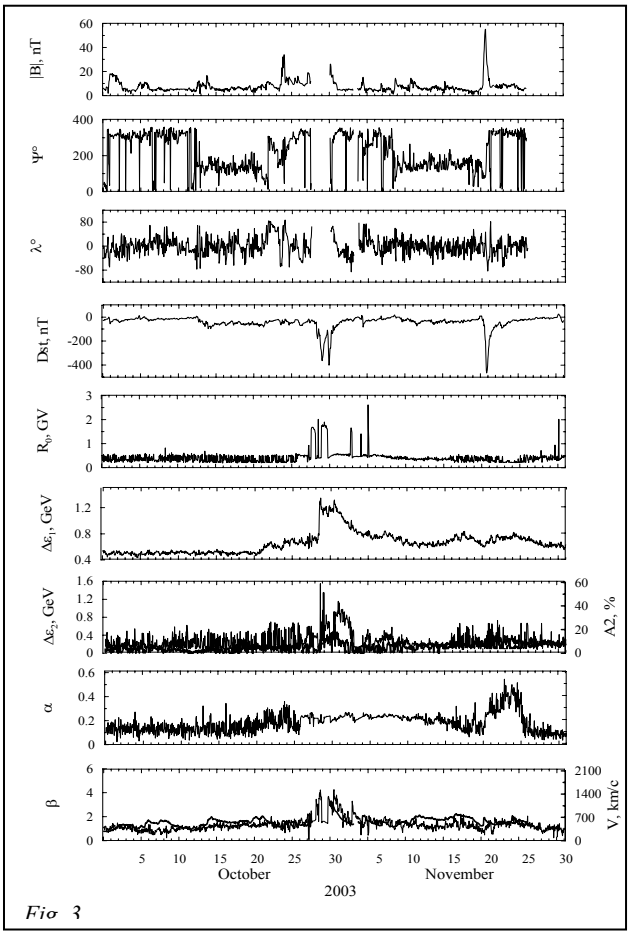

Fig. 3

Figure 4 present the rigidity spectra of relative variations of CR intensity at separate moments of the period under investigation. Curves represent the results of calculation of model spectra according to formulas (1) and (7), and triangles give the data of observations.

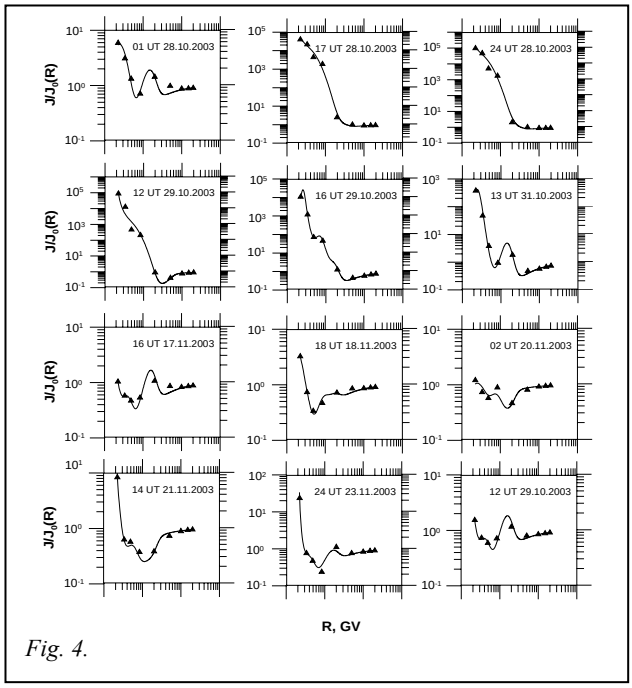

Fig. 4.

Discussion of results

When analyzing the $\Delta\varepsilon_1$ and $\Delta\varepsilon_2$ plots of the intensity of the large-scale interplanetary magnetic field and the "magnetic cloud" intensity accordingly it should be concluded that on 29 October the Earth appears to get into intensive IMF strength region that results in powerful Forbush effect. This is also confirmed by the higher amplitudes of bidirectional anisotropy which point out the passing of CME with appropriate loop-shaped IMF structure [6]. In 20 November event when the IMF module increased up to nearly 60 nT the $\Delta\varepsilon_1$ and $\Delta\varepsilon_2$ parameters practically did not react to this increase. The reason is that in the context of used conception effects of energy loss of high-energy particles and therefore their intensity decrease will be observed only if the particles traverse (because of magnetic drift) the region of increased magnetic field strength before they get on Earth. In that way if, for example, the Earth gets into the region of southern boundary of magnetic structure of the increased magnetic field strength, and the drift velocity has south–north direction, then the effect in high-energy CR will not be observed. This can be confirmed by the fact that values of α parameter in the 20 November event are significantly more than those in the October event. This parameter characterizes the particle acceleration due to the fact that particles because of inertial (polarized) drift move along the increasing electric field, and this drift direction is opposite to the magnetic drift. Therefore, when the Earth gets into "magnetic cloud" the maximum the α parameter values should be observed at minimum values of the $\Delta\varepsilon_1$ и $\Delta\varepsilon_2$ parameters.

When comparing the dynamics of β parameter and SW velocity the following fact should be accentuated that the SW velocity variations usually take place in compliance with the variations of β parameter, whence it follows that the SW and CR accelerations are caused by the same mechanisms.

Conclusion

Based on the obtained results the following scenario is proposed of CR and solar wind (SW) plasma acceleration in heliosphere. A potential difference between the pole and equator occurs in a coordinate system fixed relative to rotated source with magnetic field (Sun). If the local emergence of magnetic field flux takes place within the source then an increasing electric field is produced in heliosphere and polarization drift occurs along this field. This results in particle acceleration and formation, in this connection, of current system generating the magnetic field of loop-shaped structure in heliosphere. The increasing magnetic field of this structure causes the particle drift into it and their acceleration due to betatron mechanism. When currents forming these structures increase up to critical values then because of one or other instability a current circuit break can occur following by an explosive process with accelerated particle precipitation into solar atmosphere and their outflow into the interplanetary medium. When accelerated particle beam propagates in inhomogeneous magnetic fields of solar corona and heliosphere it becomes polarized because the protons and electrons drift in the opposite direction that results in charge separation in a spatial in homogeneity of accelerated particle density, so a potential difference occurs between beam boundaries along the magnetic drift trajectories. This causes the generation of increasing polarized electric field and as a consequence the polarized drift of background particles of SW plasma, solar corona and galactic cosmic rays (GCR) along this field, i.e. this causes particle acceleration with larmor radius less than sizes of these structures. The current system is formed again and magnetic field is generated which accelerate particles and so on. In such a way the energy exchange takes place between accelerated particles and background particles of SW plasma, solar corona and GCR as well as formation of heliosphere current structures and generation of interplanetary medium structures, so the process of particle acceleration and propagation in heliosphere is consistent with electromagnetic fields.

References

[1] E.N. Parker. “Interplanetary Dynamical Processes”, *Interscience Publishers*, John Wiley and Sons, New York, 1963

[2] http://spidr.ngdc.gov/spidr/index.html

[3] V.M. Dvornikov, V.E. Sdobnov, and M.V. Yudina. “Variations in Rigidity Spectrum and Anisotropy of Cosmic Rays during Sporadic Phenomena in the Heliosphere in October–November 2003”, *Cosmic Res,* Vol. 42, 6, 2004. pp. 619–625

[4] A.I. Morozov, and L.S. Soloviev. “The motion of charger particles in electromagnetic fields”, *Voprosy Teorii Plazmy* (*in Russian*), Vol. 2, Gosatomizdat, Moscow, 1963. p. 177

[5] H. Alfven. “Cosmic plasma”, Dordrecht, Holland, 1981. 213 p.

[6] I.G. Richardson, V.M. Dvornikov, V.E. Sdobnov, and H.V. Cane, “Bidirectional particle flows at cosmic ray and lower (~1 MeV) energies and association with interplanetary coronal mass ejections/ejecta”, *J. Geophys. Res.*, Vol. 105, A6, 2000. p. 12579

On the Highest Energies of Proton Acceleration at the Sun on January, 20 2005

N. Kh. Bostanjyan, A.A. Chilingarian, V.S. Eganov, G.G. Karapetyan
Cosmic Ray Division, Alikhanyan Physics Institute, Yerevan, Armenia 375036, bostan@crdlx5.yerphi.am

On January 20, 2005, 7:02-7:05 UT the Aragats Multidirectional Muon Monitor (AMMM) located at 3200 m a.s.l. registered enhancement of the high energy secondary muon flux (threshold ~5 GeV). The enhancement, lasting three minutes, has statistical significance of ~4σ (for the three-minute time series) and is related to the X7.1 flare seen by the GOES satellite and the Ground Level Enhancement detected by the world-wide network of neutron monitors and by muon detectors. The energetic and temporal characteristics of the muon signal from the AMMM are compared with the same characteristics of other monitors located at the Aragats Space-Environmental Center (ASEC). Various ASEC detectors select different energetic populations of the Solar Cosmic Rays (SCR). Therefore, from the multivariate time-series we conclude that in the episode of the particle acceleration at 7:00 – 7:05 UT 20 January 2005: (a) protons were accelerated up to energies of 20GeV in excess; (b) the relativistic protons with energies <10 GeV were ejected in the interplanetary space earlier than the highest energy protons (>20 GeV); (c) protons accelerated in the episode (maximum at 7:12 -7:15 UT), have lower energy compared with first acceleration episode.

Introduction

On January 20, 2005 NOAA reported an X7 importance flare with helio-coordinates (14N, 67 W), which started at 6:36 UT with maximal X-ray flux at 7:01 UT. The first results from the space-born spectrometers [1] for the proton energies up to 800 MeV pointed to very hard energy spectra of the Solar Energetic Particle (SEP) event. It stimulated detailed investigation of the correspondent Ground Level Enhancement (GLE) N 69, having one of the goals to estimate the maximal energy of the solar accelerators.

Available experimental data on the GLEs confirm proton acceleration up to 20 GeV [2,3], acceleration to higher energies is not reliably proved. Middle and low-latitude neutron monitors can not be used for the reconstruction of the primary energy spectra well above 5 GeV due to very weak fluxes and rather small sizes of the detectors. Therefore, recently, surface particle detectors measuring Extensive Air Showers (EAS) were implemented for the investigation of the highest energies of the solar proton and ion "beams"[4,5,6,7]. Due to large surface and solid angle and high efficiency of the registration of the charged particles, these detectors provide valuable information about the solar proton fluxes above 5 GeV.

The *Aragats Multidirectional Muon Monitor* (AMMM) is located at (40.5°N, 44.17°E), altitude 3200 m. a.s.l.; cutoff rigidity 7.6 GV; relative accuracy of measuring 3-minute time-series ~0.17%, much better than of neutron monitor 18NM64, located at the same altitude.

The AMMM consists of 45 plastic scintillators with detecting surface of 1 m^2 and thickness of 5 cm each. The Detector is located in the underground hall of the ANI experiment [8] under 15 meters of soil and concrete, plus 12 cm. of iron bars. Only muons with energies greater than 5 GeV can reach this underground detector. 5 GeV muons correspond to an ensemble of primary protons with mode energy ~50 GeV if we assume the power law with spectral index of γ = -2.7 (Galactic Cosmic Rays) [5]; and - ~ 30GeV if we assume spectral index γ = -5 (Solar Cosmic Rays at 20 January, 2005) [9].

During GLE N 69 on January 20, 2005 from 7:02 to 7:04 UT, AMMM detects a peak with significance *~4σ* Proceeding from the detection of this peak, we perform comparisons with time series of the other *Aragats Space-Environmental Center (*ASEC) monitors [10] and present results on the temporal and energetic characteristics of the relativistic proton fluxes accelerated at the sun on January 20, 2005.

GLE N 69 as Detected by the ASEC monitors

GLE N69 was detected by several ASEC monitors on January 20, 2005, during the solar flare X7.1. The 1- minute time series of the AMMM are presented in Figure 1. Enhancement of the count rate is seen from 7:02 till 7:04 UT with maximum at 7:03 UT. Three out of the 45 one m^2 scintillators of the AMMM were not operational at the time, therefore only 42 m^2 of muon detectors were in use to measure the high energy muon flux. The estimated mean count rate of the Galactic Cosmic Rays (GCR) as measured by the 42 m^2 of the AMMM detector during the 6:30 – 7:35 UT time span, excluding the enhanced interval from 7:02 to 7:04 UT, is 123818 particles per minute. The additional signal at 7:03 UT equals to 863 particles (0.70%). Taking into account that the standard deviation of 1 minute data is 352 (0.29%) we come to the significance of 2.5σ for the 1 minute peak at 7:03 UT.

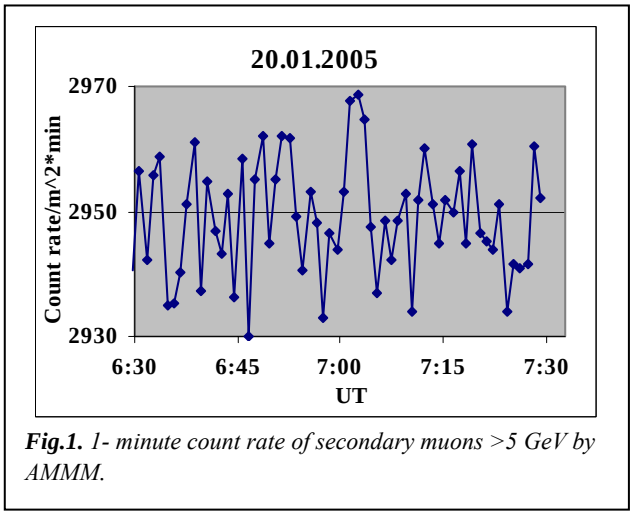

Fig.1. *1- minute count rate of secondary muons >5 GeV by AMMM.*

To emphasize the peak in the AMMM time series we group the 1 minute date in 3 minute time-intervals (see Figure 2).

The 3-minute time series demonstrates a more pronounced peak of 3.93 σ. The mean count rate of GCR again was estimated in the time span of 6:30 – 7:35 UT with the excluded point of 7:03 UT and it equals 371494 particles per 3 minutes for the 42 m^2. The additional signal at 7:02 UT equals 2354 (0.644%). If we adopt the Poisson standard

deviation for the 3 minute time series 0.164% (see detailed discussion on the method of the estimating of the standard deviation and peak significance in the attachment) we come to the significance of 3.93σ for the 3 minute peak at 7:02 – 7:04 UT. The excess count rate registered at AMMM during the interval 7:02-7:04 UT corresponds to the flux 3.1 (+/- 0.8) 10-5 muons/cm2/sec.
Due to the very short enhancement time span no corrections on the atmospheric pressure and temperature are necessary.

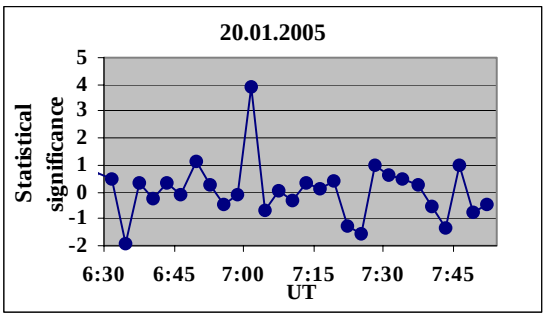

Fig.2. 3- minute count rate of secondary muons >5 GeV by the AMMM, is expressed as a statistical significance .

In Figures 3 and 4 the count rate enhancements measured by the Aragats Neutron Monitor (ANM), located at 3200 m. a.s.l. and Nor Amberd Neutron Monitor (NANM) located at 2000 m.a.s.l. are presented (both neutron monitors are 18NM64 type). From the figures we can see that the enhancement at the neutron monitors started ~3 minutes earlier than the peak detected by the AMMM at 7:03 UT.
The energies of the primary solar protons giving rise to the secondary neutrons which are registered by the neutron monitors are less compared to the primary proton energies which create the 5 GeV muons in the atmosphere. Therefore, we can conclude that relativistic protons of energies ~10 GeV are ejected in the interplanetary space earlier compared to the protons of energies >20GeV

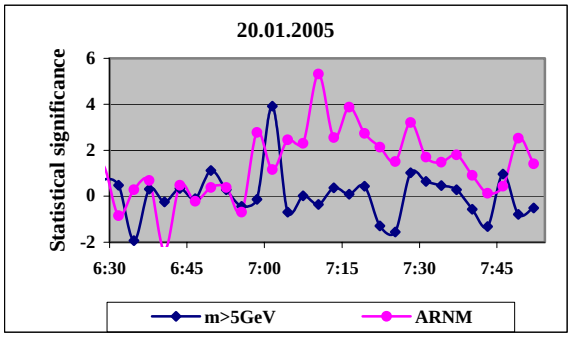

Fig.3 Comparison of the ANM and AMMM intensities are expressed as statistical significances.

As we can see from Figures 3 and 4 the ASEC neutron monitors demonstrate at least 2 peaks have significance higher than 3σ during the interval 6:55 -7:45 UT. The low energy charged particles detected by the surface scintillators as we can see in Figure 5 also detect several peaks.

Analogous patterns were detected by the neutron monitors from the world-wide network [11].

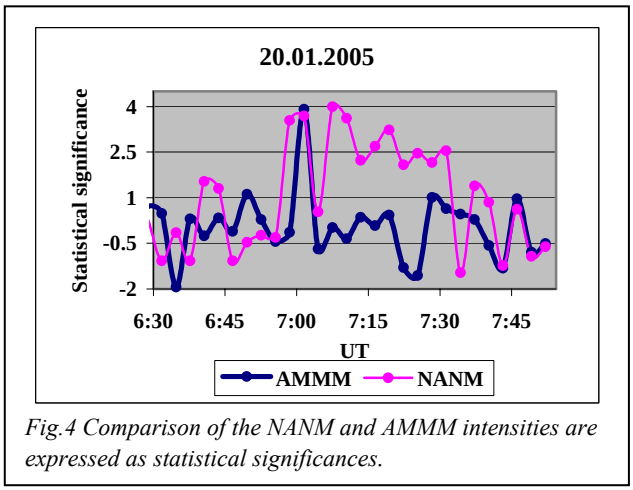

Fig.4 Comparison of the NANM and AMMM intensities are expressed as statistical significances.

Acceleration of ions at sun is usually attributed to 2 different acceleration scenarios: the first one acceleration in the flare process itself and the second - by the CME-driven shocks propagated in the low corona. In [12-15] these 2 scenarios are considered and it was mentioned difficulties to explain the first acceleration episode by the shock acceleration. Further analysis of the event invoking data from world-wide networks measuring particle fluxes will answer the question if the highest energy protons (>20 GeV) can be accelerated only in direct flare process.

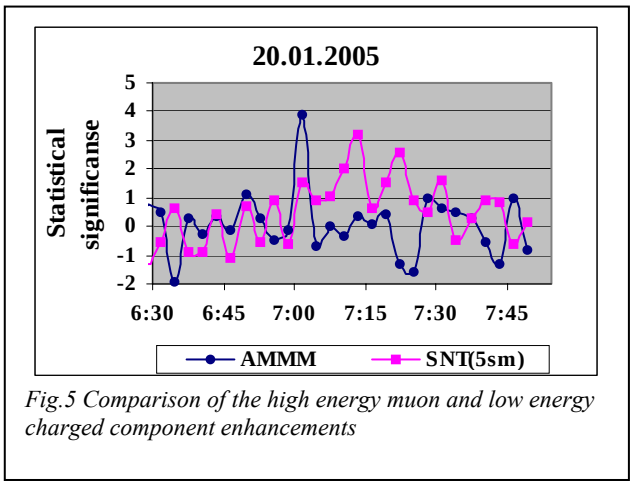

Fig.5 Comparison of the high energy muon and low energy charged component enhancements

Conclusions

1. On January 20, 2005 at 7:02-7:05 UT the Aragats Multidirectional Muon Monitor registered additional flux of - high energy muons equal to 3.1 (+/- 0.8) 10^{-5} particle/cm^2/sec.
2. Relativistic protons with energies ~ [7.6 – 10] GeV giving rise to the enhancement of the count rate of neutron monitors located at slope of mt. Aragats were ejected into the interplanetary space ~3 minutes earlier than the ~20 GeV protons.
3. Particles forming the second peak of the GLE have less energy compared with the first peak. And if we adopt the hypothesis that the event in the first interval was from a flare-

acceleration process while the event in the second interval was from the shock acceleration, as discussed in reference [12-15], then we can conclude that the highest energy protons were accelerated in the flare-process.

Acknowledgement
Authors thank the scientific and technical staff of the Aragats and Nor-Amberd research stations for the assistance in the experiment and Hamlet Martirosyan for useful discussions

Attachment: Statistical treatment of the problem of signal significance determination

To illustrate that detected peaks are not only background flux (GCR) fluctuation, but signal candidate (SCR), we perform additional investigations of the AMMM count rates at 20 January. All statements about signal significance made in the paper are valid only if the assumption about "Normality" (belonging to the Gaussian population) of the residuals is valid. The difficulty of testing this hypothesis lies in the slow drift of the mean count rate because of disturbances of the Interplanetary Magnetic Field (IMF) and magnetosphere due shocks and magnetized plasma clouds of the interplanetary CMEs (iCME) connected with four X class flares occurred at sun at 16-20 January. To account for the changing mean of the AMMM counting rates we calculate the hourly mean values and corresponding residuals for the 3-minute time series (20 numbers) each hour out of 24, according to the Gaussian model:

$$X_{i,j} = \frac{C_{i,j} - \overline{C}_j}{S_j}, \quad i = 1,20 \quad j = 1,24 \qquad \textbf{(1)}$$

where $X_{i,j}$ are normalized residuals, $C_{i,j}$ are 3 minute count rates of the AMMM at j-th hour, $\overline{C}_j$ are hourly means of the 3-minute time series and $S_j \approx \sqrt{\overline{C}_j}$ - are the hourly Poison deviation of the count rates.

To account for the arbitrary choice of the start minute of the 3-minute time series we integrate other all 3 possibilities of different starts of the 3-minute time series.

The resulting histogram of the normalized residuals is shown in the figure 6. We see rather good agreement with standard normal distribution. 3 points forming the right tail of histogram are coinciding with GLE time 7:02-7:05 and are equal to 3.2, 3.93 and 2.6 (outlined by the oval in the figure 6). Proceeding from rather large value of the biggest residual (3.93), we can accept the hypothesis that there is additional signal superimposed on the galactic cosmic ray background. Of course, within validity of the Gaussian hypothesis this and larger values can encounter, therefore we'll need additional physical proves that detected peak is caused by the highest energy solar protons (to be discussed in the end of chapter)

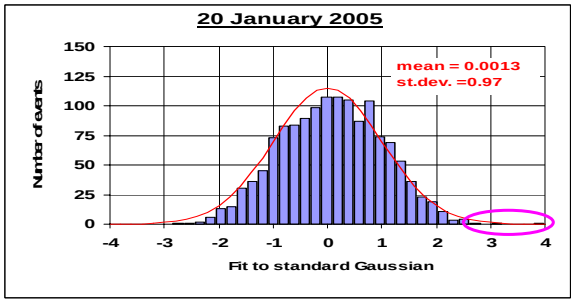

Figure 6 Normalized residuals calculate by hourly averaging 3-minute AMMM time series at 20 January 2005.Note in the oval the outlier attributed to the high energy proton flux at 7:02-7:05 UT

Nonetheless, obtain large value of residual at 7:02, gives as basis to perform comparisons of obtained signal candidate with other detectors time series. To be sure that our assumption on the Poisson nature of time series is valid we perform another check. We perform calculation of the Relative Mean Square Deviations (RMSD) by the hourly data of 20 January:

$$RMSD_j = \sqrt{\left(\frac{\sum_{i=1}^{i=N}(C_{i,j} - \overline{C}_j)^2}{N-1}\right)} \Big/ \overline{C}_j, \quad j = 1,24 \qquad \textbf{(2)}$$

where $C_{i,j}$ are 3 minute count rates of the AMMM at j-th hour, $\overline{C}_j$ is hourly mean of the 3-minute time series and N =20, is the number of 3 minutes counts in 1 hour.

To account for the arbitrary choice of the start minute of the 3-minute time series we integrate other all 3 possibilities of different starts of the 3-minute time series. Figure 7 demonstrates rather stable hour-to-hour standard deviations proving high quality of AMMM operation at 20 January.

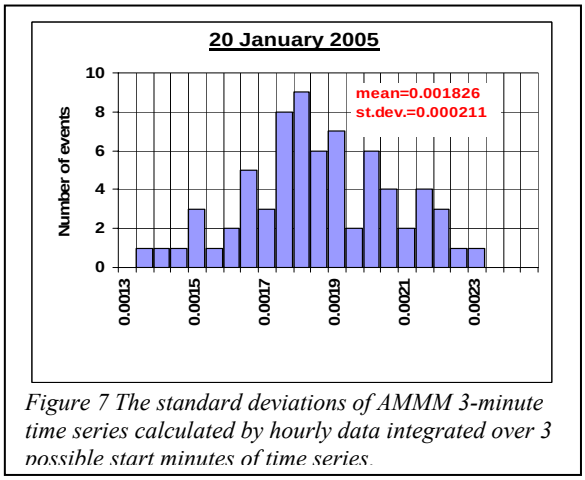

Figure 7 The standard deviations of AMMM 3-minute time series calculated by hourly data integrated over 3 possible start minutes of time series.

Obtained from the Figure 7 hourly mean value of RMSD $\overline{\sigma}_{rel} = 0.00182 \pm 0.0002$ is slightly greater than Poisson relative accuracy calculated by $\sigma_p = 1/\sqrt{Count\ rate} = 0.00164$. In turn the Poisson accuracy is bigger comparing with actual value of the standard deviations calculated at the hour of GLE occurred (6:30 – 7:35), equals to 0.0015. Therefore, we adopt a decision to use for the signal significance calculations the Poisson relative accuracy σ_p = 0.164%, than randomly obtained "better" value of RMSD correspondent to the particular hour when GLE occurred.

The relative accuracy of detector is the characteristic of detector itself, and not of the particular time-span when this characteristic was measured (of course if detector operates properly during this time-span).

We perform numerous calculations of the detector accuracies before and after the January 20 solar events and obtained

accuracies was in very good agreement with Poisson ones. The signal significance usually is measured in the, so called, "number of σ" – obtained by dividing of the enhancement of the count rate by the accuracy of the detector. Using corresponding values of 0.644% and 0.164% we come to the signal significance of 3.93σ.

Another possibility to reveal the peak provides standard procedure of the CERN ROOT package [21]. The background is interpolated by the polynomial function with not very much degrees of freedom and the peak separately by Lorentzian [21] or Gaussian function.

In Figure 8a and 8b we present results of this approach. The red line in the Figure 8a is the second order Polynomial function describing background and the blue curve in Figure 8b – the extracted peak only.

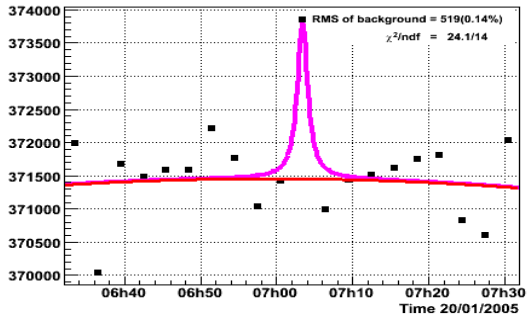

Figure 8a Polynomial fit of the background and corresponding Lorentzian peak

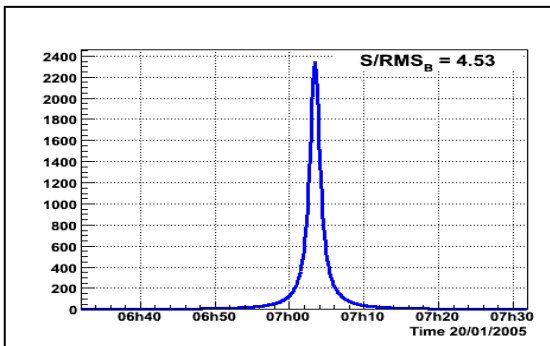

Figure 8b Extracted Lorentzian peak

Estimates of RMS of background, number of additional counts in the peak are very close to already obtained ones by simple techniques (Figures 6 and 7). The larger value of the peak significance (~4.5) can be explained by using the actual value of background variance (0.14%), instead of hourly-averaged other 20 January day and other days (0.164%). As we discuss above as measure of background fluctuation we prefer to use stable characteristic measured by detector in long periods, rather than random value obtained at particular time of the GLE. However, when calculated the chance probability we have to take into account the experimental procedures we use to reveal the signal. We made 3-minute time series from the 1 minute ones and then test 3 rebinning variants to finally obtain 3.93σ

The rebinning of time series is ordinary operation used by the all groups running the solar monitors. However, it have to be taken into account in calculating of the chances that particular large value of σ is only random rare fluctuation. As one can see from Figure 9 different start points of the 3-minute time series corresponds to slightly different pattern of the peaks.

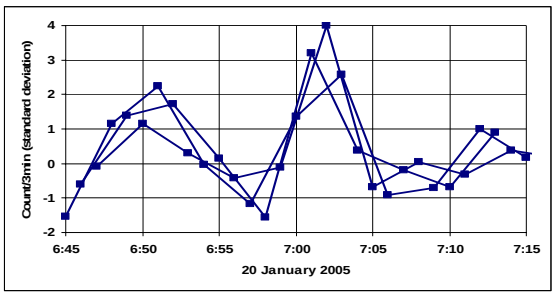

Figure 9 Three-minute time series of AMMM with 3 different starts

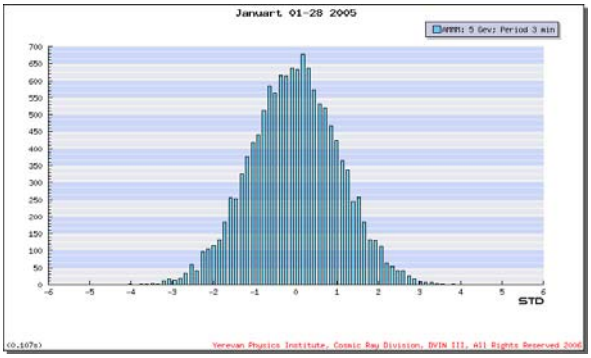

Figure 10 Normalized residuals calculate by hourly averaging 3-minute AMMM time series for 1-30 January 2005. Note in the right tail of distribution the outlier attributed to the high energy proton flux at 7:02-7:05 UT

As we already demonstrate in Figure 6 (points in the oval) each of 3 time-series have own maximal peak value and one started at 7:02 provides maximal significance of 3.93σ. Therefore, we have to take into account that we examine 3 possibilities and finally chose one with maximal signal significance. In reference [16] we consider the rebinning problem in context of cosmic ray point source searches and demonstrate that the probability density distribution of the maximal deviation of the residuals can be described by the so called, extremal statistics distribution (Chapmen et al., 2002):

$$P_M(x) = M \cdot g(x)(1 - G_{>x})^{M-1} \qquad (3)$$

Where g(x) is standard Gaussian probability density;

$$G_{>x} = \int_x^{\infty} g(t)dt \qquad (4)$$

is so called test statistics p–value: the probability to obtain the value of test statistics in the interval greater than x.

Let now consider the simple statistical problem: what is the chance to detect during 1 day the 4σ residual in the absence of any signal? Or equivalent definition: how many days we have to

wait to detect the random rare fluctuation of 4σ? To obtain the probability to observe in one from 481 (i.e. during the day) of 3-minute time-spans number of events equivalent or more than 4 standard deviations (p-value of the distribution $P_M(x)$) we have to integrate $P_M(x)$ in the interval [4, +∞). For M = 481 we obtain:

$$\int_4^\infty P_M(x)dx \sim 1.5\cdot 10^{-2}. \qquad (5)$$

It means that in absence of any signal in approximately 15 cases from 1000 we will detect the deviation of the mean value equal to 4σ using 3 minute time series during a day. Or equivalent statement: approximately once in 67 days only we will detect 4σ enhancement in the 3-minute time

series of AMMM. To check the obtained probabilistic statements we calculate with the DVIN3 Internet software [23] the distribution of residuals for the 30 days of January 2005 (see Figure 10). The overall shape of distribution fitted the standard Gaussian distribution very well and the ~4 σ value of 20 January 7:02 is apparent on the plot. There is no positive excess comparable with 7:02 peak on the plot in accordance with our calculation of expected random fluctuations (5).

However, calculating probability of obtaining randomly large values of the residual one have to take into account the rebinning of the time series which can enlarge the probability of obtaining large σ values.

Obviously, different attempts to obtain "best signal" considering different rebinnings (3 in our case) enlarge the M value in the equation 3, thus the correspondent probability to obtain ~4σ should enlarge 3 times. Therefore, we can expect random fluctuation equal to 4σ once in 22 days when using 3 minute time series with rebinning. To check this assumption and demonstrate the influence of the rebinning procedure we perform simulations with simple model of time series. The model consists in following operations:

(i) generate 1443 numbers from the standard normal distribution N(0,1);

(ii) form 3 time series summing 3 consequent numbers of the raw, starting from the first, second and the third elements. Each of time series will contain 481 element (a day);

(iii) perform normalization procedure to each of three "3-minute" time series;

(iv) determine and store the maximal element of each of normalized time series;

(v) determine and store the maximal element among time-series maximums (we model in this way selection of the largest signal from 3 equivalent time-series shifted by one minute from each other);

(vi) repeat i-vi 1000 times and form a histogram of residuals;

(vii) from the histogram calculated the frequency of obtaining residual value equal or greater than 4 (this fraction is shown in the Figure 10 by red).

Results are depicted in the figure 11. In the real live when having 3 possibilities physicist will choose one that emphasis the presence of signal (the situation (v)). But as we can see from the Figure 11 it dramatically change the probability to obtain the fake signal (4σ) increasing it approximately 3 times.

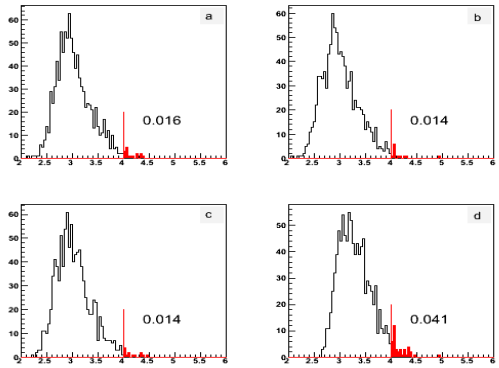

Figure 11 Histograms of the extremal statistics of different variants of rebinning of standard normal random variables. a) - c) and with selecting the maximal value – "best binning" d).

We can conclude, that in accordance with statistical model (3) our numerical modeling confirm that when testing different data binning the probability of obtaining "fake" signal during a given time period (in our case ~4σ during a day) increases proportional to number of tests.

In addition to large "significances" we can take into account the coincidences with independent detection of the signal. The 20 January GLE was detected by several EAS detectors, measuring shower charge particles (mostly muons) [18,20] and by Tibet NM [19]; all ensuring registration of highest energies of up to 10 GeV.

In Figure 12 the patterns of detection of the GLE N 69 by the solar monitors are compared.

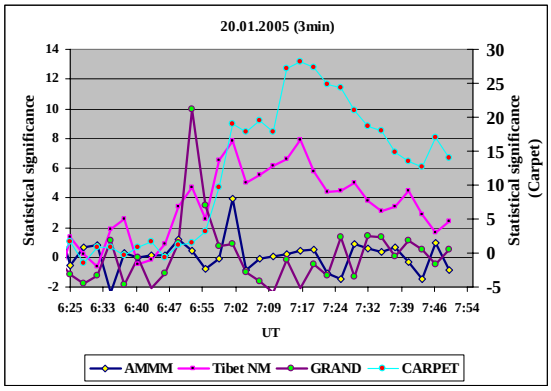

Figure 12 Comparison of the time series of the low energy charged particles monitors (GRAND, CARPET, (energy range > 6 GeV), Tibet NM (> 13 GeV) and AMMM (>20GeV)

We can see in the Figure 12 rather good coincidence of monitors time series profiles at 7:02-7:04. The 20 January event was extremely anisotropic [18] therefore the GRAND detector located in North America demonstrates its highest peak at 6:54. Tibet, Baksan and Aragats (AMMM) solar monitors demonstrate high significance peak in the same tame at 7:02,

those proving that AMMM ~4σ peak was not rare fluctuation, but detection of the protons accelerated on sun with energies greater than 20 GeV. Smaller significance values of AMMMcomparing with CARPET and Tibet is explained by the much higher threshold of AMMM and large index of the proton flux energy spectra < -5.

REFERENCES

[1] R.A. Mewaldt, M. D. Looper, C.M.S. Cohen, G.M. Mason, D.K. Haggerty, M.I. Desaic, A.W. Labrador, R.A. Leske, J.E. Mazur. "Solar-article Energy Spectra during the Large Events of October-November 2003 and January 2005". Official CD of 29th I.C.R.C., Pune, India(2005)

[2]I.N. Toptigin, *Cosmic Rays in the Interplanetary Magnetic Fields*, Moscow, 1983, p.108. (in russion).

[3] L.I. Dorman, *Cosmic Rays in the Eart`s Atmosphere and Underground*, P. 3., Kluwer Academic Publishers., 2004

[4] J.M. Ryan, 26th ICRC, Salt Lake City (1999) 6, 378.

[5] L. Ding, 27th ICRC, Hamburg (2001) SH1.07, 3372.

[6] J. Poirier and C. D'Andrea, J. Geophys. Res. 107, 1815 (2002).

[7] A. Chilingarian et al., "Monitoring and Forecasting of the Geomagnetic and Radiation Storms During the 23RD Solar Cycle: Aragats Regional Space Wheather Center, Adv. Space Res. Vol. 31, №. 4, pp861-865, 2003.

[8] A.Chilingarian, K.Avakyan et. al, Aragats Space-Environmental Center: Status and SEP Forecasting Possibilities, Journal of Physics G:Nucl.Part.Phys., Vol.29 (2003), pp 939-952.

[9] M.Zazyan, and A.. Chilingarian. "On the possibility to deduce solar proton enerhy spectrum of the 20 January 2005 GLE using Aragats and Nor-Amberd neutron monitor data",*; Solar Extreme Events. International Simposium, Nor-Amberd, Armenia.2005*

[10] A. Chilingarian et al., ."Corrlated measurements of secondary cosmic ray fluxes by the Aragats Space Enviromental Center monitors", *NIM,A543,483 (2005)*

[11] E.O. Fl¨uckiger, R. B¨utikofer, M.R. Moser, L. Desorgher "The Cosmic Ray Ground Level Enhancement during the Forbush Decrease in January 2005, Official CD of 29th I.C.R.C., Pune (2005)

[12] A. S´aiz, D. Ruffolo, M. Rujiwarodom , J. W. Bieber, J. Clem, P. Evenson, R. Pyle, M. L. Duldig, J. E. Humble, "Relativistic Particle Injection and Interplanetary Transport during the January 20, 2005 Ground Level Enhancement". Official CD of 29th I.C.R.C., Pune, India (2005)

[13] N. Gopalswamy, H. Xie, S. Yashiro, I. Usoskin, Coronal Mass Ejections and Ground Level Enhancements, Official CD of 29th I.C.R.C., Pune, India (2005)

[14] S.N. Kuznetsov, V.G. Kurt, et al., Proton acceleration during 20 January 2005 solar flare: CORONAS-F observations of high-energy gamma emission and GLE, Official CD of 29th I.C.R.C., Pune, India(2005)

[15] E.V. Vashenyuk, Yu.V. Balabin et al., Relativistic solar cosmic rays in January 20, 2005 event on the ground based observation, Official CD of 29th I.C.R.C., Pune, India(2005)

[16] A.Chilingarian, G.Karapetyan et al., Statistical Methods for Signal Estimation of Point Sources of Cosmic Rays, Astroparticle Physics, in press.

[17] Chapman S.C., Rowlands G., Watkins N.W. (2002), Extremum statistics – a Framework for Data Analysis, Nonlinear Processes in Geophysics, 9, 409-418

[18] H. Moraal, K.G. McCracken, C.C. Schoeman, P.H. Stoker. "The Ground Level Enhancements of 20 January 2005 and 28 October 2003" 29th International Cosmic Ray Conference Pune (2005) Official CD of 29th I.C.R.C., Pune, India (2005)

[19] H. Miyasaka, K. Makishima, E. Takahashi, S. Shimoda, Y. Yamada, I. Kondo, H. Tsuchiya, F. Zhu, Y. Tan, H. Hu, Y. Tang , J. Clem, and YBJ NM collaboration. "The Solar Event on 20 January 2005 observed with the Tibet YBJ Neutron monitor observatory". Official CD of 29th I.C.R.C., Pune, India (2005)

[20] C. D'Andrea and J. Poirier "Ground level muons coincident with the 20 January 2005 solar flare" Official CD of 29th I.C.R.C., Pune, India (2005)

[21] MICHAEL DZIOMBA "A NEW METHOD OF ANALYZING SOLAR FLARES USING SECONDARY MUONS" 2005 REU/NSF Program. Physics Department, University of Notre Dame. ADVISORS: John Poirier, Chris D'Andrea

Event of January 20, 2005: Ion, Proton and Electron Injection Times

H.S. Martirosyan

Cosmic Ray Division, Alikhanyan Physics Insitute, Yerevan, Armenia, hmati@crdlx5.yerphi.am

Knowledge of CR injection time is very important in terms of location detection and acceleration mechanism of these particles (flare or interplanetary shock wave). During some large events (e.g. 15-04-01, 26-12-01, 20-01-05) the first CR protons (electrons) with energies from 0,1MeV to ~1GeV (~1KeV to 0,5MeV) at the distance of 1 au are simultaneously registered within 5 minutes-long intervals.

In contrast to protons and electrons the first ions in these events were registered with relative delay. We can assume that the first ions of this type of all energies were injected simultaneously and propagated without collisions. This assumption allows assessing ion injection times for the event of 15-04-01[1] with great precision by using linear regression method.

This article provides assessment of He, C, O, Mg, Fe ion injection times for the event of 20-01-05, during which the largest GLE in the 23rd cycle of solar activity was registered.

Simultaneous registration does not allow applying this technique with protons and electrons. In this paper we used another method of assessing proton and electron injection times. Neutron monitors data were also used

Ion Injection Times

ACE/SIS [2] data were used to determine ion injection time. For the analysis we choose only those ions for which fluxes in all 8 energetic intervals of ACE/SIS were registered. Ion injection time was determined in two ways:

A) it is assumed that the first ions propagate without collisions. Then, injection time is a linear function of 1/β, where β is ion speed in light speed units:

$$T(injection) = T(registration) - L/c*1/\beta \qquad (1)$$

Here L is a nominal length of magnetic force line connecting Sun and Earth, c is the speed of light.

B) It is assumed that ions in interplanetary space propagate diffusively. For this event, ion passage time is $\Delta T \sim L^2/D \sim L^2/v.\lambda$; D – is diffusion coefficient, λ – is free path length. Taking into consideration the dependence of free path length from rigidity $\lambda=\lambda_0.R^{2-\delta}$, where δ is the indexes of magnetic inhomogeneity in interplanetary space, we obtained the following expression to determine injection time in case of ion diffusive propagation

$$T(injection) = T(registration) - K.(E_{total}/Z).R^{\delta-3} \qquad (2)$$

K- some coefficient, E_{total} – full energy on nucleon, , Z – ion charge. Fig. 1 presents the results of determining ion injection time for collision less propagation. Linear regression correlation coefficients are >0.9 for all ions, which allowed to realize linear regression extrapolation from (1) to relativistic energies (β=1) and to determine possible times for the arrival of these ions.

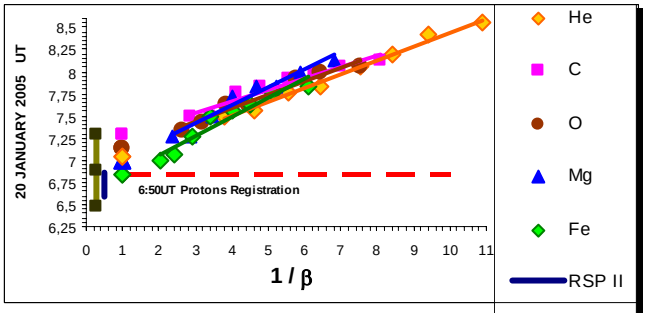

Fig. 1. Expected ion arrival times with.

Fig. 1 shows that in collision less propagation all ions except iron should have come much later (>10min) than protons, which were registered by GOES10 [3] satellite detectors at 16:50UT. Then we checked the reliability of the assumption concerning collision less propagation of ions. To do it, we determined ion injection times with the help of expression (2) and then assessed the path covered by ions as $S = K.(E_{total}/Z).R^{\delta-3}.V = [T(registration) - T(injection)].V$, where V is ion speed. The obtained ion path values were compared to nominal length of magnetic force line which was ~1.02au on January 20(solar wind speed ~700κm/s, solar flare coordinates N12W58). Results for iron and helium ions are presented in Fig. 2.

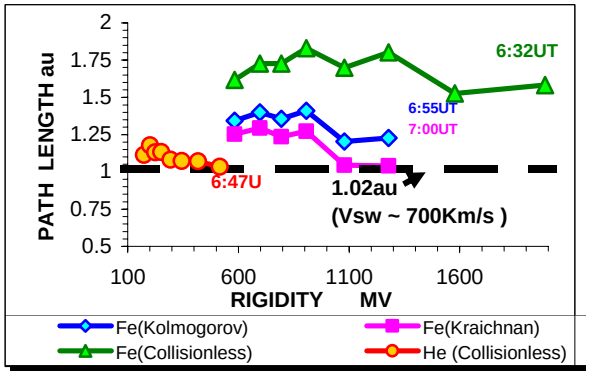

Fig.2. Ion path length form Sun to Earth depending on magnetic rigidity. The corresponding injection time values are provided next to the lines

Path length for all ions is calculated for three assumptions: a) collision less propagation, b) diffusive propagation - interplanetary inhomogeneity spectra looks like Kolmogorov` s spectrum (δ=5/3), c) diffusion movement - interplanetary inhomogeneity spectra looks like Krishnan` s spectrum (δ=3/2). Results revealed that movement of light ions and ions of medium weight (from He to Mg) corresponds to collision less propagation (path length < 1.2au). Fig.2 shows dependence of path length of He ions rigidity for the case of collision less propagation. Calculated medium path length proved to be too large for iron ions during collision less propagation (~1.7 au), whereas injection time was too early (injection 6:32UT, flare start 6:28 UT).

The situation is more realistic for iron ions when examining diffusive propagation. According to calculations, iron ions with R<1GV, which propagate diffusively, were injected at 6:55UT and 7:00UT in case of Kolmogorov` s and

Krishnan` s spectra. However, we chose variant with Krishnan` s specter after comparing ion path length to nominal length of Sun-Erath magnetic force line. The medium path length for ions with R>1GV was 1.21au for Kolmogorov`s spectrum whereas for Krishnan` s spectrum it was 1.04au, which is closer to magnetic force line length (1.02au). Thus, as injection time of light ions and ions of medium weight we used the values corresponding to collision less propagation, whereas for iron ions injection time we used the value (7:00UT) corresponding to diffusive propagation with Krishnan` s inhomogeneity spectrum. These data are presented in Fig. рис. 7.

Proton and Electron Injection times

The propagation of the first light ions was collision less, that is why, we can assume that the first protons and electrons also propagated without collisions. Proceeding from this assumption we determined proton and electron injection time as

$$T_{p,e}(\text{injection}) = T_{p,e}(\text{registration}) - \Delta t \qquad (3)$$

$\Delta t = 1.02\text{au}/V_{p,e}(E)$ is the lower limit of Sun-Earth propagation time, $V_{p,e}(E)$ are proton and electron speeds. We used GOES 10 (protons) and WIND (electrons) data [3,4].

Fig. 3 presents Δt values for each proton energy in the form of horizontal lines the beginning of which corresponds to the assumed proton injection times.

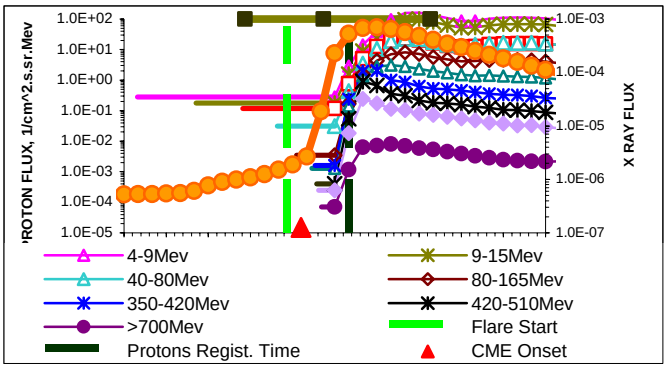

Fig 3. Proton fluxes registered by GOES10 on 20-01-05г in different energy intervals and the corresponding injection times.

The length of each horizontal line corresponds to the propagation time of protons with given energy in hours, whereas the beginning of the same line on the abscissa axis determines injection time for protons with the given energy.

In all their energy intervals GOES10 registered protons at 6:50UT, 22min after flare start till flare maximum (6:53UT). Fig. 3, shows that the assessed injection times are within flare interval only for protons with E>~50MeV. RHESSI registered a high flux of gamma quanta with energies 0.3÷0.8MeV 15min before X-ray flare start in the interval 6:13÷7:19UT. The evaluative injection time values of protons with energies E>~15Мэв are also included in this temporal interval. However, it is difficult to establish any connection between these events.

Consequently, we can conclude that only protons with E>~50Мэв were accelerated and injected during the flare whereas proton fluxes with E<50Мэв were generated in the interplanetary space. Moreover, protons with energies 1÷50Мэв and protons with high energies were simultaneously registered. With the decrease of energy their fluxes should have generated nearer and nearer to Earth with the decrease of energy.

WIND data show that the same situation (simultaneous registration and dependence of injection time of energy) is also observed for electrons. These data are provided in Fig.4.

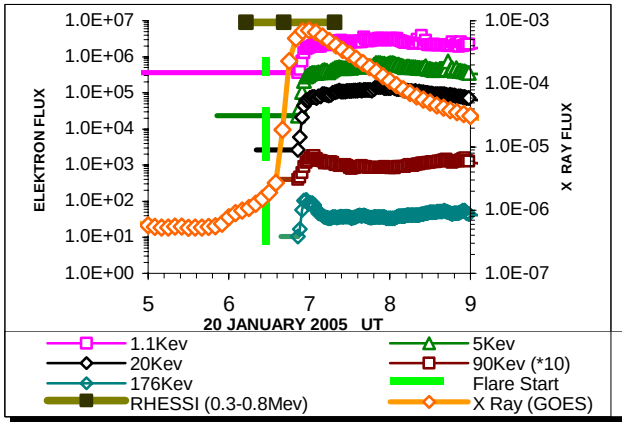

Fig. 4. Electron fluxes registered by WIND on 20-01-05 in different energy intervals and the corresponding injection times. The horizontal lines have the same meaning as for protons.

Here the evaluative injection times for electrons with E>~20Kev only are within X-ray flare area. The injection times of protons with E>50MeV and electrons with E>20KeV will be presented below after discussing neutron monitor data.

Neutron Monitor Data

We have discovered that injection time for protons (electrons) should depend on the energy obtained during acceleration as a result of simultaneous registration. The greater energy of the accelerated protons the longer they should have stayed in the acceleration area and the later injected. This assumption is confirmed by neutron monitor data on GLE of January 20.

We compared the beginning of GLE according to 12 neutron monitor data with magnetic cutoff rigidity from 0.8GV to 8 GV (see. Table 1) [5].

Table 1.Beginning of GLE 20-01-05 according to neutron monitor data

Neutron Monitor	Rigidity Cut off, GV	GLE Onset
Oulu	0.8	6:51 UT
Sanae	1.06	6:49 UT
Yakutsk	1.7	6:50 UT
Kiel	2.29	6:51 UT
Moscow	2.46	6:51 UT
Novosibisk	2.91	6:53 UT
Lomnicki St.	4	6:55 UT
Jungfraujoch	4.48	6:59 UT
Hermanus	4.9	7:00 UT
Bacsan	5.6	7:00 UT
Alma Ata	6.61	7:03 UT
Aragats	7.6	7:05 UT

The table shows that neutron monitors with geomagnetic cutoff rigidity $0.8 \le R_c \le 2.5$GV started registering GLE almost at the same time at 6:50UT, i.e. simultaneously with protons of low energies. At the same time monitors with R_c >2.5GV registered with GLE delay with the increase of cutoff of magnetic rigidity. For example, according to the data of Aragats Monitor (R_c =7.6GV) the beginning of GLE was 15 min later than the first group.

This can be explained by the fact that in case of relatively low energies (R_c<2.5GV) when proton speed greatly depends on energy, proton with greater energy which is later injected "manages" to catch up the previously injected proton with less energy at the distance of 1au (Fig.5). For the same reason, GOES10 simultaneously registered the protons.

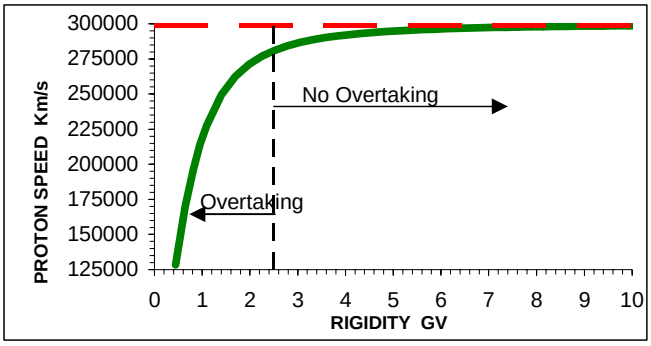

Fig.5. Dependence of proton velocity on rigidity.

The strong dependence area where the later injected proton can catch up with the previously injected proton and both of them are registered is shown in Fig. 5 left. The area where speed values are almost constant is shown in Fig.5 right.

Velocity of protons from high-energy areas (R_c >2.5GV) are hardly dependent on energies (R_c >2.5GV); at the distance of 1au the proton of high energy which was injected later cannot catch up with the previously injected low-energy proton. Two protons with different energies are registered with the same temporal interval as they are injected. This is demonstrated by neutron monitor data on GLE beginning presented in Fig. 6.

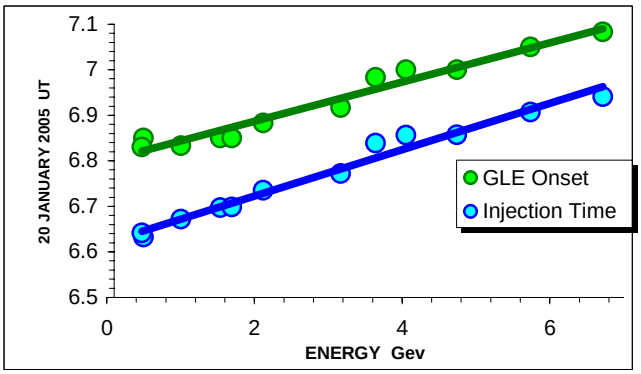

Fig.6. The dependence of GLE beginning of 20-01-05 and injection time of the primary solar CR particles on the threshold energy of neutron monitor registration.

Knowing the threshold energy and the time of GLE beginning for each monitor we assessed the injection times of the corresponding primary solar CR particles according to expression (3). Fig.6 also demonstrates the dependence of injection time on the primary particle energy. The dependence of both parameters (GLE start and injection times) on the energy were successfully approximated by the linear functions (correlation coefficients 0.96 and 0.98 respectively). These functions are presented below:

$$T_{GLE\ Onset}(E) = 0.043 \cdot E + 6{:}48UT \quad (4)$$

$$T_{injection}(E) = 0.05 \cdot E + 6{:}37UT \quad (5)$$

Energy unity is GeV.

The expression (4) shows that solar CR particles with the energies of E>0.5GeV (threshold for high-latitudinal monitors) begin to register at 6:48UT, i.e. 11min after their injection (6:37UT). The errors of time determining in the expressions (4) and (5) are ~2.5min.

Discussion and Conclusions

To summarize our results, we present the obtained ion, proton and electron injection times in Fig. 7, where the abscissa shows injection time value while the ordinate shows the particle energy (the right axis). To provide comparison, we also present the temporal profile of the flare X-radiation flux and trajectory of coronal mass ejection.

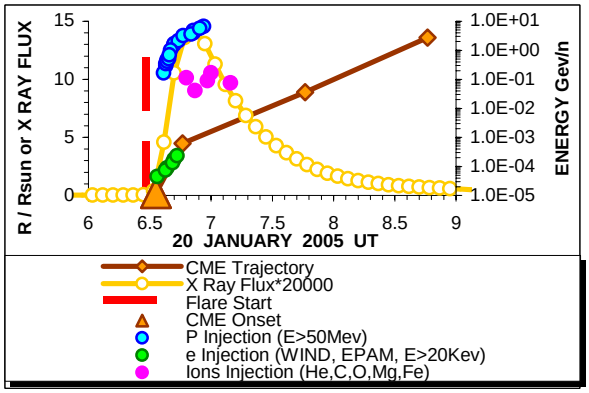

Fig. 7. Injection times of ions, protons, electrons and GLE trajectory on the time profile of 20-01-05 flare X-radiation.

According to the obtained results, electrons with E>20KeV begin to inject at 6:33UT, while the injection of protons with E>50MeV starts at 6:36UT. They are 5 and 8 min late than X-ray flare start and it is very likely that the process of proton and electron started together with the flare and was accompanied by the observed X-ray radiation. Fig.7 shows that injection of relativistic protons took place in the area of X-ray flare maximum (6:53UT). The beginning of the proton injection coincides with the time of the start of radio splashes of II, III и IV types (Table 2). Electrons begin to inject 3 min earlier than protons and this time coincide with the start of the flare in the optic range and with the GLE described in the paper.

Table 2.

Process Name	**Process beginning UT**
Flare(X-ray diapason)	6:28

Flare(optic diapason)	6:33
Coronal mass ejection	6:33
Electron injection	6:33
Proton injection	6:36
Radio splash IV	6:35
Radio splash II	6:36
Radio splash III	6:37
Ion injection	6:47

Ion injection starts at approximately 6:47UT. At that moment CME has already reached ~5$R_{sun\ altitude}$ where it certainly initiated the shock wave. Consequently, in difference to protons and electrons, ions should accelerate on the shock wave.

These time correlations enable us to conclude that the processes of proton and electron acceleration and coronal mass ejection during the event of 20.01.05 were independent and simultaneously happening components of this event. This is confirmed by the comparison of the energy dependencies of proton and electron injection times. These dependencies are presented in Fig. 8.

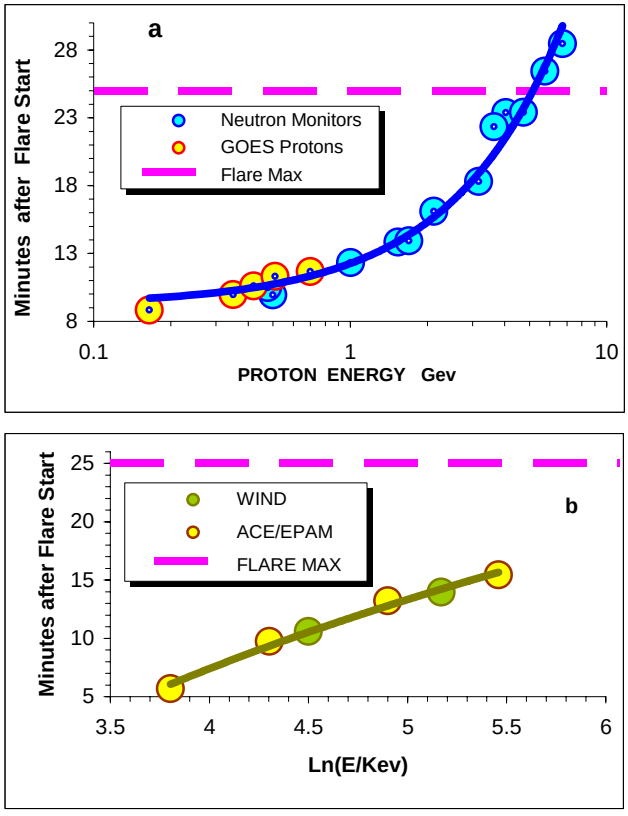

Fig 8. Energetic dependencies of injection time for GLE 20-01-05. a) protons and neutron monitors data, b) electrons.

Fig. 8 presents the unified data on protons with Ep>50MeV and neutron monitors. For this group of data injection times were successfully approximated (correlation coefficient 0.98) with the linear function of the proton energy.

$$T_{injection}(E_p) = 3.05 \cdot E_p + 9.26 \qquad (6)$$

Consequently, we can assert that for the event of 20-01-05 the dependence of proton injection times in a very large energy range (50Mev $\leq E_p \leq$ 10GeV) was linear. The expression (6) also implies that proton acceleration tempo does not depend on the energy, i.e. $dE_p/dt \sim$ const, which corresponds to Fermi's stochastic acceleration of the second type.

For electrons with E>20KeV we used WIND and ACE/EPAM [7] data. In contrast to protons, electron injection time does not greatly depend on the electron energy. (Fig.8b).

$$T_{injtction}(E_e) = 26.6 \cdot LnLn(E_e) - 29.475 \qquad (7)$$

The expression (7) implies very strong dependence of the acceleration tempo on the energy: $dE_e/dt \sim E_e \cdot Ln(E_e)$, i.e. electrons accelerate very quickly $E_e=E_0 \cdot \exp(\exp(\alpha t))$.

These results reveal that protons and electrons displayed different acceleration mechanisms and, consequently, they are accelerated in different places.

Acknowledgement

Author thanks GOES, WIND, ACE/SIS, ACE/EPAM experiment groups for using their data.

REFERENCES

1. Martorosyan H., Babyan V., Avakyan K., et al., Proceeding of Russian Academy of Science,Physics series, vol. 67, №4, p. 475
2. http://www.srl.caltech.edu/ACE/ASC/level2/lvl2DATA_SIS.html
3. http://sec.noaa.gov/Data/goes.html
4. http://sprg.ssl.berkeley.edu/wind3dp/
5. http://cr0.izmiran.rssi.ru/common/links.htm
6. Gopalswami N., Xie H., Yashiro S., Usoskin I., Coronal mass ejections and ground level enhancements, 29th ICRC, Pune, 2005, 00, p.101
7. http://www.srl.caltech.edu/ACE/ASC/level2/lvl2DATA_EPAM.html

A New Type of Solar Neutron Telescope

E. Mnatsakanyan[1,2]

[1] *Cosmic Rays Division, Alikhanyan Physics Insitute, Yerevan, Armenia*

[2] *Nor-Ambert Scientific Center of Lebedev Physics Institute, Moscow, Russia*

We discuss the problem of solar neutrons energy measurement by existing neutron telescopes and their sensitivity. In order to increase the sensitivity and to reduce existing uncertainty in energy measurement of solar neutrons, a new type of solar neutron telescope installed deep underwater is proposed for the next – 24th solar cycle. It is shown that due to installation of the telescope under thick absorber, the minimum detectable intensity can be decreased up to 10 times by decreasing background rate – from mainly neutral particles. The concept and construction of new telescope and estimations of its performances are presented. We propose to install such telescopes in some high altitude lakes such as Titicaca (Bolivia, Peru), Cucunor (China), as well as in artificial pools.

Introduction

Solar flares are the most energetic events accruing on the Sun and these provide us with a unique opportunity for studying the acceleration of charged particles. Most of the powerful flares are a strong source of high energy protons and ions, which are detected as solar cosmic rays. Some of the high energy protons and ions produce solar neutrons through collisions with the ambient gas of the solar atmosphere. High energy neutrons travel directly to the Earth without deflection by magnetic fields and provide direct information about the acceleration mechanism of charged particles.

Until recently, solar neutrons have been registered by traditional neutron monitors (NM) located at various parts in the world. Although the NM has high efficiency as a detector of solar neutrons, it is unable to determine direction and charge of the incoming particles and to measure their energies.

In order to overcome these disadvantages, at beginning of 1990s a group of scientists from Nagoya University (under the leadership of Prof. Muraki) proposed creating a world net of new type of scintillation detectors located in mountain altitudes [1],[2]. At present, similar detectors are being operated on seven stations. Since 1997 the same type of the solar neutron telescope (SNT-l) has been working in Aragats station of Yerevan Physics Institute (Armenia).

These detectors are designed to distinguish between incoming neutrons and charged particles and to get information on neutron energy by measuring the energy deposit of the recoil protons in the scintillator. However, 15 years of experience of operating such detectors, especially the registrations of the Solar Neutrons Event (SNE) in Solar Cycle 23, demonstrates, that

1) In most of the cases, the statistical significance of the signal is no more than 5σ, even when the telescope function has been used to identify neutron signals, removing the background from the other directions [3]:
2) The detectors have significant uncertainty in energy measurement of solar neutrons because of the absence of the information about kinematics of the neutron interactions and uncertainty in the recoil protons energy measurements. Therefore, estimation of primary neutron energy is still carried out via the arrival time delay, as in the case of the traditional neutron monitors.

To obtain much more qualitative information on solar neutrons, it is obvious that future observation will require detectors with more improved features.

With the aim of substantially increasing the signal to noise ratio (s/n) magnitude, decreasing the minimum detectable intensity (m.d.i.) and reducing uncertainty in energy measurement of solar neutrons, a new type of telescope installed deep underwater is proposed for the next – 24th solar cycle.

Before describing the features of the proposed detector in the following section, some problems related to the sensitivity of the solar neutron detector will be discussed.

On the sensitivity and m.d.i. of the solar neutron telescopes

The solar neutron telescope sensitivity function $S(x,E,\theta_0)$ is defined via the response of the solar neutron detector [4].

$$N_n(x,t,\theta_0) = \int I_n(E)_t S_n(x,E,\theta_0) dE\,, \quad (1)$$

where x is the atmospheric depth; E and θ_0 are energy and zenith angle of the primary neutrons; N_n - the response; and $I_n(E)_t$ - the differential energy spectrum of the primary neutron flux at the time t. For fixed neutron energy E_0 the S can be expressed via the increase of absolute counting rate:

$$S(x,E_0,\theta_0) \equiv \frac{\Delta N(x,\theta_0)}{\Delta t \cdot I_n(E_0)}\,. \quad (2)$$

This definition of the sensitivity does not express the influence of background fluctuations on the capability of detectors to measure the weak signals.

In case when the fluctuations of background are taken into account, the increase of relative counting rate is given by

$$\Delta N_r = S I_n \Delta t - k\sigma \quad (3)$$

where $\sigma = \sqrt{N_b} = \sqrt{I_b \Delta t}$ is the standard deviation of background rate N_b; I_b is the background intensity; and

$k = 1;2;3$ is the factor significance. Below we will take $k = 2$.

One can define the minimum detectable intensity I_m as:

$$I_m \equiv \frac{2\sigma}{S\Delta t} \quad (4)$$

in case when $\Delta N = 2\sigma$.

Since the values ΔN and N_b depend on detectors' area *A*,

$$I_m \sim \frac{2\sqrt{I_b}}{\sqrt{A}}, \quad (5)$$

and signal to noise ratio

$$\frac{\Delta N}{\sigma} \sim \frac{A}{\sqrt{I_b A}} = \frac{\sqrt{A}}{\sqrt{I_b}}, \quad (6)$$

two ways of improvement of parameters I_m and N/σ are evident:

-by increasing of the area;

-by decreasing of the intensity of background particles.

Until now the single method of decreasing background intensity has been by anticoincidence. But by this method the neutral particles (neutrons and γ- photons), which are a significant part of the remaining background, are not rejected. In order to significantly increase the $\Delta N/\sigma$ and reduce I_m by increasing background particles intensity, it is hereby proposed to install solar neutron detectors under a thick absorber in particularly deep underwater, which we call the SUBMARINE telescope (Fig. 1).

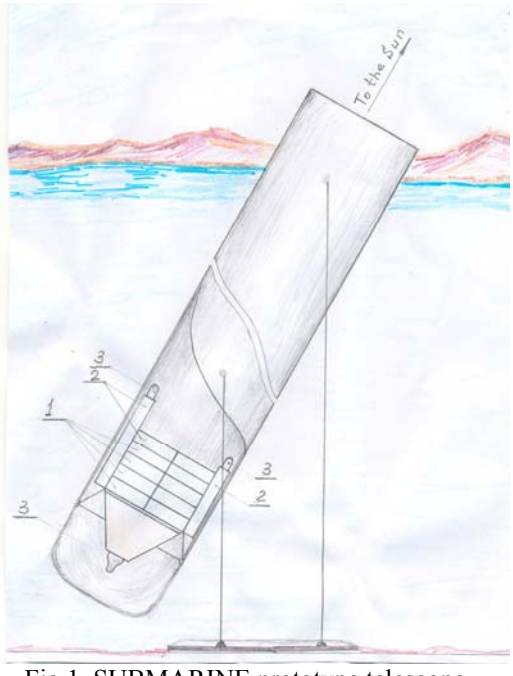

Fig.1. SUBMARINE prototype telescope.
1- Scintillators, 2 – Veto counters, 3 – PMTs.

The SUBMARINE telescope

The detector of solar neutrons of the SUBMARINE telescope is mounted inside the empty tube. The tube is oriented to the Sun and operates in tracking regime.

For the estimation of the expected characteristics of the new telescope, we have used results obtained by M. Moser in simulation on SONTEL (Gornergrat) telescope for the Solar Neutron Event of June 3, 1982. We have used only data for fixed energy E_0 = *1068MeV,* for which I_n was estimated $9.8 \times 10^2 m^{-2}s^{-1}$ and threshold > *40MeV* [5, 6]. For comparison, we take the dimensions of the SUBMARINE detectors as those of SONTEL.

TABLE 1

Simulated galactic counting rates (count/ 10 sec) for SONTEL detector > 40MeV (Moser) and adopted for SUBMARINE, for D=20 m.w.e. absorber

	SONTEL				SUBMARINE			
	without anti		with anti		without anti		with anti	
	rate	%	*rate*	%	*rate*	%	*rate*	%
N_n	1452	8.5	1216	40.5	35	3	35	28.5
N_p	695	4.0	46	1.5	17	1	1	0.8
N_μ	13142	76.7	913	30.4	1190	92	83	67.5
N_e	923	5.4	65	2.21	22	2	2	1.6
N_γ	924	5.4	763	25.4	22	2	2	1.6
N_b	17136	100	3003	100	1286	100	123	100

TABLE 2

Parameters of the SONTEL (Gornergrat) and two types of the hypothetic SUBMARINE telescopes

Parameters are estimated for Solar Neutron Event of June 3, 1982 and for 2 values of "veto" efficiency ε_V .

a) $\varepsilon_V = 0.93$			
	S O N T E L (Gornergrat)	SUBMARINE	Prototype SUBMARINE
A[m^2]	4	4	1
D[m]	0	20	20
x[$g.cm^{-2}$]	700	700	700
ΔN [cnt/10s]	285	285	71
N_b [cnt/10s]	3003	123	31
σ	54.8	11.1	5.5
$\Delta N/N_b$	0.095	2.3	2.3
$\Delta N/\sigma$	5.2	25.7	1.3
S[m^2]	$2.9 \cdot 10^{-2}$	$2.9 \cdot 10^{-2}$	$7.5 \cdot 10^{-2}$
I_m[m^2s^{-1}]	378	76	152
b) $\varepsilon_V = 0.98$			
N_b [cnt/10s]	2251	60	15
σ	47.7	7.74	3.87
$\Delta N/N_b$	0.127	4.75	4.75
$\Delta N/\sigma$	6	36.8	18.35
I_m[m^2s^{-1}]	327	53	107

The background under $D=20m$ water has been estimated without account of cosmic ray particles' angular distribution. The results are presented in Tables 1 and 2. In Table 2 the expected values of parameters for SUBMARINE prototype are also given.

Conclusions

As we can see from Tables 1 and 2, the novel approach for achieving much more qualitative information on solar neutrons has the following key advantages:

- It allows decreasing the minimum detectable intensity and increasing $\Delta N/\sigma$ more than 5 times at ε_V = 0.93, and more than 5 times at ε_V = 0.98; whereas in order to obtain these results under usual conditions, increasing the detection area ~ *25* times would be necessary;
- As seen in Table 2, even a SUBMARINE prototype telescope with a detector area of $1m^2$ will have twice more $\Delta N/\sigma$ and 2.5 times smaller I_m, than the telescope with a $4m^2$ detector area under usual conditions;
-High directional sensitivity allows reducing uncertainty in the neutron energy determination, especially while using a multiplayer position-sensitivity detector.

We propose to locate similar telescopes in the lakes Titicaca (Bolivia, Peru; 3218 m a.s.l; depth - 304m; *16°S;69°W)* and Cucunor (China, 3205m a.s.l.; depth -38 m; *37° N; 100.5° E),* as well as in artificial pools in geographical locations as near the equator as possible, such as Siera Negra (Mexico, 4600m a.s.l.; *19° N*; *97.3° W*), Mauna Keya (Hawaii, USA, 4200m a.s.l.; *19.8°; 155 W*), Cordillera (Costa Rica, 3000-3200m a.s.l.; 10° *N; 84° W*), and other places.

However, at the initial stage, the creation of a prototype with an area of $1m^2$ is proposed. Consequent testing will be carried out in the artificial pool at Aragats Station (3200m a.s.l.; 40.5° *N; 44.1° E*) of the Cosmic Rays Division of Yerevan Physics Institute, Armenia.

Acknowledgements

The author thanks A. A. Chilingarian and E. A. Mamijanian for their expressed attention and support, as well as Y. I. Stazhkov, E. O. Flückiger and Y. Muraki for useful discussion.

REFERENCES

[1] Y. Muraki et al. Proc. 23rd ICRC(Calgary), 3,171(1993)
[2] Y. Matsubara et al. Proc. 23rd ICRC(Calgary), 3,139(1993)
[3] Y. Muraki et al. 2004. Proc. 19th ECRC (Florence. 2004)
[4] Debrunner H. et al. (1997) Energetic Neutrons, Protons and Gamma Rays during the 1990 May 24 Solar Cosmic-Ray Event. Ap.J.479.997-1011.
[5] M.R. Moser Solar Neutron Telescope Gornergrat. Monte Carlo Simulation of Detector Properties. Diploma 2002.
[6] M.R. Moser, E.O. Fluckiger, R. Butikifer et. al., Proc. 28th ICRC (Tsukuba) SG1-1, 3215 (2003).

On the Possibility to Deduce Solar Proton Energy Spectrum of the 20 January 2005 GLE using Aragats and Nor-Amber Neutron Monitors Data

M.Z. Zazyan, A.A. Chilingarian

Alikhanyan Physics Institute, Yerevan, Armenia, mary@mail.yerphi.am

Modeling of Aragats and Nor-Amberd neutron monitors responses to solar proton flux was performed for different possible spectral indexes. By comparing the relative response of two neutron monitors with observations the spectral index of the power-law proton energy spectrum for the Ground Level Enhancement on January 20, 2005 at the time of maximum increase (7:15 UT) was found to be ~5. The simulation of the primary protons transport through the Earth atmosphere was performed using the well-known software package CORSIKA. The test proton spectra for the simulation were derived using the low energy proton fluence spectrum from instruments on ACE and SAMPEX spacecraft, and the intensity of >100 MeV protons measured by GOES11 spacecraft.

Introduction

The remarkable solar event of 20 January 2005 produced the highest flux of relativistic solar particles observed at many neutron monitors for nearly 50 years. The analysis of the Ground Level Enhancement (GLE) detected by Aragats Space Environmental Center (ASEC) monitors [1] is already started and will be continued with involving data from all ASEC monitors, as well as by using the new statistical analysis methods [2].

The analysis presented in this paper is based on the Aragats and Nor-Amberd neutron monitors count rates. These two neutron monitors are located at different altitudes (3200m and 2000m above sea level), but at the same geographical coordinates. The effective cutoff rigidity of the location is 7.56GV.

The idea to deduce the spectra of solar flare protons using two neutron monitors located close by at the same vertical cutoff rigidity, but at different altitudes above sea level was proposed by J.A. Lockwood et all [3]. Using Mt. Washington and Durham neutron monitors count rates, coupled with the knowledge of the proton specific yield functions, they have derived the rigidity spectra, $AR^{-\gamma}$, for selected solar flare events since 1960.

Our method is based on the modeling of the responses of Aragats and Nor-Amberd neutrons monitors to solar proton flux. The modeling technique includes Monte Carlo simulation of the propagation of primary particles through the Earth's atmosphere (air shower simulation) and calculation of neutron monitors response to secondary particles of air shower.

Simulation of the neutron monitors response

Primary particles, while entering the Earth atmosphere, interact with the atmospheric nuclei and produce a cascade of secondary particles. After production of several generations of particles, the cascade process ends when the energies of the particles become too low for the future particle production. As long as enough energy remains for the propagation of the shower and the production of cascade particles, the shower will continue down until it reaches ground level.

We used CORSIKA code [4] (version 6.204) to simulate the propagation of primary particles through the Earth's atmosphere. Electromagnetic interactions are simulated using EGS4 code [5]. For the hadronic interaction, the QGSJET01 [6] model is used at high energies, and FLUKA [7] is used at low energies (below 80 GeV). The simulation was performed for two observation levels (Aragats and Nor-Amberd stations). The threshold energies (E_0) for the primary particles correspond to the rigidity cutoff of the location. The threshold energies for secondary particles are: 50 MeV for hadrons, 10 MeV for muons and 6 MeV for electrons and photons.

The total number of particles entering the atmosphere within the solid angle $\Delta\Omega$ during the time interval Δt has been estimated according the formula:

$$N_{tot} = I(>E)\,\Delta\Omega\;\Delta t\,, \qquad (1)$$

where I(>E) is the integral energy spectrum.

We applied this formula to Galactic Cosmic Rays (GCR), which consist of protons and helium nuclei, and to solar protons. For the GCR we selected the zenith angle range of 0-70º and the input spectra of the primary particles according to the CAPRICE98 balloon-born experiment [8].

In the case of solar protons we used the zenith angles within 0-40º, because due to their softer spectrum the probability that particles entering the terrestrial atmosphere under greater zenith angles will initiate showers reaching 3200m a.s.l. is rather small. For the input spectra we used test spectra based on the low energy proton fluence spectrum from instruments on ACE and SAMPEX spacecraft and the near Earth intensity of >100 MeV solar protons measured by GOES11 spacecraft. The solar proton intensity follows a power law dependence on energy [9]. We derived the coefficient for this dependence and achieved the following equation for the intensity of protons with kinetic energy E_k<1GeV:

$$I(E_k) \sim 4.07\times10^5\, E_k^{-2.15}\ \text{part}/(\text{m}^2\ \text{sr}\ \text{s}\ \text{GeV}) \quad (2)$$

Taking indo account that ground-based instruments observed much softer spectra and assuming that the knee is around ~1GeV, a test spectrum at higher energy was adopted in the form:

$$I(E_k) \sim 4.07\times10^5\, E_k^{-\gamma}\ \text{part}/(\text{m}^2\ \text{sr}\ \text{s}\ \text{GeV}) \qquad (3)$$

The total number of solar protons of kinetic energy corresponding to R>7.56GV was calculated for different

spectral indexes. Particle fluxes at ground level were simulated, and the count rates were determined by applying the detection efficiency (as it was calculated by Clem and Dorman [10]).

Observations and simulation results

Fig.1 shows the GLE on 20 January 2005, as observed by Aragats (ArNM) and Nor-Amberd (NANM) neutron

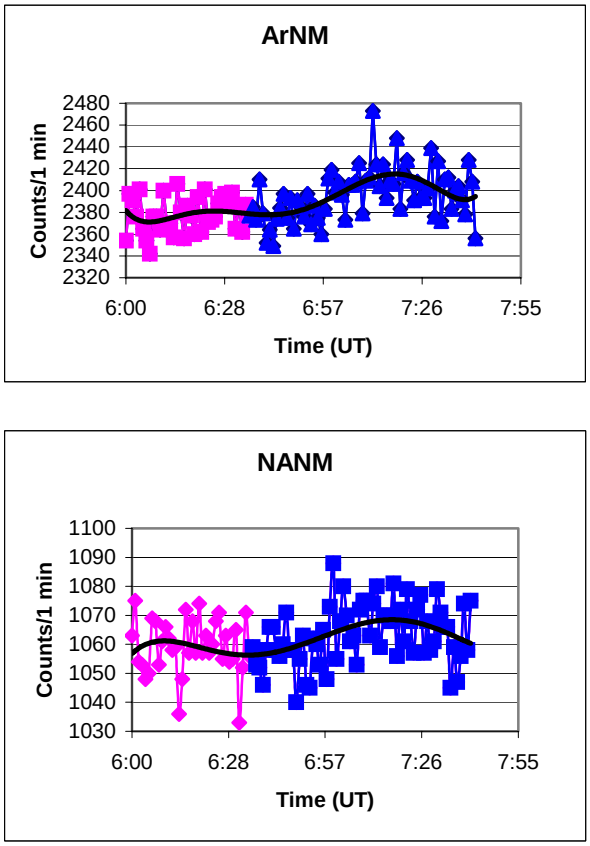

Fig.1. 1-min. count rate variations of 20 January 2005 event, observed by Aragats (ArNM) and Nor-Amberd (NANM) neutron monitors, fitted by the polynomial approximation.

monitors. It illustrates that the excess above background is not very large. The count rate increase (ΔN) due to solar protons and the background count rate (N) of Galactic cosmic rays are estimated according the polynomial approximation of 1-minute data. Near the time of maximum (7:15 UT, according the approximation) the relative increases of Aragats and Nor-Amberd neutron monitors (above the baseline of 6:37 – 6:57 UT) are estimated as 1.52% and 1.23% respectively.

A Monte Carlo simulation of the increase in the count rates of Aragats and Nor-Amberd neutron monitors has been performed for different solar cosmic ray spectra. The expected increases in the count rates, calculated for possible spectral indexes, as well as experimental increases of Aragats and Nor-Amberd neutron monitors are presented in Table 1.

One can conclude, that a spectral index of ~6 is a reasonable choice according to Table 1, because for 6 experimental data and simulations coincide best. However, we recognize that the results of simulation strongly depend on the value of the parameter **A** of solar particle spectrum. To avoid this dependence, the ratio of count rate increases of two monitors:

$$R(Ar/NA) = (\Delta N/N)_{ArNM}/(\Delta N/N)_{NANM}, \qquad (4)$$

which is a function on spectral index only, was examined. Simulated for different spectral indexes and the experimental ratios of the count rate relative increases of Aragats and Nor-Amberd neutron monitors are presented in Table 2.

TABLE I
Simulated and experimental count rate relative increases of Aragats and Nor-Amberd neutron monitors at 7:15UT

γ	Aragats NM	Nor-Amberd NM
4	105%	88%
5	10.5%	8.5%
6	1.4%	1.1%
7	0.15%	0.12%
Exp.	1.52%	1.23%

TABLE 2
The ratio of simulated and experimental count rate relative increases of Aragats and Nor-Amberd neutron monitors at 7:15UT

γ	R(Ar/NA)
4	1.19
5	1.26
6	1.29
7	1.30
Exp	1.24

From the comparison of the computed and observed ratios we estimated γ to be ~5 at 7:15. It should be noted that we have derived the total energy spectral index, because CORSIKA simulation requires the spectrum as a power law in total energy. For the rigidity range above 7.56GV, where $E_0 \cong R$, it can be considered as a spectral index of the rigidity spectrum.

Summary

With the modeling of Aragats and Nor-Amberd neutron monitors responses to the solar proton flux and comparing those with observations we deduced that the spectral index of the power law rigidity spectrum is ~5. Statistical errors and simulation uncertainties do not allow us to derive a precise value of the spectral index. To obtain reliable solution we plan to combine this analysis with data from other ASEC monitors.

References

[1] A. Chilingarian, K. Arakelyan, K. Avakyan et al., " Correlated measurements of secondary cosmic ray fluxes by the Aragats Space-Environmental Center monitors", NIM, A 543, 483 (2005)

[2] G.G. Karapetyan, A.A. Chilingarian, "Chanel-to-chanel analysis of Aragats muon monitor detection of >5GeV muons in 20 January 2005 ground level enhancement", this proceeding.

[3] J.A. Lockwood, H. Debrunner, E.O. Flukiger and J.M. Ryan. “Solar proton rigidity spectra from 1 to 10 GV of selected flare event since 1960.” Solar Physics, 208 (1), pp 113-140 (2002)
[4] D. Heck and J. Knapp, Forschungszentrum Karlsryhe, FZKA Report 6019 (1998)
[5] W.R Nelson, H. Hirayama and D.W.O. Rogers, Report SLAC 265 (1985)
[6] N.N. Kalmykov and S.S Ostapchenko, Yad. Fiz. 56, 105 (1993)
[7] A. Fasso,A. Ferrari, J. Ranft and P.R. Sala, FLUKA, Status and Prospective of Hadronic Applications, Proc. Monte Carlo 2000 Conf., Lisbon, Oct. 23-26 2000, 955
[8] M. Boezio, V. Bonvicini, P. Schiavon, A. Vacchi and N. Zampa. “The cosmic-ray proton and helium spectra measured with the CAPRICE98 ballon experiment”, arXiv:astro-ph/0212253, 1,11 (2002).
[9] ACE News #87 - Feb 23, 2005. “Space Weather Aspects of the January 20, 2005 Solar Energetic Particle Event” www.srl.caltech.edu/ACE/ACENews/ACENews87.html
[10] J.M. Clem and L.I. Dorman, “Neutron monitor response functions” Space Sci. Rev., 93, 335 (2000)

Radiation Storms in the Near Space Environment by Coronas-F Satellite

M.I. Panasyuk, S.N. Kuznetsov

Skobeltsyn Institute of Nuclear Physics of Lomonosov Moscow State University, 119899, Moscow, Russia, panasyuk@sinp.msu.ru

Russian low-orbital polar satellite Coronas-F was launched on July, 2001 and since this time several extreme solar events were observed. During some of them geomagnetic activity was very light and caused significant magnetic storms. Different phenomena such as both penetration of solar particles inside the trapping region and in polar caps and variation of electron and ions radiation belts are discussed and are compared with other experiments.

Introduction

Solar storms are accompanied by plasma and energetic particle ejection into the interplanetary medium. Some of solar matter penetrates into geomagnetic field and changes typical for quite period stationary spatial and energy distributions of charged particles. On the other hand, happening during solar storms geomagnetic disturbances (substorms and storms) cause intensive transfer and acceleration of the particles both in trapped radiation region and out of it. Jointly these processes result in complex spatial-energy changes of charged particle distributions, which are called radiation storms.

Near Earth's space radiation environment is characterized by constant presence of radiation belt (RB) particles, galactic cosmic rays (GCR), as well as second and albedo radiation due to interaction of precipitating particles of radiation belts with atmosphere. These particles penetrate deep into the magnetic field of cosmic rays. During solar and geomagnetic storms solar energetic particles (SEP) can penetrate to low altitudes and fill the polar caps producing additional radiation effects in the environment. Due to its polar orbit inclination (82˚) CORONAS-F satellite gave an opportunity to study all above mentioned radiation components.

Recently the most strong radiation environment modifications in the near Earth space were registered during solar extreme events November 2001 and October-November 2003 (*see Panasyuk M., et al, 2004 and Veselovskiy I., et al, 2004*). Many of typical physical processes some of that we consider below became apparent in these events, which caused changes of the Earth's radiation environment.

Galactic cosmic rays

Penetrating deep into the heliosphere galactic cosmic rays are affected by solar modulation. In long duration scale it shows 11-year cycle fluxes changes due to solar activity variations. Shock waves accompanied by solar coronal mass ejection (CME) during solar storms produce short-term fluctuations of galactic cosmic ray fluxes in the interplanetary medium like Forbush effect. Penetrating deep into geomagnetic field additional fluctuations of GCR at hundreds MeV energies can arise due to variations of particle penetrating effectiveness during geomagnetic storms.

High-energy particles (protons with energies E>75 MeV and 200-300 MeV) were registered by SONG instrumentation onboard CORONAS-F (*see Kuznetsov S., et. al, 2005*). Fig.1 shows proton data with energies > 75 MeV obtained using SONG device at different L-values outside of South Atlantic anomaly (SAA) region, as well as South Pole neutron monitor data and GOES-10 satellite proton data with energies > 700 MeV during solar extreme events and geomagnetic storms October-November 2003.

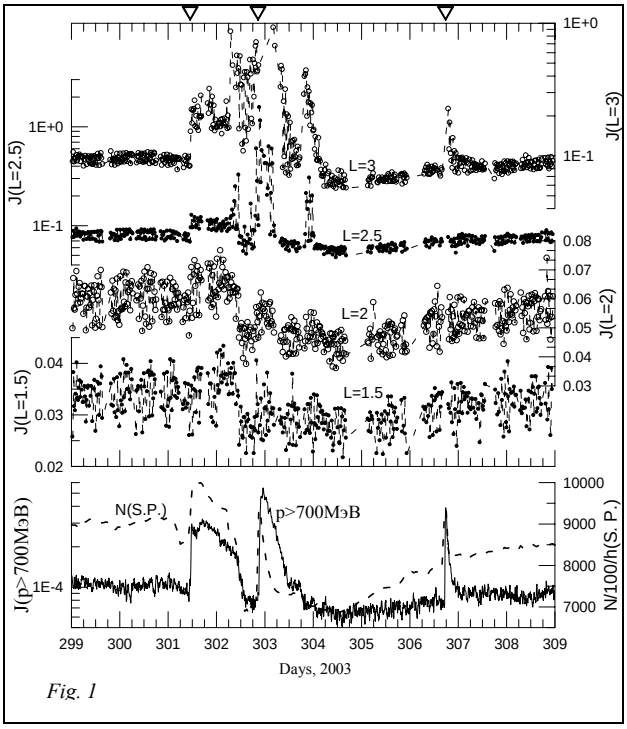

Fig. 1

Typical for GCR types of variations are revealed at low L-values: these are half-daily variations with 10-15% amplitude and Forbush-effect with up to 30% amplitude. While Forbush-effect observed at low altitudes is per se the reflection of high-speed shock wave interaction with fluxes of cosmic rays in the interplanetary medium, the half-daily variations were probably connected with changes of geomagnetic cutoff threshold due to particles penetration deep into the magnetosphere.

Against this background most strong variations of particles at high L-values were caused by SEP. Next paragraph presents in details the dynamics of SEP inside the magnetosphere.

Solar energetic particles

Over all period of CORONAS-F satellite observations most strong SEP fluxes were observed from 23 October to 06 November 2003 (shown on Fig. 2).

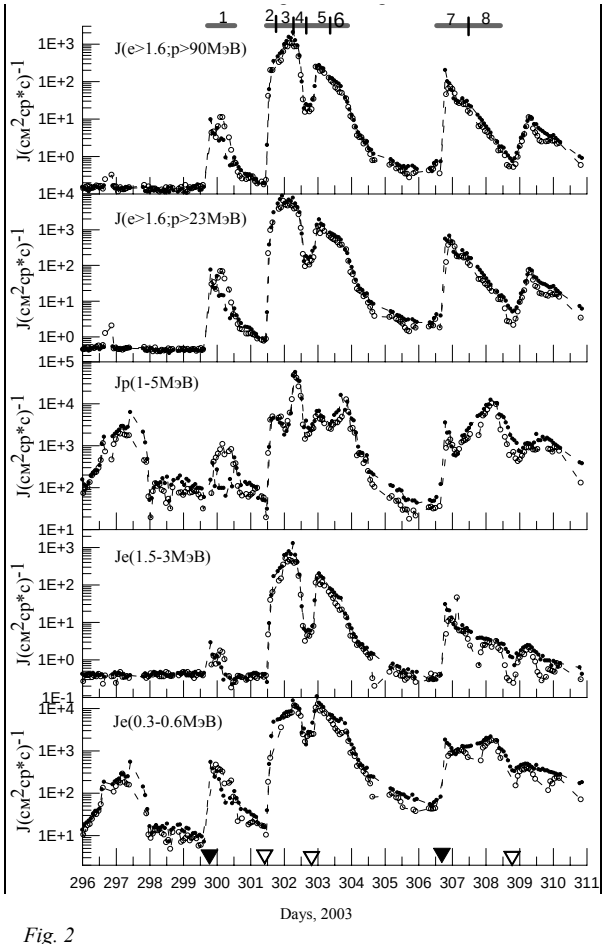

Fig. 2

The analysis carried out in the paper *Veselovskiy I., et al, 2004*, showed that most intensive solar flares were generated by one large-scale active region on the Sun. At that the most intensive and energetic SEP fluxes were produced by flare on 28 October (at 11.39 UT) with record speed of CME propagation (up to 2459 km/sec). Note that polar caps SEP data obtained onboard CORONAS-F showed fundamentally different character of particle distribution through the interplanetary medium.

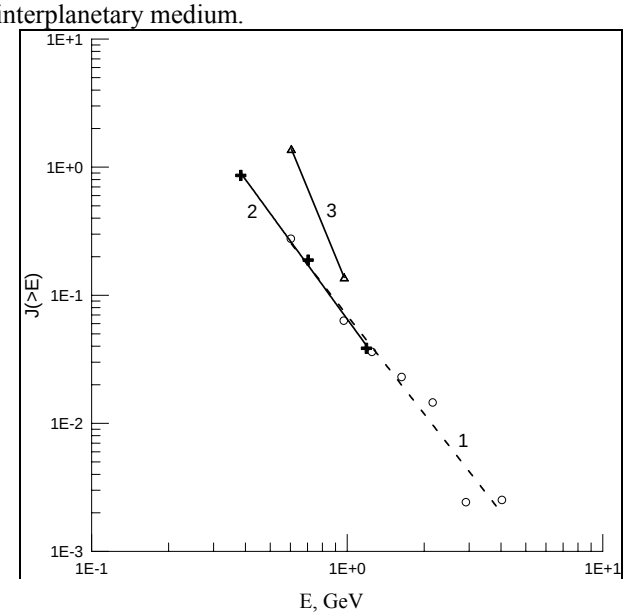

Fig. 3

While considerable SEP anisotropy observed after the flare on 26 October (at app. 12 UT) point to prolonged particle emission and comparatively large free path, SEP profile observed on 02 November was typically diffusive with short free path for low-energy particles.

Particles' generation during the strongest solar proton event on 28 October consisted of two phases. This assumption is proved by analysis of gamma rays, neutrons and relativistic electrons data obtained by SONG detectors onboard CORONAS-F satellite (*see Veselovsliy I., et al, 2004*). One of the phases is SEP acceleration on CME shock wave. Using high energy protons data on latitude effect during evolution of proton events the energy spectrum was determined (shown on Fig. 3). It is obvious from comparison of particle energetic distributions of two events on October-November 2003 that relativistic protons accelerated by shock waves with energies ~ 1 GeV and higher were observed in both events.

Energetic particles accelerated by Sun and CME shock waves penetrate deep into the magnetosphere and fill up not only polar caps region of weak magnetic field but lower latitude regions as well depending on particle rigidity and level of geomagnetic activity. Set of issues are devoted to studying of SEP penetration into magnetosphere (*for example Morfill and Scholer, 1973, Biryukov et al, 1983, Ivanova et al, 1985*). In these works shifting of low-latitude boundary (Λ°) of solar particles penetration into magnetosphere with increase of geomagnetic activity was demonstrated. At the same time it is observed Λ° asymmetry by local time (MLT).

CORONAS-F satellite experiment allowed continuing such investigations and revealed some new peculiarities of particle penetrating mechanism (*see Panasyuk M., 2004, Kuznetsov S., et al, 2005*). Among them are following. The investigation (*see Kuznetsov S., et al, 2005*) of Λ° dependence for electrons and protons on Kp and Dst indices of geomagnetic activity showed no primary correlative dependence on above mentioned geomagnetic indices during strong magnetic storms (06 and 24 November 2001, 29 October 2003). There is just tendency of Λ° boundary shifting to lower latitudes during increase of geomagnetic activity. This conclusion is clearly demonstrated by Λ° data for solar electrons and protons presented on fig. 4 in compare with Dst, Kp and Bz.

The dynamics of Λ° SEP penetration boundary demonstrates large-scale changes of magnetosphere topology. Very likely that correlation between variations of middle latitude ionosphere current (primary described by Kp index), variations of ring current in magnetosphere tail at large distances and in magnetopause region (described by Dst-index) is more complex than has been used in previous data analysis (*Kuznetsov et al 2005*):

$$\Lambda^\circ = a + b\,Dst + cKp \qquad (1).$$

It is noted that correlation of Λ° with indices increases at higher proton energies; SEP electron component mostly correlates with Kp index.

The analysis of CORONAS-F data on SEP penetration demonstrated the availability of Λ° variations not only due to evaluation of global geomagnetic storms but also during isolated substorms (*see Panasyuk et al, 2004*). During auroral activity increase SEP penetration boundary is shifted toward equatorial latitudes and return back as a substorm die out.

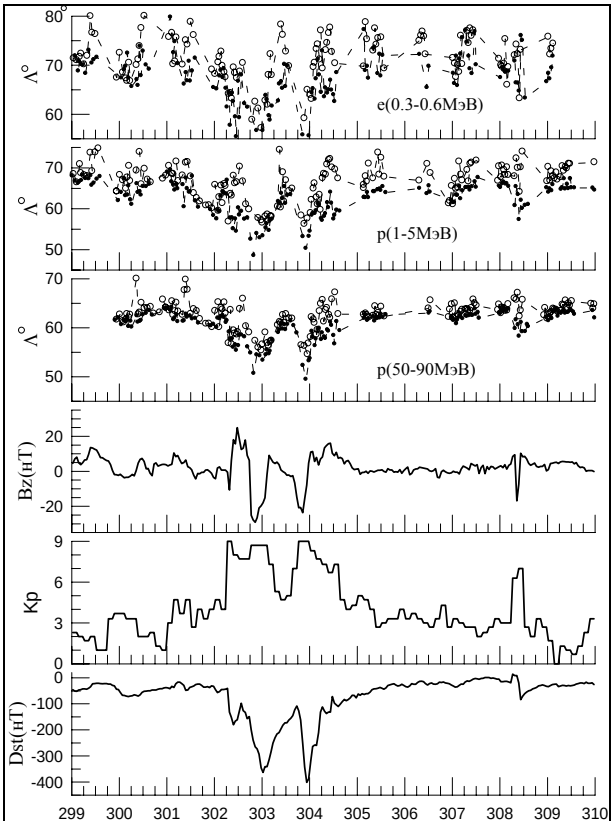

Fig. 4

This fact should also result in spread in Λ° values while searching the appropriate connection between Λ° variations and such global indices like Dst and Kp.

Radiation Belts

The dynamics of radiation belt particles during magnetic storms determined by synergetic effect of different physical mechanisms. Among them the most important ones are radial diffusion due to electric and magnetic field fluctuations, pitch-angle scattering of the particles due to its interaction with electromagnetic waves and effects caused by violation of particle adiabatic motion invariant.

The investigation of radiation belts dynamics during strong geomagnetic storms causing intense changes of its' spatial-energetic structure is of great interest. There are following typical morphology features of radiation belt particles variations during strong storms:

1. SEP penetration (both protons and electrons) on outer L-shells (see previous section)
2. SEP capture on inner L-shells;
3. Rapid transfer (radial shift) of particles toward the Earth during active phases and at the beginning of recovery phase of geomagnetic storms;
4. Impulse particle acceleration up to relativistic energies inside the trapped region.

At low altitudes the variations of particle fluxes due to its' pitch-angle scattering far off the point of observation at lower latitudes can play an essential role. Fig. 5a and b shows data on variations of radiation belt electrons and protons during 06-12 November and 23-30 November 2001. This can illustrate some physical phenomena that take place at low altitudes during strong geomagnetic storms. Analyzing time variations of electron fluxes one can mark out 3 phases:

- the first one - at the beginning of geomagnetic disturbance SEP penetrate to low latitudes ad fill up the outer L-shells;
- the second one – the intensity of electron fluxes decrease – it is a peculiar "emptying" of outer zone of trapped radiation. Right after this become
- the third phase, which is characterized by recovering and increasing of electron fluxes and its transfer to low L-shells (this process coincides with recovery phase of geomagnetic storms).

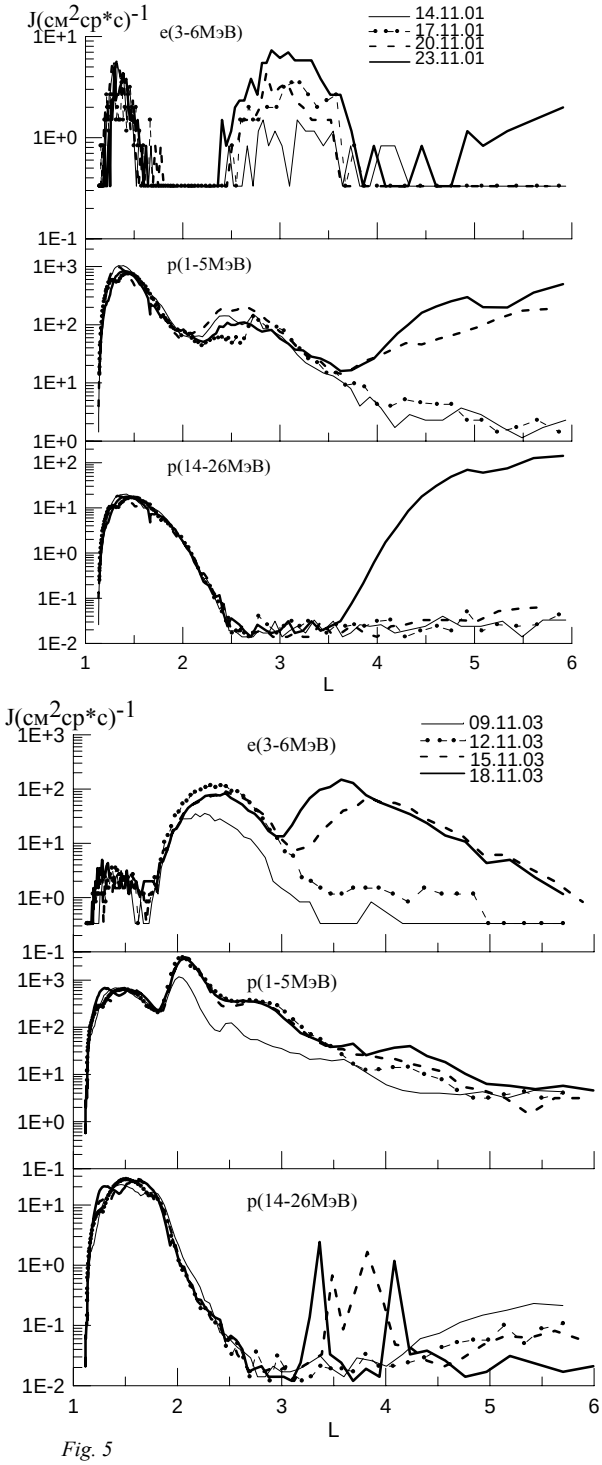

Fig. 5

Variations of radiation belt proton fluxes also can be divided into 3 similar phases. Nevertheless it should be noted that producing of "new" protons in the third phase unlike electron fluxes is extremely rare event and is observed only during strong magnetic storms (*see Kuznetsov et al, 2002*).

Detailed analysis of radiation belt particles dynamics based on CORONAS-F experimental data is presented in papers *Panasyuk et al, 2004; Kuznetsov et al, 2005*. This paper provides just the following observations.

Recent years a considerable progress in understanding of physical processes of filling with "new" electron belt particles during recovery phase was achieved. Most probably accompanied by particle acceleration up to relativistic energies radial transfer is connected with electromagnetic waves generation in the trapped region and its' subsequent interaction with electrons (*see for ex. Elkington et al, 2003*).

Concerning the question of appearance of "new" protons in the belt core during recovery phase of strong geomagnetic storms, it remains open. The process of proton pitch-angle scattering due to violation of adiabatic motion condition near the equatorial plane could play here a definite role (*see Kuznetsov et al, 1984*). However for protons with energies ~ 1 MeV this process is ineffective at L<3 and is improbable for particles of such energies.

As well the following question about sources of the particles filling inner zone of radiation belts during recovery phases remains open: what part of total source intensity consists of injected at outer L-shells SEP during initial phase of storm? Obviously most particles precipitate out of radiation belts right after the injection due to violation of adiabatic motion (*see Kuznetsov et al, 1984*). However some solar particles can be trapped and then be affected by radial diffusion into the belt. Definite answer to this question can be provided by modeling and simultaneous observations of radiation belt particles at high and low altitudes.

Conclusion

CORONAS-F satellite instrumentation system for energetic charged particles investigation gave new information about the nature of radiation storms in the near space. These are:

- ambiguous character of low-latitude boundary variations of SEP penetration in connection with Dst and Kp indices of geomagnetic activity variations;
- the existence of three different processes of trapped radiation dynamics in the near space that determine radiation environment during strong storms. These processes are:
- solar particles injection during initial phase of storm into the trapped radiation region, "emptying" of extensive outer radiation region during main and recovery phases of storm, and finally supplement with particles of outer radiation zone accompanied by acceleration and radial transfer of particles deep into the magnetosphere, and appearance of new proton radiation belt at low L-shells;
- complicated character of SEP penetration into magnetosphere not allowing to conclude about the identity of SEP flux time variations during magnetic storms at geostationary orbits and low-altitude polar orbits.

Acknowledgment

The authors thank the organizers of 2nd SEE symposium in Yerevan for the opportunity to present the solicited report.

REFERENCES

[1] A.S. Biryukov, T.A. Ivanova, L.M. Kovrygina, S.N. Kuznetsov, L. Tverskaya, E.N. Sosnovets, K. Kudela, *Space Research,* Vol. 21, 6, , p.897-906,1983

[2] I.S. Veselovsky et.al., *Space Research*, Vol.42, 5, p.453-508,2004.

[3] T.A. Ivanova, S.N. Kuznetsov, E.N. Sosnovets, L. Tverskaya, *Gemagn. and aeronomy,* Vol.,30, 6, p.8566-8580,1990,.

[4] S.N. Kuznetsov, K. Kudela, I.N. Myagkova, A.N. Podorolsky, B.Yu. Yushkov, *Astron. Vestnik*, Vol.5, 2005, p.256-261

[5] S.N. Kuznetsov, M.I. Panasyuk, V.D. Ilyin, E.N. Sosnovets, *Izvestiya AN USSR*, Vol.48, 11, 2200-2203, 1984

[6] M.I. Panasyuk et.al., *Space Research*, Vol.42, 5, 509-554, 2004.

[7] M.I. Panasyuk et.al., *Astron. Vestnik* Vol.5, 2005, p.278-284.

[8] S.R. Elkington, M.K. Hudson, A.A. Chan, Resonant acceleration and diffudion of outer zone electrons in an asymmetric geomagnetic field, *J. Geophys. Res.,* Vol.108, A3, 1116, 2003

[9] I.R. Horentxen., J.E. Mazar, M.D. Looper, J.F.Fennel, J.B.Blake, Multi satellite observations of MeV ions injected during storms, *J. Geophys. Res.,* Vol.A9, SMP.71711, 2002

[10] G. Morfill, M Scholer, Study of the magnetosphere using energetic solar particles, *Space Sci. Rev.,*Vol..15., p. 267-353, 1973

Calculation of the Threshold Energies for Aragats Solar Neutron Telescope

A.Chilingarian, L.Melkumyan, A.Reimers

Cosmic Ray Division, Alikhanyan Physics Insitute, Yerevan, Armenia

The Aragats Solar Neutron Telescope (SNT) is in operation at the Mt. Aragats research center (3200 m. above sea level) in Armenia and constitutes part of the world-wide network, coordinated by Nagoya University. In this paper we calculate the response function of the SNT to the galactic cosmic rays and determine the energy thresholds of the four SNT channels. Results of Monte–Carlo simulation and experimental calibration are compared. The capability of SNT to select different energetic populations of the primary particles is demonstrated taking as example very severe geomagnetic storm at 20 November 2003.

Introduction:

The sun influences earth in different ways by emission of radiation, plasma and high energy elementary particles and ions. Although the overall energy fraction of the high energy particles is very small compared with visible light energy, nonetheless, the study of these particles gives clues not only about fundamental and universal processes such as shock acceleration, but also provides timely information on the consequences of the huge solar explosions affecting the near-earth environment and space born and surface technologies, the so called Space Weather issues [1].

Charged particles travel and reach the Earth by way of the "best magnetic connection paths", which is not a straight line between their birthplace and the earth. The solar neutrons on the other hand, not influenced by solar and interplanetary magnetic fields, reach earth directly from their place of birth on the solar disc. This feature allows us to "map" the flare location and provide the "time stamp" of the neutron production making them excellent "probes" of solar accelerators. For this reason we need to detect the solar neutrons, distinguish them from other incoming particles, measure their energy, and determine their incoming direction. The first step to achieve these enhanced possibilities of neutron detection was to establish the network of Solar Neutron Telescopes (SNT) [2], installed at seven locations on high mountains around the world, forming the second international world-wide particle detector network, the Neutron Monitor (NM)[3] network being the first.

The large variety of solar modulation effects and the stringent limitations of space and surface based experimental techniques require new ideas for developing experimental techniques for measuring the changing fluxes of the elementary particles. New type of particle detectors with enhanced flexibility to precisely and simultaneously measure changing fluxes of different secondary particles with different energy thresholds will be key to better understanding of the sun. Establishing a new world-wide network of such detectors, at low to mid latitudes will give possibility to measure solar proton and ion energy spectra up to 50 GeV, as well as, provide cost-effective possibilities for Space Weather research.

Each type of secondary particles corresponds to different population of "parents" (the primary ions at the top of the atmosphere) initiating the showers that reach the detectors. We use Monte Carlo simulation and calibration provided by MAKET-ANI Extensive Air Shower detector [4] to obtain the characteristics of the measurement channels of the Aragats Solar Neutron Telescope (SNT) [5].

Our simulations demonstrate that the energy distributions of the primary protons which give rise to different charged and neutral particles as secondaries in the atmosphere are shifted from each other. Thus, measuring fluxes of different particles with various energy thresholds we can estimate the energy spectra of the highest energy solar ions. To do this we have to understand the detector response function on different particles. For each of the detector channels, we have to determine the efficiency and purity of the detected particles (neutrons, protons, mesons, electrons, muons, gammas). We use the GEAN3 [6] and CORSIKA [7] simulation codes for modeling the traversal of particles in the detector and atmosphere respectively. We also perform a calibration experiment with the muons and electrons of the Extensive Air Showers incident on the thick (60 cm.) and thin (5cm.) scintillators of the SNT for the validation of the simulation codes. By attaching photomultipliers to the registering channels of the MAKET-ANI experiment[2,3], located in the same building as the SNT and measuring actual count rates of the SNT, it is possible to estimate the energy releases in the 4 different energy threshold discriminating detector channels of the SNT. The Monte Carlo simulation method of determining the primary proton energy and flux is consistent with the experimentally achieved results.

Solar Neutron Telescope

The main purpose of the world-wide network of the Solar Neutron Telescopes (SNT) is to detect the very rare and interesting events of primary neutrons directly from the Sun. Starting from 1996 the group from the Solar-Terrestrial laboratory of Nagoya University has coordinated the world-wide network of solar neutron telescopes located at 7 longitudes uniformly distributed around the Earth. At least 2 neighboring detectors of this network can see the sun disc simultaneously as the earth makes its 24 hour spin around its own axis [2]

Acceleration of protons and ions on the sun is associated with the reconnection of the intense magnetic fields on the sun surface. Moving along magnetic loops, ions reach the loop roots and interacting with dense solar plasma, give birth to copious particles including relativistic neutrons. In some circumstances, which are not completely understood yet, the flux of neutrons is so intense that neutrons are detected by space born and surface detectors [8]

If the magnetic loops open due to ejected coronal plasma, the ions accelerated in the same episodes and moving along the magnetic lines connecting the sun and earth, reach the earth's magnetosphere. If the particles have enough energy to enter the magnetosphere and generate a shower of secondary particles in the atmosphere, then some of these secondary particles (including protons, neutrons, mesons,

electrons and gamma rays) can be detected by the particle detectors on Earth's surface.

The Aragats Solar Neutron Telescope (SNT) in Armenia is a part of the world-wide network of Solar Neutron Telescopes. The Aragats SNT is formed from 4 separate identical modules, as shown in Figure 1. Each module consists of standard slabs of 50x50x5 cm^3 plastic scintillators stacked vertically on a 100x100x10 cm^3 horizontal plastic scintillator slab (60 cm total thickness). One meter above the thick lower scintillator slab is another scintillator slab 100 x 100 x 5 cm^3, with the goal to register charged particles. A scintillator light capture cone and Photo Multiplier Tube (PMT) are located on the bottom and top slabs separately to measure the number of events in each of them. This collection constitutes one module. The SNT has 4 such modules arranged on a 2 m x 2 m footprint.

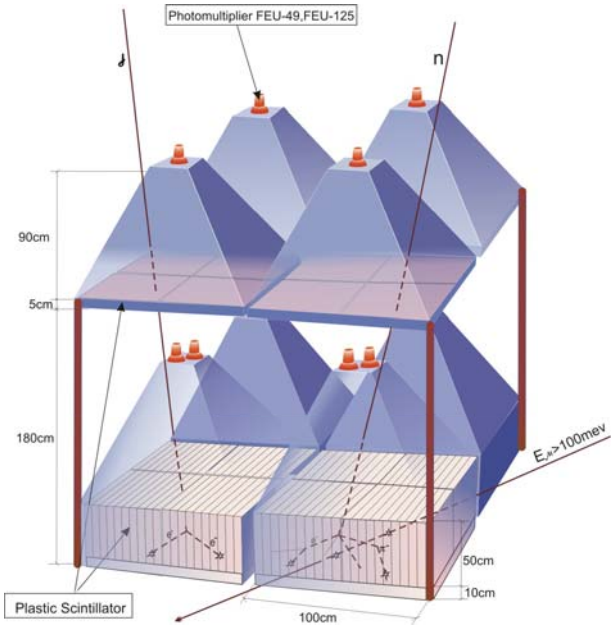

Fig.1. Aragats Solar Neutron Telescope.

Incoming neutrons undergo nuclear reactions in the thick plastic target and produce protons and other charged particles. The intensity of the scintillation light induced by these charged particles has a dependence on the neutron energy and is measured by the PMT on the scintillators. To get rough information about the incident neutron energy, we discriminate each PMT output signal according to 4 predetermined threshold settings (50, 100, 150, 200 mV) in the data acquisition electronics (4 measurement channels per module, 16 for the entire A-SNT).

In the upper 5 cm thickness of the scintillator plastic, the neutrons do not effectively interact with the scintillator nuclei. Thickness of the lower 60 cm layer is enough to produce photon emission due to the neutron interactions with the scintillator. In contrast charged particles are very effectively registered both by the upper thin 5 cm and the lower thick 60cm scintillators. When a neutral particle traverses the top thin (5cm) scintillator, typically no signal is produced. The absence of signal in the upper scintillators, coinciding with signal in the thick lower scintillators, points to neutral particle detection. When coincidences of the top and bottom scintillators register, it is possible to roughly estimate the direction of the incoming charged particle. Directional information is very useful for registration of the, so called, Ground Level Enhancements (GLE), when solar ions generate secondaries in the atmosphere with enough energy to reach to and be registered by the SNT. GLE events are usually very anisotropic and the directional information provides additional clues to understanding the origin and spectra of solar ion beams.

The light intensity produced in the scintillator is proportional to the energy release in the scintillator, which is related to the type of particle and its energy incident on the scintillator, and which in turn is related to the type and energy of the parent (primary) particle. To quantify all these relations and statements made above about detection of the different types of particles by the SNT modules, we need to perform detailed simulation of the detector response function.

Monte Carlo Simulation of SNT Response

To obtain a realistic detector response function we perform calculations with the CORSIKA Monte Carlo simulation code [7]. Using CORSIKA the simulated cascade of the secondary charged and neutral particles was followed down to the altitude of 3200m altitude, where the Aragats Solar Neutron detector is located. The threshold energies for the primary particles assumed as input for CORSIKA correspond to the rigidity cutoff of the location – 7.56 GV. All secondary particles were tracked until their energy drops below a predetermined value (50 MeV for hadrons, 10 MeV for muons and 6 MeV for electrons and photons) or reached all the way to the ground level. The spectra of primary protons and helium nuclei (99% of the flux at energies up to 100 GeV) are selected to follow the proton and helium spectra reported by CAPRICE98 balloon-borne experiment [9].

Among different species of secondary particles, generated in nuclear-electromagnetic cascades in the atmosphere, muons, electrons, γ – s, neutrons, protons, pions and kaons were followed with CORSIKA and stored. These particles were used as input for the GEANT3 package [6], used for detector response simulation. The secondary particles, their energies and angles of incidence obtained from the CORSIKA simulations allow us to develop a "particle generator", which takes secondary particles from the simulated "data bank" and generates those that would reach the top of the detector, and simulate the distribution of the energy release in the detector. Additionally we, also, take into account the light absorption in the scintillator.

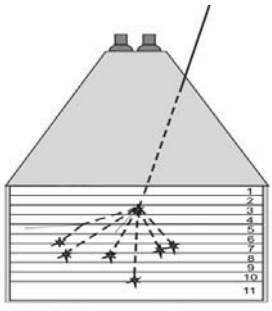

Fig.2. The division of the thick scintillation detector into 11 layers.

TABLE 1. Fraction of light intensity reaching the PMT from each layer (in %).

Scintillator layers	Light output(%)
1	89.3
2	73.96
3	61.31
4	50.1
5	40.96
6	33.64
7	27.56
8	22.56
9	18.92
10	15.6
11	11.5

The lower plastic scintillator slab in the SNT with the dimensions of 100x100x60 cm^3 consists of eleven 5-cm horizontal layers and one 10 cm layer as shown in Figure 2. The attenuation of the light intensity was calculated according to the absorption coefficients from "Light-collection in scintillation counters" by Tsyrlin J.A. [10]. The percent of flux reaching the PMT from the bottom of all 11 layers are depicted in Table 1.

In this paper we shall use the term **registered energy release** to mean the energy release as measured by the PMT, without the correction for the attenuation of light within the thick scintillator. The total energy release in the thick scintillator, which is obtained by correcting the PMT signal for the intensity lost we shall call the **genuine energy release**.

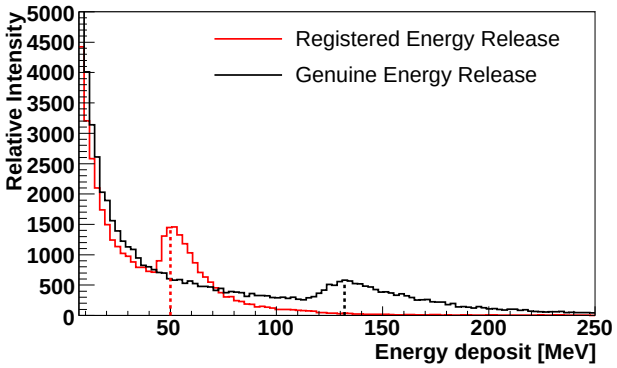

Fig.3. Histogram of Energy releases in 60 cm scintillator.

For each particle, traversing through the scintillator, we store the registered and genuine energy releases. The mode of the energy release spectra, depicted in Figure 3 changes from ~50MeV (registered) to ~130MeV (genuine) when taking into account the attenuation of light in the scintillator. As the zenith angle distribution of the incident particles pikes at 22°, we can assume that the mode of the distribution of energy releases corresponds to a single muon traversing the detector at the zenith angle of ~ 22°. We also assume that the left–hand of distribution is caused by $\gamma-$s and low energy electrons and muons stopping in the thick scintillator, or by higher energy charged particles which hit the detector at large zenith angles and traverse only part of

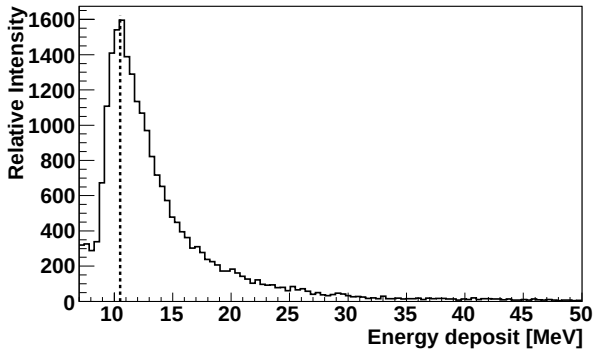

Fig.4. Simulated Energy release in the thin 5 cm upper scintillator of the SNT.

scintillator thickness.

For the 5 cm upper scintillator of the SNT which has it's own separate PMT, the light attenuation will be not greater than ~5%. The uncertainties of the modeling and the experiment errors are as minimum twice larger, and, therefore, for this paper we neglect the light absorption in the thin upper scintillator of the SNT. The mode of the energy releases distribution in the thin 5 cm upper scintillator of the SNT is ~10.75 MeV as shown in figure 4.

Experimental calculation of the threshold energies

After performing the simulation and obtaining the distribution of the genuine energy releases in the SNT, we compared the modeled and measured distributions. To make this comparison, we first have to calibrate the scintillator and PMT response to well known incident particle energy releases in previously proven instrumentation. To perform the calibration of the scintillator and PMT response, we used histograms of the energy releases when the secondary particles, initiated in the terrestrial atmosphere by protons and ions of the Galactic Cosmic Ray (GCR) flux, pass through the MAKET-ANI array [6], at the same geographic location as the Aragats SNT. The registering channels of the MAKET-ANI surface array measure Extensive Air Showers (EAS), initiated by the high energy primary protons or nuclei incident on the atmosphere known as Galactic Cosmic Rays (GCR). The GCR flux, incident on the Earth's atmosphere, has rather stable and well established parameters, although the low energy component intensity varies slightly (inversely proportional to the intensity of the solar activity) throughout out the 11-year solar cycle. These variations are insignificant for our goals and are ignored in the calculations presented here. The density of charged secondary particles can reach tens of thousands per m^2, therefore the logarithmic Analog-to-Digital Converters (ADC) are used to transform the PMT signal to a digital code and store on the on-line PC. The ADC is fabricated and tuned in such way that the digital code K, generated by the ADC, is proportional to the logarithm of the PMT signal amplitude:

$$K = \mathrm{int}\{d \cdot \ln A_{pmt}\} + c \qquad (1)$$

where A_{PMT} is the PMT signal amplitude and d is the scale factor, the so called decrement, c is the constant. The ADC is tuned with special electronics such that the decrement d ~ 10. The "registering channel" assembly, which includes the PMT and the ADC, and the on-line PC, which was tuned for the MAKET-ANI array, was transferred to the 60 cm thick scintillator of the SNT.

The histogram of the ADC codes (K) in figure 5 demonstrate pronounced peaks (distribution modes) corresponding to the energy release of a single traversing muon (or electron) through the scintillator. The position of the peak is dependent on the value of the high voltage applied to PMT. The PMT high voltage needs to be low enough so as not to amplify the PMT inherent noise, and high enough to maintain detector efficiency. The procedure for selecting the appropriate compromise includes dependencies of the particular PMT, and in our case we selected 1770 V which corresponds to $K = 5.5$ as the mode of the histogram of the registered codes, the so called "one particle spectrum" in the thin 5 cm upper scintillator of the MAKET-ANI. As it is seen from the Figure 5, for the same "registering channel" assembly, the mode code K=21 for the 60-centimeter thick scintillator, which means that the single particle registered energy release mode code generated by the ADC is shifted from 5.5 to 21 while traversing the 60 cm thick scintillator.

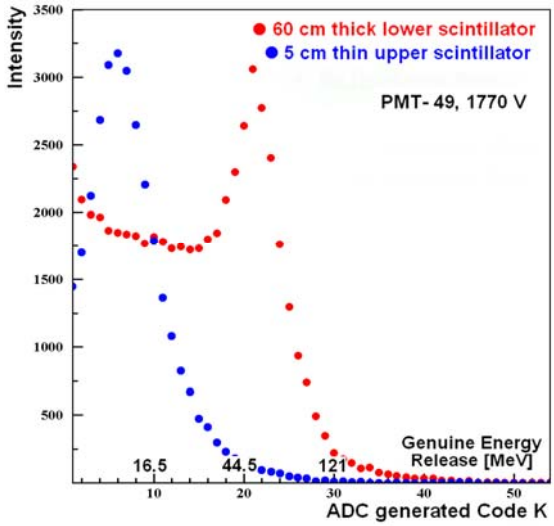

Fig.5. Energy release spectra in 5 and 60 cm scintillators, using the same measuring channel with identical settings.

This shift in the mode of the ADC generated code means that on average the amount of light reaching the photocathode of PMT from a single muon traversing the thick 60 cm scintillator is 4.7 times more, than the amount of light reaching the PMT from a single particle traversing the 5 cm scintillator. Assuming that the ADC provide linearity in the interval [0<K<~90], we can write

$$K_{60} - K_5 = d \cdot \ln\left(A_{60} / A_5\right) \qquad (2)$$

where d = 10, and the ratio of the amplitudes $A_{60}/A_5 = \exp\left(K_{60} - K_5/10\right) = 4.7$. We conclude that the amount of light released by the ionization of muons in the 60-cm scintillator is also ~ 4.7 times more than in the 5 cm scintillator. Accepting that the most probable energy release in the 5-centimeter scintillator equal to ~10.75 MeV [13], it is possible to calculate the most probable energy deposited by a near-vertical muon transiting through the thick scintillator is ~ 50.5 MeV. On the other hand, the average energy release from a single particle, under the condition of perfect transparency of the 60 cm thick scintillator, should be 12 times more than in the 5-cm think scintillator assuming the particle is energetic enough not to come to a stop in the scintillator. In other words, the PMT should measure 12 times more light intensity on the thick scintillator or the code K_{60} should be equal to 31, and not 21, indicating that the light collection from the 60 cm thick lower scintillator is 2.6 times less than expected (a 10-point difference between codes corresponds to ratio of amplitudes of 2.6). Thus, if one takes into account absorption of light in the thick scintillator the most probable energy release should be ~ $50.5 \cdot 2.6 \approx 131$ MeV. In this way we find the relation between the 2 scales (codes and genuine energy releases) using the position of the distribution (histogram) modes in measured and modeled distributions of the energy releases.

The calibration procedure we used for obtaining the "energy scale" of the PMT counts can be justified by comparing the histograms of the measured genuine energy releases and modeled energy releases. As we can see in Figure 6 the two are in very good agreement and we can pose the question of how to determine the energy thresholds.

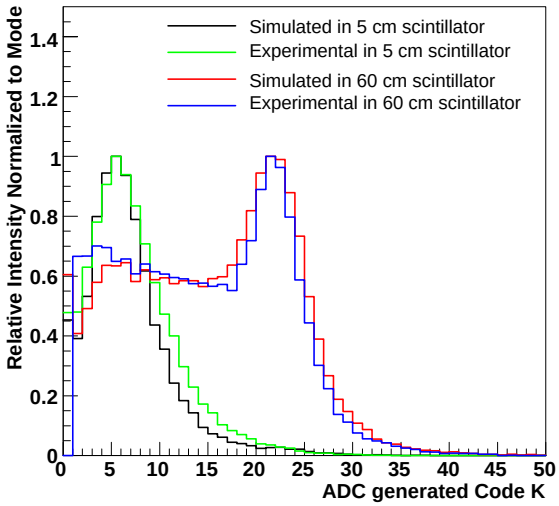

Fig.6. Comparison of modeled and measured energy releases in 5 and 60 cm. scintiullators.

Proceeding from experimentally measured count rates, we determine the corresponding energy thresholds in the 4 discrimination levels of the Aragats SNT measurement channels, by numerically integrating the histograms of each genuine energy release. We use experimentally measured intensities in each of the 4 discriminating channels (I = 228, 54, 16, 6 counts/sec). Obviously, the first (lowest energy) discrimination level has the largest intensity and the forth (highest energy) discrimination level has a rather small intensity.

By summation of histogram channels from some fixed channel (low limit of integration limit) to the right (till the maximal energy release) we can obtain the intensity of events which energy releases exceeds chosen low limit of integration. The particular value of the energy threshold is obtained by shifting the low integration limit till the sum of the higher channels coincides with the correspondent intensity. Figure 7 illustrates the method. For example to fit to the intensity I = 228 counts/sec we started the summation

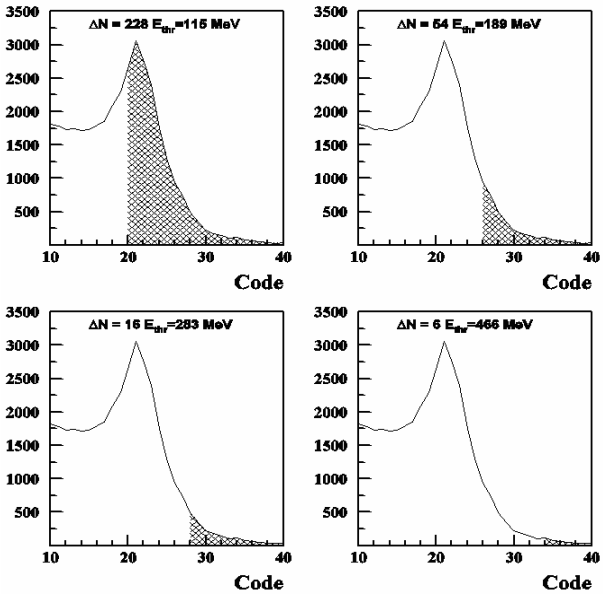

Fig.7. Illustration of the technique of obtaining thresholds of SNT. The dashed regions corresponds to 4 thresholds.

TABLE 2

SNT energy thresholds for registered and genuine energy releases of particles through the 60 cm scintillator.

№ of threshold levels	Simulated mean value of count rate [particles./min]	Simulated mean value of threshold energy for registered energy release [MeV]	Simulated mean value of threshold energy for genuine energy release [MeV]	Experimental value of threshold energy for registeredl energy release [MeV]	Experimental value of threshold energy for genuine energy release [MeV]
1	13683	48	121.9	46	119
2	2870	81	205.2	83	217
3	810	128	339.9	113	293
4	348	193	540.6	186	483

of histogram channels from code K=20 (119 MeV). For other 3 discrimination levels the energy thresholds were determined in the similar way.

We perform calculations with 10 independent model genuine energy releases distributions to estimate the statistical errors. The results of the calculations for registered and genuine energy releases are summarized in Table 2. Even though we can see from Figure 6 that the model and measured histograms coincide rather well, we made the calculations of the thresholds using both measured and experimental histograms. Table 2 also includes the results of to the registered energy releases, however only the genuine energy releases have physical meaning.

Both the experimentally measured and the simulated distribution of the energy releases give very similar values for the energy thresholds. The largest difference between experiment and simulation is in the most energetic forth threshold and can be attributed to the low intensity of the 4-th discrimination level and consequently the low statistics and large errors of numerical integration.

Calculation of the efficiency and purity of neutrons detected by the SNT

Secondary fluxes of cosmic rays (mostly muons, electrons, neutrons and gammas) are influenced (modulated) by the short periods of the solar activity. Protons and ions accelerated at sun during violent explosions (Solar Cosmic Rays – SCR) form an additional to the all-times existent Galactic Cosmic Ray (GCR) flux. In mean that approximately once in year Solar Energetic Particles (SEP) have enough energy to penetrate terrestrial atmosphere and generate cascades extended enough to reach Earth surface and be registered. These, very rare events, so called Ground Level Enhancements (GLE) are well pronounced at high latitudes in polar regions; at middle latitudes where ASEC monitors are located the count rate enhancements are not large, usually 1-2 percents. Physical inference on the GLE origin and operation of the solar accelerators heavily depend on the determination of the spectral and temporarily characteristic of the beams of solar particles incident on the terrestrial atmosphere. Only neutron monitors, due to modest sizes and low efficiency and, also, due lacking of energy resolution can not provide information about most interesting very low fluxes of relativistic particles above 5-6 GeV. Muons and electrons are tested more energetic primary particles comparing with neutrons, therefore it is vitally important to know the response function of SNT to neutrons and charged particles. Different thresholds of SNT are selecting particles in different proportions, i.e. provide different purities. We can use count rate enhancements and correlations of different channels of SNT with neutron monitors to test different populations of primary ions and, consequently, understand much more about the highest energies (>10 GeV) of the GLE events.

The efficiencies of registration of neutrons for all 4 thresholds are plotted in Figure 8.

As we can see from the figure the first channel (threshold) has efficiency ~24% for the 300 MeV neutrons, the efficiency of 4-th channel to detect 300 MeV or lower energy neutrons is near 0. At the same neutron energies the

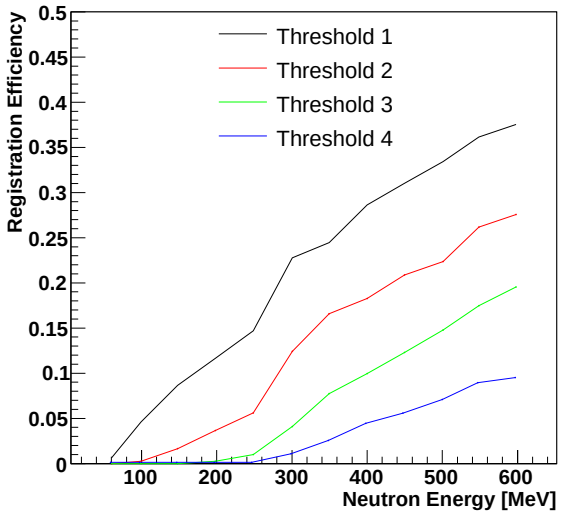

Fig.8. Efficiency of registration of the neutron by different SNT channels depending on the neutron energy.

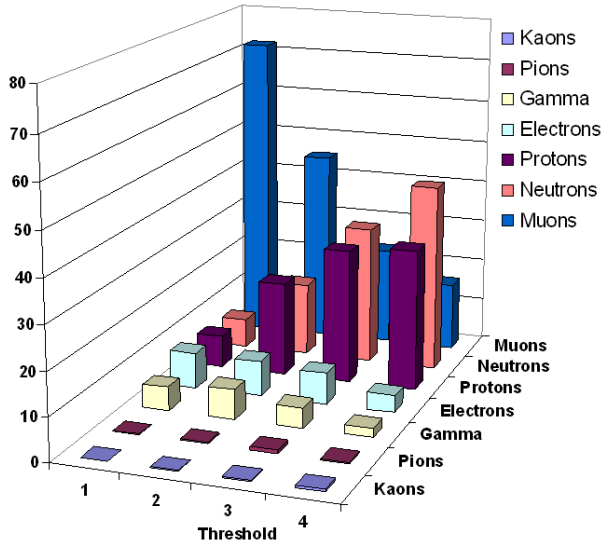

Fig.9."Purity" of selected events by the SNT channels

TABLE 3

The fraction of different particles registered by the SNT channels (in %)

№ of Thre-shold	Kaon	Pion	Gamma	Electron	Proton	Neutron	Muon
1	0.03	0.16	5.45	8.21	7.35	6.70	72.10
2	0.10	0.49	6.89	8.18	21.92	17.26	45.14
3	0.25	0.74	4.69	7.28	31.48	32.59	22.96
4	0.57	0.29	2.00	4.00	33.14	44.00	16.00

efficiency determined by the acceleration experiment for the Bolivian type of SNT (same as at Aragats) by the Nagoya university group [11] is approximately 18%. The difference can be explained by the greater thickness of the Aragats SNT – 60 cm. comparing with SNT used at Nagoya experiment – 40 cm. Consequently efficiencies of the other SNT channels are greater for the Aragats SNT.

In Figure 9 and Table 3 are posted the results on the proportion of different particles selected by the SNT channels. As we can see for the first threshold most of particles are electrons & muons (80%) and neutrons & protons only ~14%; for the 4-th channel situation is vice-versa electrons & muons (20%) and neutrons and protons (77%). This information is very important in treating the relative enhancements of SNT channels during the GLE and other solar modulation events.

Correlations of the count rates of SNT channels with particle energy.

In Figure 10 we compare the distributions of the incident neutron energies contributed to the count rates of the first and forth SNTchannels.

The simulated distributions are rather broad due to stochastic nature of particle interaction in the thick scintillator, but the apparent shift of the median energies pointed on the positive correlation of neutron energy with energy release in detector and, correspondingly, with number of SNT channel.

On the other hand, we know that more energetic primary cosmic rays can generate more energetic secondary cosmic rays. It means that registration of the secondary particles in different energy ranges give ability to investigate the different population of the primary cosmic ray and figure 10 demonstrate that ability.

In table 4 we present the correlation matrix for the monitors of Aragats Space Environmental Center

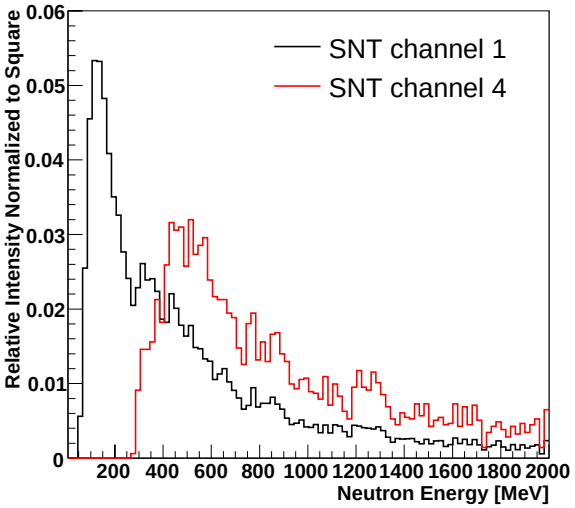

Fig.10. Energy distributions of the neutrons contributed to different SNT channels counts.

(ASEC)[12] during geomagnetic storm of 20–th of November 2003 from 14:50 to 19:10. We can see that correlations between Aragats Neutron Monitor (ANM), Nor-Amberd Neutron Monitor (NANM), and low energy secondary charged fluxes measured by 5cm detector of SNT (SNT e,μ) are very high ~ 0.9. During Geomagnetic storm (GMS) the Earth magnetic field usually prevent low-energy charged primary particles enter atmosphere and generate particle cascades is effectively reduced and some of low energy particles are entering atmosphere. Therefore, this enhanced flux of primary particles generates surplus of secondary particles. These additional secondaries are increasing flux of neutrons and low energy charged particles and consequently the correlation coefficients between these measurements are very large. To the contrary the correlations of mentioned ASEC monitors with high energy muon flux, measured by **A**ragats Multi directional Muon Monitor (AMMM**)** is rather small. It is because the secondary muons with energy higher than 5 GeV are generated by primary protons with energies ~15-20 GeV. These energies of primary particles are not influence by the geomagnetic storm and flux of high energy muons did not change coherently with change of neutrons and low energy charged secondaries.

From Table 4 we also can see that correlation of the neutron flux, measured by ANM and NANM and

TABLE 4

Correlation matrix for ASEC monitors daring geomagnetic storm of 20–th of November 2003 from 14:50 to 19:10.

	ANM	NANM	SNT e,μ	SNT Thr0	SNT Thr1	SNT Thr2	SNT Thr3	SNT Thr4	AMMM
ANM	**1.00**								
NANM	0.90	**1.00**							
SNT e,μ	0.90	0.88	**1.00**						
SNT Thr0	0.91	0.88	0.91	**1.00**					
SNT Thr1	0.83	0.82	0.83	0.88	**1.00**				
SNT Thr2	0.78	0.78	0.80	0.81	0.80	**1.00**			
SNT Thr3	0.65	0.65	0.65	0.64	0.67	0.76	**1.00**		
SNT Thr4	0.43	0.43	0.42	0.43	0.46	0.47	0.62	**1.00**	
AMMM	0.29	0.23	0.23	0.26	0.28	0.23	0.14	0.05	**1.00**

combination of neutral and charged particles measured by 4 channels of SNT (see Table 3 for details) is decreasing with increasing of number of channel (increasing of discrimination level).

It is demonstration of sensitivity of SNT detector channels to the energy of primary particles: higher SNT channels are "selecting" higher primary energies. Therefore the count rates of the SNT can be used for the reconstruction of the primary spectra of incident Solar Energetic Particle (SEP) flux during Ground Level Enhancements (GLE) registered by the ASEC monitors.

Conclusion

We perform calculations of the SNT detector response function, including determination of the energy threshold of the detector channels, efficiency of the registration of the particles of different type dependent at their energy. We also determine fraction of different particles "selected" by the detector channels. Obtained characteristics of SNT will be used in physical inference on solar extreme events detected by detector in 2003-2005 years.

Acknowledgement

Authors thank Zazyan Mary for providing CORSIKA simulation results of the Galactic Cosmic Ray traversal through the terrestrial atmosphere.

References

[1] J.Lilensten, J.Bornarel,(2006) Space Weather, Environment and Societies, Springer
[2] Matsubara, Y., and Muraki, Y., et al., Proc.of 26th ICRC, 6, 42, Salt-Lake-City, 1999
[3] H.Moraĺl, A.Belov, J.M.Clem, (2000), Design and Co-ordination of Multi-station International Neutron Monitor Networks, Space Science Reviews 93: 285-3003
[4] V.V. Avakian, E.B. Bazarov, et al., VANT. ser. Tech. Phys. Exp. 5(31)(1986) 1
[5] A.A. Chilingarian, et al., Proceeding of the 24th International Cosmic Ray Conference, Salt Lake City, vol. 1. 1999, p.240
[6] CERN 1993 GEANT3.21 Detector Description and Simulation Tool, CERN Progarm Library Long Writeups W5015[GEANT3, 1993
[7] Heck D. et al., Forschungszentrum Karlsryhe, FZKA Report 6019, 1998
[8] S.Shibata et al., Proceedings od 23-rd ICRC, Kalgary, 1993, v 3, p.95H.
[9] M. Boezio, V. Bonvicini, P. Schiavon, A. Vacchi and N. Zampa. "The cosmic-ray proton and helium spectra measured with the CAPRICE98 ballon experiment", arXiv:astro-ph/0212253, 1,11 (2002).
[10] Tsyrlin J.A., Light-collection in scintillation counters, Atomizdat, 1975 (in Russian)
[11] Tsuchiya et al., Detection efficiency of a new type of solar neutron detector calibrated by an accelerator neutron beam. Nuclear Instruments and Methods in Physics Research A 463 (2001) 183 – 193.
[12] A.Chilingarian for the ASEC team, (2005) Correlated Measurements of Secondary Cosmic Ray Fluxes by the Aragats Space- Environmental Center Monitors,NIM-A, 543, 483-496
[13] A.Chilingarian, et al., Study of Extensive Air Showers by MAKET-ANI detector on mountain Aragats. (in press)

The Extreme Cosmic Ray Ground Level Enhancement on January 20, 2005

R. Bütikofer, E.O. Flückiger, M.R. Moser, and L. Desorgher

Physikalisches Institut, University of Bern, Bern, Switzerland, rolf.buetikofer@phim.unibe.ch

In association with major solar activity in January 2005, the worldwide network of neutron monitors (NM) recorded several pronounced variations in the ground-level cosmic ray intensity. On January 20, 2005, the active region NOAA AR 10720 near the west limb produced an X7.1 solar burst with onset time at 0636 UT and peak time at 0652 UT. Less than 15 minutes after the observation of the flare onset the first relativistic solar particles arrived near Earth and a solar cosmic ray ground level enhancement (GLE) was recorded by the worldwide network of NM stations. This GLE is ranked among the largest in years with gigantic count rate increases at the south polar NM stations McMurdo (almost 3000 %) and South Pole (more than 5000 %). In the Jungfraujoch IGY NM 1-minute data the onset time of the GLE was at 0654 UT and reached a maximum amplitude of 11.4 %. From the recordings of the Swiss cosmic ray detectors and of the worldwide network of NMs, we determined the characteristics of the solar particle flux near Earth. For the evaluation of the asymptotic directions and the cutoff rigidities of the NM locations we used the Geant4 code MAGNETOCOSMICS. In the paper we discuss the method of analysis and present the obtained results.

Introduction

Between January 15 and 20, 2005, the solar active region NOAA 10720 produced five powerful solar flares. In association with this major solar activity several pronounced variations in the ground-level cosmic ray intensity were observed.

After a sudden storm commencement (ssc) on January 17, 2005, at 0748 UT the worldwide network of neutron monitors (NM) recorded a Forbush decrease (Fd). The IGY NM at Jungfraujoch, Switzerland (geogr. latitude: 46.55°N, geogr. longitude: 7.98°E; altitude: 3570 m asl; effective vertical cut-off rigidity Rc = 4.5 GV), observed a Fd with onset around noon GMT, and with a maximum amplitude of about -15 % as can be seen in Fig. 1. The Fd was associated with strongly enhanced geomagnetic activity.

Three days later, on January 20, 2005, i.e. still during the Fd, NOAA AR 10720 produced its fifth flare, an X7.1 solar burst with onset time at 0636 UT and peak time at 0652 UT. The flare position on the Sun was at 14°N, 67°W near the west limb, and therefore the Earth was well connected to the flare site along the heliospheric magnetic field (HMF) lines. Less than 15 minutes after the observation of the X-ray flare onset, the first relativistic solar particles arrived near Earth and a solar cosmic ray ground level enhancement (GLE) was recorded by the worldwide network of NM stations. This GLE is ranked among the largest in years with gigantic count rate increases at the south polar NM stations McMurdo (almost 3000 %) and South Pole (more than 5000 %).

The January 2005 GLE has a certain similarity with the GLEs on May 7, 1978, on October 24, 1989, on July 14, 2000, and on April 15, 2001. All these events occurred during a Fd.

From the recordings of the Swiss cosmic ray detectors and of the worldwide network of NMs, we determined the characteristics of the solar particle flux near Earth (spectral form, amplitude, pitch angle distribution).

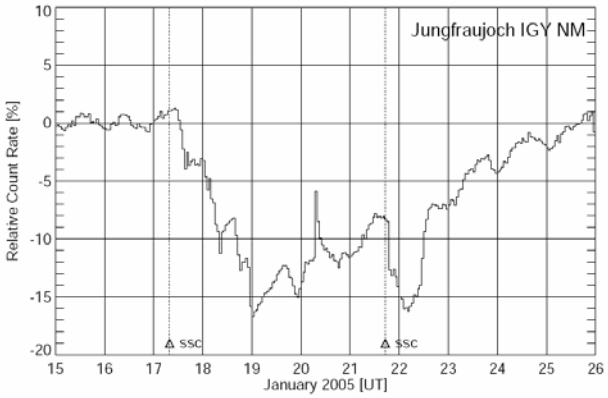

Fig.1 Relative pressure corrected hourly count rate of the IGY neutron monitor at Jungfraujoch for the time interval January 15-25, 2005.

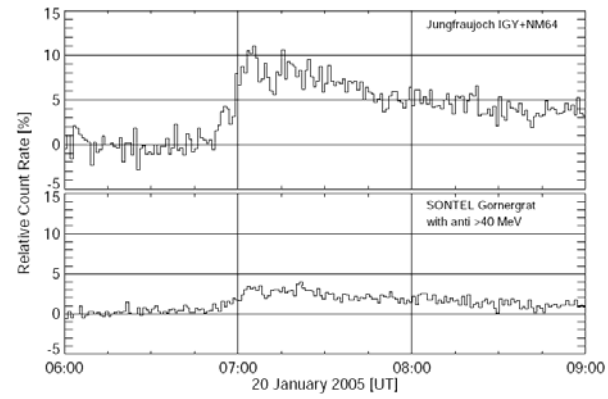

Fig.2. Relative pressure corrected 1-minute count rates of the NMs at Jungfraujoch (IGY + NM64 combined, above) and of the neutron channel >40 MeV of SONTEL at Gornergrat, Switzerland, (below) for January 20, 2005, 0600-0900 UT.

Measurements

Fig. 2 shows the relative pressure corrected counting rates of both Jungfraujoch NMs combined (IGY + NM64) and of the neutron channel >40 MeV of the Solar Neutron Telescope (SONTEL) at Gornergrat, Switzerland, [1,2] during the GLE on January 20, 2005.

Fig. 3 shows the GLE on January 20, 2005, as observed by the NMs at South Pole, Inuvik, Barentsburg, and Jungfraujoch. Fig. 3 clearly illustrates the complexity of this event. The station South Pole showed a dramatic, sharp increase of more than 5000 % after 0648 UT. The maximum count rate was reached very quickly, only 5 minutes after the GLE onset in the interval 0653-0654 UT. The onset time at the NM stations Inuvik, Barentsburg, and Jungfraujoch was 6-9 minutes later than at South Pole. The onset times of the worldwide grid of NM stations are listed in Table 1. The Inuvik NM recorded the maximum increase at ~0705 UT

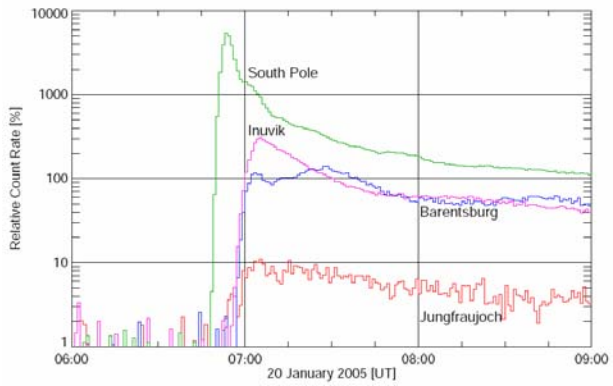

Fig.3. Relative pressure corrected 1-minute neutron monitor count rates of the NMs at South Pole, Inuvik, Barentsburg, and Jungfraujoch for January 20, 2005, 0600-0900 UT.

TABLE 1
Onset times for the January 20, 2005, GLE as recorded by the worldwide network of NM stations

Time [UT]	NM Station
0648–0649	South Pole, McMurdo, Newark
0650–0654	Apatity, Climax, Fort Smith, Hermanus, Irkutsk, Jungfraujoch, Kiel, Kingston, Larc, Lomnický Štít, Mawson, Moscow, Nain, Norilsk, Oulu, Tixie Bay, Yakutsk
0655–0657	Aragats, Barentsburg, Cape Schmidt, Inuvik, Magadan, Novosibirsk, Thule

when the count rate of the South Pole NM was only at ~20 % of its maximum increase, but still over 1000 % above the baseline of 0500-0600 UT. The NM at Barentsburg, Spitsbergen, showed a second peak around 0730 UT.
Both NMs at Jungfraujoch as well as other NM stations (Fort Smith, Irkutsk, Lomnický Štít, Newark, Novosibirsk, and Sanae) showed a significant pre-increase before 0657 UT, coincident in time with the maximum increase at South Pole. The neutron channels of the SONTEL detector at Gornergrat, however, did not show an increase at this time, as can be seen in Fig. 2. Therefore the possibility that the pre-increase was due to solar neutrons can be excluded; moreover, the zenith angles of the position of the Sun at the stations with a pre-increase were >75° at the time of the event.
On a global scale the GLE exhibited a pronounced anisotropy during the initial phase of the event and a complex intensity-time profile.

Method of Analysis

The records from 36 NM stations were used to determine the GLE parameters. The response of a NM to the anisotropic solar particles, ΔN(t), can be expressed according to Smart et al. [3] and Debrunner and Lockwood [4], by

$$\Delta N(t) = \sum_{P_c}^{\infty} S(P) I(P,t) F(\delta(P),t) \Delta P$$

where

P_c effective vertical cutoff rigidity
$S(P)$ specific yield function [5]
$I(P,t)$ solar particle intensity
$F(\delta(P),t)$ pitch angle distribution of solar particles
$\delta(P)$ angular distance between direction of vertically incident particles at the NM and direction of HMF near Earth

For the solar particle intensity near Earth a power law dependence on rigidity was adopted:

$$I(P,t) = A(t) \cdot P^{-\gamma(t)}$$

Using a trial and error procedure, the apparent source position, the functions I(P,t) and F(δ(P),t) can be determined by minimizing the difference between the calculated and the observed NM increases, ΔN(t).
For the evaluation of the asymptotic directions and the cutoff rigidities for each NM location, including effects of local time position and geomagnetic activity, the GEANT4 program MAGNETOCOSMICS [6] was used. The geomagnetic field was modeled by the IGRF [7] and by the Tsyganenko89 magnetic field model [8]. In addition we used for the analysis of this GLE the magnetosheath model by Kobel and Flückiger [9] for the first time to investigate the influence of the magnetosheath effect.
In Fig. 4 the asymptotic directions during the GLE on January 20, 2005, for the NM stations Barentsburg, Cape Schmidt, South Pole, and Thule according to the IGRF and Tsyganenko89 model are plotted. Fig. 4 also shows the asymptotic directions for the case that the magnetosheath effect is included in addition to the IGRF and Tsyganenko89 model.

Analysis

The aim of our analysis was to determine the GLE parameters during the initial and the main phase of the event. It can be assumed that the solar cosmic rays follow the HMF lines; therefore the apparent source position outside the Earth's magnetosphere is expected to correspond to the direction of the HMF near Earth. According to ACE [10] measurements the direction of the HMF near Earth during the initial phase of the GLE was in the region around 260°E and 80°S in the geographic coordinate system. However, it must be mentioned that the position of ACE is more than 200 Earth radii away from the Earth in the direction toward the Sun. Our analysis results in a slightly different apparent source

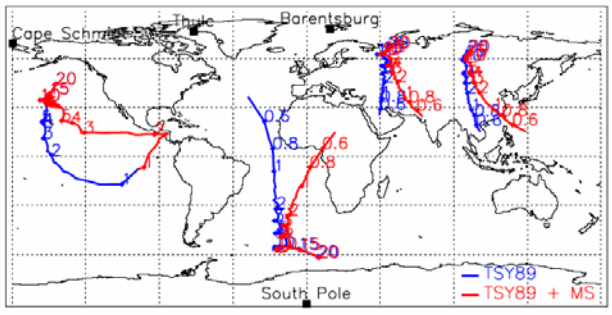

Fig.4. Asymptotic directions during the GLE on January 20, 2005, for the NM stations Barentsburg, Cape Schmidt, South Pole, and Thule according to the IGRF and Tsyganenko89 model (blue), and including in addition the magnetosheath effect (red). The numbers indicate the particle rigidity in GV.

position 300°-350°E and 50°-70°S during the initial phase of the GLE.

Fig. 5 shows a world map with the asymptotic directions of vertically incident cosmic ray particles at the NM stations with high count rate increases in the time interval 0655-0657 UT. The apparent source position and the direction of the HMF near Earth are also indicated, and contours are drawn for angular distances of 30°, 60°, and 90° from the apparent source position. The fact that only the two NM stations McMurdo (2644 %) and South Pole (3234 %) had a much higher count rate increase than all the other stations of the NM worldwide network (Nain 312 %, number three in the ranking of GLE amplitude) during this time interval implies that the pitch angle in the forward direction must have been very narrow. On the other hand, the NM station Apatity with asymptotic directions at pitch angles >90° had a relative count rate increase of more than 100 % in the time interval 0655-0657 UT, indicating that during the initial phase of this event a bi-directional flux near Earth must have already been present.

Conclusions

On January 20, 2005, almost at the end of the solar cycle 23, a giant solar cosmic ray GLE was observed by the worldwide network of NMs. As for several previous major GLEs, this event also occurred during a Fd. Its intensity-time profile is extremely structured. The initial pulse appears to be a pencil beam of particles, although soon after the start of the event a bi-directional flux was also present.

Fig. 6 shows the pitch angle distributions during the GLE on January 20, 2005, obtained from our analysis. This GLE was characterized by a very narrow pitch angle distribution during the first minutes of the event; but already some minutes later the anisotropy decreased clearly.

In Fig. 7 the spectral parameters for the assumed power law in rigidity are plotted as a function of time without and with the magnetosheath effect. The rigidity spectrum changed from very hard at the start of the GLE to a very soft spectrum within ~10 minutes, see also Bieber et al. [11]. However, it seems that after 0700 UT the spectrum was again somewhat harder. This may indicate a possible second population of solar cosmic rays that was accelerated during a second phase of the event [12,13].

The determined apparent source position differed mainly during the initial phase and mostly in the geographic longitude from the heliospheric magnetic field direction near Earth, as can be seen from Fig. 8.

From the results of this analysis it seems that the magnetosheath effect does not significantly influence the determination of the GLE parameters.

Acknowledgements

This research was supported by the Swiss National Science Foundation, grant 20-067092.01 and by the High Altitude Research Stations Jungfraujoch and Gornergrat. We thank the investigators of the NM stations from which we used the data for this analysis: Alma Ata, Apatity, Athens, Baksan, Barentsburg, Cape Schmidt, Climax, Erevan, Fort Smith, Hermanus, Inuvik, Irkutsk, Kerguelen, Kiel, Kingston, Larc, Lomnický Štít, Magadan, Moscow, Mawson, Mexico City, Nain, Norilsk, Novosibirsk, Newark, Oulu, Potchefstroom, Sanae, Thule, Tsumeb, Tixie Bay, Yakutsk. Discussions with E. Eroshenko and A. Belov are gratefully acknowledged.

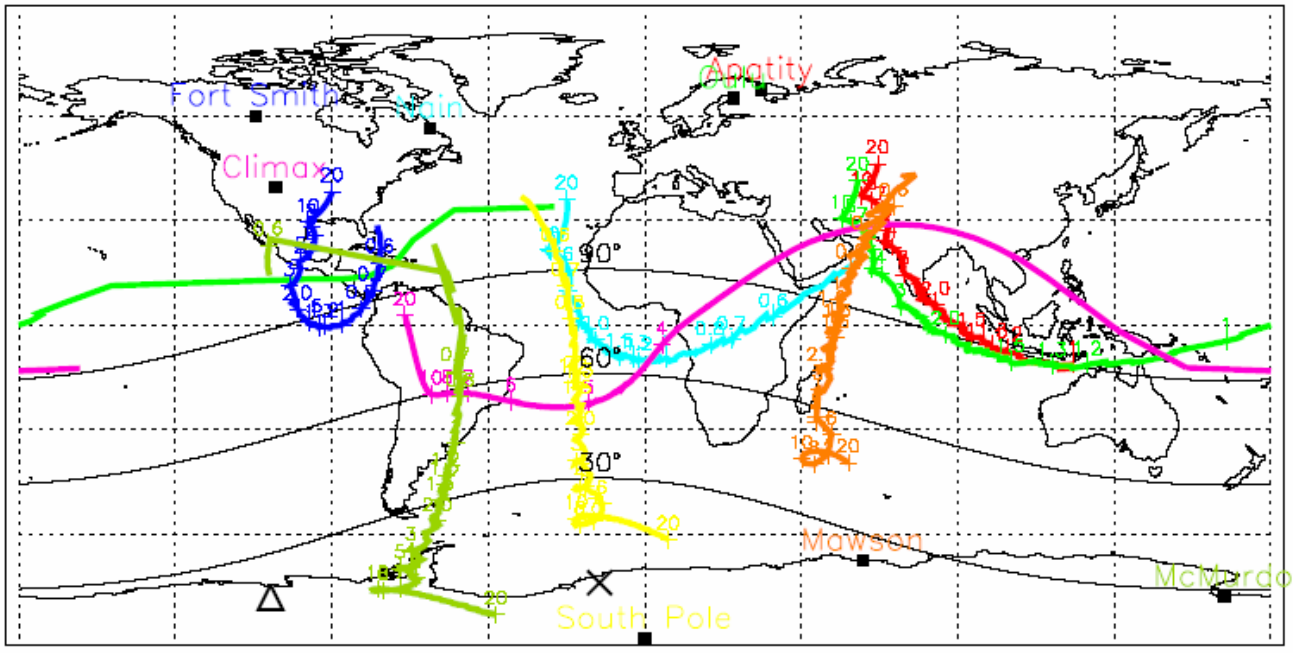

Fig.5. World map with asymptotic directions of cosmic ray particles with vertical incidence at the NM stations with high count rate increases in the time interval 0655-0657 UT. **x***: Indicates the apparent source position. The contours for angular distances are plotted for 30°, 60°, and 90°.* **Δ***: Indicates the direction of the HMF near Earth from the ACE measurements.*

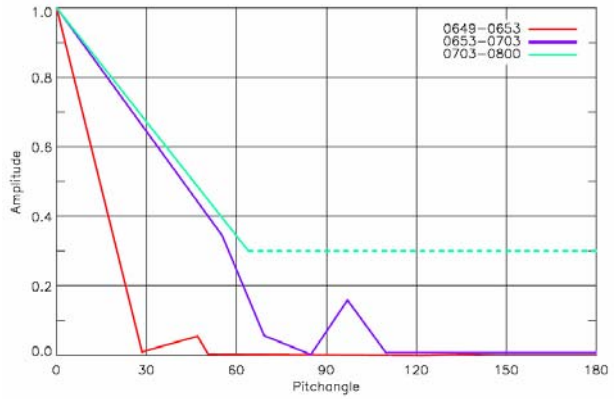

Fig.6. Pitch angle distribution for different time intervals (analysis including magnetosheath effect).

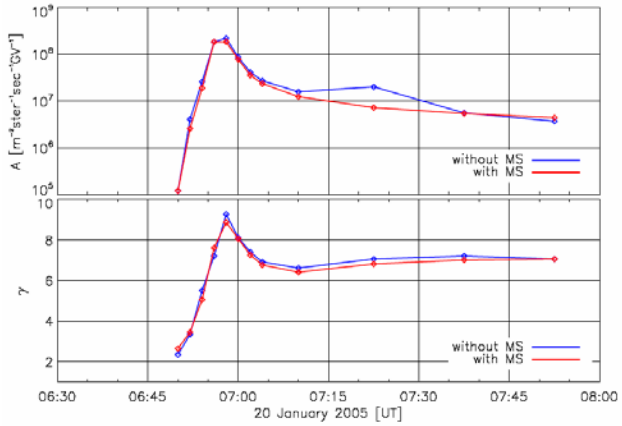

Fig.7. Parameters of the solar particle rigidity spectrum. Amplitude A (top) and spectral index γ (bottom) for the assumed power law in rigdity vs. time, without (blue) and with (red) magnetosheath effect.

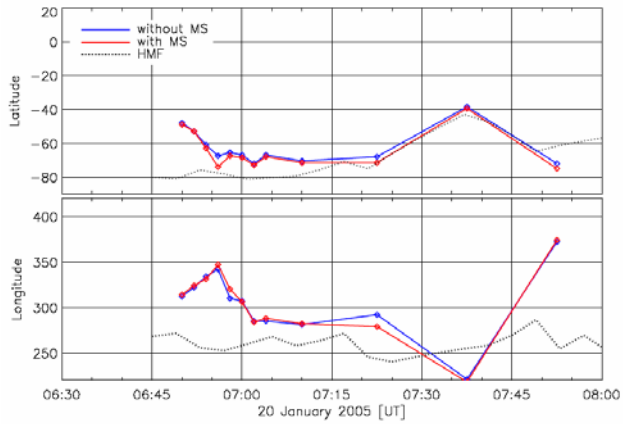

Fig.8. Apparent source positions without consideration of the magnetosheath (blue), including the magnetosheath effect (red) and direction of HMF(dotted lines) vs. time.

REFERENCES

[1] E.O. Flückiger, R. Bütikofer, Y. Muraki, Y. Matsubara, T. Koi, H. Tsuchiya, T. Hoshida, T. Sako, and T. Sakai, "A New Solar Neutron Telescope at Gornergrat", Proc. 16th ECRS, 1998, pp219-222

[2] R. Bütikofer, E.O. Flückiger, Y. Muraki, Y. Matsubara, T. Sako, H. Tsuchiya, and T. Sakai, "The Upgraded Solar Neutron Detector at Gornergrat", Proc. 27th ICRC, Vol.8, 2001, pp3053-3055

[3] D.F. Smart, M.A. Shea, and P.J. Tanskanen, "A Determination of the Spectra, Spatial Anisotropy, and Propagation Characteristics of the Relativistic Solar Cosmic-Ray Flux on November 18, 1968", Proc. 12th ICRC, Vol.2, 1971, pp483-488

[4] H. Debrunner, and J.A. Lockwood, "The Spatial Anisotropy, Rigidity Spectrum, and Propagation Characteristics of the Relativistic Solar Particles during the Event on May 7, 1978", J. Geophys. Res., Vol.85, A11, 1980, pp6853-6860

[5] H. Debrunner, E.O. Flückiger, E.L. Chupp, and D.J. Forrest, "On the Response of the Neutron Monitor at Jungfraujoch to the Solar Flare Neutron Event on June 3, 1982", (Abstract), 9th European Cosmic Ray Symposium, 1984

[6] L. Desorgher, http://cosray.unibe.ch/~laurent/magnetocosmics, 2005

[7] IAGA Division V, Working Group 8, Eos, Trans. AGU, http://www.ngdc.noaa.gov/IAGA/vmod/, 2005

[8] N.A. Tsyganenko, "A Magnetospheric Magnetic Field Model with the Warped Tail Current Sheet", Planet. Space Sci, Vol.37, 1989, pp5-20

[9] E. Kobel, and E.O. Flückiger, "A Model of the Steady State Magnetic Field in the Magnetosheath", J. Geophys. Res., 99, 1994, pp23617-23622

[10] E.C. Stone, L.F. Burlaga, A.C. Cummings, W.C. Feldman, W.E. Frain, J. Geiss, G. Gloeckler, R. Gold, D. Hovestadt, S.M. Krimigis, G.M. Mason, D. McComas, R.A. Mewaldt, J.A. Simpson, T.T. Rosenvinge, M.E. Wiedenbeck, "The Advanced Composition Explorer", Particle Astrophysics; AIP Conference Proceedings, Vol.203, 1989, pp 48

[11] J.W. Bieber, J. Clem, P. Evenson, R. Pyle, M. Duldig, J. Humble, D. Ruffolo, M. Rujiwarodom, A. Sáiz, "Largest GLE in Half a Century: Neutron Monitor Observations of the January 20, 2005 Event", Proc. 29th ICRC, 2005, in press

[12] A. Sáiz, D. Ruffolo, M. Rujiwarodom, J.W. Bieber, J. Clem, P. Evenson, R. Pyle, M.L. Duldig, J.E. Humble, "Relativistic Particle Injection and Interplanetary Transport during the January 20, 2005 Ground Level Enhancement", Proc. 29th ICRC, 2005, in press

[13] E.V. Vashenyuk, Yu.V. Balabin, B.B. Gvozdevsky, S.N. Karpov, V.G.Yanke, E.A. Eroshenko, A.V. Belov, R.T. Gushchina, "Relativistic Solar Cosmic Rays in January 20, 2005 Event on the Ground Based Observations", Proc. 29th ICRC, 2005, in press

Multidetector Correlation Study of Solar Transient Events

G.G. Karapetyan, A.A. Chilingarian

Cosmic Ray Division, Alikhanian Physics Institute,Yerevan, Armenia, gkarap@crdlx5.yerphi.am

Ground Level Enhancements (GLE), as measured by the low latitudes particle detectors are not well pronounced compared with detectors located at high latitudes due to higher geomagnetic cutoff rigidity of low latitude stations. Proceeding from the measurements of several particle detectors located at the Aragats Space Environmental Center (ASEC), we develop a methodology, which combines the data from 3 monitors to reveal solar transient events. Method utilizes correlation information from 3 detectors measuring neutrons on different latitudes and low energy charged particles. The product of 3 correlation coefficients (CC) between the time series of Aragats Neutron Monitor, Nor-Amberd Neutron Monitor and Solar Neutron Telescope gets large values when all three time series are changed similarly, otherwise the product fluctuates around zero. Thus, being a composite characteristic of three different monitors the product presents more pronounced indication of solar transient events – GLE, Forbush decreases (Fd) and geomagnetic storms (GS). Statistical distribution of the null hypotheses (H0 - no signal hypothesis), obtained by Monte-Carlo simulations, proves very low chance probability of "imitating" signal. Proposed method can find also numerous other application.

Introduction

Aragats Space Environmental Center (ASEC) [1] has the advantage to monitor cosmic rays (CR) fluxes simultaneously by several particle detectors. Neutral and charged secondary fluxes are initiated by primary Galactic and Solar Cosmic Rays (GCR – fully stripped ions, mostly protons and α-particles, SCR – protons and different isotopes of light and heavy atoms). In turn these particles (with energy up to a few hundreds of GeV) are influenced (modulated) by disturbances of the Interplanetary Magnetic Field (IMF) caused by solar activity. Huge clouds of magnetized plasma ejected during violent explosions on the Sun, are traveling in the interplanetary space with velocities up to 3,000 km/sec and interacting with ambient population of cosmic rays. Solar plasma and high energy particles accelerated by different mechanisms triggered by explosions on the Sun, are introducing anisotropy in the CR flux, those "modulating" primary and, consequently, secondary particle fluxes. The modulation effects of the "active" Sun are inducing so called, transient events, reflecting in coherent changes of the magnitude and direction of low energy secondary fluxes. At low latitudes, the changes of secondary fluxes are small, because of large cutoff rigidity. Excess in count rates due to GLEs detected by ASEC (cutoff rigidity ~7.6GV) usually don't exceed 1.5-2%. Meanwhile reliable detection of GLEs at low latitudes provides us with information about maximal energy of solar particles, which is missing in data of high latitude stations. Monitoring the event by several independent detectors compensates the lack of pronounced excess in each separate detector.

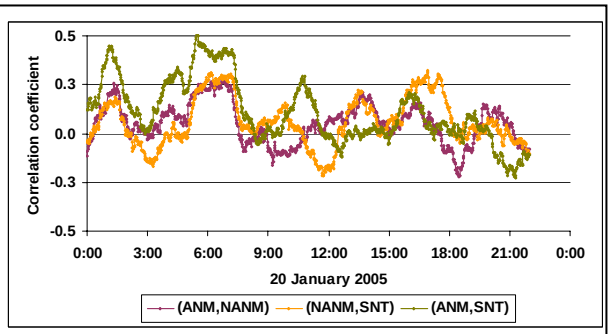

Fig.1. Time variation of 3CCs between (ANM,NANM), (ANM,SNT) and (NANM,SNT) during 20 January 2005

As we demonstrated earlier [2], the correlation coefficients between different secondary fluxes are good indicators of the space storms strength. For the magnifying of this effect we consider not one, but product of 3 correlation coefficients between Aragats Neutron Monitor (ANM), Nor-Amberd Neutron Monitor (NANM) and Solar Neutron Telescope (SNT). It is expected that using the data of multiple monitors, will enlarge signal-to-noise ratio, and the time variation of this product will indicate the periods of solar modulation more distinctly.

Product of 3 correlation coefficients

We compute correlation coefficients by using 1min data of the following pairs of monitors (ANM, NANM), (NANM, SNT) and (ANM, SNT). The correlation coefficients are calculated according to its definition [3] by "moving" 120 points, i.e. in 120 min interval of monitor time series by shifting interval to the right each time by 1 minute.

As it known, if there is perfect linear relationship between two variables, we have large correlation coefficient ~1; a correlation coefficient of ~0 means that there is no linear relationship between the variables.

In the absence of solar modulation data from all 3 monitors changes randomly by Poisson rule (which can be approximated very well by the Gaussian with mean and variance specific for each monitor). The mean count rate is determined by the value of flux of particles with particular energy threshold, by the detector surface and – detector response function. Variances are controlled by numerous random factors including stochastic nature of particle transport and detection, local changes of pressure and temperature, fluctuations of the power supply, etc. For example, mean count rates of ANM, NANM and SNT in time interval 5:00 – 7:00 20 on January 2005 are 2373, 1026 and 116716 per minute per square meter respectively. Corresponding standard deviations are 18, 11 and 364 so that their relative errors are 0.76%, 1.1% and 0.31% respectively.

We are interested in proving the existence of solar modulation and locating the time when it started.

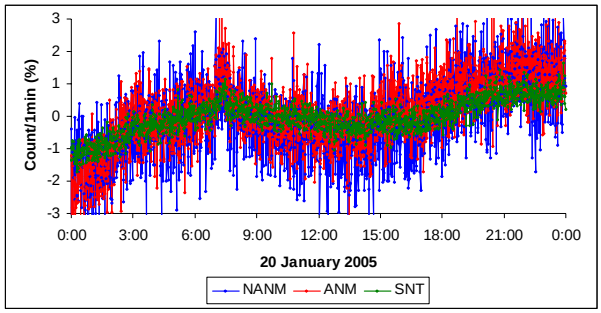

a)

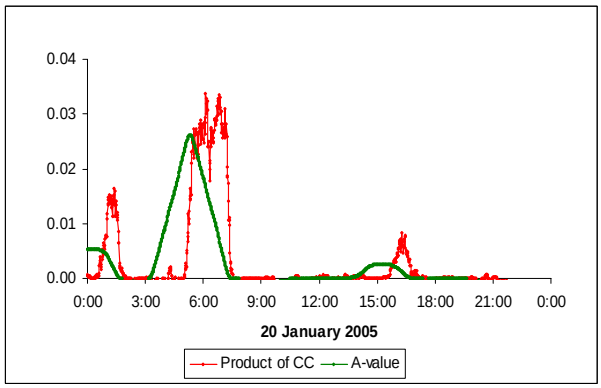

b)

Fig.2. Time variation of monitor's data (a), the product of CC and averaged product of CC (b) during 20 January 2005.

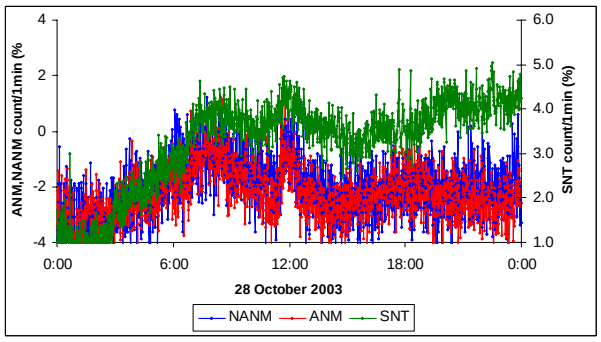

a)

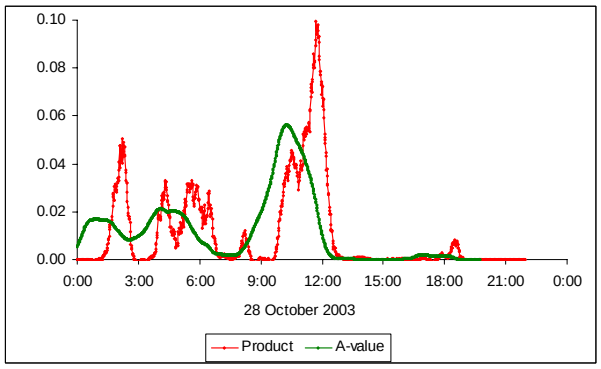

b)

Fig.3. Time variation of monitor's data (a), the product of CC and averaged product of CC (b) during 28 October 2003.

As usually in the statistical hypothesis testing we formulate so called zero hypothesis H0 (no solar modulation) and on the basis of calculated correlations we'll try to "reject" H0 with as much as possible power of confidence.

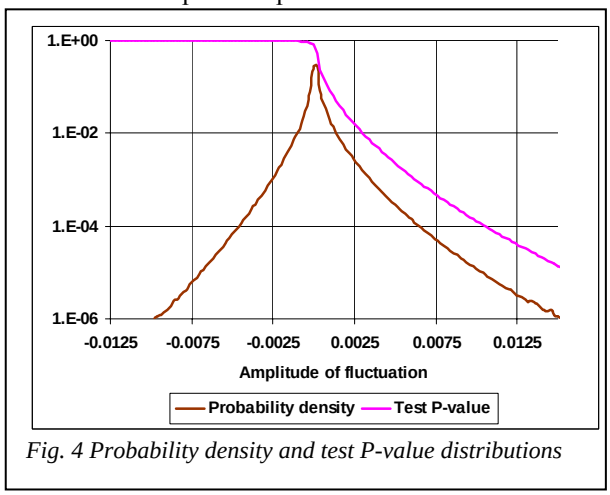

Fig. 4 Probability density and test P-value distributions

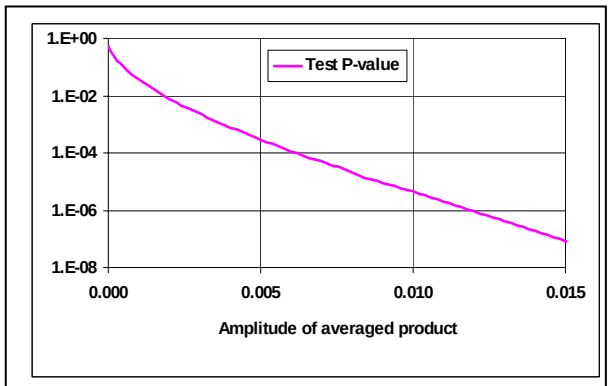

Fig. 5 Test P-value for averaged product.

Using single correlation is not effective because it has large random variations, masking the small changes due to the solar modulation effects (see Fig. 1). But in some time intervals, for example 5:00 – 8:00 of 20 January 2005, all three CCs simultaneously increase (or decrease). It means that in those intervals variation of monitor's counts is non-random. Just in such intervals the product of 3 CCs will get larger values than in other intervals where at least one of the CC is small. For this reason, we use the product of 3 CCs, rather than single CC. In Fig. 2, 3 time variations of 3 monitor's data and the product of CC are presented. It is seen that the product usually fluctuates around zero with standard deviation ~ 0.0001. However, sometimes the product gets larger values during ~ 0.5…2 hours. For example it gets the value ~ 0.03 during ~ 5:30 – 7:30, or ~ 0.015 during ~ 1:00 – 1:30 of 20 January 2005. To derive the probability that product surplus a given value, we performed Monte-Carlo simulation using 3 Gaussian time series mimicking 3 monitor's counts (each detector is modeled by Gaussian with specific mean and variance). Probability density of the product and test P-value are obtained under validity of H0 (see Fig. 4,5). Test P-value is determined as the probability to observe the product with greater than given value.

It is seen that probability distribution is not symmetric relative to zero; it means that the probability to obtain positive value of the product is larger than the probability of obtaining negative products. This asymmetry is the

feature of this approach, conditioned by cyclic procedure of CCs calculations. For this reason we plot only positive values of product because number of negative products is small and they have very small amplitudes.

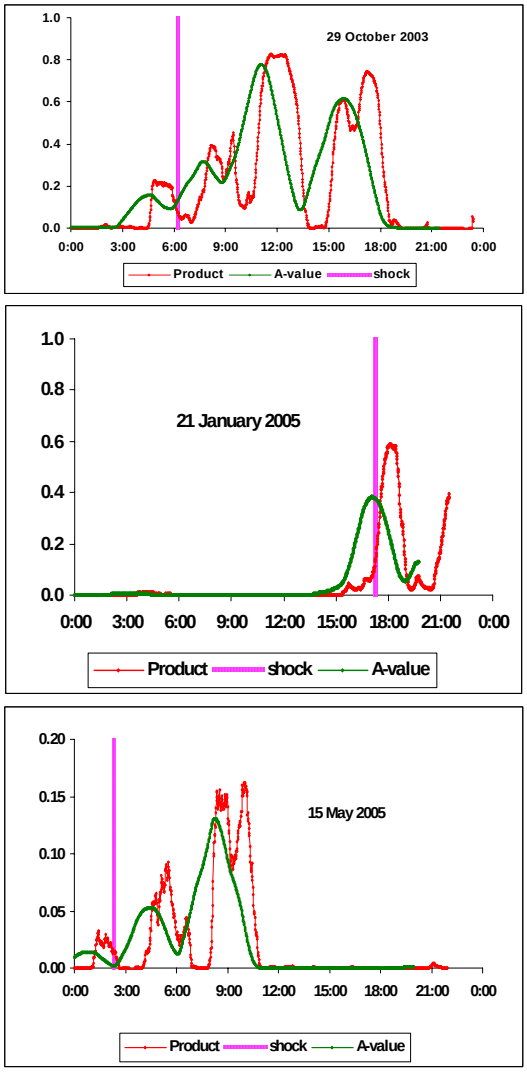

Fig. 6 Product and averaged product during different Fds: 29 October 2003, 20 January 2005 and 15 May 2005.

Using product of CCs as test value for checking the statistical hypothesis we should know the probabilistic distribution of its values under validity of H0.

As it is seen in Fig. 2, 3 enhancements of the product have rather long duration and one needs to have the probability of appearance of such continuous enhancements. For this purpose it is necessary to classify different fluctuations of the product by a parameter, which includes both the amplitude of enhancement and its duration. We introduced such a parameter (test statistics) as the averaged value of the product during 120 min interval, denoting it below as A-value or "averaged product". Time variations of averaged product are shown in Fig. 2, 3. Performing Monte-Carlo simulation for averaged product we obtain the probability to observe averaged product having amplitude greater than given, i.e. test P-value (see Fig. 5)

Study of events and discussions

Using obtained by Monte-Carlo A-test distributions one can estimate the probability of the appearance of rare fluctuations (chance probability). For example the enhancement at ~0:30 20 January 2005 has A-value ~ 0.005, and test P-value ~ 3×10^{-4}. The frequency of such fluctuation appearance per day is $3\times10^{-4}\times1440 \sim 0.4$.

Therefore this fluctuation can be considered as a random one. Analogously the fluctuation at 15:30 20 January 2005 has A-value ~ 0.003, so it also can be treated as random fluctuation. But fluctuation at ~1:30 28 October 2003 has A-value ~ 0.017 and considerably smaller test P-value, which is $< 10^{-7}$. The frequency of such fluctuation appearance per year is $10^{-7}\times1440\times365 \sim 0.05$, i.e. random fluctuation with such, or greater amplitude will appear once in ~20 years.

Analogously the enhancement at ~ 4:30 28 October 2003 we can't treat as random fluctuations, because it's A-value is ~0.02 and its test P-value is $< 10^{-8}$.

The chance probability of A-test for the GLE on 28 October 2003 (A-value 0.056) and GLE on for 20 January 2005 (0.026) have extremely small test P-values, comparing even with previously considered events.

Usually in neutron flux the enhancement due the GLE is ~3%, and in low energy charged particle flux only ~ 1.5%. Since ANM data has mean count ~ 2840 and MSD ~20, so 3% increase of ANM data during the largest amplitude GLE of 28 October 2003, corresponds to ~ 0.03/(20/2840) ~ 4.2 sigma, which gives test P-value ~1.2×10^{-5}. However test P-value for the product with averaged amplitudes ~ 0.026 or 0.056 (Fig. 1,2) is much smaller, as it follows from Fig. 4. Therefore time variation of the product pointed on coherent excess much more pronouncedly.

For scanning time-series in searching solar modulated events we need to establish some threshold value, above which we can treat enhancements as not random. For the A-test such level was chosen to be 0.015. The chance probability of random fluctuation greater than 0.015 is ~ 10^{-7} (see Fig. 4). If A-value of observed fluctuation is greater than 0.015 then such fluctuation is defined as not random (because frequency of appearance is 1 per ~20 years), but caused by an solar modulation. Proceeding from this level (~0.015) one can estimate the efficiency of detecting different kinds of events. For both of two GLE the A-value exceeded 0.015, so they were detected reliably.

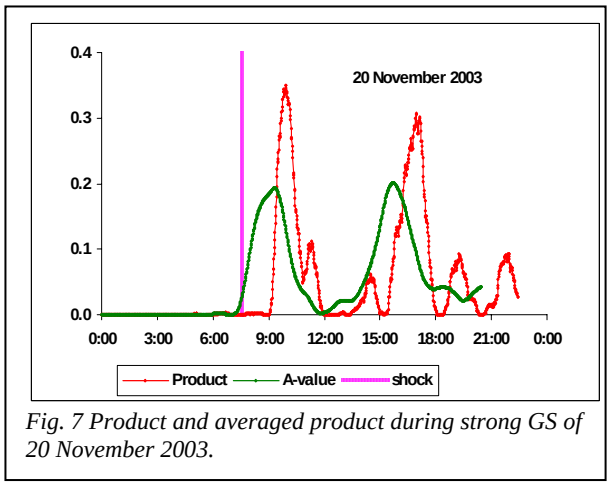

Fig. 7 Product and averaged product during strong GS of 20 November 2003.

Now let's consider averaged product distribution for the Fd and GS. In Fig. 6 there are presented A-values correspondent to the 3 Fds: 29 October 2003, 21 January 2005 and 15 may 2005. It is seen that A-values are even higher comparing with GLEs. For example for 29 Oct 2003 and 21 Jan 2005 Fd A-value surpasses 0.015 very much, being ~0.8 and ~0.4 respectively.

Analogously we considered big geomagnetic storm at 20 November 2003 (Fig. 7). Again CC product considerably surpasses the level of 0.015, providing extremely small values of probability of false alarm.

Thus in all considered 4 Fd and GS as well as 2 GLE events the A-value pointed on the event, considerably surpassing level 0.015. One can state that A-value reflects in general non-random changes in monitor's data caused by solar activity.

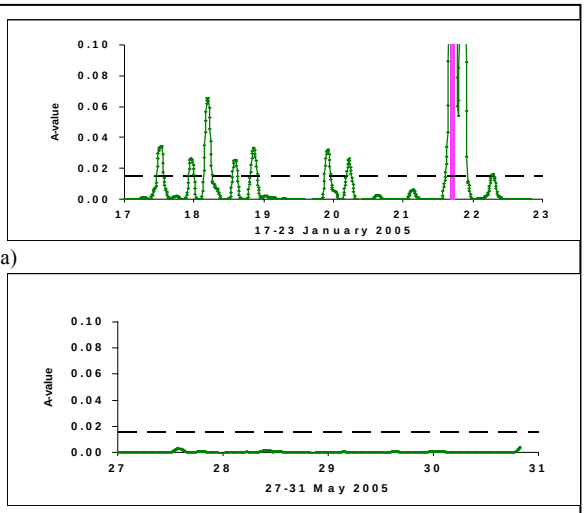

Fig.8 Averaged product during solar active period 17 – 23 January 2005(a) and during quiet period 27 – 31 May 2005 (b). Dashed line is 0.015 level, purple line represents the time of shock arrival.

For example during 17-23 Jan 2005 solar activity was high (Fig. 8a), heliosphere was filled with magnetized clouds, and solar wind brought strong and variable in time magnetic field, which cased Fds and GSs. All these events are reflected in averaged product, which gets values considerably surpassing the level 0.015. Opposite to it during quiet solar period, say 27-31 May 2005, A-value was negligibly small (Fig. 8b).

Conclusion

We propose a new method, to reveal weak signal in noise background. Unlike to existing methods, proposed method uses data of 3 independent detectors, which simultaneously monitor noisy signal.

As a result weak noisy signals are revealed with more confident level. In this paper we demonstrate efficiency of the approach in investigating solar induced changes in solar monitor's data. Proposed method is a general one, and it can be used in numerous other applications, where monitoring of noisy signal is carried out with 3 independent detectors. For example, it can be applied to detecting of gravitational waves (GW) by 3 different detectors placed in the USA and Europe. Arriving at Earth, the GW will induce the similar changes in time series of 3 independent detectors. Then A-value can reveal GW induced signal more reliably than it is capable to do single detector.

Big variety of solar transient events is reflected in different patterns of particle fluxes in vicinity of Earth. We have demonstrated the sensitivity of the product of 3 Correlation Coefficients, composed by using 3 monitors' data, to different types of events caused by solar activity: GLE, Fd and GS. The possibility of the early diagnostic of the expected hazard of geomagnetic or/and radiation storms using the correlation information on the changing fluxes of the ASEC monitors is under investigation now.

References

[1] A. Chilingarian, K. Avakyan et al.,"Aragats Space-Enviromental Center: Status and SEP forecasting possibilities" J *Phys. G. Nucl. Part. Phys.* Vol. 29, 2003, pp. 939-952.

[2] A. Chilingarian, K. Arakelyan et al., "Correlated measurements of secondary cosmic ray fluxes by the Aragats Space-Environmental Center monitors", *Nuclear Instruments and Methods in Physics Research,* Vol. A 543, 2005, pp.483-496.

[3] S. Brandt *Data analysis,* Springer, 1998.

Channel-to-Channel Analysis of Aragats Muon Monitor Detection of >5GeV Muons in 20 January 2005 Ground Level Enhancement

G.G. Karapetyan, A.A. Chilingarian, N.Kh. Bostanjyan

Cosmic Ray Division, AlikhanianPhysics Institute,Yerevan, Armenia, gkarap@crdlx5.yerphi.am

During the famous solar flare of 20 January 2005, the 3-min time series of the Aragats Multidirectional Muon Monitor (AMMM) demonstrated maximum muon count in excess of ~ 4σ at 7:02 UT. The probability that this excess is caused by random fluctuation is ~ 4.3×10^{-5}. We applied Binomial statistical analysis of excesses in each 42 independent detector channels. We estimate the probability that in n channels the count surpass the given level L, and then by changing L obtain minimal value of this probability. For example: using 3-min data we find that at 7:01 muon counts greater than 0.9σ is observed in 21 out of 42 channels, which leads to the probability about 3.1×10^{-6}, an order of magnitude less than the Gaussian chance probability. Thus the applied approach of analyzing the counts from each channel separately leads to lower value of probability of random fluctuation.

Introduction

On January 20, 2005 solar active region AR10720 produced the famous X7.1 flare, which was the strongest flare of the 23-rd cycle. The flare site (~60W solar longitude) was connected to Earth along the Parker spiral line of the interplanetary magnetic field. The NASA Geostationary Operational Environmental Satellite (GOES) detected onset of 4 – 700MeV protons flux simultaneously at ~6:50UT, with maximum at ~7:00UT [1]. The high energy protons produce muons when encountering the earth's atmosphere. Ground level enhancement (GLE) was observed by all neutron monitors around the world, with onset time between 6:50 – 7:00UT. The maximum count rate was reached at South Pole station (~5000%) during ~5 min after onset. Low latitude stations recorded smaller enhancements.

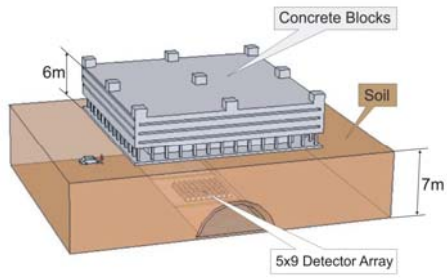

Fig.1 Sketch of Aragats Multidirectional Muon Monitor installation at 3200 m elevation

In present paper we investigate the response of Aragats Multidirectional Muon Monitor (AMMM) to this GLE. AMMM is one of the detectors of Aragats Space Environmental Center (ASEC) [2], which is capable to register high energy muons. It is installed on Mt Aragats, Armenia ($40^o30'$N, $44^o10'$E) at altitude 3200m asl. AMMM consists of 45 scintillation detectors, each with surface of 1 m^2, located in the underground hall (see Figure 1). The absorption in the 6m thick concrete blocks and 7m soil sets the energy threshold of registered muons ~ 5 GeV for vertically incident muons so that mainly muons with energies > 5 GeV can reach detector location. Total count rate of AMMM is ~ 130000 per minute; standard deviation is close to the Poissonian value ~360, so that relative error of one minute count is ~ 0.3%. Thus AMMM constitutes very sensitive muon monitor, rather robust to atmospheric condition and temperature.

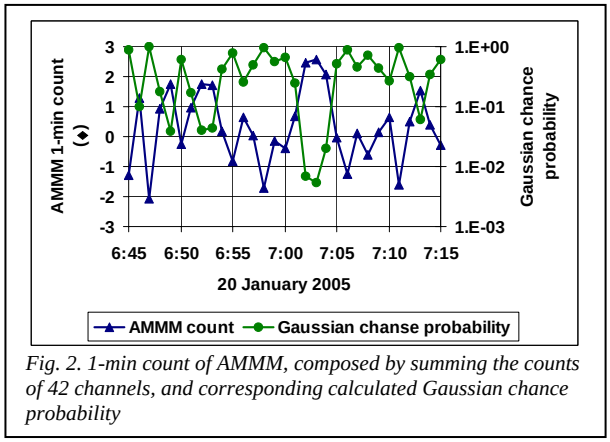

Fig. 2. 1-min count of AMMM, composed by summing the counts of 42 channels, and corresponding calculated Gaussian chance probability

Starting from commissioning in 2002 we were looking for the excess in ANMM count rates correlated with solar activity during GLE events of August 2002, October 2003, and January 2005. However, till 20 January 2005 no significant excess of 5 GeV muon flux was observed. At 20 January 2005 monitors of ASEC detected GLE onset at ~ 6:58UT, which corresponded to 10:58 of local time. AMMM data showed the excess with the peak at 7:03 (see Figure 2), which was considered as the candidate of GLE event in high energy muon flux. According to numerical calculations [3,4] muons with energies greater than 5 GeV are produced in atmosphere by protons of galactic cosmic ray having median energy ~50GeV, whereas solar protons, producing >5GeV muons have median energy ~ 20 - 25 GeV. Thus if observed excess was caused by solar protons, then it means that in solar flare 20 January 2005 protons were accelerated till 20 – 25 GeV.

Channel-to-channel analysis

At 20 January 2005, 42 out from 45 scintillators of AMMM was operating; summarized 1 min count rates of 42 scintillators in standard deviation units are presented in the Figure 2.

Mean count rate of the detector was calculated by averaging the counts in the time interval of 6:30 – 7:35 removing 5 points of interval 7:00 – 7:04 (the peak

candidate). As a result the mean value 123818 and standard deviation 352 was obtained; using of which we obtain 1 min count in units of standard deviation. Chance probability P(x) at given value of the peak counts x is defined as the probability that this or greater value is obtained by random fluctuation. Because of large count rate of AMMM, Poissonian distribution can be replaced by Gaussian one, as a result the chance probability is written as P(x) = 1 – F(x), where F(x) is Gaussian distribution function [5]. Computed values of P are presented in Figure 2 by green circles. Statistical significance of peak at 7:03 is about 2.5σ corresponding to chance probability P(2.5) = 6.2×10^{-3}. To increase statistical significance we rebin the time series in larger than 1min intervals. We group 1-minute time series in the 3-minute ones. To avoid arbitrariness of choosing the start of the time series we perform calculations for the 3 possible start points. Therefore, each point in the Figure 3a represents the 3 minute count rates shifted from each other by 1 minute. Such technique, called moving sum, suppresses the fluctuations and increases statistical significances of event peaks.

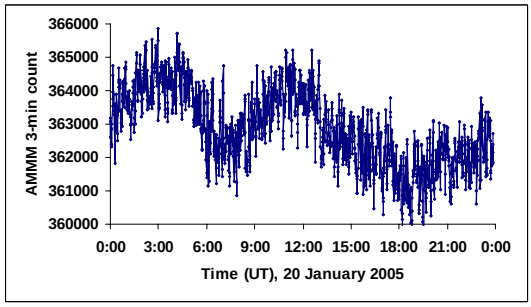

a)

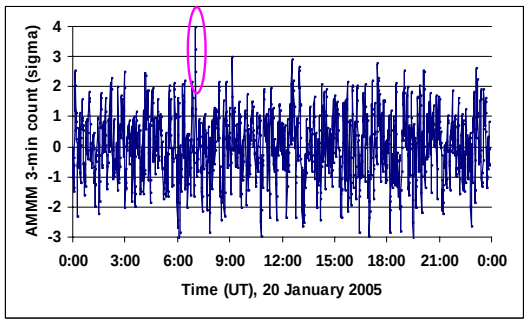

b)

Fig.3 3-min count of AMMM composed by summing 3-min counts of 42 channels (a) and the same count in units of standard deviation (b), when slow drift removed. Red oval outlines the counts 3.05σ, 3.93σ and 2.49σ, observed in time interval 7:01 – 7:03

Slow drift of counts, apparent in the Figure 3a is caused by solar modulation effects and diurnal variations of muon flux [6]. To remove this drift we calculate average values of count in 24 separate 1 hour intervals and obtain count variation in units of standard deviation (Figure 3b). The maximal excess of 3.93σ is seen at 7:02. Distribution of counts is well fitted by Gaussian distribution, so chance probability of this excess is computed by Gaussian distribution function and proves to be ~ 4.3×10^{-5}. Such an excess caused by random fluctuation rather than by solar event can appear once in every ~ $1/(1440\times4.3\times10^{-5})$ ~ 16 days.

This value is rather large to reject the assumption of random origin of observed peak. Below we apply another method of analysis of channel counts trying to use all information on the signal contained in detector channels.

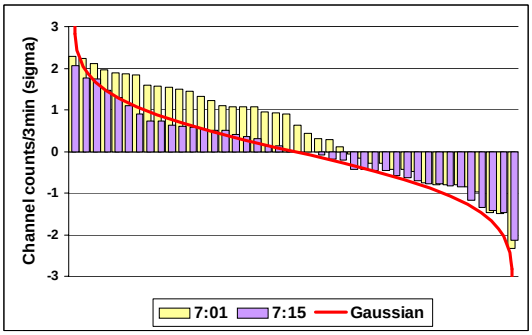

Fig. 4 Distribution of channel counts at 7:01 and 7:15. Red curve represents Gaussian random distribution

Distribution of channel counts in units of standard deviation σ, placed in descending order is presented in Figure 4. Red curve shows pure Gaussian distribution. It is seen that at 7:01 the counts in many channels essentially surpass Gaussian values, whereas at, for example 7:15 they are close to Gaussian random distribution. Such positively biased pattern of channel counts at 7:01 allows one to assume that it is caused by the additional flux of solar protons. For giving to this hypothesis probabilistic meaning one should calculate the probability of observing particular distribution of channel counts. Suppose that we set a level L, so the probability P(L) of observing in one channel the count greater than L is P(L) = 1 – F(L), where F(x) is Gaussian distribution function [5]. Then the probability of observing greater than L excess in n channels from N is given by binomial distribution [5]

$$b(n,N,P(L)) = \frac{N!}{n!(N-n)!}P(L)^n(1-P(L))^{N-n} \quad (1)$$

and the probability of observing greater than L excess in n, or n+1, or n+2…or N channels is given by the sum

$$B(N,P(L)) = \sum_{i=n}^{N} b(i,N,P(L)) \quad (2)$$

where N = 42.

Changing L we find minimal value of B(n,N,P(L)), denoting it below as B_{min}. Doing this procedure each minute in time interval 6:45 – 7:15 we obtain time variation of B_{min}, presented in Figure 5 along with Gaussian chance probability. For example: at 7:01 B_{min} is obtained when setting the level 0.9σ, then 21 channels is observed above this level (see Figure 4) so B_{min} proves to be 3.1×10^{-6}.

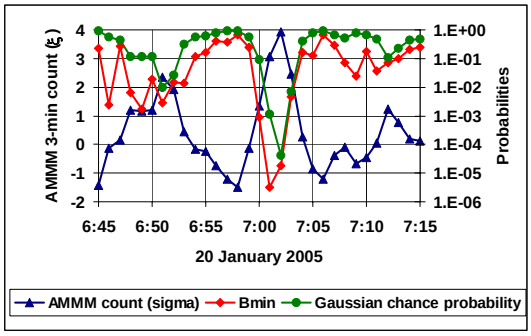

Fig. 5 Comparison of Gaussian chance probability (green) and B_{min} (red)

From Figure 5 one can see that these two probabilities are compatible; both related to the peak interval of 7:01 – 7:03. Gaussian chance probability gets the minimum value 4.3×10^{-5} at 7:02 when count excess reaches its maximum 3.93σ, whereas B_{min} gets its minimal value ~ 3.1×10^{-6} at 7:01.

Conclusion

We studied AMMM count during solar flare 20 January 2005 by using more detailed analysis of channel counts than traditional Gaussian method utilizing their sum. Applied channel-to-channel analysis investigates distribution of channel counts by computing the probability to observe several number of channel counts surpassing given value of statistical significance. Obtained value of B_{min} (3.1×10^{-6}) is ~ 14 times smaller than Gaussian chance probability.

References

[1] ACE News #87 –Feb 23, 2005, Space Weather Aspects of the January 20, 2005 SEP event.
[2] A. Chilingarian, K. Avakyan et al.,"Aragats Space-Enviromental Center: Status and SEP forecasting possibilities" J Phys. G. Nucl. Part. Phys Vol. 29, 2003, pp. 939-952.
[3] A. Chilingarian, K. Arakelyan et al., "Correlated measurements of secondary cosmic ray fluxes by the Aragats Space-Environmental Center monitors", Nuclear Instruments and Methods in Physics Research, Vol. A 543, 2005, pp.483-496.
[4] M. Zazyan, A. Chilingarian. "On the possibility to deduce solar proton energy spectrum of the 20 January 2005 GLE using Aragats and Nor-Am,berd neutron monitor data", Solar Extreme Events. International Symposium, Nor-Amberd, Armenia.2005
[5] S. Brandt Data Analysis, Springer, 1998
[6] M.L. Duldig, "Muon observations", Space Science Reviews Vol. 9, 2000, pp. 207-226.

Magnetic Clouds and Major Geomagnetic Storms

K.Georgieva[1], B. Kirov[2]

[1] Solar-Terrestrial Influences Laboratory, Bulgarian Academy of sciences, Sofia, Bulgaria, kgeorg@bas.bg
[2] Solar-Terrestrial Influences Laboratory, Bulgarian Academy of sciences, Sofia, Bulgaria, bkirov@space.bas.bg

Abstract. *It is known that the most intense geomagnetic storms in both minimum and maximum sunspot activity are caused by coronal mass ejections (CME's). We study the major geomagnetic storms (Dst<-100) during the last solar cycle and demonstrate that the solar drivers of almost all of them are not CME's in general but magnetic clouds, a subclass of CME's distinguished by a smooth magnetic field rotation. The main factor determining whether a CME will be a magnetic cloud is the helicity in its source region on the Sun which depends on the amount of helicity transferred from the solar interior, and on the surface differential rotation. The sign of the helicity transferred from the solar interior into the corona is independent of the solar magnetic cycle, and is always negative in the north, and positive in the south (hemispheric helicity rule). Emerging magnetic flux tubes carrying helical magnetic fields are subjected to the solar differential rotation which can additionally twist or untwist the field lines, depending on the sign of helicity which it creates. We check the helicity in the magnetic clouds – drivers of major geomagnetic storms whose source regions have been identified, and find that out of the 12 cases when the hemispheric helicity rule is violated, in 10 cases the differential rotation in the source region is reversed (higher angular velocity at higher latitudes).*

Introduction

Richardson et al. [1] studied the sources of geomagnetic storms over nearly three solar cycles (1972-2000) and found that the most intense storms at both solar minimum and solar maximum are almost all associated with CME's, weaker storms are preferentially associated with high speed solar wind from solar coronal holes at solar minimum and with CME's at solar maximum, and slow solar wind generates a small fraction of the weaker storms at solar minimum and maximum.

Our previous studies [2] have shown that the sources of the most intense geomagnetic storms are nor CME's in general but magnetic clouds – a subclass of CME's distinguished by low plasma temperature or low plasma beta (the ratio of the magnetic pressure to the plasma pressure) and enhanced magnetic field with smooth rotation inside the structure. Fig.1 and Fig.2 compare the geomagntic disturbances caused by an average CME and an average MC as expressed by the Kp and Dst indices, respectively. The figures are superposed epoch analyses of the daily average values of Kp and Dst indices on days of the event (day 0), one day before and after the event (days -1 and +1, respectively), etc. This study covers the period 1997-2002 in which we have 73 MC's from [2] completed by the events from http://cdaw.gsfc.nasa.gov/ geomag_cdaw/. For the CME's we use the list of Richardson and Cane [1] from which all events identified as MC's have been removed, which leaves us with a total of 128 cases.

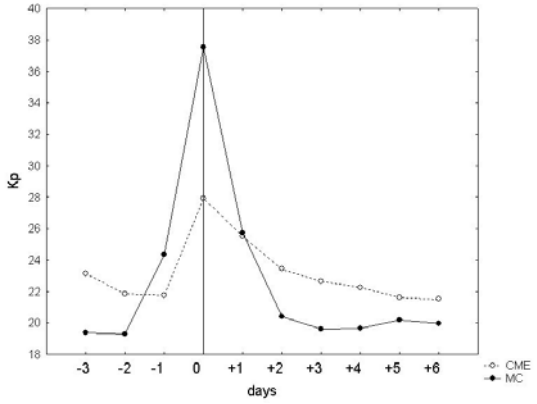

Fig.1. Superposed epoch analysis of average daily Kp index on days with MC's and CME's in the period 1997-2002.

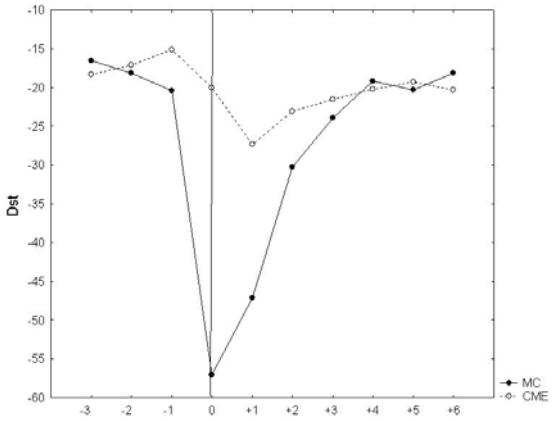

Fig.2. Superposed epoch analysis of average daily Dst index on days with MC's and CME's in the period 1997-2002.

The geoeffectiveness of both CME's and MC's as expressed by the Kp index follows the sunspot cycle, and in all phases of the ctcle MC's are more geoeffective than CME's (Fig.3).

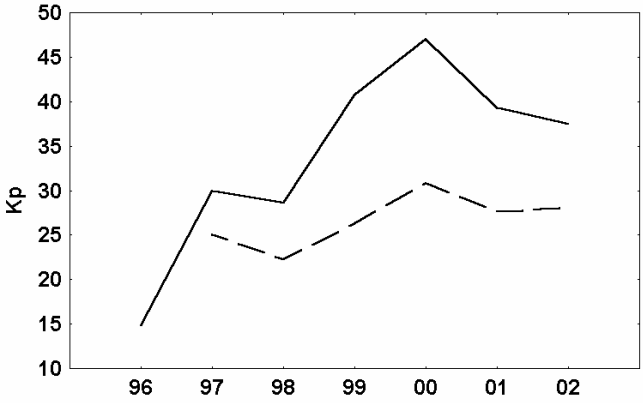

Fig.3. Yearly averaged Kp index for geomagnetic disturbances caused by MC's (solid line) and CME's (broken line)

The geoeffectiveness of MC's as expressed by the Dst index is strongly solar cycle dependent, while the average Dst index for disturbances caused by CME's which are not MC's practically doesn't change (Fig.4). Therefore, the sunspot cycle variations of the CME's reported in previous studies in

which CME's have not been divided into MC's and non-MC's [4] are due to the sunspot cycle dependence of MC's.

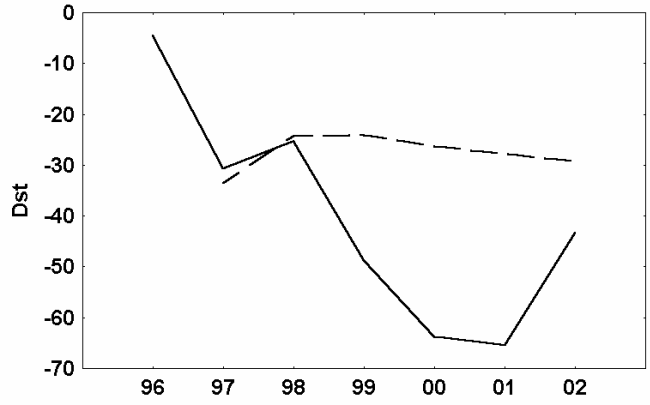

Fig.4. Yearly averaged Dst index for geomagnetic disturbances caused by MC's (solid line) and CME's (broken line)

The main factor determining the geoeffectiveness of MC's are the prolonged periods of negative Bz provided by the magnetic field rotation (Fig.5). Therefore, the magnetic field rotation is of great importance for the geoeffectiveness of these solar drivers. This magnetic field rotation depends on the helicity contained in the corona.

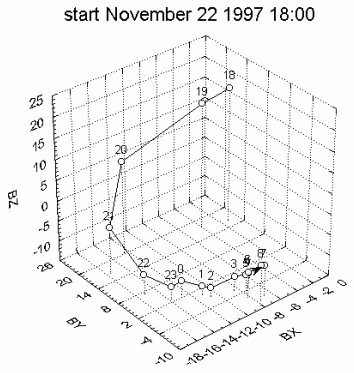

Fig.5. Rotation of the magnetic field in a magnetic cloud

Helicity in magnetic clouds

The amount of helicity in the corona depends on 2 factors: the net helicity transferred from the solar interior into the southern and northern corona [5], and the surface differential rotation which can increase or reduce, or even reverse the twist of emerging magnetic tubes [6].

Helicity transfer from the interior

The net helicity transferred from the solar interior into the northern corona is given by [5]:

$$\frac{dH_{CN}}{dt} = -\frac{\Omega_0}{2\pi}\Phi^2$$

where $\boldsymbol{H_{CN}}$ is the net helicity from the solar interior into the northern solar hemisphere, $\boldsymbol{\Omega_0}$ is the solar equatorial rotation rate (considered constant), and

$$\Phi = \pi R_\nu^2 B_1$$

is the net dipole flux through the northern photosphere. The expression for the southern hemisphere is with a positive sign. As the net dipole flux is maximum in sunspot minimum and minimum in sunspot maximum, the net transferred helicity has maximum positive values in the southern hemisphere and maximum negative values in the northern hemisphere around sunspot minimum, and is close to zero in both hemispheres around sunspot maximum (See Fig.3 in [5]).

Surface differential rotation

In the corona, the emerging flux tubes are subjected to differential rotation [6]:

$$\Omega(\varphi) = \Omega_0 + b \sin^2\varphi$$

where $\boldsymbol{\Omega(\varphi)}$ is the rotation rate at latitude $\boldsymbol{\varphi}$, $\boldsymbol{\Omega_0}$ is the equatorial rotation rate, and b is the latitudinal gradient of the rotation rate; $\mathbf{b}<0$ so that the equator rotates faster than the higher latitudes. Fig.6 illustrates the dependence of the rotation rate on latitude derived from observations. The grid of the data used for the calculation of the rotation velocities averaged over one Carrington rotation is available online at http://wso.stanford.edu/synoptic. html and consists of 30 equal steps in sine latitude from 75.2 North to 75.2 South degrees and 5 degrees step in the heliographic longitude. The details of the calculations of the rotation velocity are described in [7].

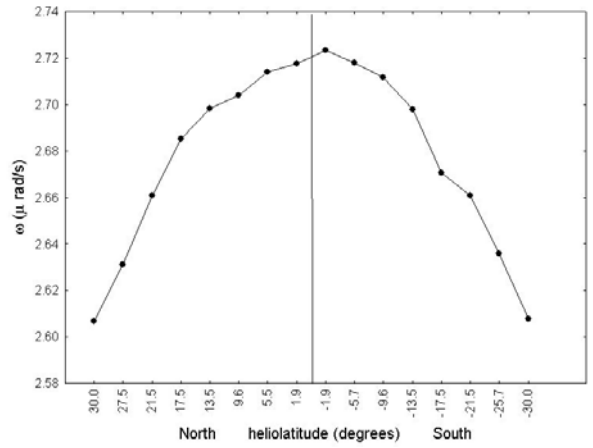

Fig. 6. Dependence of the rotation rate on latitude averaged over 333 Carrington rotations from 1976 to 2001 (from Mt.Wilson Doppler shift measurements)

The generated helicity is negative in the north and positive in the south

$$H \sim -\mathrm{sgn}(\varphi)\ \pi/32\ \cos(\varphi)$$

It twists initially untwisted or containing a finite amount of initial helicity flux tubes, and unwinds fields with opposite initial helicity.

The magnetic clouds carry the helicity of their source regions [8]. Therefore, MC's originating from the northern solar hemisphere, should have negative helicity (counterclockwise rotation of the magnetic field), and from the southern hemisphere – positive helicity (clockwise rotation). However, this is true in only 70-80% of the cases [9].

Violation of the hemispheric helicity rule

79 major geomagnetic storms (Dst<-100) have occurred in the period 1997-2001. 70 of them were caused by magnetic clouds. For 39 of the MC's the solar source regions have been reliably identified (http://cdaw.gsfc.nasa.gov/geomag_cdaw/). In 27 cases (73%) a MC was observed at Earth's orbit with the expected hirality; In 7 cases MC's originating from the northern solar hemisphere exhibited right-handed helicity (clockwise rotation of the magnetic field); In 3 cases MC's originating from the southern solar hemisphere exhibited left-handed helicity (counterclockwise rotation of the magnetic field), and in 2 cases CME's originating from the southern solar hemisphere were not MC's (no magnetic field rotation).

In 10 out of the 12 cases when the hemispheric helicity rule was violated, the solar differential rotation in the source region of the CME was "reversed" (increasing with latitude). The dates of the CME's, their identified source regions, the magnetic field rotation in the structure at the Earth's orbit, and the differential rotation in the source region are summarized in the Table.

Table. CME's violating the hemispheric helicity rule

Date	Source region	CME at the Earth's orbit	rotation in source region
23.11.97	N20E05	Right-handed MC	normal
04.05.98	S18E20	No rotation	**reversed**
14.11.98	N18W02	Right-handed MC	**reversed**
12.02.00	N25E26	Right-handed MC	**reversed**
14.10.00	N01W14	Right-handed MC	**reversed**
18.04.00	S20W58	No rotation	**reversed**
17.08.01	N16W36	Right-handed MC	normal
26.09.01	S12E23	Left-handed MC	**reversed**
01.10.01	N10E18	Right-handed MC	**reversed**
03.10. 01	S13E03	Left-handed MC	**reversed**
06.11.01	N06W18	Right-handed MC	**reversed**
24.11.01	S17W36	Left-handed MC	**reversed**

Fig.7 demonstrates a case of differential rotation reversed in the source region of a CME (marked by a circle).

Reversed (anti-solar) differential rotation

The origin and maintenance of the solar differential rotation is usually explained by the interaction between rotation and convection [10]. Convective turbulence in rotating medium is subjected to the Coriolis force, and the feedback distorts rotation and makes it nonunuform. Models for differential rotation based on this theory provide rotation law for the Sun [11] in close agreement with helioseismology [12].

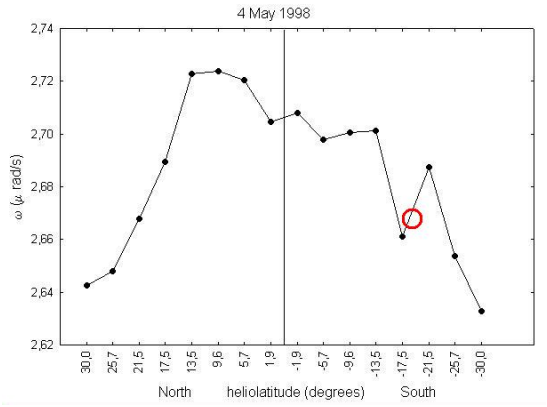

Fig. 7. An example of reversed differential rotation in the source region of a CME

On the other hand, the theory of the reversed, or "anti-solar" differential rotation, is still in its initial phase. The suggestion is that this type of rotation can result from a fast meridional flow which in turn can be caused by deviation from the spherical symmetry in the gravity or temperature distributions. The reason can be large-scale thermal inhomogeneities or tidal forcing from a companion star. About ten stars have already been identified with anti-solar type of differential rotation [13], six of them are close binaries, and one is a giant for which dark spots have been observed at low latitudes with temperature contrast of about 200° K [11].

In the case of the Sun, the anti-solar type of rotation is only observed in narrow latitudinal zones as in the case illustrated in Fig.7, and in limited temporal intervals. In some of the cases listed in the table above, the planetary configurations hint at a possibility for tidal forcing. Fig.8 presents the planetary configuration for February 12, 2000 where almost almost all planets from Mercury to Saturn are aligned and most of them are on the one side of the Sun.

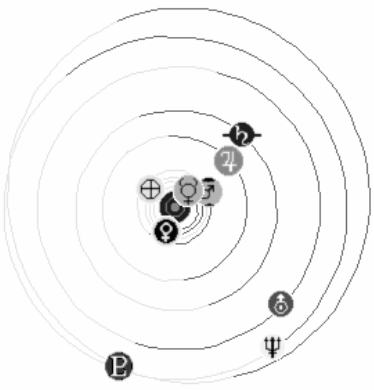

Fig.8. Planetary configuration for February 12, 2000

However, much additional study is needed to confirm this suggestion, completed by detailed data for the meridional circulation and the temperature distribution on the Sun.

Summary and conclusions

The high magnetic field magnitudes and especially the field rotation providing prolonged intervals of Bz negative – the properties distinguishing the magnetic clouds as a subclass of coronal mass ejections – make them the most geoeffective solar drivers. The magnetic field rotation is determined by two factors: the amount of helicity transferred from the solar interior into the corona, and the surface differential rotation. The helicity transferred from the solar interior into the corona is always positive in the southern solar hemisphere and negative in the northern hemisphere, irrespective of the magnetic polarity cycle. The surface differential rotation can additionally wind or unwind the rising magnetic flux tubes. The well known "solar type" of differential rotation with the rotation rate decreasing from the equator toward the poles, generates again negative helicity in the north and positive helicity in the south. Magnetic clouds preserve the helicity of their source regions, so left-handed rotation should be observed in magnetic clouds originating from the northern hemisphere, and right-handed rotation in magnetic clouds originating from the southern hemisphere. However, this hemispheric helicity rule holds in only 70-80 of the cases.

We study the major geomagnetic storms (Dst<-100) in the last solar cycle (1996-2004). 70 out of 79 storms were caused by magnetic clouds. For 39 of them the solar sources were identified, and in 73% the magnetic clouds had the expected helicity. In 10 out of the 12 cases of violation of the hemispheric helicity rule, the magnetic clouds originated from regions on the Sun with reversed - "anti-solar type" of differential rotation with the higher latitudes rotating faster than lower latitudes. Such "anti-solar" differential rotation has been observed in about 10 stars. The theory of "anti-solar" differential rotation which is still in its initial phase, relies on the fast meridional circulation which could be caused by gravitational or thermal asphericities. Six of the stars are close binaries, and one is a spotted giant. In the case of the Sun, "anti-solar" differential rotation is observed in limited latitudinal regions and time intervals. The Sun has no companion star, however it has planets, and the planetary configurations in some cases hint at the possibility that "anti-solar" differential rotation could be a result of gravitational asphericity caused by tidal forces due to planetary alignments.

REFERENCES

[1] Richardson, I.G., Cane, H.V., "The fraction of interplanetary coronal mass ejections that are magnetic clouds: Evidence for a solar cycle variation", *Geophysical Research Lett.*, Vol. 31 (18), 2004, CiteID L18804.

[2] Georgieva, K. and Kirov, B., "Helicity of magnetic clouds and solar cycle variations of their geoeffectiveness". *Coronal and Stellar Mass Ejections, IAU 226,* Cambridge University Press, 2005, pp. 470-472.

[3] Georgieva, K. et al, "Solar rotation and solar wind - magnetosphere coupling". *Planet. Space Sci.*, Vol. 53 (1-3), 2005, pp. 197-207.

[4] Webb, D.. "CMEs and the solar cycle variation in their geoeffectiveness", *In: Proceedings of the SOHO 11 Symposium on From Solar Min to Max: Half a Solar Cycle with SOHO, 11-15 March 2002, Davos, Switzerland*, pp. 409 – 419.

[5] Berger, M.A. and Ruzmaikin, A. "Rate of helicity production by solar rotation". *J. Geophys. Res.*, Vol. 105 (A5), 2000, pp. 10481-10490 .

[6] DeVore, C. R., "Magnetic helicity generation by solar differential rotation", *Astrophys. J.*, 539 (2), 2000, pp. 944-953.

[7] Gavryuseva, E. and Godoli, G., "Structure and rotation of the large scale solar magnetic field observed at the Wilcox Solar Observatory", *PCE*, 2005 (In press).

[8] Kumar, A. and Rust, D., "Interplanetary magnetic clouds, helicity conservation, and current-core flux-ropes". *J. Geophys. Res.*, 101 (A7): 1994, pp. 15,667-15,684.

[9] Pevtsov, A. A.et al., "Latitudinal variation of helicity of photospheric magnetic fields" , *ApJ,* vol. 440 (2), 1995, pp. L109-L112.

[10] Kitchatinov, L.L., "Star differential rotation", *Physics-Uspekhi,* Vol. 48, 2005, pp. 475-494.

[11] Kitchatinov L.L. and Rűdiger, G., "Differential rotation in solar-type stars: revisiting the Taylor-number puzzle", *A&A* Vol.299, 1995, pp. 446-452.

[12] Schou, J. et al., "Helioseismic Studies of Differential Rotation in the Solar Envelope by the Solar Oscillations Investigation Using the Michelson Doppler Imager", *Ap.J* Vol. 505 (1), 1998, 390-417.

[13] Strassmeier K.G. et al., Doppler imaging of stellar surface structure. XX. The rapidly-rotating single K2-giant HD 31993 = V1192 Orionis, *A&A,* Vol. 408, 2003, pp. 1103-1113.

Modelling of the Aragats Space Environmental Center Monitors Response to Galactic and Solar Cosmic Rays

M.Z. Zazyan, A.A. Chilingarian

Alikhanyan Physics Institute, Yerevan, Armenia, mary@mail.yerphi.am

Detectors of Aragats Space Environmental Center (ASEC) are monitoring different species of secondary cosmic rays at 2 altitudes according to various energy thresholds. Using CORSIKA code we have calculated the response of ASEC monitors to galactic cosmic rays and to different transient events, such as Ground Level Enhancements (GLEs) and geomagnetic storms, influencing cutoff rigidity threshold values. The response of ASEC monitors, simulated for historic events of 23-rd solar cycle, is compared with corresponding measurements.

Introduction

Monitors of Aragats Space Environmental Center (ASEC) [1] register secondary fluxes generated by high energy particles as they enter the Earth's atmosphere. The information about primary particle type and energy is mostly smeared during its interactions with atmospheric nuclei. To be able to reconstruct the primary particle fluxes incident on the Earth's atmosphere it is necessary to know the relationship between the count rates of the monitor and the primary particles fluxes. This relationship can hardly be determined experimentally or analytically. To obtain it modelling of particle cascades developed from cosmic ray interactions in the Earth's atmosphere was performed and ASEC detectors response to galactic and solar cosmic rays was calculated.

Modelling of ASEC monitors response to the galactic cosmic rays.

Primary particles, while entering the Earth atmosphere, interact with the atmospheric nuclei and produce a cascade of secondary particles. After production of several generations of particles, the cascade process ends when the energies of the particles become too low for the further particle production. As long as enough energy remains for the propagation of the shower and the production of cascade particles, the shower will continue down until it reaches ground level.

We used CORSIKA code [2] (version 6.020) to simulate the propagation of primary particles through the Earth's atmosphere. Electromagnetic interactions are simulated using EGS4 code [3]. For the hadronic interaction, the QGSJET [4] model is used at high energies, and GHEISHA2002 [5] is used at low energies (below 80 GeV). The simulations are performed for two observation levels: 3200m a.s.l. (Aragats station) and 2000m a.s.l. (Nor-Amberd station). The threshold energies for the primary particles correspond to the rigidity cutoff of the location – 7.56 GV. All secondary particles are followed until they are below the threshold energy (50 MeV for hadrons, 10 MeV for muons and 6 MeV for electrons and photons) or reach ground level. The input spectra for the simulation are selected to follow the observed proton and helium spectra of CAPRICE98 balloon-borne experiment [6].

The simulated ground level particle intensities are used to estimate ASEC monitors count rates. Count rates of muon monitors (registering low energy charged particles, muons with the energy threshold of 350MeV and high energy muons with the energy threshold of 5GeV) are calculated as a number of corresponding particles per 1 m^2. To calculate Aragats and Nor-Amberd neutron monitors count rates we used a NM-64 neutron monitor detection efficiency as a function of rigidity from the report of Clem and Dorman [7]. As far as neutron monitor responds mostly to neutrons and protons, only these secondary particles are taken into account.

The mean count rates with the statistical errors calculated from 5 independent simulated samples for primary protons and helium nuclei are presented in Tables 1 and 2. For the comparison, experimentally measured count rates of ASEC monitors on a quiet day (no solar modulation), are presented as well. Of course, the experimental values are changing with the phase of solar cycle and other solar modulation effects, but one can conclude that there is a reasonable agreement between the simulated and the measured count

TABLE 1

ASEC monitors count rates at Aragats level (3200m a.s.l) due to secondary galactic cosmic rays (cts/m^2 min)

	neutrons, protons	low energy charged particles	muons (>350 MeV)	muons (>5GeV)
Simulated	2919±33	23378±214	12479±92	3223±239
Experimental	3218±22	24985±320	-	3688±35

TABLE 2

ASEC monitors count rates at Nor-Amberd level (2000m a.s.l) due to secondary galactic cosmic rays (cts/m2 min)

	neutrons, protons	low energy charged particles	muons (>350 MeV)	muons (>5GeV)
Simulated	1196±19	15320±138	9997±89	2839±20
Experimental	1325±12	14540±130	9600±150	-

Variations of cosmic rays caused by cutoff rigidity changes during geomagnetic storm.

Disturbances of the Earth's magnetic field during the magnetic storms can cause the changes of effective cutoff

rigidity. These changes may be sufficiently large to distort essentially cosmic ray (CR) intensity measured by ground-based detectors. We have studied the CR intensity dependences on cutoff rigidity. The count rates for the ASEC monitors for the four different values of rigidity cut-off are calculated. The relative increases $\Delta N_{cnts}/N_{cnts}$ in the 5-minute count rates due to the decreases of rigidity cut-off are presented in Table 3. One can see that the neutron flux is much more influenced by the cutoff rigidity decrease than charged particle flux. The greater energy of the secondary charged particles – the less intensity changes are.

For the comparison the relative increases of the measured count rates for the two events detected by ASEC monitors are presented in Table 4. The experimental increases are estimated above pre-event background, calculated by one-hour data prior shock arrival. The comparison of simulated and experimental increases in count rates shows that the *November 20, 2003* event could be associated with the cut-off rigidity changes of ~1GV. This is in a good agreement with the cut-off rigidity variation (~1.2 GV for Aragats station) calculated by Belov et al. [8] using data from the worldwide neutron monitor network and the global survey method.

The decrease of cut-off rigidity at September 7, 2002 is less than 0.5GV.

TABLE 3

The simulated increase $\Delta N_{cnts}/N_{cnts}$ in the 5-minute count rates of ASEC monitors due to the changes of rigidity cut-off.

R_c decreases	neutrons, protons	low energy charged particles	muons (>350 MeV)
from 7.56 to 7.00GV	3.1%	0.74%	0.43%
from 7.56 to 6.50GV	6.0%	1.34%	0.74%
from 7.56 to 6.00GV	9.2%	1.93%	1.00%

TABLE 4

The experimental increases $\Delta N_{cnts}/N_{cnts}$ in the 5-minute count rates of two events.

event	neutrons, protons	low energy charged particles	muons (>350MeV)
November 20, 2003	6.2%	0.8%	0.5%
September 7, 2002	2%	0.5%	0%

Intensity-time profile of November 20, 2003 event

Aragats neutron monitor (ArNM) count rates along with variation of Dst (Disturbance storm time) index during magnetic storm on 20 November 2003 are shown in Fig. 1 [9]. Assuming that Rc time variations are exactly following the Dst variations we have calculated the count rates of ASEC monitors for the time-interval 10 – 20 UT. Proceeding from our result, that the cut-off rigidity is changing from 7.56 GV to 6.56 GV, we have fixed Rc to 7.56GV at 0:00UT and to 6.56GV at 20:00UT.

A time variations of simulated and experimental 5-minute count rates of Aragats NM for November 20, 2003 event are shown in Figure 2. Each simulated point represents a count rate, averaged from 10 independent samples. Errors are estimated according to Poisson distribution.

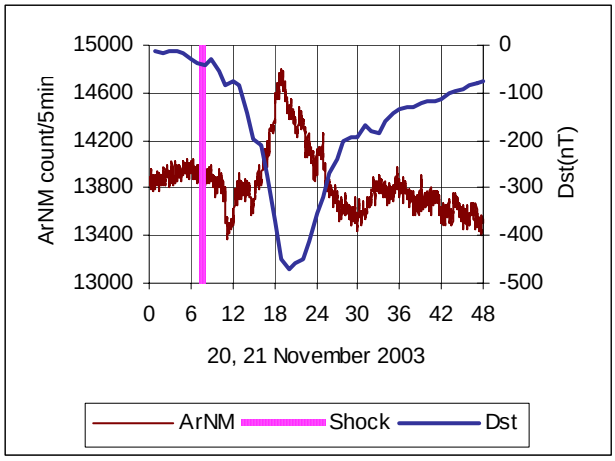

Fig.1. Aragats Neutron Monitor 5-minute count rate and Dst-index for November 20, 2003 event

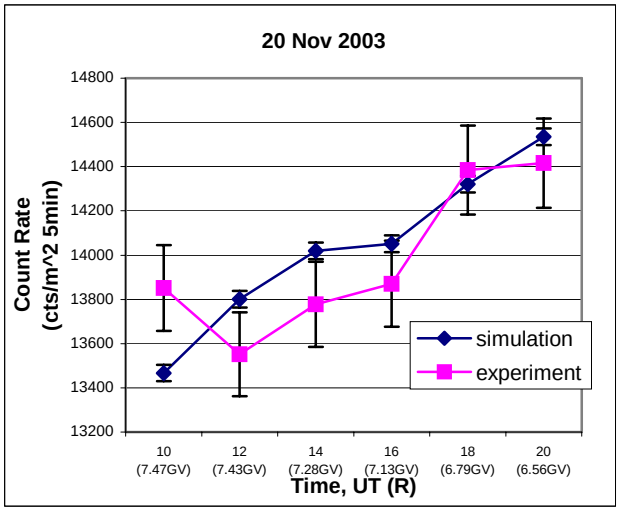

Fig.2. Simulated and experimental 5-minute count rate variations of Aragats NM during November 20, 2003 event.

Simulated and experimental variations, although very close to each other, are not exactly the same, because the linear dependence dRc on Dst can be used only as a first approximation. However, as a next step, by using the calculated time-profile of the event the cutoff rigidity can be corrected at each moment of time.

Conclusions

It was shown a good agreement between calculated and measured ASEC monitors count rates.

A cut-off rigidity variation was defined to be ~1GV for severe magnetic storm on 20 November 2003 by modeling of the response of Aragats neutron monitor and comparing it with observations.

The time-profile of the November 20, 2003 event was simulated for Aragats NM. Comparing experimental and calculated values we can see rather good agreement between them. Thus, our calculations can estimate not only mean values of the detected secondary particle fluxes, but also time history of flux evolution during severe geomagnetic storms.

This work demonstrates that the ground level monitors response to galactic and solar cosmic rays can be successfully calculated using CORSIKA code. For further detailed study of solar events FLUKA interface, which is better adjusted for the low energies, will be used.

REFERENCES

[1] A. Chilingarian, K. Arakelyan, K. Avakyan et al., " Correlated measurements of secondary cosmic ray fluxes by the Aragats Space-Environmental Center monitors", NIM, A 543, 483 (2005)

[2] D. Heck and J. Knapp, Forschungszentrum Karlsryhe, FZKA Report 6019 (1998)

[3] W.R Nelson, H. Hirayama, and D.W.O. Rogers, Report SLAC 265 (1985)

[4] N.N. Kalmykov, S.S. Ostapchenko, and A.I. Pavlov, Nucl. Phys. B (Proc. Suppl.) 52B 17 (1997).

[5] H. Fesefeldt, Report PITHA-85/02 (1985)

[6] M. Boezio, V. Bonvicini, P. Schiavon, A. Vacchi, and N. Zampa, "The cosmic-ray proton and helium spectra measured with the CAPRICE98 ballon experiment", arXiv:astro-ph/0212253, 1,11 (2002)

[7] J.M. Clem and L.I. Dorman, "Neutron monitor response functions" Space Sci. Rev., 93, 335 (2000)

[8] A. Belov, L. Baisultanova, E. Eroshenko, H. Mavromichalaki, V. Yanke, V. Pchelkin, C. Plainaki, and G. Mariatos (2005), Magnetospheric effects in cosmic rays during the unique magnetic storm on November 2003, *J. Geophys. Res.*, *110*, A09S20, doi:10.1029/2005JA011067

[9] G.G. Karapetyan, CRD report, 2004.

Highest Energy Solar Neutrons Detected in the Solar Flare on November 28th, 1998

Y. Muraki

Solar-Terrestrial Environment Laboratory, Nagoya University, Nagoya 464, Japan muraki@stelab.nagoya-u.ac.jp

In 1990, we have proposed a new method to study particle acceleration mechanism at the Sun by observing solar neutrons [1]. In this paper, the advantages of the new method of detecting solar neutrons are discussed. After giving a review of past events of solar neutrons, one of the solar neutron telescopes constructed at the observatory in Tibet is introduced. Then new and important results using this detector are presented.

Observation of solar neutrons by a new method

Particle acceleration mechanism at the Sun has been zealously investigated using several instruments located at ground level or aboard spacecraft. However information obtained by these observations is mainly related to phenomenon induced by electron acceleration, and comparatively little information has been obtained until now on the iron acceleration processes. Therefore even whether or not irons are accelerated at the same time as electrons has not yet been established.

Although a plenty of data on ions is available, difficulties arise when we want to determine the exact acceleration time of those ions because they propagate from the Sun to the Earth through the interplanetary magnetic field. Much information as the production time of ions at the solar surface is usually destroyed by the transportation process.

Therefore it is natural to consider observing only neutral particles when trying to understand the acceleration mechanism of irons, since they travel from the Sun to the Earth in straight lines unperturbed by the interplanetary magnetic field. Neutrinos are essentially undetectable in the numbers expected from a flare, so the practically accessible neutral particles are gamma-rays and neutrons. There are advantages and disadvantages connected with both gamma-rays and neutrons.

Electrons can produce gamma-rays of virtually any energy, so it is only neutrons that are exclusively produced in the accelerator process of ions. This has been well known for some time but actual observation of solar neutrons was delayed for several reasons, principally the difficulty of identifying solar neutrons in the presence of large backgrounds. Even today, it is only the comparatively rare, large events that produce detectable fluxes of neutrons. Neutrons are absorbed in the atmosphere, so observation at high altitude or in space is a requirement, and low energy neutrons (less than about 10 MeV) decay in flight between the Sun and the Earth.

Furthermore, even though there is no effect of the magnetic field on their path, the flight time of neutrons from the Sun to the Earth depends on the energy. Since neutrons have mass, high energy neutrons from the Sun arrive on the Earth sooner than low energy neutrons even if they are emitted at the same time at the Sun. We cannot escape from the time dispersion unless we measure the energy of neutrons. Without energy determination we cannot identify whether monoenergetic neutrons are emitted at the Sun continuously or neutrons are emitted instantaneously with a spectrum. On the other hand if we measure the neutron energy, we can determine the production time at the Suns and therefore the acceleration time of ions.

Our approach is designed to make this important energy measurement in that we use plastic scintillator as the target for detecting the neutrons. When neutrons enter the plastic scintillator, they can interact either with hydrogen or with carbon. When neutrons collide with a hydrogen target, protons are emitted in the forward direction following a formula determined by pure kinematics: $T_p = T_n \cos^2\theta$. The kinetic energy of protons T_p is determined from their energy loss by ionization. The scattering angle of the protons is measured by proportional counters located below the plastic scintillator. Since we know the direction from the Sun the energy of neutrons T_n can be measured.

However when neutrons make collisions with carbon target of the plastic scintillator, several neutrons and protons can be produced. Break-up of carbon nuclei emits additional neutrons and protons. In this case we only know the minimum energy of incoming neutrons, and we can use our detector as a threshold detector that identifies the energy of neutrons higher than 40 MeV, 80 MeV, 120 MeV and 160 MeV. We can change the threshold using data which from counters located below the main detector.

This method is generally superior to a standard neutron monitor, which detects thermal neutrons initially produced as lead nuclei are broken up by incoming neutrons. Most of the information about the energy of the incoming neutron is lost in the process. Although the neutron monitor is relatively immune to background from the muons and electrons that dominate the background it is sensitive to the entire hadronic component of the cosmic rays, not just the neutrons as the name might imply. The detection efficiency of neutron monitor depends on the energy, but roughly speaking it is about 30-40%, in other words quite high. Using the plastic scintillator, detection efficiency depends on the thickness of scintillator and is approximately 10% for every 10cm in thickness. Because of the sensitivity to minimum ionizing background, anti-counters are usually required.

Past observations of solar neutrons

The possibility of detecting solar neutrons was pointed out by Biermann, Haxel and Schulter in 1951 [2]. However, actual detection of solar neutrons was delayed 30 years until June 21st 1980, when they were identified by the detector GRS (Gamma Ray Spectrometer) aboard the SMM (Solar Maximum Mission) spacecraft [3]. The flare of June 21st 1980 had a "typical" feature in photons in that there were two sharp spikes of photons separated by 35 seconds, together with a long continuous emission resulting from the diffusion and interaction of neutrons in the solar atmosphere. The energy spectrum of neutrons can be modeled by assuming that those neutrons are emitted with the same time structure as the with photons

spikes. The observations are consistent with production as a single power law in energy with an index $\gamma = -3.5 \pm 0.1$. The long duration of the neutron event (over nine minutes) arises from the velocity dispersion of the neutrons.

Solar neutrons were first detected by ground based detectors in the June 3rd 1982 flare with the neutron monitors located at Jungfraujoch and other two stations in Europe [4], [5]. In this flare, the time profile of gamma-rays (>25 MeV) consisted of a strong spike at 11:42:30 UT which clearly corresponded to the photon emission, followed by a small spike at 11:43:40UT. Then the HE matrix channel (> 25 MeV) of GRS observed a long continuous emission which from neutrons. In this event, the ground based neutron monitor at Jungfraujoch observed high energy neutrons (En > 100 MeV) for over 11minutes. It is worthwhile to mention that neutron decay protons were also first detected in this event. These neutron-decay-protons were produced from neutrons that crossed the interplanetary magnetic field in straight lines until they eventually decayed in flight. After decay, the resulting protons were captured by the magnetic field and transported to the Earth. Those protons arrived at the spacecraft sooner than the protons emitted into the solar corona which had to propagate along the magnetic field all the way to the Earth. According to Monte Carlo calculations by Shibata [6], the neutrons detected at Jungfraujoch can be interpreted as being emitted at the same time with photons. With this assumption, the spectrum index of solar neutrons can be expressed as a power law with $\gamma = -4.0 \pm 0.2$.

Only two solar neutron events were detected in the solar cycle 21, but in solar cycle 22 four more events were observed. Solar neutrons in association with a large solar flare on May 24th 1990 was the first event in the solar cycle 22, detected by neutron monitors located in North and South America. The first peak of this event was so strong that GLE was observed, which was the first GLE event induced by neutrons [7], [8]. The production spectrum of neutrons was very hard and could be fitted by a power law with $\gamma = -2.5 \pm 0.2$ [9].

In 1991, extraordinary flares were observed on the Sun. From June 1st to 15th six large flares occurred with intensity $X \approx 10$. Fortunately the CGRO spacecraft was operating at that time and many important data on high energy channels were collected. On March 22nd a large flare was observed as the Sun was over Hawaii and the neutron monitor at Mt. Haleakala observed solar neutrons [10]. The production spectrum could be expressed by a single power law with $\gamma = -2.7 \pm 0.1$. Then in June 1991 large solar flares were seen repeatedly in the sunspot region 6659. Among those flares, the new solar neutron detector located at Mt. Norikura observatory, Japan (2,770m) which is made of plastic scintillators succeeded in catching the signal of neutrons even though the size of the neutron telescope is only 1 m^2 [11]. Signals of neutrons were detected simultaneously by the 12 m^2 neutron monitor [12] and the 36m^2 muon detector (made of plastic scintillator) which are located at the same observatory. Therefore we can compare the detection efficiency of each detector in this event. Two days after the June 4th flare, on June 6th 1991, another large solar flare was observed. In association with this flare three detectors located at Mt. Norikura (2,770m) and also Haleakala (3,030m) detected solar neutrons, the first time solar neutrons were detected at different longitudes over the Pacific Ocean [13]. All these 6 events observed in solar cycle 21 and 22 can be explained by impulsive production in association with an identified solar flare.

For the new solar cycle 23, we have prepared several solar neutron telescopes around the world, installed at Gornergrat, Switzerland (3,250m), Mt. Aragats, Armenia (3,500m) [14], Yangbajing, Tibet (4,300m) [15],[16], Mauna Kea, Hawaii (4,200m), Mt. Chacaltaya, Bolivia (5,250m) [17] and most recently Mt. Sierra Negra, Mexico (4,600m) [18]. The solar neutron telescopes are operated so that they separate signals from backgrounds by using the telescope function. Owing to these efforts, 40 solar neutron events were collected with the statistical significance over 3 σ and 15 events were collected with the statistical significance over 4 σ. The details have been published in elsewhere [19]. In this paper we describe a very interesting event in data obtained at Yangbajing international cosmic ray station, Tibet, China in association with the large flare on November 28th, 1998

Solar Neutron Event observed by Tibet neutron telescope

A new solar neutron telescope was constructed in Tibet during October of 1998. By chance large solar flares occurred at the Sun in November 22nd, 23rd and 28th, 1998.The new solar neutron telescope detected neutrons on November 23rd and 28th, but not from the flare of November 22nd. In this paper we discuss on the event recorded on November 28th. This solar neutron event is unusual because (1) neutrons were detected in the northern hemisphere winter when the solar angle was 53 degrees, (2) the flare had a comparatively modest intensity of X3.3 and (3) the event involved quite high energy neutrons [20]. These observations thus have important implications for solar physics. A schematic view of the Tibet solar neutron detector is shown in Figure 1.

On February 22nd 1999, Japanese solar physicists who observe the Sun at different wave lengths met at the Solar-Terrestrial Environment Laboratory, Nagoya University to discuss this event [21]. One of the questions considered was: "If high energy neutrons were observed by the solar neutron telescope why were the low energy neutrons not detected by a large neutron monitor?" In fact, the Tibet neutron monitor observed a small (1.7 σ) enhancement consistent with the observation by the scintillator part of the solar neutron telescope [22]. At that time, we assumed that the neutron spectrum had a cutoff at a few GeV. In this case, it is not necessary to take account of pion production in the atmosphere, and we could use the Monte Carlo code developed by Shibata [6].

One of the difficulties in understanding this event is that the number of events detected by the channel 3 (E_p or $E_e > 120$ MeV) of the upper scintillators is the same as that in the down side proportional counters ($E_p > 270$ MeV). If the excess of the event were due to neutrons, according to Monte Carlo calculations, the number of events detected by upper scintillator should be greater than the number of penetrating events. Trigger pulses are produced by the coincidence between the upper channels (at least > 40 MeV deposited energy is necessary in the scintillator) and lower four layers of the proportional counters. Inside the four layers of the proportional counters are two layers of wood with a total thickness of 20cm. According to the Monte Carlo calculation the ratio of the upper channel to coincidence signal is expected as to be a factor of four to

ten, depending on the energy of the neutrons in the range 270 – 1000 MeV [20].Recently we have concluded that high energy neutrons, beyond 5 GeV, were involved in this event. Therefore photons must be included in the calculation. Only the most recent version of GEANT 4 can treat neutron cascade in the atmosphere correctly down to a few MeV (Koi et al, private communication). We have determined the best model using a new version of GEANT 4 and compared the results to those of Shibata [6]. In this process, we discovered that the intensity of photons is expected as to be the same order as that of neutrons as shown in Fig. 2 [23].

Hence we have arrived at a new interpretation for this event, namely that the flare must have accelerated protons to beyond 100 GeV and thereby also produced high energy neutrons. In our simulation we have assumed a power law spectrum of neutrons with index γ = - 2.5. Such high energy neutrons produce not only charged pions in the atmosphere but also neutral pions, which immediately decay into two photons and initiate an electromagnetic cascade. Those photons penetrate the solar neutron telescope through the anti-counter which cannot separate neutrons from photons. The radiation length of upper scintillator is just one radiation length, so most photons are converted into electron positron pairs in the scintillator. These are minimum ionizing particles which can penetrate both layers of wood and all four layers of the proportional counters.

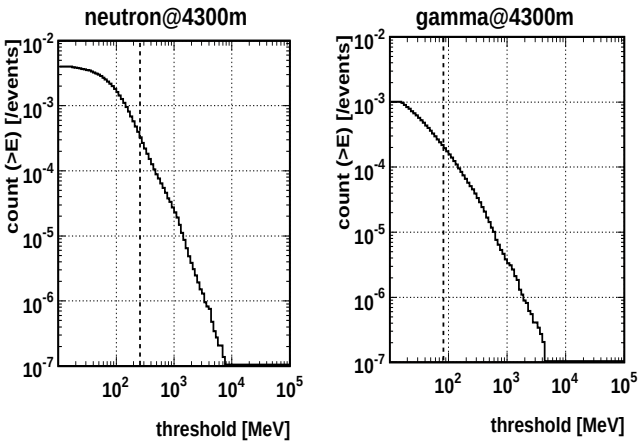

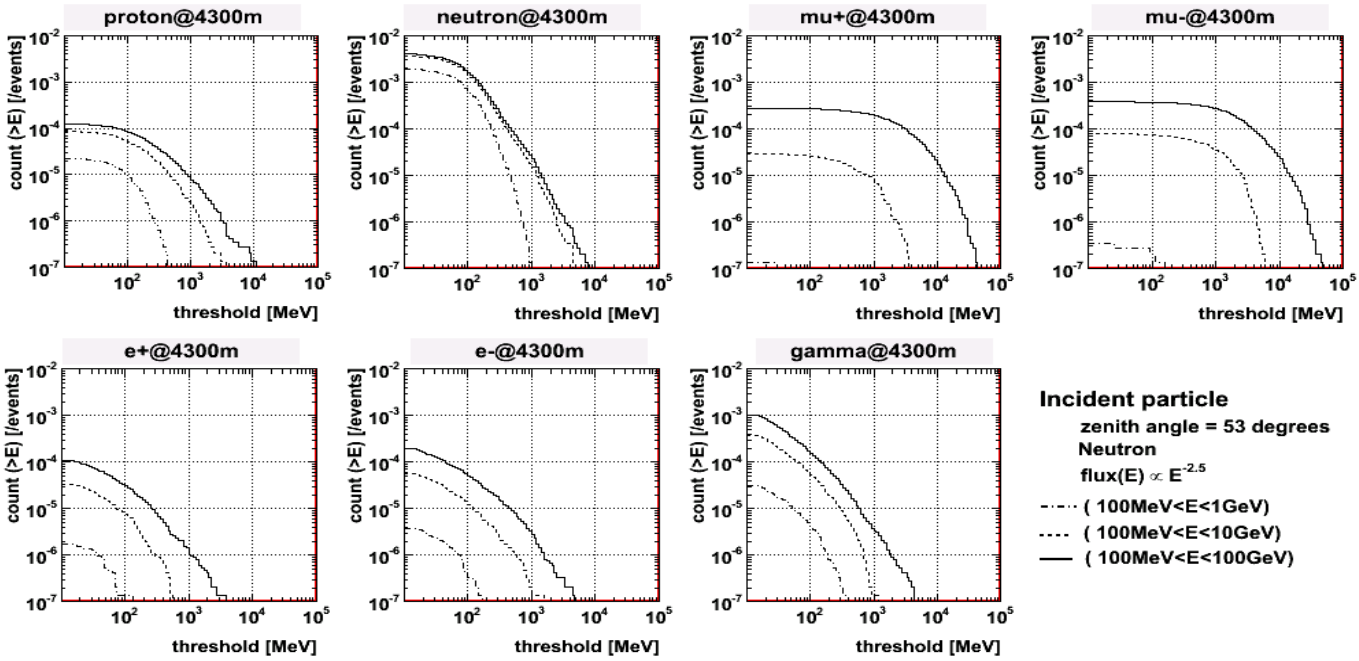

Summary and Conclusions

In the solar flare on November 28th, 1998, ions were accelerated up to 100 GeV with a similar time profile as the X-rays observed by the Yohkoh Hard X-ray Telescope. Those high energy ions collided with the atmosphere of the Sun to produce high energy neutrons. When the neutrons entered the atmosphere of the Earth, they produced charged and neutral pions. The neutral pions decayed immediately and started the electromagnetic cascades, with the photon component of the cascade shower that able to penetrate the atmosphere to the depth of the solar neutron telescope.

The detector responds to both photons and neutrons and cannot differentiate between them. Electrons and positrons produced in the scintillator can penetrate two layers of the wood and trigger four layers of the proportional counters. This must be the source of the enhancement observed in the solar direction by the neutron telescope since the adjacent neutron monitor, which is insensitive to photons, showed only a weak enhancement in its counting rate. In future versions of the neutron detector is will be possible to separate photons from neutrons by installing a thin lead layer over the anticoincidence shield.

We conclude that in this solar flare, particles were accelerated to at least 10 GeV, and probably to over 100 GeV over a time interval of a few minutes. Confirmation of such high energy solar particles will be one of the most important tasks of the next solar cycle 24. The author acknowledges Mr. Hiroaki Menjyo for providing us his Monte Carlo results before publication.

REFERENCES

[1] Y. Muraki et al., Proceed. 22nd ICRC (Dublin), 3 (1991) 45, 49.
[2] V.L. Biermann et al., Z. Naturforsch. 6a (1951) 47.
[3] E.L. Chupp et al., ApJL 263 (1982) L95.
[4] E.L. Chupp et al., ApJ 318 (1987) 913.
[5] L.I. Efimov, G.E. Kocharov and K. Kudela, Proceed. 18th ICRC, 10 (1983) 276.
[6] S. Shibata, JGR, 99 (1994) 6651.
[7] H. Debrunner et al., ApJL 387 (1992) L51., ApJ 479 (1997) 997.
[8] D.F. Smart et al., Proceed 24th ICRC, 4 (1995) 171.
[9] Y. Muraki and S. Shibata, AIP Conf. Proceed. 374 (1996) 256.
[10] K.R. Pyle and J.A. Simpson, Proceed 22nd ICRC, 3 (1991) 53.
[11] Y. Muraki et al., ApJL 400 (1992) L75.

Solar and Heliospheric Disturbances Resulted in Magnetic Storm of November, 2004

Yu. Yermolaev[1], L. Zelenyi[1], V. Kuznetsov[2], I. Chertok[2], M. Panasyuk[3], I. Myagkova[3], I. Zhitnik[4], S. Kuzin[4]

and other members of the SEE'04 collaboration

[1] *Space Research Institute (IKI), Russian Academy of Science, Profsoyuznaya 84/32, 117997, Moscow, Russia, yermol@iki.rssi.ru*

[2] *Institute of Terrestrial Magnetism, Ionosphere and Radio Propagation (IZMIRAN), Russian Academy of Science, Moscow Region, Troitsk, Russia*

[3] *Skobeltsyn Institute of Nuclear Physics, Moscow State University, Moscow, Russia*

[4] *Lebedev Physical Institute, Russian Academy of Science, Moscow, Russia*

This paper presents a portion of data on observations of the Sun, interplanetary medium, and magnetosphere, obtained by participants of the "Solar Extreme Events in 2004 (SEE'04)" collaboration before and during the strongest magnetic storm of November 08, 2004 (Dst= –373 nT). These events were observed in year after the series of the strongest solar flares (including flares of class > X17) and the magnetic storm with Dst = –401 and –472 nT during October – November, 2003 studied by previous SEE'03 collaboration [1-3]. Although the number and power of the flares were much smaller during the period under study, the magnetic storm was one of the strongest for the entire period of Dst index observation and was apparently caused by the interaction of frequently occurred coronal mass ejections in the interplanetary space, as a result of which the region of interaction was compressed and the southward IMF component increased to less than –45 nT [4].

Introduction

Investigation of the effects of solar and interplanetary (heliospheric) events on the near-Earth space is one of the most important components of the solar–terrestrial physics. In spite of the fact that the general concept of such an effect has been almost constant for many years and the large body of experimental and theoretical data has been accumulated it is to a certain degree difficult to predict effects of the space weather. The greatest difficulties on the prediction of space weather effects exist for the strongest, extreme disturbances as a number of such events was sufficiently low and datasets of measurements on these events were insufficiently complete. An excellent example of interdisciplinary approach is the collaboration of the researchers (SEE'03) from more than ten Russian scientific institutions, which was organized in order to study the extreme events that occurred on the Sun, in the heliosphere, and on the Earth in October–November 2003 [1-3].

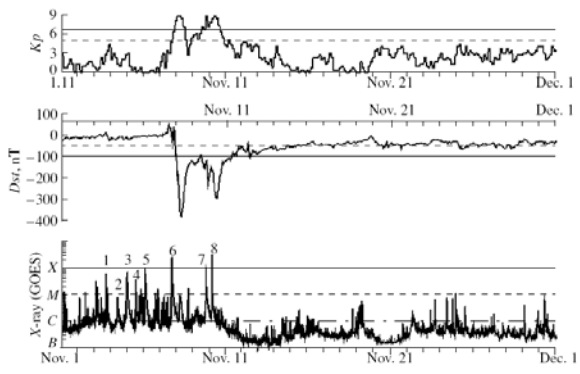

Fig.1. The series of solar and ground-based measurements in November 2004. Nos. 1–8 correspond to the flares presented in Table 1.

Exactly a year later, at the end of October–beginning of November 2004, the Sun was again very active and generated a number of strong interplanetary and magnetospheric disturbances (Fig. 1, Table 1) [4]. The values of some parameters measured during this period of 2004 were slightly smaller than the extreme values observed in 2003, nevertheless, solar activity in 2004 can be considered among the strongest events not only in the current solar activity cycle (cycle 23) but also during the entire period of space observations. The aim of this paper prepared mainly by group of researchers of the previous active period is to generally describe the state of different spatial regions during that period and to present the main Russian experimental data.

TABLE I

Flare events in AR 10696 in November 2004

N	Date, UT	Coordinates	Class	CME
1	Nov.3, 15:35	N11 E40	M5.0/SN	NE
2	Nov.4, 08:45	N08 E28	C6.3/SN	P.Halo
3	Nov.4, 21:42	N11 E19	M2.5/1N	P.Halo
	Nov.4, 22:34		M5.4/1N	P.Halo
4	Nov.5, 11:23	N08 E15	M4.0/1F	-
	Nov.5, 19:10	N09 E07	M1.2/SF	-
5	Nov.6, 00:11	N10 E08	M9.3/2N	Halo
	Nov.6, 00:44		M5.9	Halo
	Nov.6, 01:40		M3.6	Halo
6	Nov.7, 15:42	N09 W17	X2.0/2B	Halo
7	Nov.9, 16:59	N07 W51	M8.9/2N	Halo
8	Nov.10, 01:59	N09 W49	X2.5/3B	Halo

Solar observations

The burst of solar-flare and eruptive activity at the decline phase of the current solar cycle (cycle 23) was observed at the end of

October–beginning of November 2004. This burst was related to the passage of two sunspot groups – active regions (ARs) 10691 and 10696 – over the visible solar disk.

The SPIRIT telescope on the CORONAS-F satellite was used in the Sun observations performed on November 1–8, 2004. In this case the full disk images in the channels 175 and 304 Å were registered four times a day at intervals of 4–8 h and complete spectrograms were registered two times a day. Several obtained telescopic images are shown in Fig. 2.

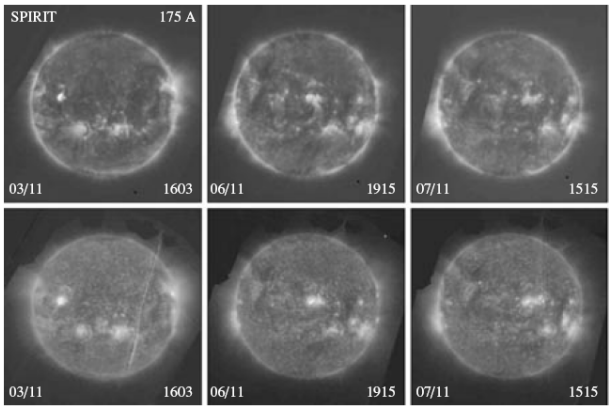

Fig.2. SPIRIT/CORONAS-F images of the Sun in the 175 and 304 Å channels obtained on November 3–7, 2004.

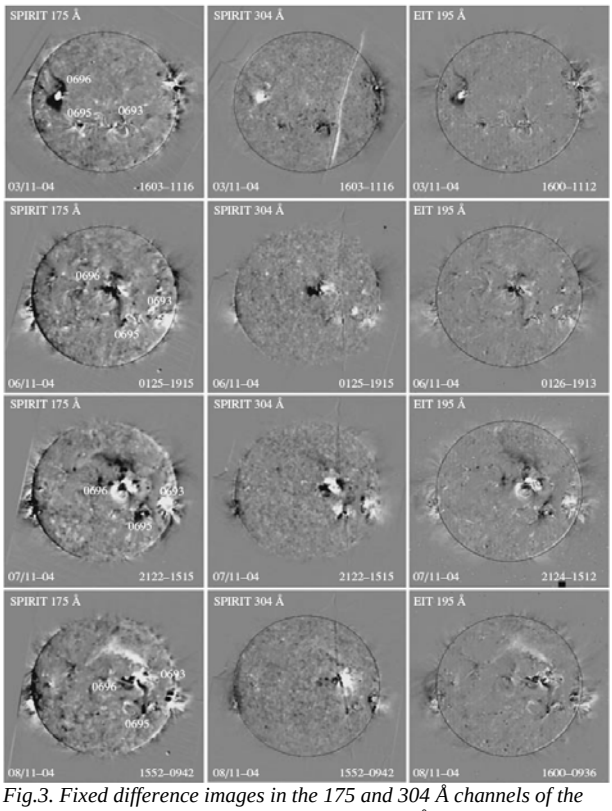

Fig.3. Fixed difference images in the 175 and 304 Å channels of the SPIRIT telescope and similar images in the 195 Å channel of the SOHO/EIT telescope obtained on November 3, 6, 7 and 8, 2004.

Fixed difference images obtained using the SPIRIT telescope and similar SOHO/EIT images are compared in Fig. 3. A classical pair of compact dimmings, corresponding to footpoints of an eruptive magnetic loop, was generated as a result of the flare and eruptive event occurred on November 3 near AR 10696. These dimmings are very contrasting in the channels 175 and 195 Å and are much less distinct in the channel 304 Å, which can be caused by the delay in the dimming development in the transition layer.

Interplanetary measurements

In contrast to the situation in 2003, when large fluxes of energetic particles caused serious failures in the operation of instruments that measured parameters of the interplanetary medium on spacecraft, the complete sets of data on the solar wind and IMF were obtained (see Fig. 4). An analysis of Fig. 4 makes it possible to preliminarily conclude that the studied time interval was characterized by strongly disturbed conditions in the solar wind. Thus, six interplanetary shocks and several magnetic clouds (interplanetary coronal mass ejections ICMEs) were observed on November 7–11. The values of all plasma parameters (velocity V, temperature T, and density N) were not extreme. At the same time, the values of B and IMF Bz component reached extremely large values (>45 and –45 nT, respectively) on November 8, precisely which resulted in the generation of the strongest magnetic storm.

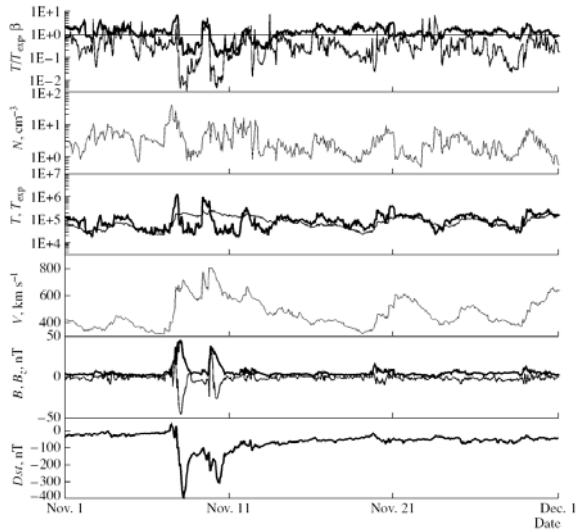

Fig.4. Interplanetary space parameters in November 2004. Panels: 1- parameter β (the ratio of the thermal and magnetic pressures, thin line) and the ratio of the proton temperature to such a temperature calculated from the average dependence of temperature on velocity, T/Texp (thick line), 2- density, N, 3- proton temperatures T (thick line) and Texp (thin line), 4- solar wind velocity, V, 5- IMF magnitude B (thick line) and Bz component (thin line), 6- Dst index.

Fig.5 indicates that a considerable increase in the flux of protons with energies of 1–5 MeV was registered by CORONAS-F on November 5–6 and, consequently, was caused by a flare that occurred before November 7. Fig.5a demonstrates that the fluxes of protons with energies of 14–26 MeV and higher started increasing only on November 7 after an X2 flare. We assume that this increase in SCRs of low energies could be caused by an M9.3 flare that occurred near midnight on November 4–5 in the AR 10696 (N09E05). Fig.5b indicates that fluxes of electrons with energies higher than 3 MeV appeared together with protons with energies higher than 14 MeV, and an insignificant (by a factor of 3–4) increase in the fluxes of electrons in the channels 300–600 and 600–1500 keV, probably related to the earlier flare mentioned above, was observed on the previous two days.

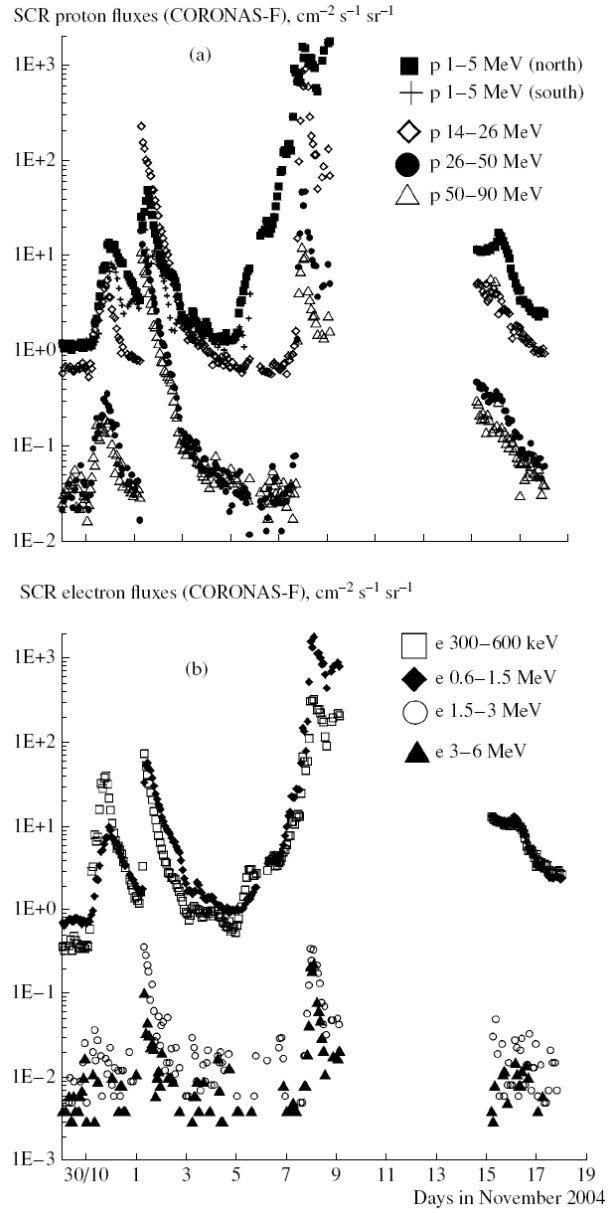

Fig.5. Fluxes of (a) protons in both polar caps and (b) electrons in the northern polar cap from October 29 to November 18, 2004, according to the CORONAS-F satellite data.

Magnetospheric and ground observations

The dynamics of the Earth's radiation belts is one of the main physical processes during magnetic storms. Fig.6 shows the radiation belt dynamics during the strong magnetic storms at the beginning of November 2004 based on the CORONAS-F satellite. At the parameters of the orbit, the CORONAS-F

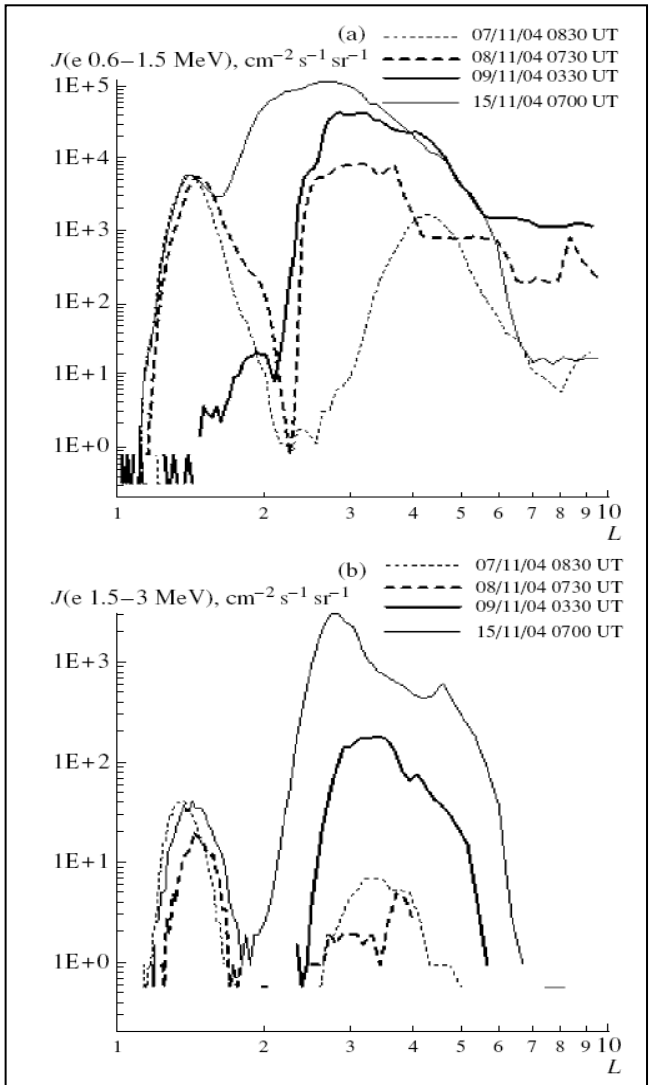

Fig.6. Comparison of the profiles of the radiation belt particle fluxes: electrons with energies of (a) 600 keV–1.5 MeV and (b)1.5–3 MeV.

instruments could register trapped radiation only in the region of the South Atlantic magnetic anomaly.

The presented data indicate that the radiation belt dynamics during the November 2004 storms was rather similar to such a dynamics during the strong storms of October–November 2003 [2,3], namely:

(i) the intensity of the flux of 1.5–3 MeV electrons decreased during the magnetic storm main phase;

(ii) during the recovery phase the intensity of the electron fluxes from the Earth's outer radiation belt pronouncedly increased, the electron belt widened, and the belt maximum shifted to smaller L;

(iii) the additional maximum of protons with energies of 1–5 MeV appeared near $L = 3$.

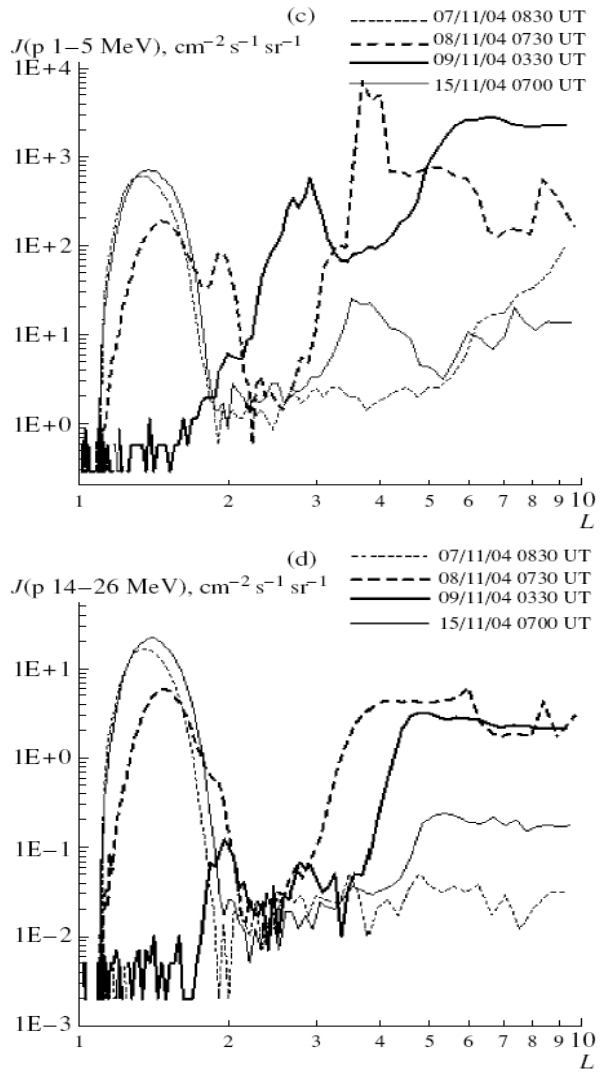

Continuation of Fig.6 for protons with energies of (c) 1–5 MeV and (d) 14–26 MeV.

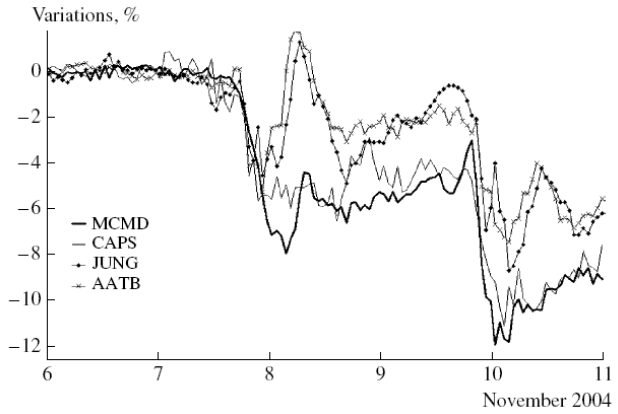

Fig.7. Variations in the neutron monitor count rate relative to the base on November 6 at the stations: McMurdo (MCMD), Rc =0.01 GV; Cape Schmidt (CAPS), Rc = 0.52; Jungfrauioh (JUNG), Rc = 4.48; Alma Ata 3300 m (AATB), Rc = 6.69 GV in November, 2004.

Fig. 7 shows that the cosmic ray density behavior was slightly unusual on November 8 at the Forbush effect. At that time the density increased (by about 2%) for approximately 12 h. The peak of this increase coincides with the solar wind disturbance and with the *Dst* minimum -373 nT.

Conclusions

As follows from the observations performed for the last several years, the main surprises took place during the phase of decline of the current 23-rd solar cycle. Solar activity was high in 2001–2003, although the solar maximum (at least with respect to the number of sunspots) was observed in 2000. For example, the events of October–November 2003 are extreme with respect to a number of parameters [1-3]. In our previous [4] and this papers, we presented the experimental observations of the Sun, heliosphere, and magnetosphere and performed a preliminary analysis for the next period of high disturbance, which was accompanied by the strongest geomagnetic storm of November 8–10, 2004, with *Dst* = –373 nT. This work not only presents comprehensive and various experimental data of observations in different regions but also demonstrates possible cause–effect relations between different phenomena in the complex chain of solar–terrestrial physics.

Acknowledgments

We are grateful to the teams operating the SOHO/LASCO coronagraph; SOHO/EIT telescope; CORONAS-F, GOES, and ACE satellites; Big Bear and Medon observatories; and the series of ground-based stations for data used in the present work.

This work was supported by the Russian Foundation for Basic Research (project nos. 03-02-16049, 03-51-6206, 04-02-16131, 04-02-16152, 04-02-17332, and 05-02-16228); INTAS (project 03-51-3738); OFN RAN programs “Plasma Processes in the Solar System” and “Physics of the Atmosphere: Electric Processes and Radar Methods of Studies”; RAN program “Solar Activity and Physical Processes on the Sun–Earth System”.

REFERENCES

[1] I.S, Veselovsky, M. I. Panasyuk, S. I. Avdyushin, G. A. Bazilevskaya et al., "Solar and Heliospheric Phenomena in October–November 2003: Causes and Effects", *Cosmic Research.*, Vol. 42, No. 5, 2004, pp435–488

[2] M. I. Panasyuk, S. N. Kuznetsov, L. L. Lazutin, S. I. Avdyushin et al.,. "Magnetic Storms in October 2003", *Cosmic Research.*, Vol. 42, No. 5, 2004, pp489–534

[3] Yu. I. Ermolaev, L. M. Zelenyi, G. N. Zastenker, A. A. Petrukovich et al., " Solar and Heliospheric Disturbances that Resulted in the Strongest Magnetic Storm of November 20, 2003”, *Geomagnetism and Aeronomy*, Vol. 45, No. 1, 2005, pp20–46.

[4] Yu. I. Yermolaev, L. M. Zelenyi, G. N. Zastenker, A. A. Petrukovich et al., A Year Later: Solar, Heliospheric, and Magnetospheric Disturbances in November 2004, *Geomagnetism and Aeronomy*, Vol. 45, No. 6, 2005, pp681–719

Prediction of Geomagnetic Storm Using Neural Networks: Comparison of the Efficiency of the Satellite and Ground-Based Input Parameters

M. V. Stepanova[1-3], E.E. Antonova[1],

F.A. Muños-Uribe[3], S.L. Gomez-Gordo[3], M.V. Torres-Sanchez[3]

[1] *Scobelstyn Institute of Nuclear Physics Moscow State University, Moscow, 119992, Russia; tel. +7-095-9392488; fax: +7-095-9390896, e-mail: marinastrepanova@vtr.net, antonova@orearm.msk.ru*
[2] *Departamento de Física, Universidad de Santiago de Chile, Santiago, Chile, marinastepanova@vtr.net*
[3] *Chilean Air Force Aeronautic Polytecnic Academy, Santiago, Chile, Departamento de Física, Universidad de Santiago de Chile, Santiago, Chile, marinastepanova@vtr.net*

Different kinds of neural networks have established themselves as an effective tool in the prediction of different geomagnetic indices, including the Dst being the most important constituent for determination of the effects of Space Weather on technology infrastructure. Feed-forward networks with one hidden layer is used to forecast the Dst variation, using separately the solar wind VB_z, polar cap index, and auroral electrojet index as input parameters. It was found that in all three cases the storm-time intervals were predicted much more precisely as quite time intervals. The majority of cross-correlation coefficients between predicted and observed Dst of strong geomagnetic storms are situated between 0.8 and 0.9. Changes in the neural network architecture, including the number of nodes in the input and hidden layers and the transfer functions between them lead to an improvement of a network performance up to 10%.

Introduction

Different types of neural networks have established themselves as effective tools in the prediction of time series behavior, especially for noisy data in the lust decades. They have successfully been used in the space weather forecasting. Several models have been developed for the prediction of the ring current index Dst, which is commonly used for geomagnetic storm description despite difficulties in its determination [1,2].

Different combinations of solar wind parameters and different kinds of neural networks were used for Dst prediction [3-5]. It was found that good prediction of the storm recovery phase requires knowledge about previous values of the Dst index. The causal aspects of the storm-substorm relationship were studied by examining the correlation between the westward auroral electrojet (AL) index and the ring current index Dst [6]. The polar cap (PC) index was used in [7] for the Dst prediction using the time-delay neural networks. In this work we make the comparative study of the neural network performance in case of the solar wind, PC, and Al indices as input parameters for the years, abundant in geomagnetic storms.

Neural Architecture and Training

Various types of neural networks have been used for geomagnetic activity forecasting. For example, Elman recurrent networks were used for prediction of geomagnetic storms from solar wind data [5], the radial basis function neural network were used for prediction of the solar wind velocity [4], and the self-organized maps were used to identify structures in the geoeffective solar wind [8].

Feed-forward multilayer perceptrons are generally used for pattern recognition problems. However in this work the input data sets are organized as a temporal sequence. The data, sampled during a time window of duration ξ, is shown to the network simultaneously, i. e. the information about the previous stages of the magnetosphere is embedded into the input vector. This window is stepwise in time, nevertheless it is possible to present the learning patterns randomly. Therefore the presence of data gaps does not affect the learning process as it does in the case of recurrent networks. The feed-forward neural network together with this type of organization of the input data is often referred to as a time-delay neural network [4,7,9]. This kind of networks was used in current research.

The architecture of a feed-forward network is specified by the number of neurons used in the input, hidden, and output layers. The output O_i^μ of a single hidden-layer neural network with an input pattern ξ is given by

$$O_i^\mu = g_1\left(\sum_j w_{ij} g_2\left(\sum_k w_{jk}\xi_k^\mu\right)\right) \qquad (1)$$

where w_{ij} and w_{jk} are the weights between the input and hidden layers and between the hidden and the output layers, respectively, $g_{1,2}$ are the transfer functions.

In this work we used 8 neurons in the input vector, which represents the time delay line of 1 hour averaged indices, extended over 8 hours, previous to the predicted Dst value (one neuron in the output layer). We used the linear scale function as a scaling function to scale all input values into an interval <<-1, 1>>. The double brackets indicate that larger numbers are allowed later when we apply the neural network to the validation set inputs, conserving the same scaling factor as in case of training and validation sets.

Different numbers of neurons in the hidden layer have been checked to establish the best network configuration. The logistic $f(x) = 1/(1+\exp(-x))$ function was used as the transfer one. The weights were updated by the scaled conjugate gradient method.

To make a direct comparison between the results, obtained using the VB_z (where V is the solar wind plasma bulk velocity and B_z is the z component of the interplanetary magnetic field (IMF)), and the PC index, we selected the 1999 and 2000 data sets divided into training, test, and validation subsets. The validation data sets were provided to the networks preserving the time sequence, allowing analysis of the results from a physical point of view.

The accuracy of predictions was estimated by calculating the linear prediction-target correlation coefficient as

$$\rho = \frac{\sum_{\mu=1}^{N}\left(T^{\mu}-\langle T\rangle\right)\left(O^{\mu}-\langle O\rangle\right)}{\sqrt{\sum_{\mu=1}^{N}\left(T^{\mu}-\langle T\rangle\right)^{2}}\sqrt{\sum_{\mu=1}^{N}\left(O^{\mu}-\langle O\rangle\right)^{2}}} \qquad (2)$$

where T is the target vector.

Results

The performance of the networks was checked by applying the neural networks to predict the Dst variation during 16 storm time intervals in July-December 2000. It was found the network performance generally does not depend strongly on the number of neurons in the hidden layer and transfer functions, and all storms, except one, were reasonable well predicted. However, slightly better results have been achieved, when the number of hidden neurons was equal to 8 for PC-index and equal to 12 for VB_z. The results, provided by these two networks were used for the following analysis.

Fig. 1 and 2 show the relationship between the observed and predicted Dst minima for each of 16 storms analyzed. As it can be seen, the minimum values of the Dst variation are predicted correctly in case of the VB_z input and are underestimated in case of PC index for strong storms.

However, if we analyze the dependence of cross-correlation coefficient between observed and predicted value of Dst variation for each storm on the minimum Dst (see Fig. 3 for VB_z and Fig. 4 for PC index), it is possible to see, that the values of this coefficients are almost independent on the value of Dst minima for both cases, and the cross-correlation coefficient is almost the same for strong and weak geomagnetic storms.

Also it is possible to see, that both graphs follow the same tendency, and the storms predicted well using the solar wind data generally are also predicted well using the PC index. It is true also for the unsatisfactory predictions. For example, the strongest storm has very good correlation coefficients in both cases, and the worth predicted storm is the same and has very low cross-correlation coefficient also in both cases.

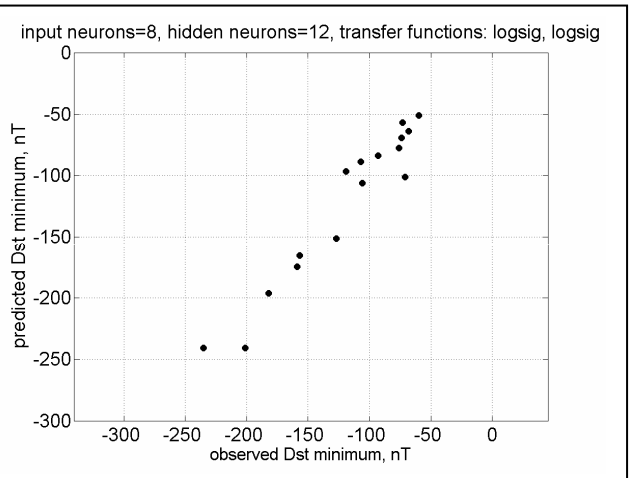

Fig.1. Relationship between observed and predicted D_{st} minima. VB_z data were used as an input.

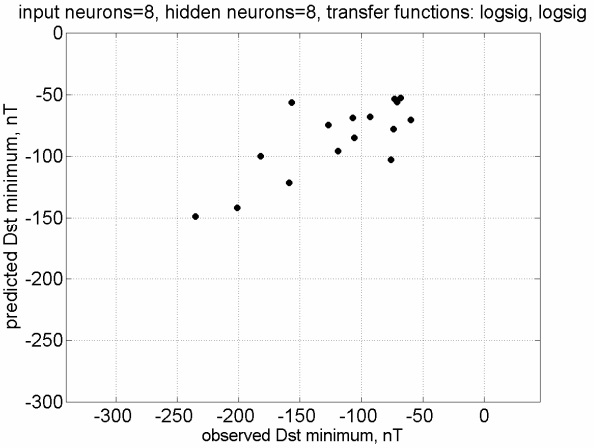

Fig. 2 Relationship between observed and predicted D_{st} minima. PC index data were used as an input.

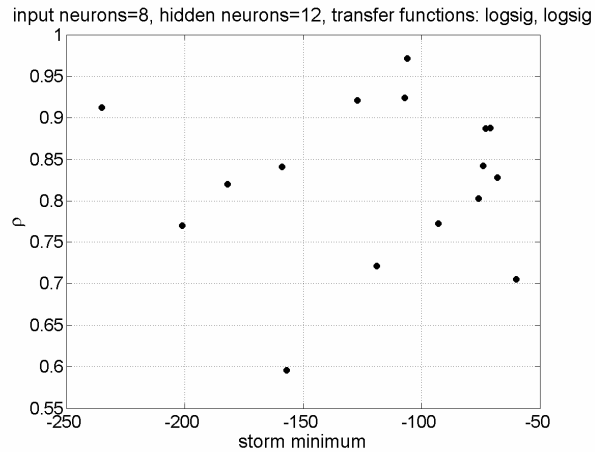

Fig.3. Dependence of the cross-correlation coefficient on the storm amplitude. VB_z data were used as an input.

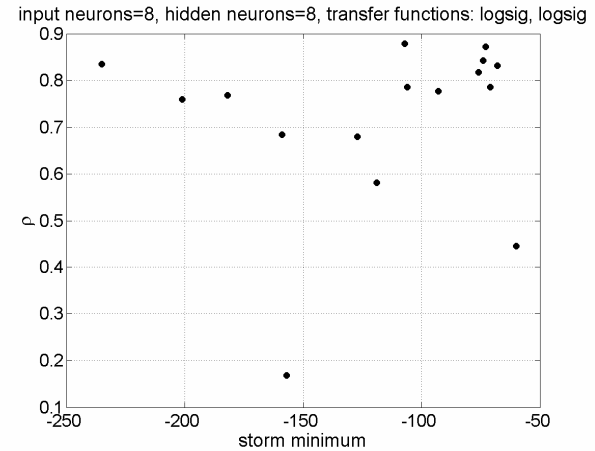

Fig.4. Dependence of the cross-correlation coefficient on the storm amplitude. PC data were used as an input.

Fig. 5 and 6 show the observed and predicted Dst variation for the strongest storm of the validation data set, occurred August 10-15, 2000. As it can be seen, the amplitude of the Dst variation is well predicted in the first case and it is underestimated in the second one. However, this underestimation does not occur generally when the Dst amplitude does not exceed -100 nT.

To complement our study of possible sources of input parameters measured on the ground, we also explored the possibility to use the auroral electrojet indices for this purpose. It was found that the use of the AL-index gives considerably better results. The definitive AL index is available up to 1988 only, therefore it was not possible to select the same data sets for AL, PC and VB_z. Fig. 7-9 summarize the results obtained using the 1981-1982 data sets. It is possible to see, that generally the geomagnetic storm amplitude is well reproduced, although the points are much more spread in comparison with Fig. 1 and even with Fig. 2.

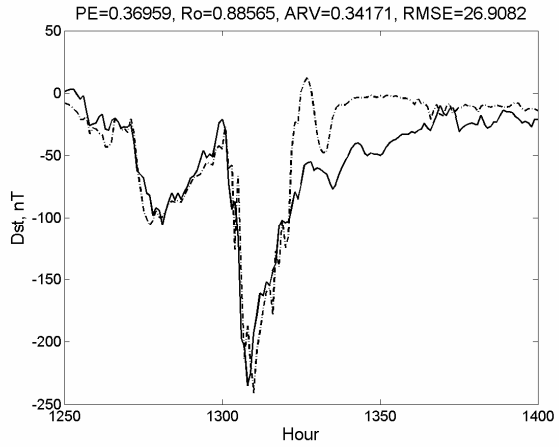

Fig.5. August 10-15, 2000 storm. Dashed line corresponds to the predicted Dst variation. VB_z data were used as an input.

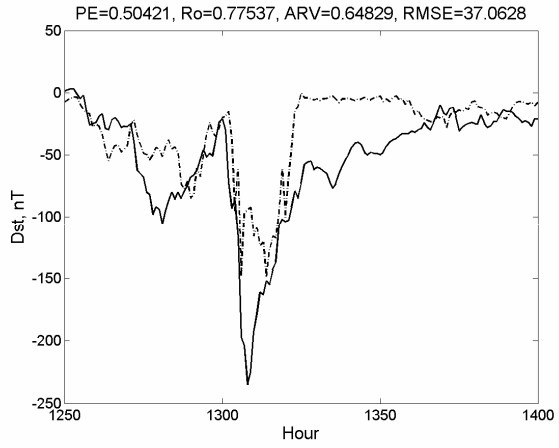

Fig.6. The same as in Fig. 8. PC index was used as an input.

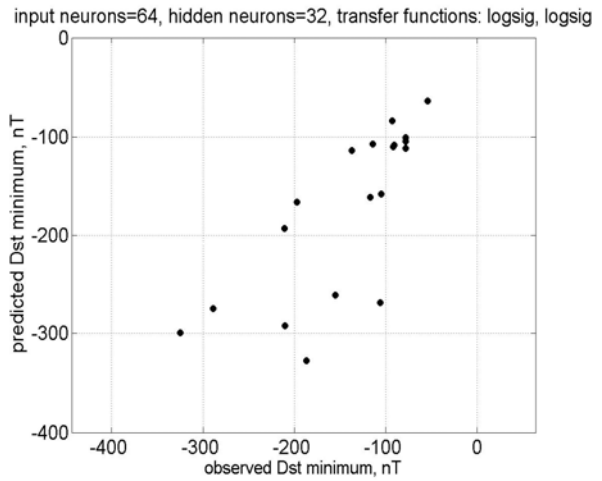

Fig.7. Relationship between observed and predicted D_{st} minima. AL-index was used as an input.

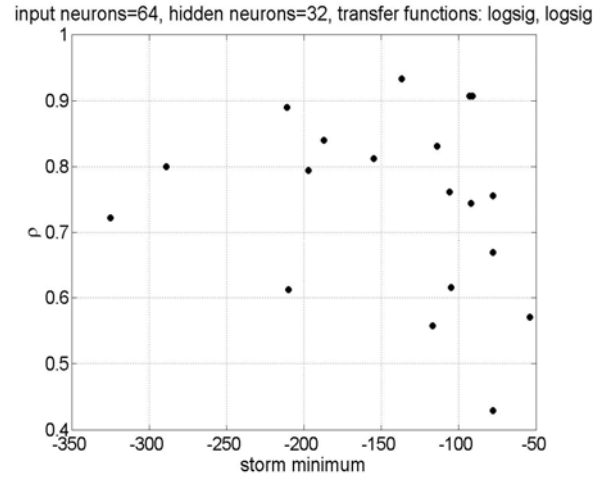

Fig.8. Dependence of the cross-correlation coefficient on the storm amplitude. AL index was used as an input.

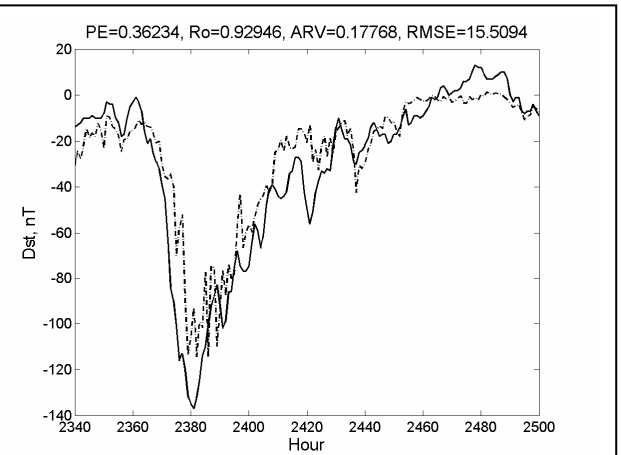

Fig.9. August 10-15, 2000 storm. Dashed line corresponds to the predicted Dst variation. AL index was used as an input.

Fig. 8 indicates that the neural networks based on the AL index reproduce better strong geomagnetic storms. Six geomagnetic storms with Dst<-150 nT have the cross-correlation coefficient between the observed and predicted Dst more than 0.7, and only one is situated below this value. On the contrary, when the Dst>-150, we have more scattering values of ρ. Another feature of the use of AL index is the better reproduction of the recovery phase (Fig. 9) then in the case of using PC and VB_z.

Discussion

The use of the solar wind VB_z and the PC index for Dst prediction is physically connected to the convective transport of plasma sheet particles into the ring current during geomagnetic storms. The high level of correlation of VB_z with large-scale magnetospheric electric field is well known. PC index is linearly correlated with the cross polar cap voltage [10] under conditions of low or moderate magnetic activity PC<8). However, [11] showed that under conditions of extremely high increase of magnetic activity (PC > 10) the polar cap electric field tends to saturate at $E_{ion} \approx$ 40-45 mV/m. It would be stressed that the PC index is sensitive not only to VB_z in the solar wind, but to a number of factors influencing activity in the polar cap. The relationship between the polar cap potential and the PC-index can be more complicated than the description of [10]. Antisunward convection in the polar cap is driven by the interplanetary electric field. The PC index is also strongly affected by solar wind pressure pulses [12], which produces antisunward convection (positive PC) under southward IMF, and which produces sunward convection (negative PC) under northward IMF. Therefore PC contain the information not only on VB_z, but also on the solar wind dynamic pressure. The auroral AL index is used for the description of substorm activity. Therefore it contains not only information on the large-scale electrostatic electric fields, but also on impulsive electric fields producing substorm pressure injections in the inner magnetosphere.

Conclusions

To date the most promising techniques of the space weather forecast are based on the study the early precursors of geomagnetic storms, like the prediction of daily solar wind velocity days ahead. However, sometimes the solar wind properties in the libration point (230 Earth Radii) differ significantly from those measured in the vicinity of the magnetosphere (tens Earth Radii) [13,14]. Sometimes also there are gaps in the satellite data. Therefore, it is reasonable to develop an alternative secondary predicting methods relying solely on ground-based measurements.

AL index is a good tool of Dst prediction, but it is not available in real time. Currently the Kyoto World Data Center provides the provisional values for Dst variation in real-time. This makes it possible to realize a direct verification of Dst predictions as well as include the previous values of Dst as an input parameters using another index.

In this work we have shown that the PC index seems to be a good candidate for the Dst index forecast. It is the only index available now in real time. However, to make the PC index based Dst forecast more reliable, it will be necessary to improve the quantitative understanding of variations in ionospheric conductivity. PC index as an input parameter for the time-delayed neural networks gives the possibility to predict Dst values up to -100 nT. We suggest that the proper inclusion of the observed nonlinearity of the PC index and the simultaneous use of PC index from both hemispheres will lead to an increase in the accuracy of the prediction of Dst for great geomagnetic storms.

Acknowledgments

The research was supported by FONDECYT grant 1020293, INTAS grant 03-51-3738, RFBR grant 05-05-64394-a and the program Universities of Russia.

REFERENCE

[1] Y.Kamide, W.Baumjohann, I.A.Daglis, W.D.Gonzalez, M.Grande, J.A.Joselin, R.LMcPherron, J.LPhillips, E.G.D.Reeves, G.Rostoker, A.S.Sharma, H.J.Singer, B.T.Tsurutani, V.M.Vasyliunas, "Current understanding of magnetic storms: Storm-substorm relationship", *J. Geoph. Res.*, vol.103, 1998, pp17,705-17,732.

[2] R.L.McPherron, "Influence of the substorm current wedge on the *Dst* index". *J. Geoph. Res*. vol.104, 1999, pp4567-4575.

[3] H.Lundstedt, P.Wintoft, "Prediction of geomagnetic storms from solar wind data with the use of a neural network, *Ann. Geophys.*, vol.12, 1994, pp676-686.

[4] H.Gleisner, H.Lundstedt, P.Winfoft, "Predicting geomagnetic storms from solar wind data using time-delay neural networks", *Ann. Geophys.*, vol.14, 1996, pp676-686.

[5] J.-G.Wu, H.Lundstedt, H., "Prediction of geomagnetic storms from the solar wind data using Elman recurrent neural networks", *Geoph. Res. Lett.*, vol.23, 1996, pp319-322.

[6] V.Munsami, "Determination of the effects of substorms on the storm-time ring current using neural networks", *J. Geoph. Res.*, vol.105,A12, 2000, pp27,833-27,840.

[7] M.Stepanova, E.Antonova, O.Troshichev, "Prediction of Dst variations from Polar Cap indices using time-delay neural network", *J. Atm. Sol. Terr. Phys.*, vol.67, 2005, doi:10.1016/j.jastp.2005.02.027.

[8] P.Wintoft, P., H.Lundstedt, H., "Prediction of daily average solar wind velocity from solar magnetic field observations using hybrid intelligent systems", *Phys. Chem. of the Earth*, vol.22, 1997, pp617-622.

[9] M.Stepanova, P. Peres, "Autoprediction of Dst index using neural network techniques and relationship to the auroral geomagnetic indices", *Geofis. Int.*, vol.39, 2000, pp143-146.

[10] O.Troshichev, H.Hayakawa, A.Matsuoka, T.Mukai, K.Tsuruda, "Cross polar cap diameter and voltage as a function of PC index and interplanetary quantities". *J. Geoph. Res.*, vol.101, 1996, pp13429-13435.

[11] O.Troshichev, R.Lukianova, V.Papitashvili, F.Rich, O.Rasmussen, "PC index as a proxy of electric field in the polar region ionosphere". *Geoph. Res. Lett*., vol.27, 2000, pp3809-3812.

[12] R.Y.Lukianova, O.A.Troshichev, "Magnetospheric response to the solar wind dynamic pressure inferred from the PC index". Sixth international conference on substorms, March 25-29, 2002, Seattle, Abstracts, pp38.

[13] P.Dalin, G.Zastenker, K.Paularena, J.Richardson, "The main features of solar wind correlations of importance to space weather strategy". *J. Atm. Sol.Terr. Phys.*, vol.64.5-6,2002, pp737-742.

[14] G.N.Zastenker, P.A.Dalin, A.A.Petrukovich, M.N.Nozdrachev, S.A. Romanov, K.I.Paularena, J.D.Richardson, A.J.Lazarus, R.P.Lepping, A.Szabo, "Solar wind structure dynamics by multipoint observations". *Phys Chem. of the Earth, Part C*, vol.25(1-2), 2000, pp137-140.

Data Visualisation Interactive Network for the Aragats Space-environmental Center

A.Eghikyan, A.Chilingarian

The ASEC (Aragats Space Environmental Center) facilities provide real time monitoring of cosmic particle fluxes with a number of particle detectors located at high-altitude research stations at mt. Aragats, Armenia. For the issuing of warnings and alerts on sudden changing of the near-earth radiation environments and for the detailed collaborative analysis of the most important solar modulation events we developed distributed counting system with automatic data storage and processing. For the physical inference based on the changing particle fluxes the DVIN (Data Visualization Interactive Network software is used). Data from ASEC monitors is accessible on-line from http://crdlx5.yerphi.am/DVIN3 *and currently is widely used in research of the solar physics and Space Weather. In the paper we illustrate the DVIN implementation with the Ground Level Enhancement (GLE) event analysis during famous Halloween events (28October -2 November 2003).*

Introduction

Networks of particle detectors are continuously monitoring changing fluxes of particles reaching earth surface. Charged and neutral particles are born in cascade processes initiated by protons and nuclei incident on the terrestrial atmosphere. Fast majority of these primaries are from numerous galactic sites traveling tens of million years in Galaxy and arriving to solar system as rather stable and isotropic population. Balloon and satellite spectrometers enumerate the Galactic Cosmic Ray (GCR) fluxes with rather high accuracy (Caprice, ei dr.). Our nearest star, the sun, by disturbing interplanetary magnetic field and by accelerating protons and ions (producing so called Solar Cosmic Rays – SCR) is modulated the GCR flux, and as a result – the particle fluxes measured by surface detectors. Among numerous sun modulation effects Ground Level Enhancements (GLE), is one of most essentials, both from point of view of fundamental physics processes and Space Weather effects. The universal processes of particle acceleration in the Universe can be studied although on the smaller however much more detailed by measuring fluxes of protons and ions from solar accelerators. The satellite spectrometers due to tiny sizes can measure only huge fluxes of low energy particles, surface detectors are much larger and they use atmosphere as particle multiplier. Therefore, rather small highest energy fluxes of solar particles can be recovered by measured secondary particle flux on earth surface. The problem of revealing signal (SCR) against overwhelming background (GCR) is one of the most complicated in high energy astrophysics.

We implement several data analysis procedures in DVIN to solve this problem.

Measuring highest energy particles it will be possible to determine the spectra of the major solar event in progress. Hard spectra at heist energies will manifest abundant SCR flux at low and medium energies and consequently radiation hazard to crew of space stations, to space-born and surface industries. There is not much time for issuing warnings and alerts (from 15-45 minutes), therefore data analysis and physical inference should be made very fast. Physical analysis should invoke also data from space spectrometers and particle detectors from world-wide networks.

It is why DVIN is strategically important as a scientific application to help develop space science and to foster global collaboration in solar physics and in space weather research. The system is highly interactive and exceptional information is easily accessible online. Data can be monitored and analyzed for desired time spans in a fast and reliable manner by the remote users world-wide.

Data from particle detectors from space and earth surface is automatically downloaded and stored in DVIN for joint analysis with ASEC monitors.

DVIN provides wide possibilities for sharing data and sending warnings and alerts to scientists and world-wide, which have fundamental and practical interest in knowing the space weather conditions.

DVIN gives opportunity to remote groups to share the process of analyzing, exchange data analysis methods, prepare joint publications and maintain networks of particle detectors. DVIN gives users set of online features for physical interface from the ime series of changing secondary particle fluxes.

DVIN Structure

DVIN structure presented at the Figure 1.

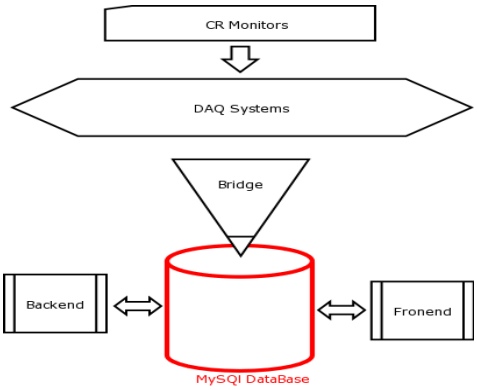

Figure 1. DVIN structure

DVIN developed at the base of several software technologies:

- MySQL Database for data store
- PHP, DHTML as a front-end

The structure of the DVIN presented in Figure 1. Backend is a set of software which interconnects users with database. Software developed at the base of a number of programming languages like Python, Perl, C/C++.

Front-end software developed at the base of PHP as a server side part and DHTML as a client side part. The splitting of Front-end to two parts allows optimization of Internet bandwidth to make the number of reloads of the site minimal.

Figure 2 presents a screenshot of the DVIN operation menu. In the "Operations" menu user performed and displayed following operations with different time-series obtained from particle detectors:

- Plot time series with rich styles;
- Make Distributions from time series;
- Calculate Correlation Matrix;
- Perform Periodic operations on time series;
- Add Time Series to analysis;
- SQL operations;
- Exchange of the Work Areas.

It is possible to display simultaneously up to 6 time series on one plot for the comparative purposes. The distributions of residuals of time series point on the peaks and check for the proper operation of the detector channels;

Periodic operations perform detailed analysis of the time series, revealing the peaks, estimating the statistical significance of peaks, inspecting the detector channels, etc… Add Time series is for importing data from database. SQL operation gives additional functionality for the experienced with SQL users and imports data from Internet. Work areas operation stores "work areas" - sets of processed time series for continuing analyses later and for sharing with collaborators of data and analysis methods. In Figure 3 the toolbox of Operations menu is presented. Each string corresponds to definite time series initial, before or after performing desired operation.

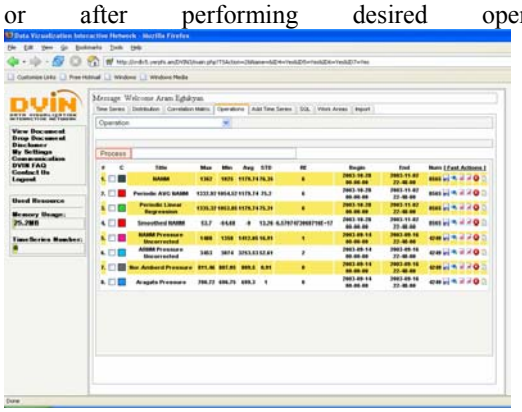

Figure 2. Operations Menu

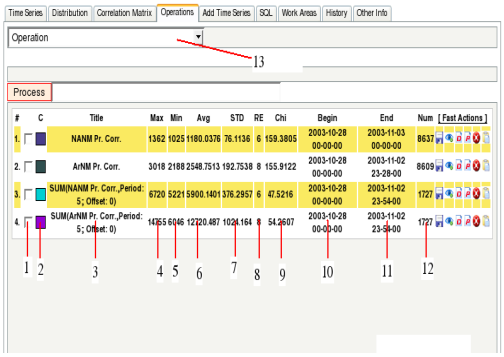

Fig. 3 Toolbox of the "Operations" menu

1. Check box for selecting Time Series
2. Color used for plots (time series and diagrams)
3. Title of time Series
4. Maximum value of Time Series
5. Minimum value of Time Series
6. Average value of Time Series
7. Standard Deviation of Time Series
8. Relative Error of Time Series
9. Begin Time Stamp
10. End Time Stamp
11. Number of Elements in Time Series
12. Operations Drop Down menu

Fast Actions

Most important operations are displayed at the right of each Time Series string in the Drop Down menu, as shown in Figure 4.

Fig. 4 "Fast Actions" panel

Following operations menu are presented in Figure 4 from left to right:

1. Save Time Series to local system
2. View Time series (in ASCII format, for not too large time series)
3. Plot Distribution of Time Series
4. Plot Time Series
5. Delete time series
6. View Notes attached to this Time Series.

"Add Time Series" Section

"Add Time Series" section is developed for easy data import from MySQL database into DVIN and contain following operations:

1. Select Time Range
2. Select preserved solar events
3. Select Monitor
4. Select Time Series of Monitor
5. History of selected Time Ranges

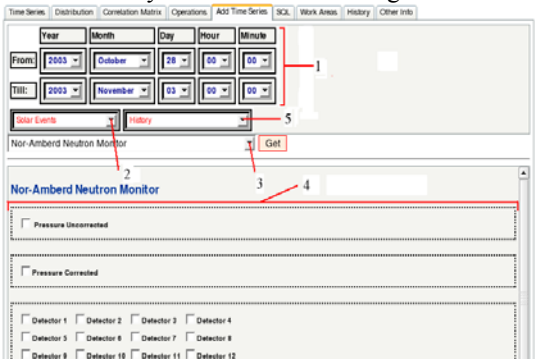

Fig. 5. "Add Time Series" Section

The "Check boxes" of Time Series give users ability to import any number of Time Series of selected monitor in one action. The Time Series of monitors are divided to subsections. For example Nor-Amberd Neutron Monitor data consisted of several groups: Pressure Corrected data, Pressure uncorrected and raw data (data from each detector separately).

"SQL" Section

"SQL" section's main purpose is to grant a direct access to MySQL database for importing data, see menu in Figure 6. It is more complicated then "Add Data" section, but gives to user flexible tool for importing data. Users can make "plot" data processing during the import, for example, to import sum of several detectors, check the data for upper-down limits and replace ones with another set if necessary, or produce another filtering operation. To use this feature user must be familiar with SQL language.

1. Easy SQL generation form
2. Advance SQL generation window
3. Name of imported Time Series

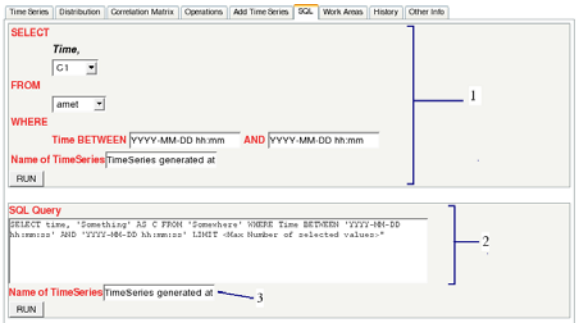

Fig. 6. "SQL" Menu

"Work Areas" Section

This section is implemented for managing user's work areas. 3 operations are available:

1. "Switch" is for switching current work area to the saved one. The old one will be lost if not saved
2. "Concatenate" produces the concatenation of two sets of Time Series from the current and saved.

"Remove" just removes the saved work area.

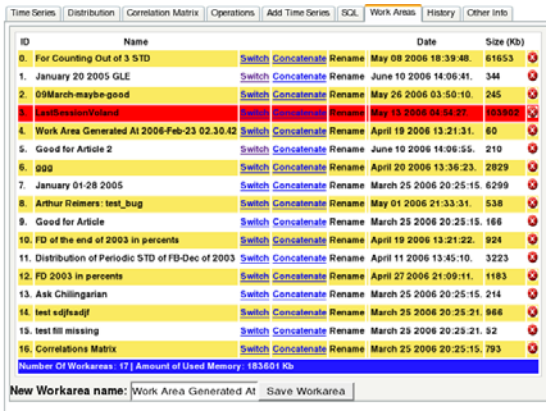

Figure 7 "Work areas" menu

Overview of the Main Operations

There are two main types of Operations so called moving and periodic operations.

The periodic and moving operation are calculated by 3 given values. Length of period, function type and offset. The difference between the moving and periodic operations is in defining of the next portion of time series. In periodic operations the next portions are change with step Period and in the moving operations the step is 1.

Periodic functions are following:

- Average;
- Standard Deviation;
- Median;
- Linear Regression;
- Periodic rebinning (adding successive time series in larger time unit) of the initial time series

Periodic and moving operations provide very flexible and powerful tool for examining of time series. User controls the time period, offset of period (start point of rebinning operation) and interpolation mode (within chosen time period) of time series. Using these options user can rebin (add) successive monitor counts for examining long time periods and reveal non-trivial structures in time series. For example adding initial (parent) 1-minute time series in 3 minute by the "periodic sum operation" helps to discover the Ground Level Enhancement (GLE) detection on 20 January 2005 by the AMMM monitor, obscured by the large fluctuations of 1-minute time series. "Offset" option defines the particular grouping of initial time series. There is 3 possible ways to group 1 minute time series in 3 minute ones; each outlining slightly different structures. "Periodic Average Operation" and "Linear Regression Operation" are interpolating time series by the piecewise continuous functions (see Figure 8). All the periodic operations have "compatibility" option, leaving the number of elements in time series unchangeable. For example, if we interpolate 1 minute time series by hourly average, in each of 60 hourly minutes of transformed time series will be the same average value.

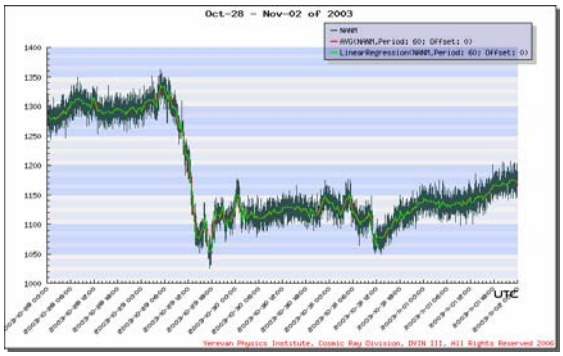

Figure 8 Average (red) and Linear Regression (green) interpolation of the Nor Amberd neutron monitor time series.

Then, by subtracting one time series from another user can obtain the residuals time series (see Figure 9). By dividing obtained residuals to the variance we obtain the, so called, Normalized residuals obeying the standard Gaussian law (see Figure 11). By the time series of normalized residuals we can select the outliers for the further analysis. The histograms of the residuals (see Figure 10) can be compared with standard Gaussian probability density function by χ^2 test. Large values of χ^2 point on failures in detector channel operation. Therefore, the described operations modes of DVIN can be used for the check of detector channels.

After proving the "Gaussian" nature of the residuals positive outliers are examined as candidates for the Ground Level Enhancement (GLE) or "Geomagnetic storm" events. Large positive deviations (greater than 4σ) point on the possible non-random character of the deviation from mean count rate, i.e. on the solar modulation effects.

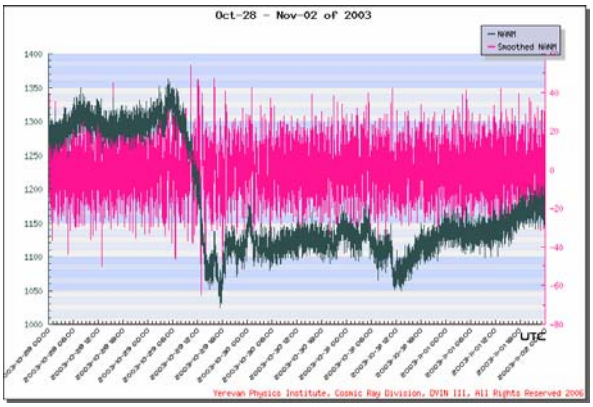

Figure 9. The residuals time series (in red) of Nor Amberd NM time series (black).

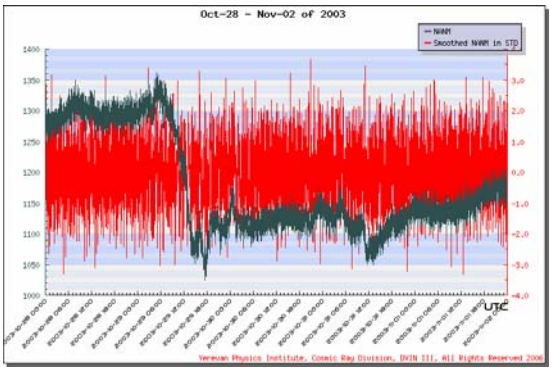

Figure 10. Standard Deviation of residuals, of Nor-Amberd Neutron Monitor

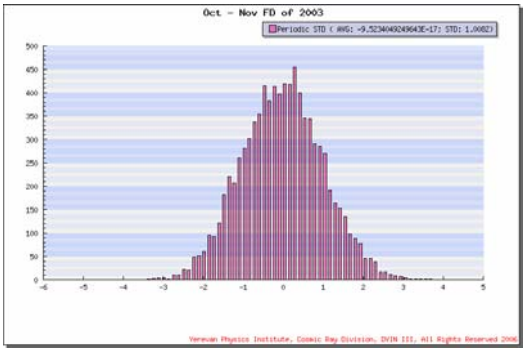

Figure 11. Distribution of the GLEs in Standard Deviations of Nor-Amberd Neutron Monitor

At the figure 12 presented the same FD in percents. To calculate the decrease in percents we get the average count rate at the normal period Oct 28 and using this value as a 100 percent recalculating the values into percents.

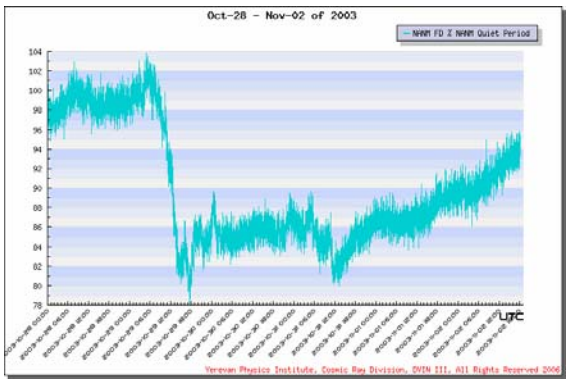

Figure 12 Nor-Amberd Neutron Monitor, FD of Oct-Nov of 2003. FD: 22 Percent in comparison

The transformation of the time series into percents of observed period relatively to the "quiet" period is widely used for getting quantitative description of the "deepness" of Forbush decrease.

Transformation of Time Series into percents relatively to the other time series are made by following steps

1. Selection examined time perios;
2. Selection of reference time period;

Using "%" operation in "Binary Mode" .

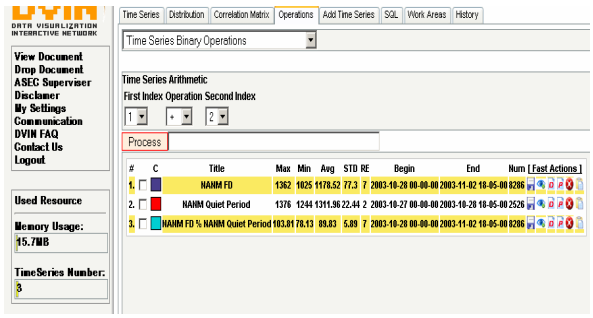

At the Fig 13 presented the "Operations".

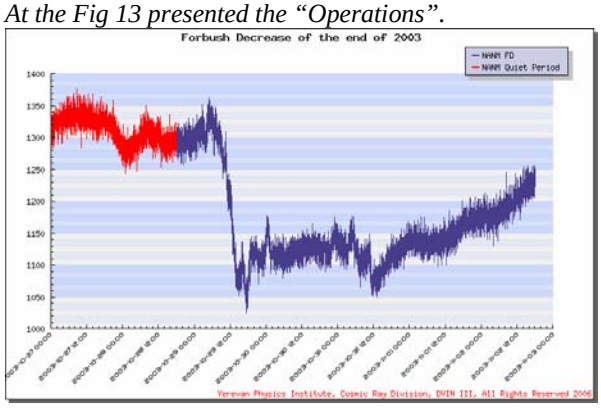

Fig. 14 Red part is the normal period, Blue part is observed period. The transformation to percents are

produced relatively the "Red" one.

At the plot 14 presented the normal and Forbush Decrease of 2003 which must be translated to percents and the relative quiet range.

Analyzes of the candidate of GLE with AMMM detector

Varieties of the ASEC monitors are "selecting" different populations of the primary energy spectra, because of different energy thresholds. Among ASEC monitors the Aragats Multidirectional Muon Monitor (AMMM) selects highest primary energies, because detector is located in the underground hall and 14 m. of soil and concrete fileter low energy muons and electrons. Only muons with energy greater than 5 GeV can reach
Detector location. The energy of "parent" proton should be greater than 20 GeV to give birth to 5 GeV muon. These energies are extremely rare in SCR and if encounter lasting several minutes only. Therefore, in AMMM time series we are looking to very narrow peaks in coincidence with solar flares and GLEs detected by surface particle detectors sensitive to lower primary energies.

The 1- minute time series of the AMMM are presented in Figure 15. Enhancement of the count rate is seen at 10:12 10:14 UT. Unfortunately from 45 channels of the AMMM detector were not operational at the time, therefore only 31 m^2 of muon detectors were in use to measure the high energy muon flux. The estimated mean count rate of the Galactic Cosmic Rays (GCR) as measured by the 31 m^2 of the AMMM detector during the 10:40 – 11:40 UT time span, excluding the enhanced interval from 10:12 to 11:14 UT, is 92040 particles per minute.

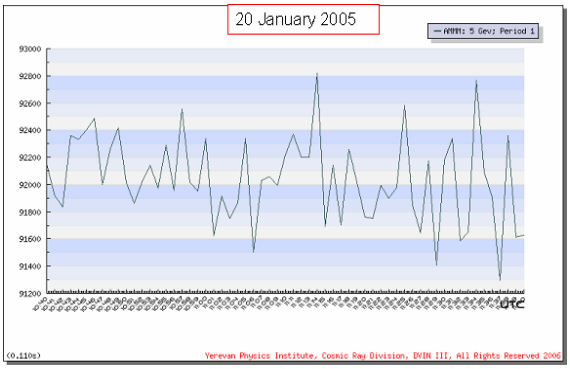

Fig. 15 . Minutely data of AMMM.

In the Table 1 are depicted the statistical parameters of one minute time series. To check significance of the GLE candidate we calculate the significance according to the Poisson distribution and standard Relative Mean Square Deviation:

$$RMSD = \sqrt{\left(\frac{\sum_{i=1}^{i=N}(C_i - \bar{C})^2}{N-1}\right)} / \bar{C},$$

Where normalized residuals $X_i = \frac{C_i - \bar{C}}{S}$, $i = 1,60$, C_i, are 1 minute count rates of the AMMM, $\bar{C}$ is hourly mean of the 1-minute time series and $\sqrt{\bar{C}}$ - is the hourly Poisson deviation of the count rates.

	Max	Min	$\bar{C}$	STD	RMSD	S
1 min counts	92821	91296	92040	315.45	0.34	0.33

Maximal value at 10:14 – 92821, enhancement (possible signal) Δ=781. The relative enhancement $\Delta_r = \Delta / \bar{C} = 0.85\%$, correspondent to significance of Δ_r / RMSD = 2.5σ.

To emphasize the peak in the AMMM time series we group the 1 minute time series in the 3 minute time-intervals. In Figure 16 three different possibilities of regrouping of 1 minute time series in 3 are presented. All 3 are presented slightly different temporal pattern of time series. The particular time series started from the second element (10:41) provide biggest peak. In Figure 14 The 3-minute time series emphasized the peak, offset 2 provides maximal . However, the size of peak is not large enough to claim that AMMM detect the SCR and not only GCR fluctuation.

In the next steps of processing used offset 2 as a Time Series with a maximum Peak.

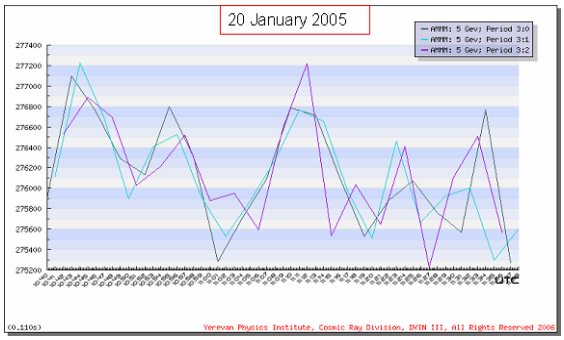

Fig. 16. 3 Minutely data with all the offsets.

For farther calculation we remove the Peak. To remove the peak we used "Up-Down Limit Cut" which replaces

the points which are do not located in the given range with Periodic Median. At the Fig. 17 Presented two Time Series with and without Peak.

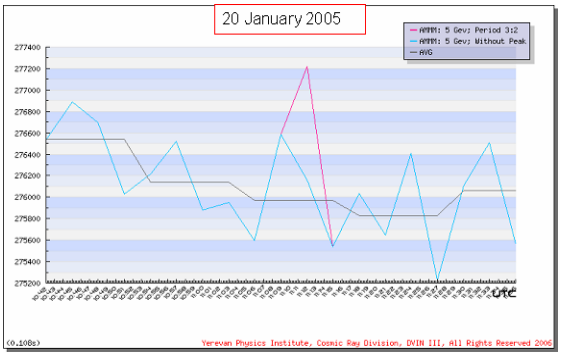

Figure 17. AMMM: 5 Gev; Period 4:3 with and without peak and periodic AVG of the Time Series without Peak

At the following table presented statistical parameters of the time series with peak and without peak.

Name	Max	Min	Avg	STD	R.E.(100*STD/AVG)
AMMM: 5 Gev; Period 3:2	277219	275225	276165	497	0.178
AMMM: 5 Gev; Period 3:2 without peak	276892	275225	276109	434	0.159

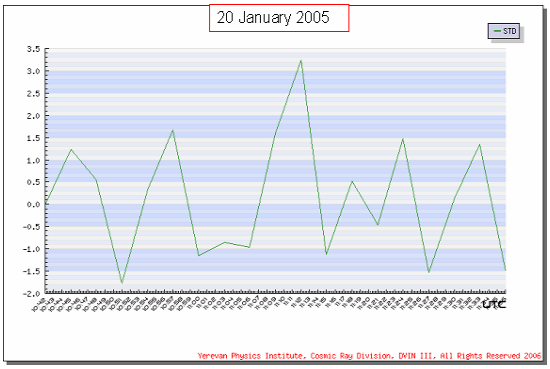

Figure 18 Normalized residuals of AMMM 3 minute counts

From the Picture 18 we can see that significance of the peak did not exceed 3.3, such enhancements we can detect several times during the day.

Therefore we can not reject the hypothesis that detected peak is background fluctuation only.

Correlation Analysis

Correlation Analysis is a new tool for the physical inference on multiple time series. Different ASEC monitors are sensitive to different populations of the primary protons and ions. If Neutron Monitors are detecting neutrons generated by primary protons with energies just after cuttof rigidity, the 5 GeV muons are generated mostly by >20 GeV protons. Also different channels of the Solar Neutron Telescope (SNT) also are selected slightly different populations of primaries. Therefore, measuring correlations between changing count rates of ASEC monitors we can get information about energy spectra of the solar cosmic rays (SCR), or about the nature of geomagnetic disturbance changing the actual value of the threshold rigidity.

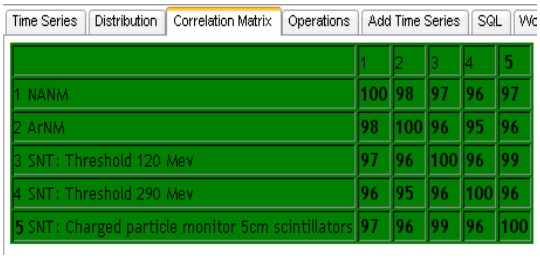

Figure 4.1 Correlation matrix of 2003-10-29 in percents

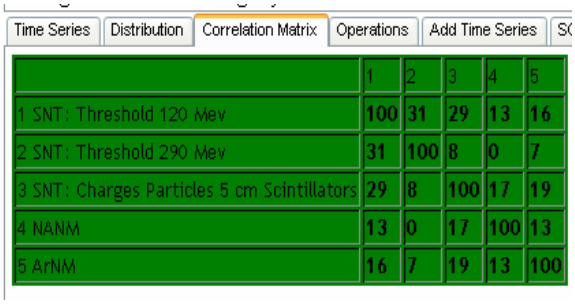

Figure 4.3 Correlation matrix of 2006-04-08 in percents

In the Figure 19 and Figure 20 are depicted the correlation matrixes of two periods, 2003-10-29 which corresponds to the enormous Forbush decrease (correlations are large approaching 1). At 2004-03-05 which corresponds to the calm phase of the Space Weather (no geomagnetic disturbances) there are no significant correlations detected..

Work Areas issue

Work Areas in DVIN defined as a set of Time Series which can are related to solar modulation effect and should be treated mutually. Saving work area gives users a very convenient feature for localizing the work, splitting the data analysis to several succeeding stages in time. Using work areas allows producing temporary or so called middle stage time series. During work with data from Aragts monitors the number of different time series can rapidly grew and make the work with the DVIN very complicated. Therefore, we provide to user possibility to split the work (in programming this method called "Functional Programming" or "Procedural Programming") to several sub stages and concentrate attention at small number of time series at a time.

Data Exchange between Users

Users of DVIN can interchange processed data and establish virtual collaboration. They interchange work areas using communication section. When user gets data from another user he can continue analyzing at the received work area or concatenate own work area with new one. In the figure 21 we illustrate this process by "Communication" section of the DVIN.

Fig. 21 Communication Areas Subsection

1. Drop down menu of Recipients (DVIN Users)
2. Work Areas for sent.

Conclusion

DVIN is the first online system used in Cosmic Ray Division where users can make online collaborations not only at the level of information interchange but also at the level of physical analysis, using general interconnected platform. It allows scientists from different countries to work.

Acknowledgment

We are grateful to Suren Chilingaryan and Tigran Hovhannisyan for technical assistance and idea generation and ASEC members for stimulating interest and support.

Reference

[1] MySQL Reference Manual (URL:http://dev.mysql.com/doc/)

[2] PHP Manual (URL: http://www.php.net/docs.php)

[3] MathWorld (URL: http://mathworld.wolfram.com/)

First European Space Weather Telescope – MuSTAnG

F. Jansen
University of Greifswald, Institute for Physics, WWW Greifswald, Germany
and 1A-First Applications Greifswald, Germany

Abstract

MuSTAnG is the abbreviation for "Muon Spaceweather Telescope for Anisotropy at Greifswald". MuSTAnG will be the first European Space Weather Telescope to measure in real time form the ground the propagation of interplanetary Coronal Mass Ejections (CMEs). MuSTAnG will be part of an International Muon Telescope Network, which delivers forecast and nowcast information about plasma cloud propagation and cosmic ray flux changes for space weather users up to 20 hours in advance. The physics, technical characteristics and construction status of MuSTAnG will be described. In addition the role of MuSTAnG within several space weather activities – towards an European Space Weather Programme (ESWP) - carried out in the last ten years in Europe will be sketched.

1. Introduction

Space based coronagraph on SOHO like LASCO observes in near real time CMEs up to 30 solar radii - or about only to 1/3 of Mercury orbit [1]. This restricted field of view means a gape of real time observation for CMEs in the order of two days until the moment Earthward directed CMEs are arriving at L1 point or nearby Earth orbits, where SOHO, ACE and other satellites measure in-situ the CMEs. After its foreseen launch in August 2006 STEREO will improve the quantity and quality of real time detection of earthward directed CMEs within its operational time of about two years [2]. Nevertheless a very long and real time detection of CME until the next solar maximum is demanded from the space weather community [3].
MuSTAnG will fulfil these demands and will measure in real time from the ground the propagation of interplanetary CMEs and forecast their arrival time at Earth, i.e. by means of the international muon telescope network in the order of 20 hours prior CME arrival, which means about from Venus orbit. In addition cosmic ray flux changes induced by interaction of primary cosmic rays with the interplanetary CMEs are measured in real time.
MuSTAnG measurement and detection principles are the following:

a) the nearly isotropic distribution galactic cosmic ray in the interplanetary space between the Sun and Earth will be disturbed by the interaction of cosmic ray flux with CMEs and related shockwaves propagating towards Earth from the Sun [4]. A decrease or increase of the anisotropic compared with the isotropic component of the galactic cosmic rays is detectable by cosmic ray muon telescopes. The ratio of anisotropy to isotropy is in the order of 0.1% to 4 % [5].
b) The relativistic, primary cosmic ray particles deliver the information towards muon telescopes at Earth ground up to 20 hours before arrival of the interplanetary CME and shock wave at Earth: because the primary cosmic rays produce secondary particles like muons in the atmosphere, which still have the same arrival direction on ground as the originally primary cosmic ray particle.
c) The secondary cosmic ray muons produce on MuSTAnG plastic scintillators light flashes, which will be detected by photomultiplier tubes and recorded by the telescope electronic. The directional information will be re-constructed by coincidence logic from the two plastic scintillator detector layers.
d) MuSTAnG operates with a new detection technique (compared with the Australian, Japanese and Brazil scintillator telescopes), originally developed for L3 experiment at CERN [6] and first applied to a space weather telescope.

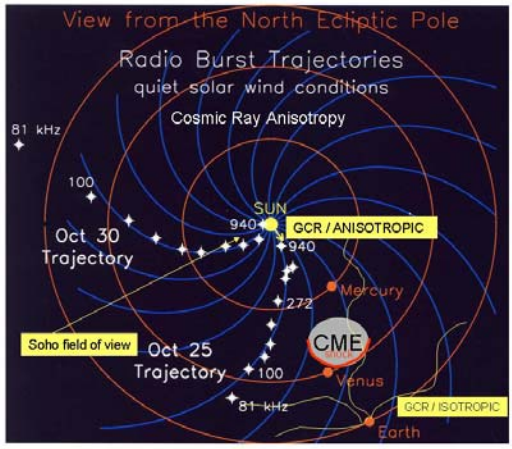

Fig. 1 Sketch of the inner heliosphere: Parker spiral magnetic field lines (blue), Soho field of view, cosmic ray anisotropy and radio burst trajectory. Data transfer on interplanetary type II and III radio bursts currently not observable in real time on the ground [7], but galactic cosmic rays – which are mostly isotropic distributed in the GeV energy range - obtain an anisotropic distribution towards the Sun direction, only in the case if a CME is propagating between the Sun and the Earth.

MuSTAnG is funded by ESA and DLR (ESA/ESTEC contract 18835/04/NL/MV under the supervision by E. Daly, A. Glover and F. Gampe). The construction of MuSTAnG started in January 2005 and will be finished in fall 2006. The MuSTAnG consortium consists of the following members: the University and 1A company in Greifswald (R. Hippler & F. Jansen), HTS Dresden (Germany, W. Göhler), UAS Stralsund (Germany, G. Kolbe & B. Zehner), the University of Bern (Switzerland, E. Flückiger & R. Bütikofer), Austrian research Seibersdorf (P. Beck), Shinshu University (Japan, K. Munakata & S. Yasue), Australian Antartic Division (Hobart, M. Duldig & J. Humble), University of Delaware (J. W. Bieber & T. Kuwabara) and IEPSAS (Slovakia, K. Kudela).

2. Physics and Technical Characteristics of MuSTAnG

Ground-level cosmic ray telescopes scan various directions in space (including to the Sun) as Earth rotates. The daily variations in counting rates on ground reflect the anisotropic intensity distribution of cosmic rays in space. In addition the telescopes observe a reduced flux of cosmic ray particles moving away from the shock (with small pitch angles), due to cosmic ray depleted region behind the interplanetary shock in front of the CME. A cosmic ray intensity deficit or increase in the order of 1% to 4% - so-called precursor anisotropy decrease (PAD) and precursor anisotropy increase (PAI) were already measured in the early 1990s [5]. A first detection of the shock is in principle possible at a distance of

$$r \sim 0.1\ \lambda_P \cos ß$$

(λ_P scattering mean free path of cosmic rays, ß angle between Sun - Earth line and the mean interplanetary magnetic field at Earth). For instance λ_P is about 1 AU for 10 GeV cosmic ray neutron monitor. Insofar shock wave arrival may be detected by neutron monitors about 5 hours before arrival at Earth. The muon telescopes of the international network measure at about 50 GeV, where λ_P much longer. Depending on the actual situation during CME propagation λ_P in the interplanetary space between Sun and Earth is in the order of 2 AU [8]. Therefore by means of a single respectively the entire network of muon telescopes it is calculated to observe the cosmic ray anisotropy between 10 to 20 hours before shock wave arrival at Earth.

Operating cosmic ray ray muon telescopes have two different detection principles: measurements by proportional counter (PC) and plastic scintillator (PS). PC telescopes are installed at Australian Mawson station (detection area: underground 2 x (2.5 x 1.8 sqm), ground 3 x (2.4 x 2.5 sqm)), Mt. Norikura in Japan (5 x 5 sqm) and the Kuwait PC has an detection area of 3 x 3 sqm. The Armenian muon telescope is a combination of PC and PS telescopes with a detection area of 3 x 2 sqm. The Nagoya Scintillator Telescope (NST) has 6 x 6 sqm, the Australian Hobart Scintillator Telescope (HST) has currently 3 x 3 sqm and the San Martinho Scintillator Telescope (SMST) in Brazil is extended to 7 x 4 sqm [9]. NST, HST and SMST always have one Photomultiplier Tube (PMT) per one sqm. The PMTs are observing the muon induced UV light from top of the PS plates. In contrast MuSTAnG has 4 PMTs per sqm to obtain a higher angular resolution and in addition the optical coupling between the PS and the PMTs is done by means of wavelength shifter fibre optics glued on the top of each PS. This enables MuSTAnG telescope to receive a maximum efficiency. The UV light produced by the cosmic ray muon in the PS will be shifted to green light, in which the selected PMT of MuSTAnG have the maximum response. MuSTAnG has 49 viewing directions (see Fig.4).

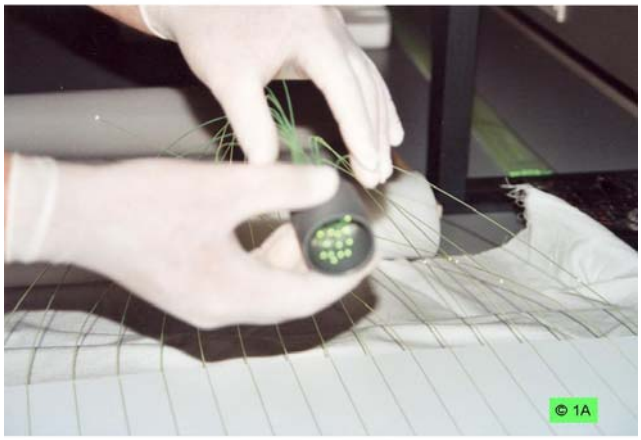

Fig. 2 White painted PS with green emission of WLS fibres on the top of MuSTAnG detector plate. The tube socket for the PMT is also seen.

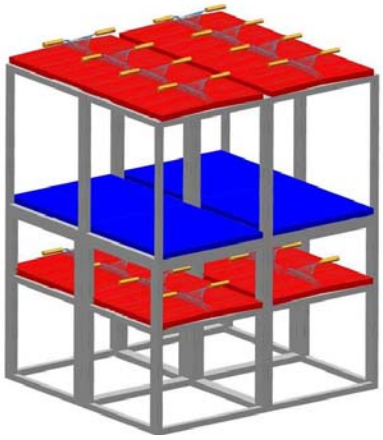

Fig 3. MuSTAnG telescope layout: two layers of PS (red) with WLS (grey) and PMT (yellow). The lead layer (blue) is foreseen to stop low energy cosmic electrons and gamma rays. MuSTanG will have two PS layers – each of them has 4 sqm detection area. The distance between the PS layers will be 1.83 m. The PS layers will protected by light-save metal detector boxes.

The electronical components of MuSTAnG consist of the following part:

1) local units for each of 32 PMTs, which contains preamplifier, high voltage supply and a signal

conditioner with discriminator and pulse shaper and

2) a recording system as a coincidence unit based on advanced logical circuit using Field Programmable Gate Array (FPGA) and VHDIS Hardware Description Language (VHDL) [10].

The local units are new developed electronic components, but the foreseen data recording system is already successful used in NST, HST, SMST, Mt. Norikura and Kuwait PC, as well as at the Armenian muon telescope.

The MuSTAnG software components contain three parts:

1) telescope status software,
2) the software for reduction of cosmic ray muon anisotropy data from the recording system (Fortran 90) and
3) the display of cosmic ray muon anisotropy data for the network based on IGOR Pro software.

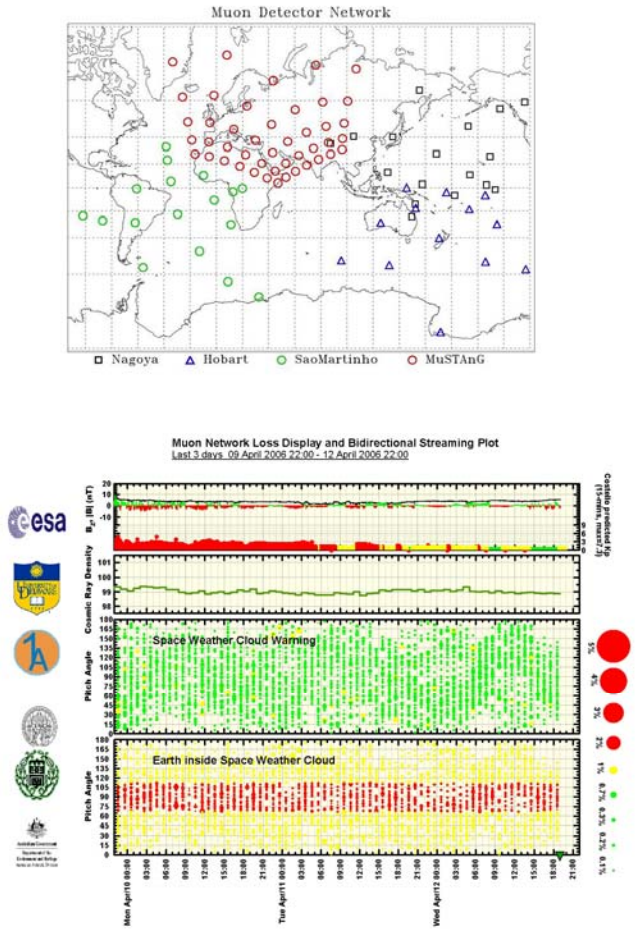

Fig. 4 Top: The 49 asymptotic viewing directions of MuSTAnG reach from about Ural mountain up to the Atlantic Ocean. The calibration of MuSTAnG data is foreseen with the NST and SMST telescope data. Bottom: space weather user orientated online plots (from top to bottom) - B_Z (ACE) and calculated K_p, cosmic ray density. The two circle plots will be also displayed on-line from the international muon telescope network and inform users about cosmic ray anisotropies due to Earthward directed CMEs.

3. Space Weather Activities and MuSTAnG

Within the space weather feasibility study for ESA carried out in 2000 – 2001 by the Alcatel Space Industry (France) consortium it was proposed to build a space and ground based segment as part of an European Space Weather Programme (ESWP). The results of the study are available online under http://esa-spaceweather .net/spweather/esa_initiatives/spweatherstudies/ public_doc.html.) It was proposed for the so-called space based segment an entire fleet of spacecraft and satellites including instrumentation, orbits and communication links to ESA.

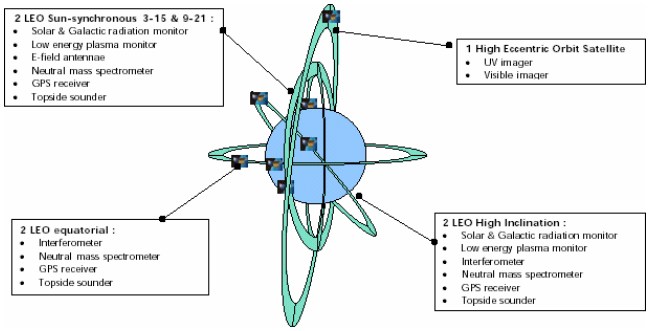

Fig. 5: The Alcatel Space Industry consortium proposed to ESA this space based full scenario of satellites and instruments on HEO and LEO Sun-synchronous, equatorial and high inclination in the ionosphere and thermosphere.

For the ground segment within ESWP a space weather cosmic ray muon telescope was recommended. Insofar MuSTAnG has to forecast the onset of disturbances in the magnetosphere/ionosphere for the European region as well. The Regional Warning Centres (RWC) Warsaw, RWC Prague and the Space Weather Application Center – Ionosphere (SWACI) at DLR in Germany will level up – by means of MuSTAnG - their information about space weather storm on-set time and reliability of impacted communication and satellite navigation systems for the European user community on a routine basis. In addition by means of MuSTAnG the space weather user groups from power line and pipeline companies at RWC Lund and at Finnish Meteorological Institute Helsinki may obtain a more precise onset time for geomagnetically induced currents (GICs). More details of space weather activities in Europe over the last 10 years are described in [11]. Airline operations in Europe may diminish the radiation hazards to their crew during flight and will receive reports about potential communication and navigation failures [12].

4. References

[1] B.Fleck, V. Domingo, A.I. Poland. "The SOHO Mission", Kluwer Academic Publishers, Dordrecht/Boston/London, ISBN 0-7923-3894-4, 1995

[2] R. Howard, D. Moses, A. Vourlidas, J. Davila, J. Lemen, R. Harrison, C. Eyles, J.-M. Defise, V. Bothmer, M.-F. Ravet. "The SECCHI

Experiment on the STEREO Mission", 36th COSPAR Scientific Assembly Beijing, July 2006, subm.

[3] F. Jansen, R. Pirjola. "Space Weather Elucidates Risks to Technological Infrastructures", Eos 85(25), 2004, pp242-246

[4] D. Ruffolo. "Transport and Acceleration of Energetic Charged Particles near an Oblique Shock", The Astrophysical Journal, vol. 515, 1999, pp787-800

[5] K. Munakata, J.W. Bieber, S. Yasue, C. Kato, M. Koyama, S. Akahane, K. Fujimoto, Z. Fujii, J.E. Humble, M.L. Duldig. "Precursors of geomagnetic storms observed by the muon detector network", J. Geophys. Res., vol. 105, 2000, pp27457-27468

[6] O. Adriani, et al. (94 co-authors). "The L3+C detector, a unique tool-set to study cosmic rays", Nucl. Instr. and Meth., vol. A488, pp.209-225

[7] G. Mann, F. Jansen, R.J. MacDowall, M.L. Kaiser, R.G. Stone. "A heliosperic density model and type III radio bursts", Astronomy and Astrophysics, vol. 348, 1999, pp.614-620

[8] K. Leerungnavarat, D. Ruffolo, J.W. Bieber. "Loss Cone Precursors to Forbush Decreases and Advance Warning of Space Weather Effects", The Astrophysical Journal, vol. 593, 2003, pp.587-596

[9] F.Jansen, M. Duldig, K. Munakata, R. Hippler "Cosmic Ray Muon Telescopes: Physics with Space Weather Applications", AOGS Conference, ST-21 Space Weather Session, Singapore, July 2006, subm.

[10] S. Yasue, K. Munakata, C. Kato, T. Kuwabara, S. Akahane, M. Koyama, P. Evenson, J.W. Bieber. "Design of a Recording System for A Muon Telescope Using FPGA and VHDL", Proc. 28th ICRC, Universal Academy Press, 2003, pp.3461-3464

[11] F. Jansen. "European Space Weather Activities", NATO / IST-056 Characterising the Ionosphere, Fairbanks June 2006, subm.

[12] F. Jansen, P. Beck, L. Cander. "Space weather impacts on aviation and radio communications", IHY First European General Assembly, Paris, Proceedings p.9 & CD-Rom, 2006

Forecasting Solar Activity with the Aid of Fuzzy Descriptor Models and Singular Spectrum Analysis

M. Mirmomeni [1], C. Lucas [2], M. Shafiee [3]

[1] *Control and Intelligent Processing Center of Excellence, Electrical and Computer Engineering Department, University of Tehran, Tehran, Iran.*
m.mirmomeni@ece.ut.ac.ir
[2] *Control and Intelligent Processing Center of Excellence, Electrical and Computer Engineering Department, University of Tehran, Tehran, Iran; and School of Intelligent Systems, Institute for Studies in Theoretical Physics and Mathematics, Tehran, Iran.*
lucas@ipm.ir
[3] *Electrical Engineering Department, University of Amirkabir, Tehran, Iran.*
shafiee@aut.ac.ir

Abstract

In the last two decades, researches indicate that the physical precursor and solar dynamo techniques are preferred as practical tools for long term prediction of solar activity. But, why more than 23 cycles of solar activity history should be omitted and just use the empirical methods or simple autoregressive methods on the basis of observations for the latest eight cycles? In this article, a method based on fuzzy descriptor systems (as a generalization of ordinary T-S neuro-fuzzy models) and singular spectrum analysis (SSA) as one of the spectral analysis is proposed to forecast some of solar activity's indexes in the way that, A fuzzy descriptor model is optimized for each of the principal components obtained from singular spectrum analysis, and the multi step predicted values are recombined to make the disturbance storm time (Dst). The proposed method is used for forecasting hourly Dst index in 2001. The results are remarkably good in comparison to the predictions made by solar dynamo and precursor methods.

Keywords: Solar Activity, DST Index, Forecasting, Singular Spectrum Analysis, Fuzzy Descriptor Models, Neuro-fuzzy Modeling, Principal Components, GLOLIMOT.

Introduction

Most of the space weather phenomena are influenced by variations in solar activity. The solar activity time series shows chaotic behavior [1, 2, 3], which leads to long time unpredictability.

On the other hand, descriptor systems [4] describe a wider class of systems, including physical models and non-dynamic constraints. It is well known that the descriptor system is much tighter than the state-space expression for representing real independent parametric perturbations [5]. In addition, the fuzzy descriptor models as a generalization of the locally linear neuro-fuzzy models are general forms that can be trained by constructive intuitive learning algorithms.

In this article a decomposition method based on singular spectrum analysis is used to make an intuitive nonlinear black box modelling technique applicable to prediction of Dst time series. The Singular Spectrum Analysis (SSA) [6, 7] performs a data adaptive filtering in the lag coordinate space of data and yields the principal components of the time series which have narrow band frequency spectra and obvious temporal patterns. In addition, this paper proposes a new method for fuzzy descriptor systems to adjust the parameters of such systems for modeling problem. This method is called "generalized locally linear model tree algorithm (GLOLIMOT)". To show the advantage of this method, the performance of fuzzy descriptor system is compared with several neural and neuro-fuzzy models in the prediction of Dst index. Results depict the great performance of such systems in prediction of this index in compare of other neuro-fuzzy models.

The article consists of five sections. The mathematical description of SSA algorithm is presented in section 2. Section 3 is devoted to describe the learning method used for fuzzy descriptor systems to predict solar activity's indexes. In section 4, the fuzzy descriptor system is used to predict Dst index to show the performance of fuzzy descriptor system in compare of other methods. The last section contains the concluding remarks.

Spectral Analysis

SSA is defined as a new tool to extract information from short and noisy chaotic time series [6]. It relies on the Karhunen-Loeve decomposition of an estimate of covariance matrix based on *M* lagged copies of the time series. Thus as the first step, the embedding procedure is applied to construct a sequence $\{\tilde{X}(t)\}$ of *M*-dimensional vectors from time series $\{X(t): t = 1,\ldots,N\}$:

$$\tilde{X}(t) = (X(t), X(t+1),\ldots, X(t+M-1)), \quad t = 1,\ldots,N', \quad N' = N - M + 1 \tag{1}$$

The $N' \times M$ trajectory matrix (*D*) of the time series has the *M* dimensional vectors as its columns, and is obviously a Hankel matrix (the elements on the diagonals *i+j=const* are equal). In the second step, the $M \times M$ covariance matrix C_x is calculated as

$$C_X = \frac{1}{N'} D^T D \qquad (2)$$

and its eigenelements can be determined by Singular Value Decomposition (SVD):

$$C_X = U \Sigma V^T \quad ; \quad U^T U = I \ , \ V^T V = I \qquad (3)$$

The elements of diagonal matrix $\Sigma = [diag(\sigma_1, \ldots, \sigma_M)]$ are the singular values of D and are equal to square roots of the eigenvalues of C_X .The eigenelements $\{(\lambda_k, \rho_k) : k = 1, \ldots, M\}$ of C_X are obtained from

$$C_X \rho_k = \lambda_k \rho_k \qquad (4)$$

Each eigenvalue, λ_k estimates the partial variance in the direction of ρ_k , and the sum of all eigenvalues equals the total variance of the original time series. In the third step, the time series is projected onto each eigenvector, and yields the corresponding principal components:

$$A_k(t) = \sum_{j=1}^{M} X(t + j - 1)\rho_k(j) \qquad (5)$$

Each of the principal components, being a nonlinear or linear trend or a periodic or quasi-periodic pattern, has narrow band frequency spectra and well defined characteristics to be estimated. As the fourth step, the time series is reconstructed by combining the associated principal components:

$$R_K(t) = \frac{1}{M_t} \sum_{k \in K} \sum_{j=L_t}^{U_t} A_k(t - j + 1)\rho_k(j) \qquad (6)$$

The normalization factor (M_t), and the lower (L_t) and upper (U_t) bounds of reconstruction procedure differ for the center and edges of the time series, and are defined by the following formula

$$(M_t, L_t, U_t) = \begin{cases} \left(\frac{1}{t}, 1, t\right), & 1 \le t \le M - 1 \\ \left(\frac{1}{M}, 1, M\right), & M \le t \le N' \\ \left(\frac{1}{N - t + 1}, t - N + M, M\right), & N' + 1 \le t \le N \end{cases} \qquad (7)$$

strictly proper and a polynomial subsystem by a proper transformation [9]. Fig. 1 shows such action.

It is obvious that the polynomial subsystem in discrete domain will be a moving average subsystem. Fortunately, each sub system could be identified by classical identification methods. Therefore, one can adjust the parameters of a descriptor system by decoupling it in to two subsystems, and then adjust these parameters simultaneously.

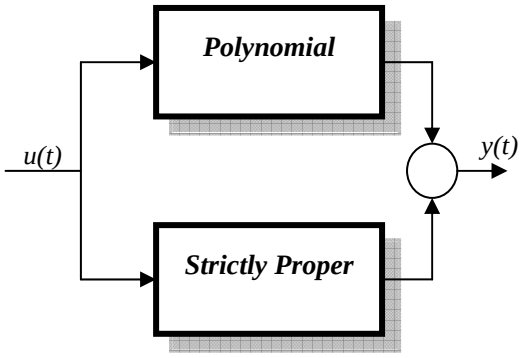

Fig. 1: A decoupled descriptor system.

After adjusting the linear descriptor system's parameters, it times to adjust the parameters of validity functions for each locally linear descriptor system by GLOLIMOT algorithm. This algorithm is simple and intuitive, but to achieve a good performance one should tune some parameters like the splitting ratio and the standard deviation. The number of neuron is also important to be optimized to attain the most accurate predictions and avoid over-fitness.

The GLOLIMOT algorithm is described in five steps:

Learning Methodologies

This section is devoted to describe the new learning method for fuzzy descriptor systems to adjust its parameters. As it said before, the consequent part of a fuzzy descriptor system, is a descriptor system which is an improper system. Therefore, to adjust the parameters of consequent parts, we need an extended method which arises from classical identification methods. This method is based on decoupling technique [8, 9]. A descriptor system can be decoupled to a

1. ***Start with an initial model:*** start with a single LLDM, which is a global linear model over the whole input space with $h_1(\underline{z}) = 1$ and set $M = 1$. If there is a priori input space partitioning it can be used as the initial structure.
2. ***Find the worst LLDM*:** Calculate a local loss function e.g. MSE for each of the $i = 1, \ldots, M$ LLDMs, and find the worst performing LLDM.
3. ***Check all divisions*:** The worst LLDM is considered for further refinement. The hyper rectangle of this LLDM is split into two halves with an axis orthogonal split. Divisions in all dimensions are tried, and for each of the p divisions the following steps are carried out:
   a. Construction of the multi-dimensional membership functions for both generated hyper rectangles.
   b. Construction of all validity functions.
   c. System identification of linear descriptor systems for both generated hyper rectangles by decoupling method introduced above.
   d. Construction of new fuzzy descriptor system according to new linear descriptor systems via Silverman-Ho algorithm.
   e. Calculations of the loss function for the current overall model.
4. ***Find the best division*:** The best of the p alternatives checked in step 3 is selected, and the related validity functions and LLDMs are constructed. The number of LLDM neurons is incremented $M = M + 1$.
5. ***Test the termination condition*:** If the termination condition is met, then stop, else go to step 2.

Solar Activity Forecasting

The proposed method is used in prediction of the Dst index in hourly state during 2001, where the results can be compared to actual values and the predictions made by MLP and BEL techniques. First we look to the hourly prediction of Dst index in 2001.

The hourly and daily averaged value of Dst index is accessible through several web sites from the sunspot Index Data Center in Belgium or US National Oceanic and Atmospheric Administration. The number of data for Dst index in year 2001 is about 4800. We use 4000 data for training the fuzzy descriptor system and other 800 data will be used for testing the performance of the algorithm.

After implementing SSA to training data, 20 components are held to use for prediction. After that the GLOLIMOT algorithm is implemented as a MATLAB m-file and is used to predict the Dst index. The standard deviation of validity functions is set to 0.7. A linear search between 0.5 and 1 shows the optimality of this value. For splitting ratio optimization a random search algorithm is included, which has three points and lower the number of iterations (neurons) to reach the optimum performance. The number of iterations is also optimized by an intelligent program: the model will be checked by the test data in each iteration and the training will be stopped when the mean square error (MSE) of test data starts to increase. In this way, the over-fitness is avoided and the most accurate prediction is prepared.

After 9 iterations, the error index starts to increase and the training is stopped. Fig. 2 shows the actual Dst index and the prediction of this index by fuzzy descriptor systems in training mode.

Fig. 3 depicts the performance of the fuzzy descriptor model in predicting the Dst index during 2001 in test mode. It can be easily seen that the combination of fuzzy descriptor system with SSA has very good results.

The comparison between this combined method results and MLP and BEL techniques' results in hourly predicting Dst during 2001 is presented in Table 1.

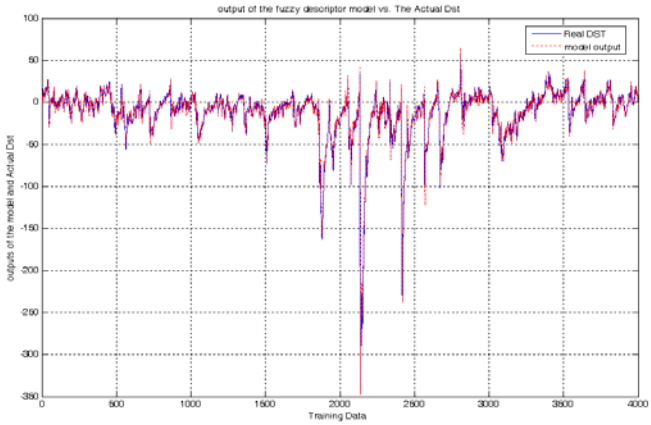

Fig. 2: the actual Dst index and the prediction of this index by fuzzy descriptor systems with the aid of SSA in training mode.

Table 1. *NMSE* of several methods in the prediction of hourly Dst index.

Method	NMSE in predicting Dst
MLP	0.0534
BEL	0.0365
GLOLIMOT with SSA	0.0305

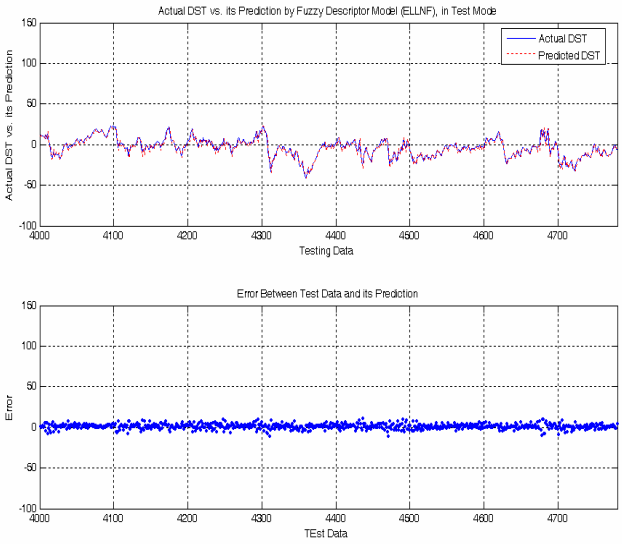

Fig. 3: prediction of Dst index during 2001 by a fuzzy descriptor model with the aid of SSA; Upper: Predicted and Observed values of test set, Lower: Prediction error.

Discussion and Conclusions

This paper has defined a fuzzy descriptor system by extending the ordinary T-S fuzzy model. Such system can be used as predictor when it is trained by constructing learning methods.

In this research, several optimization methods have been used with GLOLIMOT algorithm, to predict some important measures of solar activity: the DST index.

This paper goes back to the numerical techniques to extract the most available information from the history of Dst time series. By applying a nonlinear spectral analysis tool, the singular spectrum analysis, the principal patterns of such indexes are extracted. An optimal fuzzy descriptor model is constructed for each of the components by an incremental learning algorithm (GLOLIMOT) and is used in prediction of solar activity. The original time series is reconstructed from the extrapolated components. The results of predictions by this method are superior in comparison to predictions made by MLP and BEL techniques.

Acknowledgements

The authors are thankful to Iran Telecommunicating Research Centre (ITRC) which supports the authors of this paper during this research.

References

[1]. A. Weigend, B. H. Berman, and D. Rumelhart, "Predicting the future: A Connectionist Approach," *Int. Journal of Neural systems*, 1(3), pp. 193-209, 1990.

[2]. A. Weigened, B. H. Berman, and D. Rumelhart, "Predicting sunspots and exchange rates with connectionist networks," M. Casdalgi, S. Eubank, editors, *Nonlinear modeling and forecasting*, Addison-Wesley, pp. 395-432, 1992.

[3]. M. Casdagli, "Chaos and deterministic versus stochastic and nonlinear modeling," *Roy. Statistics. Soc. B*, 54, pp. 303-328, 1992.

[4]. D. G. Luenberger, "Dynamic equations in descriptor form," *IEEE Trans. Automat. Contr.*, vol. AC-22, pp. 312-321, 1977.

[5]. T. Taniguchi, K. Tanaka, H. O. Wang, "Fuzzy descriptor systems and nonlinear model following control," *IEEE Trans. On Fuzzy Systems*, vol. 8, No. 4, pp. 442-452, Aug. 2000.

[6]. R. Vautard, M. Ghil, "Singular spectrum analysis in nonlinear dynamics, with applications to paleoclimatic time series," *Physica D*, 35, pp. 395-424, 1989.

[7]. R. Vautard, P. Yiou, M. Ghil, "Singular spectrum analysis: A toolkit for short noisy chaotic signals," *Physica D*, 58, pp. 95-126, 1992.

[8]. S. L. Campbel, *Singular systems of differential equation*, Pitman, London, 1980.

[9]. G. C. Verghese, B. C. Levy, and T. Kailath, "A generalized state-space for singular systems," *IEEE Trans. Auto. Contr.* Vol. AC-26, No. 4, Aug. 1981.

The Sunspots Roads: A Morphology-Based Sunspots Detection Method and Delaunay Triangulation Surface for Prediction

A. Poursaberi[1], C. Lucas[2]

[1] Control and Intelligent Processing Center of Excellence, Electrical and Computer Engineering Department, University of Tehran, Tehran, Iran.
a.poursaberi@ece.ut.ac.ir
[2] Control and Intelligent Processing Center of Excellence, Electrical and Computer Engineering Department, University of Tehran, Tehran, Iran; and School of Cognitive Sciences, Institute for Studies on Theoretical Physics and Mathematics, Tehran, Iran.
lucas@ipm.ir

Abstract

In this paper a new approach for automatic detection and identification of sunspots on the full disk solar images is presented. The technique uses morphological operators on image such as image cleaning, morphological "bottom hat" operation, image closing and H-maxima transform. Applying some filtering processes on image to enhance the contrast and remove the high frequency noises are considered. Edge detection via Sobel mask is applied to find sunspot candidates. A new transformation which is used in iris recognition strategy is utilized to map the sunspots road from Cartesian coordinates to the normalized non-concentric polar representation to analysis the sunspots trajectories. Delaunay triangulation which is a set of lines connecting each point to its natural neighbors is applied to the sunspots centers which are detected from the suggested process. The Delaunay triangulation is related to the Voronoi diagram and via this technique the surface of the connected sunspots roads is achieved for each month. By using a search mechanism that requires a triangulation of the desired points obtained by Delaunay, the prediction of the sunspots is obtained. The technique was tested on two years of full disk SOHO/MDI images. The detection results are promising with a good preciseness and the sunspots location estimation is noticeable.

Introduction

The Sun is a source of light and heat for life on Earth. Our ancestors realized that their lives depended upon the Sun and they held the Sun in reverent awe. We still recognize the importance of the Sun and find the Sun to be awe inspiring. In addition we seek to understand how it works, why it changes, and how these changes influence us here on planet Earth. The Sun was much dimmer in its youth and yet the Earth was not frozen. The quantity and quality of light from the Sun varies on time scales from milli-seconds to billions of years. During recent sunspot cycles the total solar irradiance has changed by about 0.1% with the sun being brighter at sunspot maximum. Some of these variations most certainly affect our climate but in uncertain ways. The Sun is the source of the solar wind; a flow of gases from the Sun that streams past the Earth at speeds of more than 500 km per second (a million miles per hour). Disturbances in the solar wind shake the Earth's magnetic field and pump energy into the radiation belts. Regions on the surface of the Sun often flare and give off ultraviolet light and x-rays, that heat up the Earth's upper atmosphere. This Space Weather can change the orbits of satellites and shorten mission lifetimes. Solar as a gas and plasma clouds of ions have very mysteries properties and some of magnetic field properties such as 11 year cyclic behavior of it, is well-known for every one. Also it's a well-known property for scientist that based on Magneto Hydro Dynamic (MHD) model of solar core, the particles of solar have very complicated motions such as meridional flows, etc. sunspots are the places on the sun surface which are darker than other regions and have more compact magnetic fluxes. Sunspot images taken by SOHO satellite shows those sunspots have 27 day rotation over the sun surface. We use these images of year 2002 and based on these images performed our algorithm. The compilation of the Zurich relative sunspot numbers, or since 1981 the Sunspot Index Data (SIDC), is one of the most commonly used measures of solar activity (Hoyt & Schatten [1] and Temmer, Veronig, and Hanslmeier [2]). Some related works in sunspot detection is summarized in [1-6]; called thresholding methods but also including region growing techniques, rely on sunspots lower intensity variations. There are also methods, called border methods developed by Győri [8], Pettauer and Brandt [7], making use of the intensity gradient of the sunspot image.

Methodology

For sunspots detection we applied morphological operators to the image and the sunspot points are extracted from the image with its characteristics such as area, center, bounded square and etc. The construction of the proposed algorithm will be discussed in this section step by step and the results will be depicted as follows.

Sunspot lines

After getting the image, by converting image to binary image by thresholding and adding the resulted image three times to sharp the sunspots area, a logical image will be obtained. Since we want to get the road map of sunspots movement, the exact positions of sunspots are not necessary. Then based on the whole images of the suns for example in one month, we extract all the positions of sunspots and accumulate them in one image. In Fig.1 this algorithm process is depicted. Fig.1 (a) shows the input image to the algorithm and in Fig.1 (b) the detected sunspots positions is shown. After this stage, we used Sobel edge detection method to obtain the accurate edges of the detected sunspots. After that by imposing these edges to the original image, the sunspots are limited by their edges carefully. In Fig.2 these process are shown. Fig.2 (a) and 2(b) shows the original and selected sunspots positions such as Fig.1 In Fig.2(c) the edge

of Fig.2 (b) is gotten and then finally in Fig.2 (d) the positions of spots of original image is depicted. Finally in Fig.3 we show the accumulated sunspots of a month for example to show the boundaries of sunspots. As you can see in this picture all the sunspots can be assumed in some arcs and we used this curves for determining the roads of sunspots in the next stage.

In each image we can also calculate the properties of sunspots which are useful for prediction of the other months. We calculate areas, cancroids and boundaries of the detected sunspots in this paper. We can also obtain the number of the sunspots in each image by morphological labeling. It means that if we have an image that its spots are detected, by labeling it's connected components that are bigger than a threshold (in our algorithm we chose 2 which means connected components bigger that 2 pixel will be counted), the number of spots are gotten. Fig.4 shows this process.

Iris Recognition Idea

In iris recognition which is pioneered by John Daugman [9], he suggested a transformation for overcoming the problem of inconsistency in matching process. This transformation (that we called it normalization) projects iris region into a constant dimensional ribbon so that two images of the same iris under different conditions have characteristic features at the same spatial location. The proposed transformation is a normal Cartesian to Polar transformation that remaps each pixel in iris area into a pair of polar coordinates (r,θ) where r and θ is on the interval $[0 \quad 1]$ and $[0 \quad 2\pi]$respectively. This unwrapping is formulated as follows:

$$I(x(r,\theta),y(r,\theta)) \rightarrow I(r,\theta)$$

that

$$x(r,\theta) = (1-r)x_p(\theta) + rx_l(\theta)$$

$$y(r,\theta) = (1-r)y_p(\theta) + ry_l(\theta)$$

Where $I(x,y),(x,y),(r,\theta),(x_p,y_p),(x_i,y_i)$ are the iris region, Cartesian coordinates and corresponding polar coordinates, coordinates of the pupil and iris boundaries along the θ direction respectively. This process is shown in Fig.5 (a) and (b) which in (a) we select some pixels along with radius with different intensities and applied the mentioned transformation. The output of mapping is shown in (b) that clarifies the structure of mapping. We used this idea for mapping the sunspot roads in each month to a constant-size ribbon in order to perform the strategy of prediction.

Delaunay Triangulation

Given a set of data points, the Delaunay triangulation is a set of lines connecting each point to its natural neighbors. The Delaunay triangulation is related to the Voronoi diagram-- the circle circumscribed about a Delaunay triangle has its center at the vertex of a Voronoi polygon (Fig.6). We used the centroid of the sunspots in each image and apply the Delaunay function where the outputs of this function is a set of triangles such that no data points are contained in any triangle's circumscribed circle. The plot of triangles is defined in the m-by-3 matrix that each row of the m-by-3 matrix defines one such triangle and contains indices into x and y (the centroid coordinate). We used the transformed sunspots positions from the previous step and applied Delaunay Triangulation to find the lattice of the spots connection. The triangular plot and its mesh are shown in Fig.7 By applying the nearest point search mechanism for finding the probable position of the subsequent sunspots we design our prediction algorithm. With the unknown point in the domain of spots and using the centers of the nearest existed spots and their Delaunay triangulations the coordinates of the new spot will be determined. We examined the system by the one year sun images (2002) and observed that the estimated coordinate is very close to the real spot position. In Fig.7 complete demo of the system is depicted. You can choose your desired spot by the mouse and then its real and approximate coordinates will be shown.

Conclusion

In this paper a morphology method for sunspot detection was introduced. This method extracted the exact coordinate of sunspots in an each day and by gathering the positions of them, the road of sunspots was obtained. Using the idea of normalization in iris recognition, the roads of spots was mapped to a constant rectangular shape. By applying the Delaunay Triangulation method and a search mechanism which could find the nearest position of the sunspot, the prediction of new spot was done with promising results. The results showed that relying on the roads of sunspots which construct arc shapes is a suitable mechanism for prediction.

REFERENCES

[1] D.V. Hoyt, K.H. Schatten, " Group sunspot numbers: A new solar activity reconstruction. Part 2 ", *Solar Physics*, 1998b, 491-512.

[2] M. Temmer, A. Veronig, A. Hanslmeier, " Hemispheric Sunspot Numbers R_n and: R_s Catalogue and N-S asymmetry analysis", *Hemispheric Astronomy and Astrophysics*, 2002, 707-715.

[3] M. Steinegger, M. Vazquez, J.A. Bonet, P.N. Brandt, "On the energy balance of solar active regions", *Astrophysical Journal*, 1996, 461-478.

[4] G. A. Chapman, G. Groisman, "A digital analysis of sunspots areas", *Solar Physics*, 1984, 45-50.

[5] M. Steinegger, P. N. Brandt, J. Pap, W. Schmidt, "Sunspot photometry and the total solar irradiance deficit measured in 1980 by ACRIM", *Astrophysics and Space* Science, 1990, 170: 127-133.

[6] P. N. Brandt, W. Schmidt, M. *Steinegger, "On the umbra-penumbra area ratio of sunspots ", Solar Physics, 1990, 129: 191.*

[7] T. Pettauer, P.N. Brandt,"On novel methods to determine areas of sunspots from photoheliograms"*, Solar Physics, 1997, 175- 197.*

[8] S. Zharkov, V.V. Zharkova, S.S. Ipson, , A. Benkhalil, " Automatic Identification of Active Regions (Plages) in the Full-Disk Solar Images Using Local Thresholding and Region Growing Techniques", *Proc. of the AISB'03Symposium on Biologically-inspired Machine Vision, Theory and Application, University of Wales, Aberystwyth, 7th-11th April 2003, pp. 74-84, ISBN 1- 902956*-33-1, 2003.

[9] J. Daugman, "High Confidence Visual Recognition of Persons by a Test of Statistical Independence", *IEEE Trans. Pattern Analysis and Machine Intelligence*, vol. 15, no. 11, pp. 1148-1161, Nov. 1993.

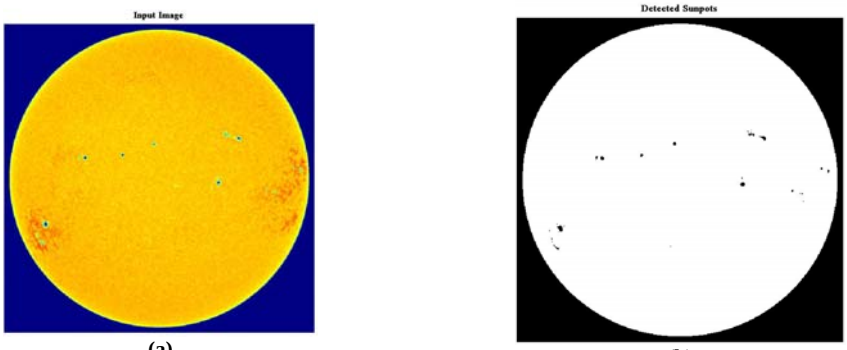

(a) **(b)**

Fig. 1. Determining the sunspots positions. (a) Input image, (b) Detected sunspots

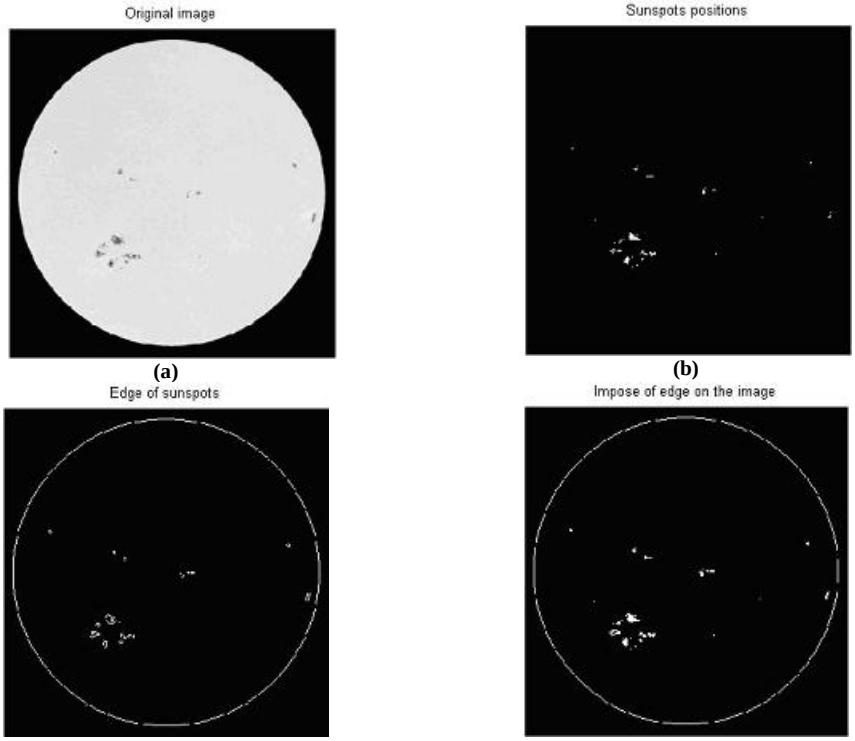

(a) **(b)**

(c) **(d)**

Fig. 2. (a) Original image, (b) Positions of sunspots, (c) Edge of detected sunspots, (d) Imposed edge of sunspots

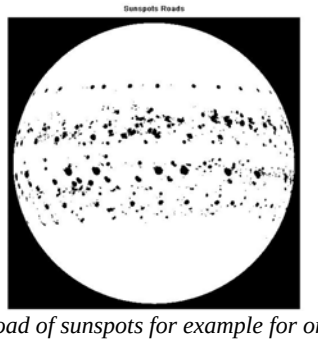

Fig. 3. The road of sunspots for example for one month. The roads are such as some arcs in the middle of sun area.

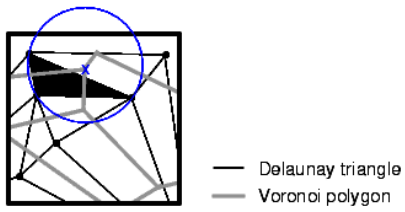

Fig.6. The structure of Delaunay triangulation and Voronoi diagram.

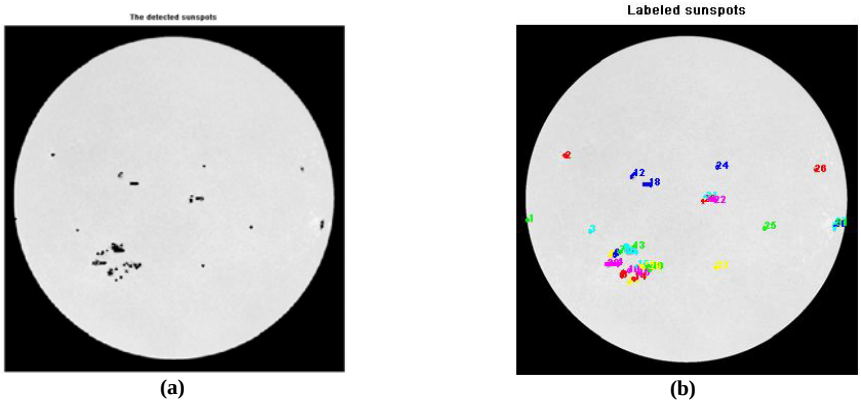

(a) **(b)**

Fig.4. (a) Detected sunspots in sun mage, (b) The labeled sunspots. The number of all sunspots easily is calculated.

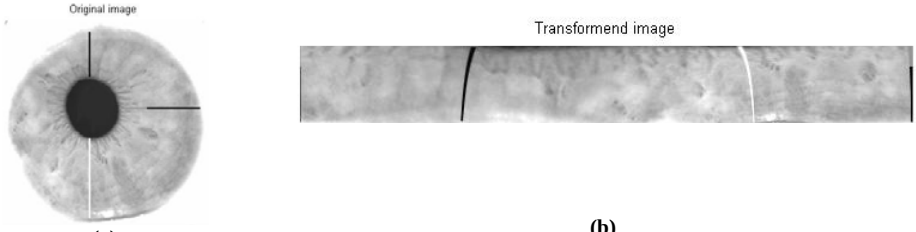

(a) **(b)**

Fig. 5. (a) An eye image with some typical lines with different intensities. (b) The mapped iris region.

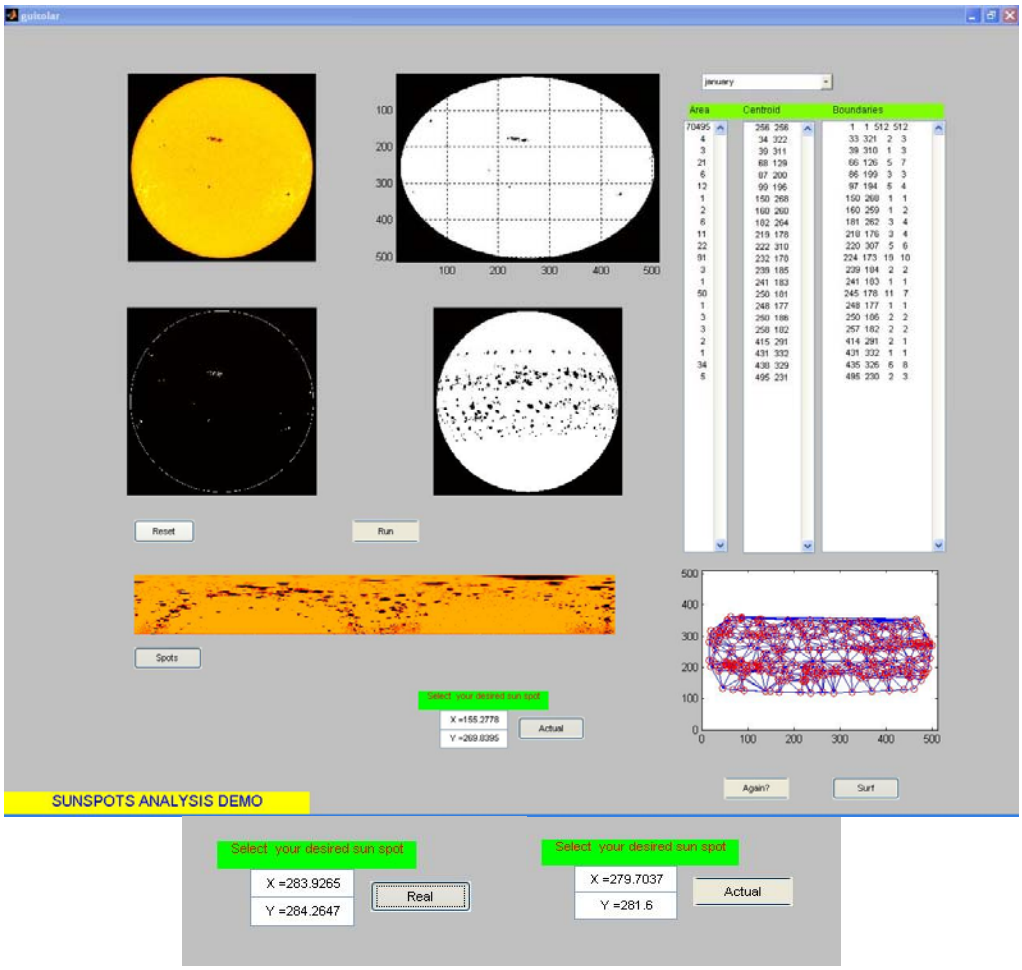

Fig.7. The schematic of the program. By selecting an unknown spot in the trained lattice to the system by mouse, the nearest spot to this point will be gotten. An example is shown in the picture that in left the position of the selected point is depicted and in right the nearest spot's coordinate is allocated.

Real Time Prediction of Extreme Events 2005 by Singular Spectrum Analysis and Neurofuzzy Modeling

Javad Sharifie [1], Caro Lucas [2], Babak Araabi [3]

[1] *Control and Intelligent Processing Center of Excellence, Electrical and Computer Engineering Department, University of Tehran, Tehran, Iran and School of Cognitive Sciences, Institute for Studies in Theoretical Physics and Mathematics, Tehran, Iran. j.sharifie@ece.ut.ac.ir*

[2] *Control and Intelligent Processing Center of Excellence, Electrical and Computer Engineering Department, University of Tehran, Tehran, Iran and School of Cognitive Sciences, Institute for Studies in Theoretical Physics and Mathematics, Tehran, Iran. lucas@ipm.ir*

[3] *Control and Intelligent Processing Center of Excellence, Electrical and Computer Engineering Department, University of Tehran, Tehran, Iran and School of Cognitive Sciences, Institute for Studies in Theoretical Physics and Mathematics, Tehran, Iran. araabi@ut.ac.ir*

Introduction

The solar corona is constantly losing particles. Protons and electrons evaporate off the sun, and reach the earth at velocities of 500 km/s. large gradual solar energetic particle (SEP) events pose threat to probe components and space operations, making necessary to develop reliable space weather forecasting models. Protons accelerated by interplanetary shocks generated by coronal mass ejections (CMEs) [1, 2].When these charged particles head for the Earth through the interplanetary magnetic field with high flux and energy, a solar proton event (SPE) is recorded. Strong SPEs, in which energetic protons penetrate the atmosphere in large numbers, are rare, but do have chemical effects. solar energetic particle (SEP) events or solar radiation storms stronger than S3 (according to NOAA classification) are dangerous for communication and operation systems, computer memory, astronauts in space stations, passengers and crew in commercial jets, and even for technology and people on the ground. In this study a singular spectrum analysis is applied for extracting the principle components (PC) of proton time series and then for each PCs, a locally linear neurofuzzy model is used for modeling and one-step prediction of next values of each PCs and finally predicted PCs are recombine to obtain the one-step prediction of main series (proton event).

Singular Spectrum Analysis

SSA is a tool to extract information from short and noisy chaotic time series [3]. It relies on the Karhunen-Loeve decomposition of an estimate of covariance matrix based on *M* lagged copies of the time series. Thus as the first step, the embedding procedure is applied to construct a sequence $\{\tilde{X}(t)\}$ of *M*-dimensional vectors from time series $\{X(t): t = 1,\ldots, N\}$:

$$\tilde{X}(t) = (X(t), X(t+1),\ldots, X(t+M-1)), \quad t = 1,\ldots, N', \quad N' = N - M + 1 \qquad (1)$$

The $N' \times M$ trajectory matrix (*D*) of the time series has the *M* dimensional vectors as its columns, and is obviously a Hankel matrix (the elements on the diagonals ($i + j = consant$) are equal). In the second step, the $M \times M$ covariance matrix C_X is calculated as

$$C_X = \frac{1}{N'} D^T D \qquad (2)$$

C_X Eigenelements can be determined by Singular Value Decomposition (SVD):

$$C_X = U \Sigma V^T \quad ; \quad U^T U = I \ , \ V^T V = I \qquad (3)$$

The elements of diagonal matrix $\Sigma = [diag(\sigma_1,\ldots,\sigma_M)]$ are the singular values of *D* and are equal to square roots of the C_X eigenvalues. The C_X eigenelements $\{(\lambda_k, \rho_k): k = 1,\ldots, M\}$ are obtained from:

$$C_X \rho_k = \lambda_k \rho_k \qquad (4)$$

Each eigenvalue, λ_k, estimates the partial variance in the ρ_k direction, and the sum of all eigenvalues equals the total variance of the original time series. In the third step, the time series is projected onto each eigenvector, and yields the corresponding principal component (PC) for each $PC_k(t)$:

$$PC_k(t) = \sum_{j=1}^{M} X(t + j - 1)\rho_k(j) \qquad (5)$$

Each of the principal components, a nonlinear or linear trend, a periodic or quasi-periodic pattern, or a multi-periodic pattern, has a narrow band frequency spectrum and well defined characteristics to be estimated. As the fourth step, the time series is reconstructed by combining the associated principal components:

$$R_K(t) = \frac{1}{M_t} \sum_{k \in K} \sum_{j=L_t}^{U_t} PC_k(t - j + 1)\rho_k(j) \qquad (6)$$

The normalization factor (M_t), and the lower (L_t) and upper (U_t) bounds of reconstruction procedure differ for the center and edges of the time series, and are defined by following formula

$$(M_t, L_t, U_t) = \begin{cases} (t,1,t), & 1 \le t \le M-1 \\ (M,1,M), & M \le t \le N' \\ (\min(t, N-t+1), t-N+M, M), & N'+1 \le t \le N \end{cases} \qquad (7)$$

To enhance signal to noise ratio, one can use the singular spectrum (the logarithmic scale plot of singular values of covariance matrix in decreasing order). The principal components related to lower singular values can be omitted in the reconstruction stage, to obtain adaptive noise cancellation. If all the components are used in reconstructing the time series, no information is lost.

Locally Linear Neurofuzzy with Model Tree Learning

The main idea for utilizing the locally linear neurofuzzy (LLNF) model for function approximation is dividing the input space into small linear subspaces with fuzzy validity functions, $\phi_i(\underline{u})$, which describe the validity of each linear model in its region. The validity function is used in this study

is Gaussian function which defined as $\mu(x) = \exp(-\frac{(x-c)^2}{2\sigma^2})$, where c is the center and σ is the standard deviation of the Gaussian.

Any produced linear part with its validity function can be described as a fuzzy neuron. Thus the total model is a neurofuzzy network with one hidden layer, and a linear neuron in the output layer which simply calculates the weighted sum of the outputs of locally linear models (LLMs) as follows:

$$\hat{y}_i = \omega_{i_0} + \omega_{i_1} u_1 + \omega_{i_2} u_2 + \ldots + \omega_{i_p} u_p \,,\; \hat{y} = \sum_{i=1}^{M} \hat{y}_i \phi_i(\underline{u}) \qquad (8)$$

Where $\underline{u} = \begin{bmatrix} u_1 u_2 \cdots u_p \end{bmatrix}^T$ is the model input, M is the number of LLM neurons, and ω_{ij} denotes the LLM parameters of the ith neuron. The validity functions are chosen as normalized Gaussians; normalization is necessary for a proper interpretation of validity functions.

$$\phi_i(\underline{u}) = \frac{\mu_i(\underline{u})}{\sum_{j=1}^{M} \mu_j(\underline{u})} \qquad (9)$$

$$\mu_i(\underline{u}) = \exp\left(-\frac{1}{2}\left(\frac{(u_1 - c_{i1})^2}{\sigma_{i1}^2} + \ldots + \frac{(u_p - c_{ip})^2}{\sigma_{ip}^2}\right)\right) = \qquad (10)$$

$$\exp\left(-\frac{1}{2}\frac{(u_1 - c_{i1})^2}{\sigma_{i1}^2}\right) \times \ldots \times \exp\left(-\frac{1}{2}\frac{(u_p - c_{ip})^2}{\sigma_{ip}^2}\right)$$

Each Gaussian validity function has two sets of parameters, centers (c_{ij}) and standard deviations (σ_{ij}) which are the Mp parameters of the nonlinear hidden layer. Optimization or learning methods are used to adjust both the parameters of local linear models (ω_{ij}) and the parameters of validity functions (c_{ij} and σ_{ij}). Global optimization of linear parameters is simply obtained by Least squares technique. The complete parameter vector contains $M(p+1)$ elements:

$$\underline{\omega} = \lfloor \omega_{10} \;\; \omega_{11} \;\; \ldots \;\; \omega_{1p} \;\; \omega_{20} \;\; \omega_{21} \;\; \ldots \;\; \omega_{M0} \;\; \ldots \;\; \omega_{Mp} \rfloor \qquad (11)$$

and the associated regression matrix $\underline{X}$ for N measured data samples is

$$\underline{X} = \begin{bmatrix} \underline{X}_1 & \underline{X}_2 & \ldots & \underline{X}_M \end{bmatrix} \qquad (12)$$

$$\underline{X}_i = \begin{bmatrix} \phi_i(\underline{u}(1)) & u_1(1)\phi_i(\underline{u}(1)) & \ldots & u_p(1)\phi_i(\underline{u}(1)) \\ \phi_i(\underline{u}(2)) & u_1(2)\phi_i(\underline{u}(2)) & \ldots & u_p(2)\phi_i(\underline{u}(2)) \\ \vdots & \vdots & & \vdots \\ \phi_i(\underline{u}(N)) & u_1(N)\phi_i(\underline{u}(N)) & \ldots & u_p(N)\phi_i(\underline{u}(N)) \end{bmatrix} \qquad (13)$$

Thus

$$\hat{\underline{y}} = \underline{X}\,\hat{\underline{\omega}} \quad ; \quad \hat{\underline{\omega}} = \left(\underline{X}^T \underline{X}\right)^{-1} \underline{X}^T \underline{y} \qquad (14)$$

The remarkable properties of locally linear neurofuzzy model, its transparency and intuitive construction, lead to the use of least squares technique for rule antecedent parameters and incremental learning procedures for rule consequent parameters as introduced below:

Learning Algorithm

Locally Linear Model Tree (LOLIMOT) is an incremental tree-construction algorithm that partitions the input space by axis orthogonal splits in all directions of input space. It implements a heuristic search for the rule premise parameters and avoids a time consuming nonlinear optimization.

The LOLIMOT algorithm is described in five steps according to [4, 5]:

1. **Start with an initial model:** start with a single LLM, which is a global linear model over the whole input space with $\Phi_1(\underline{u}) = 1$ and set $M = 1$. If there is a priori input space partitioning it can be used as the initial structure.
2. **Find the worst LLM:** Calculate a local loss function e.g. Mean Square Error(MSE) for each of the $i = 1, \ldots, M$ LLMs, and find the worst performing LLM.
3. **Check all divisions:** The worst LLM is considered for further refinement. The hyper rectangle of this LLM is split into two halves with an axis orthogonal split. Divisions in all dimensions are tried, and for each of the p divisions the following steps are carried out:
   a. Construction of the multi-dimensional membership functions for both generated hyper rectangles;
   b. Construction of all validity functions.
   c. Estimation of the rule consequent parameters for newly generated LLMs.
   d. Calculations of the loss function for the current overall model.
4. **Find the best division:** The best of the p alternatives checked in step 3 is selected, and the related validity functions and LLMs are constructed. The number of LLM neurons is incremented $M = M + 1$.
5. **Test the termination condition:** If the termination condition is met, then stop, else go to step 2.

The termination condition is reaching to a predefined error between output ($\underline{y}$) and LLNF output with M neuron ($\hat{\underline{y}}$), i. e. when the condition: $\left\|\underline{y} - \hat{\underline{y}}\right\| \le \varepsilon$ is satisfied. In practice we used a predefined number of neurons in LOLIMOT, plotted the error as a function of this number, and kept increasing the number of neurons until satisfactory performance was obtained.

Proton density prediction

Proton density hourly data of October, November, September 2004 and first 15 day of January 2005 is used for modeling this data set and 16 January 2005 for prediction. Also the data sets of year 2005 prior to events are used for training the model to predict the events in this year. The main proton density series is extracted to 50 new series with equation5 then for each newly produced time series, a locally linear neurofuzzy network with model tree learning (as introduced in part3) was used for modeling and one-step prediction of each Principle Component. After prediction, by using

equations6,7, recombine the predicted values of each PC to obtain the one-step prediction of the main series (proton density). The correlation coefficient of 0.95 is achieved with our method for one-step prediction of extreme events of this year. The prediction is without delay for prediction of peak points of most of the extreme event. Also the event of 7, 15 May 2005 is predicted with our method with correlation coefficient 0.91, 0.8. in figure1, one-step prediction with SSA+LOLIMOT method for prediction of events in 18 July and 7 May in 2005 is depicted.

Conclusion

In this study a combination of singular spectral analysis and powerful neurofuzzy model with tree learning algorithm was applied for modeling and prediction of some of solar energetic particles in 2005 and a high correlation coefficient between observed and predicted values was obtained with our model. The modeling method is applied for long-term prediction of 22, 23solar cycles and also for 24 solar cycles [6] and had shown good performances for long-term prediction of solar activity and also for one-step prediction of Disturbance storm time (Dst) index [7,8]**.**

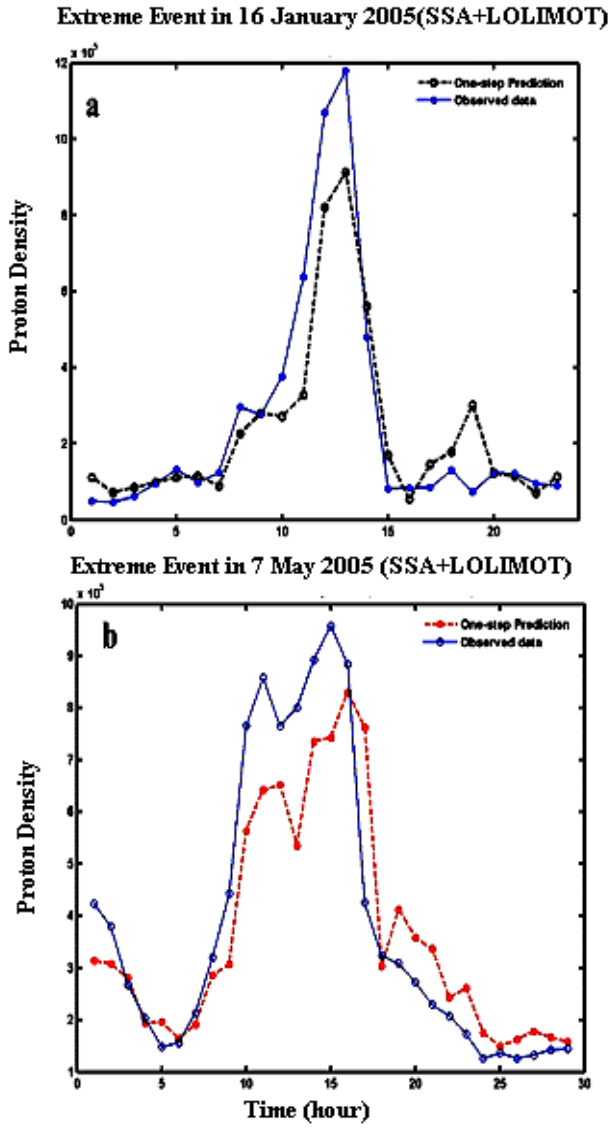

Fig.1. one-step prediction of proton density with LOLIMOT+SSA method: (a)-16 July; (b)-7 May 2005

REFERENCES

[1] Feynmann J., Gabriel S.B., On Space Weather Consequences and Predictions, *J.Geophys. Res.*, 105, 10543, 2000

[2] Cane H.V., Reames D.V., von Rosenvinge T.T., The Role of Interplanetary Shocks in the Longitude Distribution of Solar Energetic Particles, *J. Geophys. Res.*, 93, 955, 1988

[3] Vautard R., Yiou P., Ghil M., Singular spectrum analysis: A toolkit for short noisy chaotic signals, Physica D, 58: 95-126, 1992.

[4] Nelles O., Nonlinear System Identification with Local Linear Neuro-Fuzzy Models, PhD Thesis, TU Darmstadt, Shaker Verlag, Aachen, Germany, 1999

[5] Nelles O., Nonlinear system identification, Springer Verlag, Berlin, 2001

[6] Gholipour A., Lucas C., Shafiee M., Araabi B.N., Extracting the Main Patterns of Natural Time Series for Long Term Prediction, *J. of Aymospheric and Solar Terrestrial Physics*, Vol 67, Issue 6, p 595-603, 2005.

[7] Sharifie, J., B. N. Araabi, and C. Lucas, Multi-step prediction of Dst index using singular spectrum analysis and locally linear neurofuzzy modeling, Earth Planets Space, Vol 58, p 331-341, 2006.

[8] Javad Sharifie, Caro Lucas, Babak N. Araabi, Locally linear neurofuzzy modeling and prediction of geomagnetic disturbances based on solar wind conditions, Space Weather, Vol 4, p 1-12, 2006.

TIME SERIES PREDICTION USING BRAIN EMOTIONAL LEARNING CASE STUDY: SUNSPOT NUMBER

R.KARIMIZANDI[1], T.BABAIE[1], C.LUCAS[1,2]
[1]Control and Intelligent Processing Center of Excellence, Electrical and Computer Engineering Department, University of Tehran, Tehran, Iran
[2]School of Cognitive Sciences, Institute for Studies in Theoretical Physics and Mathematics, Tehran, Iran
r.zandi@ut.ac.ir; t.babaie@ut.ac.ir; lucas@ipm.ir

Abstract

In this paper we present a novel method for predicting chaotic time series which is based on Brain Emotional Learning. Many researchers attempt to model learning process in human brain. Moren and Balkenius have developed a new approach to modeling brain emotional learning. The Brain Emotional Learning (BEL) algorithm is derived from this model to be used in prediction applications. The proposed method simulates the emotional learning process in human brain. This system has been shown to be an efficient tool of learning and decision making. In this work we develop a methodology to use BEL for time series prediction. The method is applied for the Sunspot number time series. Sunspot number is a good measure of solar activity. Solar activity is a quasi periodic phenomenon with a period of about eleven years. Finally, we discuss the strong points of the new method against other intelligent methods such neuro-fuzzy networks.

Key words: *Emotional learning, Time series prediction, Sunspot number.*

1 Introduction

Predictions of solar and geomagnetic activity are important to various technologies, including the operation of low-Earth orbiting satellites, electric power transmission grids, geophysical exploration, and high-frequency radio communications and radars. The scale height of Earth's upper atmosphere (and thus the drag on satellites in low Earth orbit) is dependent on the intensity of short-wavelength solar radiation and the level of geomagnetic activity, so knowledge of the profile and magnitude of the next solar and geomagnetic cycle is crucial for logistical planning for reboosting the Hubble Space Telescope and assembly of the International Space Station. Solar activity is a quasi periodic phenomenon with a period of about eleven years. The solar cycle consists of a period of activity, called solar maximum, and a period of quiescence, called solar minimum. During the solar maximum there are more coronal mass ejections, solar flares, and sunspots. Nowadays, predicting the solar cycle and solar activity is more than a matter of scientific curiosity. Prediction of solar activity is specifically useful to space mission centres because the orbital trajectory parameters of satellites are greatly affected by the changing solar activity. Solar flares are also the origin of high energy particles which affect the lifetime of satellites. The Wolf's sunspot number, as a reliable and useful index of solar activity, has been a difficult benchmark for prediction purposes. Various numerical prediction techniques have been used for the sunspot number time series, which can be classified as Fourier analyses , curve fitting , artificial intelligence, neural networks, and adaptive filtering. In this study we present a novel method for predicting sunspot number which is based on Brain Emotional Learning (BEL). This learning method is based on the emotional learning procedure in human brain and modeled by Moren and Balkenius [1,2].

2 Brain Emotional Approach to Prediction

A recent work on modeling emotions in human brain has been used for designing a more realistic emotional learning based intelligent system for decision making. The emotional learning in human brain takes place mainly in amygdala, a small area with multiple layers of interconnected parts, and extensive connections with several other areas like hippocampus, hypothalamus, and orbitofrontal cortex.

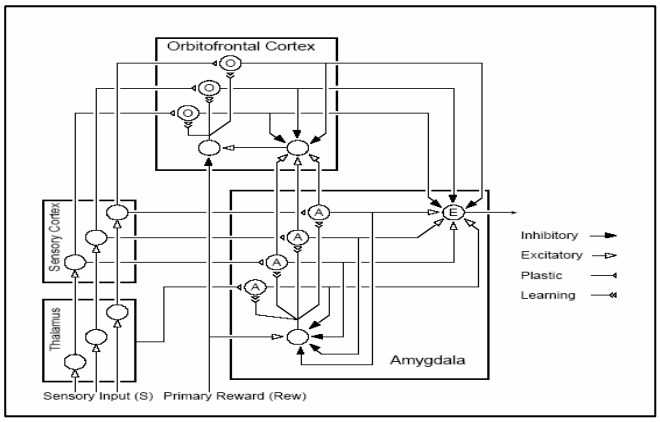

Fig.1. *A graphical depiction of the model At the top is the rudimentary orbitofrontal part at the bottom right is the amygdaloid part and at left are the thalamic and sensory cortical modules. The thalamic and sensory-cortical parts are just place-holders in this version of the model. The sensory inputs S enter the thalamic part, where a thalamic input to the amygdala is calculated as the maximum over all inputs. A primary reward signal Rew enters both the amygdaloid and orbitofrontal parts*

The distinctive feature of the BEL model is that the weights of amygdala cannot decrease. In other words, the emotional learning in amygdala is monotonic (once an emotional reaction is learned, it is permanent and can not be unlearned. When needed, the Orbitofrontal Cortex (OFC) will inhibit the amygdala reaction). It is remarkable that the learning rate in amygdala is proportional to the strength of stimuli signals. Meaning the emotions are more sensitive to strong sensory inputs. This property is useful in some of the

practical problems, when the large input signals are more important to be estimated or predicted. The BEL algorithm is derived from this model to be used in prediction applications. the
thalamic stimulus).

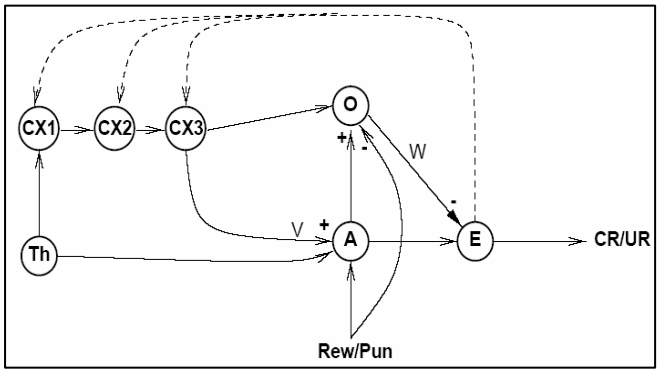

Fig.2. *The preliminary model Th: thalamus. CX1, CX2, CX3: sensory cortex. A: input structures in the amygdala. E: output structures in the amygdala. O: orbitofrontal cortex. Rew/Pun : external signals identifying the presentation of reward and punishment. CR/UR: conditioned response/unconditioned response. V: associative strength from cortical representation to the amygdala that is changed by learning. W: inhibitory connection from orbitofrontal cortex to the amygdala that is changed during learning.*

There is also one node for each of the stimuli (except for the thalamic node).There is one output node in common for all outputs of the model, called *E*. The *E* node simply sums the outputs from the *A* nodes, then subtracts the inhibitory outputs from the *O* nodes. For each *A* node, there is a plastic connection weight V.

$$A_n = V.S$$

Where A_n is the output of amygdala nodes in nth iteration, and the total output is:

$$E_a(n) = E_a(n-1) + \sum_i A_n(i)$$

$$\Delta V_n = diag(\alpha.\max(R_n - E_a(n),0).S)$$

Where **α** is the learning rate of amygdala. The output nodes of OFC are calculated as:

$$O_n = W.S$$

And its total output is the sum of all output nodes and the previous value of itself:

$$E_o(n) = E_o(n-1) + \sum_j O_n(j)$$

$$\Delta W_n = diag(\beta.R_o.S)$$

β is the learning rate of OFC. The internal reinforcement signal, (R_0), is calculated by:

$$R_o = \begin{cases} \max(E_a(n) - R,0) - E_o(n) & if\ R \neq 0 \\ \max(E_a(n) - E_o(n),0) & Otherwise \end{cases}$$

The system output is calculated by

$$E(n) = E_a(n) - E_o(n)$$

Stimuli inputs to the system are described by the *S*. There is one *A* node for every stimulus S (including one for

The choice of external reinforcement signal provides the degrees of freedom for multi objective learning procedures. A simple form is

$$R_n = \sum_j \omega_j r_j$$

Where r_j s are the factors of the reinforcement agent, and w_j s are the related weights.

3 Sunspot Time-Series Prediction

Solar activity is a quasi periodic phenomenon with a period of about eleven years. The solar cycle consists of a period of activity, called solar maximum, and a period of quiescence, called solar minimum. During the solar maximum there are more coronal mass ejections, solar flares, and sunspots. Nowadays, predicting the solar cycle and solar activity is more than a matter of scientific curiosity. The sunspot number is a good measure of solar activity and is computed according to the Wolf formulation $R=k(10g+s)$, where g is the number of sunspot groups, s is the total number of spots in all groups and k is a variable scaling factor which is related to the conditions of observation. In this study BEL algorithm is used to make a one year ahead prediction of sunspot number and compared to a prediction which made by a strong locally linear neurofuzzy network, this locally linear neurofuzzy predictor is developed on the basis of Locally Linear Model Tree (LOLIMOT) [3]. Fig.3 shows the one year ahead predicted and observed values of sunspot numbers and the related prediction error by the BEL based predictor, while Fig.4 presents the observed and prediction of sunspot number using LOLIMOT algorithm in the test set and Comparing different error indices of the BEL predictor and LOLIMOT algorithm in prediction of sun spot number is shown in Fig.5. The years of 1800 to 2000 are used for BEL predictor. The years of 1700 to 1919 are used for training and the years from 1920 t0 2000 are used as test set for LOLIMOT predictor. The test set (years from 1920 to 2000) is used for comparison. Error indices are: average error of solar peaks (2.02 for BEL and 5.5 for LOLIMOT) and error of the highest peak (0.4 for BEL and 8 for LOLIMOT).

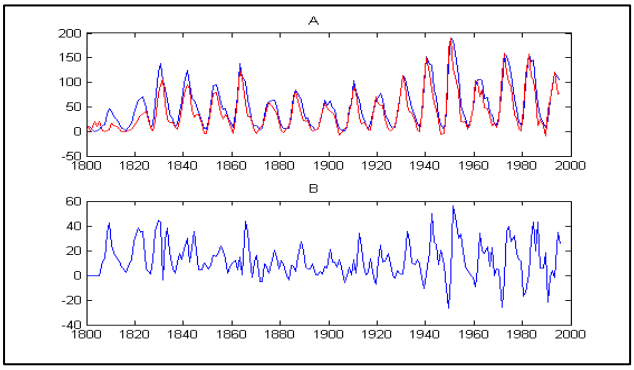

Fig.3*. One year ahead prediction by BEL based predictor;*

(A):Observed and predicted values of sunspot numbers,(B): prediction error

Fig.4. *One year ahead prediction by LOLIMOT predictor;*

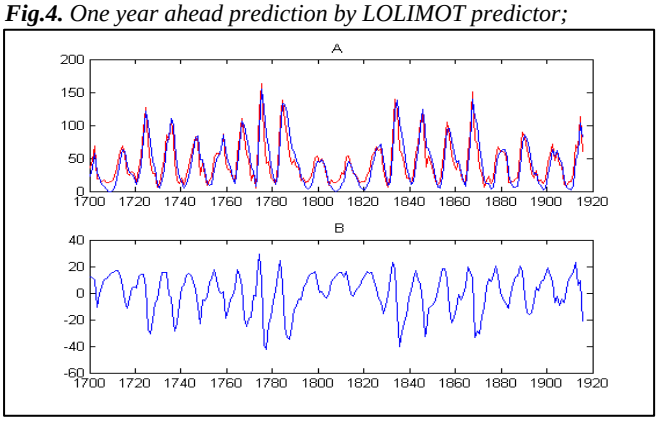

(A): Observed and predicted values of sunspot numbers on training set,(B): prediction error

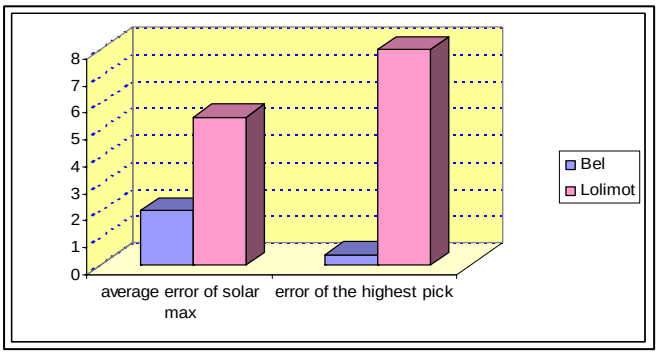

Fig.5. *Comparing different error indices of BEL predictor and LOLIMOT algorithm, in prediction of sunspot number*

4 Conclusions

We have achieved non-model based solutions in multi objective contexts with low computational burden and with no need to worry about the differentiability of the objective function. BEL based predictor can predict the peak values of yearly sunspot better than LOLIMOT. The average error of solar max and the error of predicting the highest peak for BEL in comparison to LOLIMOT algorithm is less. This method is based on the Brain Emotional learning procedure in human mind and its remarkable properties are: low computational complexity, fast training, and its simplicity in multi objective problems.

References:

[1] J. Moren, Emotion and Learning: A computational model of the amygdala, PhD thesis, Lund university, Lund, Sweden, 2002.

[2] J. Moren, & C. Balkenius, A computational model of emotional learning in the amygdale, In J.A. Mayer, A. Berthoz, D. Floreano, H.L. Roitblat, & S.W. Wilson (Ed.), From animals to animats 6, (MIT Press, Cambridge, MA, 2000), 383-391.

[3] Gholipour A., Abbaspour A., Araabi B. N., Caro Lucas, Enhancements in the Prediction of Solar Activity by Locally Linear Model Tree, proc. of MIC2003: 22nd Int. Conf. on Modeling, Identification and Control, Innsbruck, Austria, 2003, pp. 158-161

[4] M. Fatourechi, C. Lucas, & A. Khaki Sedigh, Reducing Control Effort by means of Emotional Learning, Proc. of 9th Iranian Conf. on Electrical Engineering, ICEE'01, Tehran, Iran, 2001, (41)1-8.

[5] A. Jazbi, C. Lucas, Intelligent control with emotional learning, 7th Iranian Conference on Electrical Engineering, ICEE'99, Tehran, Iran, 1999, 207-212.

[6]Schatten, K., Solar activity prediction: Timing predictors and cycle 24, Journal of Geophysical Research, 107(A11), 2002

[7]Schatten, K., Correction to "Solar activity prediction: Timing predictors and cycle 24" by Kenneth Schatten, J. Geophys. Res., 108(A3), 1100, 2003

Predicting Solar Activity with the Aid of Fuzzy Descriptor Models

M. Mirmomeni[1], C. Lucas[2], M. Shafiee[3], B. Nadjar Araabi[2]

[1] *Control and Intelligent Processing Center of Excellence, Electrical and Computer Engineering Department, University of Tehran, Tehran, Iran.*
m.mirmomeni@ece.ut.ac.ir
[2] *Control and Intelligent Processing Center of Excellence, Electrical and Computer Engineering Department, University of Tehran, Tehran, Iran; and School of Cognitive Sciences, Institute for Studies on Theoretical Physics and Mathematics, Tehran, Iran.*
lucas@ipm.ir, araabi@ut.ac.ir
[3] *Electrical Engineering Department, University of Amirkabir, Tehran, Iran.*
shafiee@aut.ac.ir

Abstract

The cyclic solar activity has significant effects on earth, climate, satellites and space missions. Several methods have been introduced for the prediction of sunspot number, which is a common measure of solar activity.

In the past two decades, descriptor systems and related fuzzy descriptor systems have been the subjects of interest due to their many practical applications in modeling complex phenomena. In this study, a new learning method, generalized locally linear model tree (GLOLIMOT) algorithm for fuzzy descriptor models as an intuitive incremental learning algorithms, has been used in the prediction of sun spot number. The contribution of this paper is to provide some methods for adjusting the parameters of fuzzy descriptor model, e.g. the splitting ratio and the standard deviation, the number of locally linear neurons and the number of linear descriptor systems for the consequent part in fuzzy descriptor model and specially the parameters of such descriptor systems which need some special methods for these systems. By these modifications an accurate prediction of sunspot number is obtained which is compared with several other methods.

Keywords: Chaotic Prediction, Solar activity, Sunspot number, Fuzzy Descriptor Models, Neurofuzzy Models, GLOLIMOT.

Introduction

Among the various conditions that affect space weather, the sun-driven phenomena dominate the others. The sunspot number time series shows chaotic behavior [1, 2, 3], which leads to long time unpredictability.

On the other hand, descriptor systems [4, 10] describe a wider class of systems, including physical models and non-dynamic constraints. It is well known that the descriptor system is much tighter than the state-space expression for representing real independent parametric perturbations [5]. In addition, the fuzzy descriptor models as a generalization of the locally linear neuro-fuzzy models are general forms that can be trained by constructive intuitive learning algorithms.

This paper defines a fuzzy descriptor system whose consequent parts are represented by descriptor forms. The ordinary T-S fuzzy model is a special case of the fuzzy descriptor system. This paper proposes a new method "generalized locally linear model tree algorithm (GLOLIMOT)" to fuzzy descriptor systems to adjust the parameters of such systems for modeling problem. To show the advantage of this method, the performance of fuzzy descriptor system with this extended learning algorithm is compared with several neural and neuro-fuzzy models in the prediction of sunspot numbers. Results depict the great performance of such systems in prediction of sunspot numbers in compare of other neuro-fuzzy models.

The article consists of five sections. Section 2 presents the fuzzy descriptor model. Section 3 is devoted to describe the learning method used for fuzzy descriptor systems to predict sunspot numbers. In section 4, the fuzzy descriptor system is used to predict sunspot numbers to show the performance of fuzzy descriptor system in compare of other methods. The last section contains the concluding remarks.

Fuzzy Descriptor Systems

In this section the mathematical formulation of fuzzy descriptor models are considered. The fundamental approach with such systems is dividing the input space into small linear subspace with fuzzy validity functions and their appropriate linear descriptor systems. Therefore the total fuzzy descriptor model is an extended neurofuzzy network with one hidden layer for locally linear descriptor systems and a linear neuron in the output layer which simply calculates the weighted sum of the outputs of locally linear descriptor systems. Therefore, in this paper a fuzzy descriptor system can be defined by extending the T-S fuzzy model [6]. The fuzzy descriptor system is defined as

$$\sum_{k=1}^{r^e} v_k(z(t))E_k\dot{x}(t) = \sum_{i=1}^{r} h_i(z(t))\left(A_i x(t) + B_i u(t)\right)$$
$$y(t) = \sum_{i=1}^{r} h_i(z(t))C_i x(t) \qquad (1)$$

where $x(t) \in R^n$, $y \in R^q$, $u(t) \in R^m$

$$h_i(z(t)) \geq 0, \qquad \sum_{i=1}^{r} h_i(z(t)) = 1$$

$$v_k(z(t)) \geq 0, \qquad \sum_{k=1}^{r_e} v_k(z(t)) = 1$$

$x(t) \in R^n$ is the descriptor vector, $u(t) \in R^m$ is the input vector, $y \in R^q$ is the output vector, $E_k \in R^{n \times n}$, $A_i \in R^{n \times n}$, $B_i \in R^{n \times m}$, and $C_i \in R^{q \times n}$. Note that E matrix in the fuzzy descriptor system is assumed to be not always nonsingular. Equation (4) is a generalized system for [7] and [8].

By defining $x^*(t) = \left[x^T(t) \quad \dot{x}^T(t) \right]^T$, the fuzzy descriptor system (4) can be written as

$$E^* \dot{x}^*(t) = \sum_{i=1}^{r} \sum_{k=1}^{r^e} h_i(z(t)) v_k(z(t)) \left(A_{ik}^* x^*(t) + B_i^* u(t) \right)$$

$$y(t) = \sum_{i=1}^{r} h_i(z(t)) C_i^* x^*(t)$$

(2)

where

$$E^* = \begin{bmatrix} I & 0 \\ 0 & 0 \end{bmatrix}, \qquad A_{ik}^* = \begin{bmatrix} 0 & I \\ A_i & -E_k \end{bmatrix}$$

$$B_i^* = \begin{bmatrix} 0 \\ B_i \end{bmatrix}, \qquad C_i^* = \begin{bmatrix} C_i & 0 \end{bmatrix}$$

The structure of fuzzy descriptor systems is depicted in fig. 1.

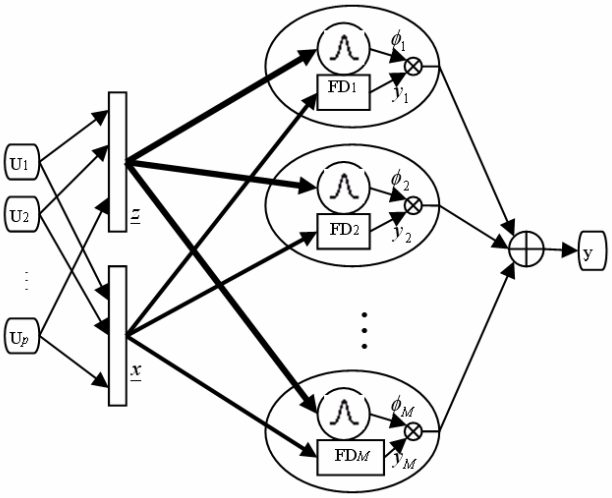

Fig. 1: Network structure of a fuzzy descriptor system with M neurons.

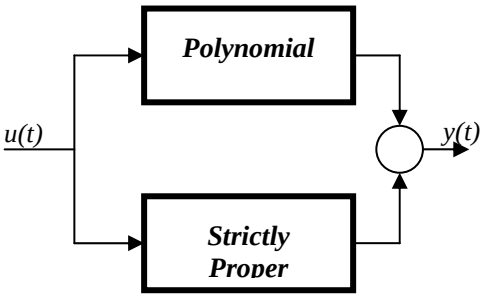

Fig 2: A decoupled descriptor system.

Learning Methodologies

This section is devoted to describe the new learning method for fuzzy descriptor systems to adjust its parameters. As it said before, the consequent part of a fuzzy descriptor system, is a descriptor system which is an improper system. Therefore, to adjust the parameters of consequent parts, we need an extended method which arises from classical identification methods. This method is based on decoupling technique [8, 9]. A descriptor system can be decoupled to a strictly proper and a polynomial subsystem by a proper transformation [9]. Fig. 2 shows such action.

It is obvious that the polynomial subsystem in discrete domain will be a moving average subsystem. Fortunately, each sub system could be identified by classical identification methods. Therefore, one can adjust the parameters of a descriptor system by decoupling it in to two subsystems, and then adjust these parameters simultaneously.

After adjusting the linear descriptor system's parameters, it times to adjust the parameters of validity functions for each locally linear descriptor system by GLOLIMOT algorithm. This algorithm is simple and intuitive, but to achieve a good performance one should tune some parameters like the splitting ratio and the standard deviation. The number of neuron is also important to be optimized to attain the most accurate predictions and avoid over-fitness.

The GLOLIMOT algorithm is described in five steps:

1. ***Start with an initial model:*** start with a single LLDM, which is a global linear model over the whole input space with $h_1(\underline{z}) = 1$ and set $M = 1$. If there is a priori input space partitioning it can be used as the initial structure.

2. ***Find the worst LLDM*****:** Calculate a local loss function e.g. MSE for each of the $i = 1, \ldots, M$ LLDMs, and find the worst performing LLDM.

3. ***Check all divisions*****:** The worst LLDM is considered for further refinement. The hyper rectangle of this LLDM is split into two halves with an axis orthogonal split. Divisions in all dimensions are tried, and for each of the p divisions the following steps are carried out:

a. Construction of the multi-dimensional membership functions for both generated hyper rectangles;

b. Construction of all validity functions.

c. System identification of linear descriptor systems for both generated hyper rectangles by decoupling method introduced above.

d. Construction of new fuzzy descriptor system according to new linear descriptor systems via Silverman-Ho algorithm.

e. Calculations of the loss function for the current overall model.

4. ***Find the best division*****:** The best of the p alternatives checked in step 3 is selected, and the related validity functions and LLDMs are constructed. The number of LLDM neurons is incremented $M = M + 1$.

5. ***Test the termination condition*:** If the termination condition is met, then stop, else go to step 2.

Predicting the Sunspot Numbers

The sunspot number is a good measure of solar activity and is computed according to the Wolf formulation:

$$R=k\,(10g+s) \qquad (3)$$

The GLOLIMOT algorithm is implemented as a MATLAB m-file and is used to predict the sunspot number. The number of iterations is also optimized by an intelligent program: the model will be checked by the test data in each iteration and the training will be stopped when the mean square error (MSE) of test data starts to increase. In this way, the over-fitness is avoided and the most accurate prediction is prepared.

Three other networks have been implemented to be compared with fuzzy descriptor models and its algorithm GLOLIMOT; the MLP network with conjugate gradient learning method, the RBF network, and its predecessor LLM network with LOLIMOT learning method. All of these models are compared in their optimum performance.

Table 1 contains the results of several methods; the RBF and the MLP and the LLM networks.

Fig. 3 and fig. 4 present the prediction of sunspot number (training set and total test set respectively) by GLOLIMOT algorithm. This algorithm shows good performance in the solar maximum (peak points of sunspot number), especially in 1958, while the other methods do not.

Table 1. *NMSE* of several methods in the prediction of yearly sunspot numbers

	Test set 1	Test set 2	Test set 3	Total test
MLP	0.2	0.3	0.22	0.23
RBF	0.1186	0.184	0.1421	0.1392
LOLIMOT	0.0702	0.1518	0.1519	0.1136
GLOLIMOT	0.0634	0.1056	0.1392	0.0873

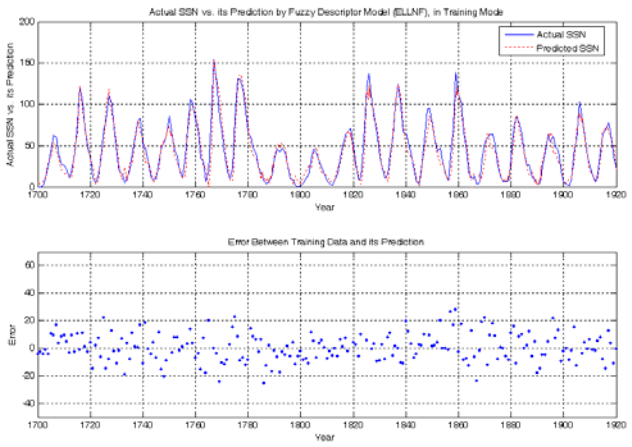

Fig 3: prediction of sunspot number by a fuzzy descriptor model with GLOLIMOT algorithm; upper: Predicted and Target values of train set, lower: Prediction error.

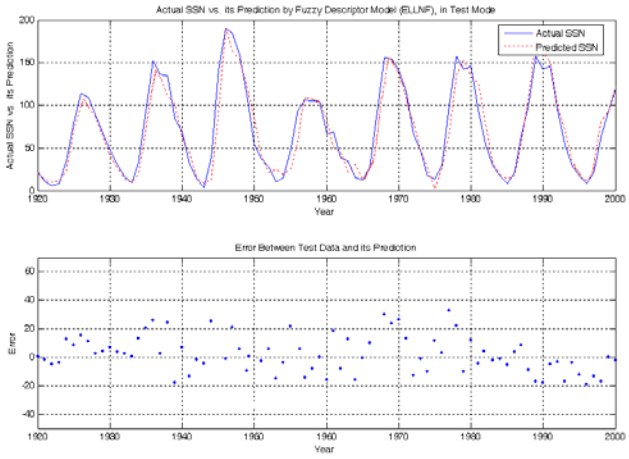

Fig 4: prediction of sunspot number by a fuzzy descriptor model with GLOLIMOT algorithm; Upper: Predicted and Observed values of test set, Lower: Prediction error.

Conclusion

This paper has defined a fuzzy descriptor system by extending the ordinary T-S fuzzy model. Such system can be used as predictor when it is trained by constructing learning methods.

In this research, several optimization methods have been used with GLOLIMOT algorithm, to predict an important measure of solar activity: the sunspot number. By optimizing the number of neurons, the splitting ratio and the standard deviations, an accurate prediction has been provided. The especially low prediction error of the proposed method in the peak points of sunspot number (solar maximum), even with few neurons in its structure is an interesting achievement. Due to its high generalization and low prediction error, this method can be used in predicting the solar activity several years in advance.

Acknowledgements

The authors are thankful to Iran Telecommunicating Research Centre (ITRC) which supports the authors of this paper during this research.

REFERENCES

[1]. A. Weigend, B. H. Berman, and D. Rumelhart, "Predicting the future: A Connectionist Approach," *Int. Journal of Neural systems*, 1(3), pp. 193-209, 1990.

[2]. A. Weigened, B. H. Berman, and D. Rumelhart, "Predicting sunspots and exchange rates with connectionist networks," M. Casdalgi, S. Eubank, editors, *Nonlinear modeling and forecasting*, Addison-Wesley, pp. 395-432, 1992.

[3]. M. Casdagli, "Chaos and deterministic versus stochastic and nonlinear modeling," *Roy. Statistics. Soc. B*, 54, pp. 303-328, 1992.

[4]. D. G. Luenberger, "Dynamic equations in descriptor form," *IEEE Trans. Automat. Contr.*, vol. AC-22, pp. 312-321, 1977.

[5]. T. Taniguchi, K. Tanaka, H. O. Wang, "Fuzzy descriptor systems and nonlinear model following control," *IEEE Trans. On Fuzzy Systems*, vol. 8, No. 4, pp. 442-452, Aug. 2000.

[6]. T. Takagi, and M. Sugeno, "Fuzzy identification of systems and its applications to modeling and control, " *IEEE Trans. System, Man, Cybernetics*, vol. SMC-15, pp. 116-132, 1985.
[7]. T. Taniguchi, K. Tanaka, K. Yamafuji, and H. O. Wang, "Fuzzy descriptor systems: stability analysis and design via LMIs, " in *1999 Amer. Contr. Conf.*, San Diego, CA, June 1999, pp. 1827-1831.
[8]. T. Taniguchi, K. Tanaka, K. Yamafuji, and H. O. Wang, "Fuzzy descriptor systems and fuzzy controller designs, " in *8th Int. Fuzzy Syst. Assoc. World Congress*, vol. 2, Taipei, Taiwan, Aug. 1999, pp. 655-659.
[9]. S. L. Campbel, *Singular systems of differential equation*, Pitman, London, 1980.
[10]. G. C. Verghese, B. C. Levy, and T. Kailath, "A generalized state-space for singular systems," *IEEE Trans. Auto. Contr.* Vol. AC-26, No. 4, Aug. 1981.

Ajabshirizadeh	Ali	Iran	Research Institute for Astronomy & Astrophysics of Maragha	a-adjab@ tabrizu. ac.ir
Antonova	Elizaveta	Russia	SINP MSU	antonova@orearm.msk.ru
Arakelyan	Karen	Armenia	Alikhanyan Physics Institute	karen@crdlx5.yerphi.am
Babayan	Valeri	Armenia	Alikhanyan Physics Institute	babayan@mail.yerphi.am
Baishev	Dmitry	Russia	Yu.G.Shafer Institute of Cosmophysical Research and Aeronomy	baishev@ikfia.ysn.ru
Bazilevskaya	Galina	Russia	Lebedev Physical Institute	bazilevs@fian.fiandns.mipt.ru
Belov	Anatoly	Russia	IZMIRAN	abelov@izmiran.ru
Bieber	John	USA	Bartol Research Institute, University of Delaware	john@bartol.udel.edu
Bostanjyan	Nikolay	Armenia	Alikhanyan Physics Institute	bostan@crdlx5.yerphi.am
Buetikofer	Rolf	Switzerland	Physikalisches Institut, University of Bern	rolf.buetikofer@phim.unibe.ch
Bunuatov	Karen	Russia	ISTC	bunyatov@istc.ru
Chilingarian	Ashot	Armenia	Alikhanyan Physics Institute	chili@crdlx5.yerphi.am
Dvornikov	Valery	Russia	Institute of Solar-Terrestrial Physics, SB RAS	dvornikov@iszf.irk.ru
Eghikyan	Aram	Armenia	Alikhanyan Physics Institute	eghikyan@crdlx5.yerphi.am
Eroshenko	Eugenia	Russia	IZMIRAN	erosh@izmiran.rssi.ru
Feigin	Victor	Russia	Research Center for Earth Operative Monitoring	feigin@dbs.ntsomz.ru
Flueckiger	Erwin	Switzerland	Physikalisches Institut, University of Bern	flueckiger@phim.unibe.ch
Gavrilova	Elena	Russia	ISTC	gavrilova.istc.ru
Georgieva	Katya	Bulgaria	Solar-Terrestrial Influences Laboratory, Bulgarian Academy of Sciences	kgeorg@bas.bg
Gevorkyan	Nerses	Armenia	Alikhanyan Physics Institute	nerses@crdlx5.yerphi.am
Ghazaryan	Sergei	Armenia	Alikhanyan Physics Institute	ssk@crdlx5.yerphi.am
Gopalswamy	Nat	USA	NASA/GSFC	n_gopalswamy@yahoo.com
Gushchina	Raisa	Russia	IZMIRAN	rgus@izmiran.rssi.ru
Hayrapetyan	Aram	Armenia	Web-Limited	aram@r.am
Hovhannisyan	Armen	Armenia	Alikhanyan Physics Institute	harmen@web.am
Hovhannisyan	Armen	Armenia	Alikhanyan Physics Institute	armen@crdlx5.yerphi.am
Hovsepyan	Gagik	Armenia	Alikhanyan Physics Institute	hgg@crdlx5.yerphi.am
Ishkov	Vitaly	Russia	IZMIRAN	ishkov@izmiran.ru
Ivanov	Vitaly	Armenia	Alikhanyan Physics Institute	ivanov@crdlx5.yerphi.am
Jansen	Frank	Germany	University of Greifswald	jansen@physik.uni-greifswald.de
Karapetyan	Grigory	Armenia	Alikhanyan Physics Institute	gkarap@crdlx5.yerphi.am
Kleimenova	Natalia	Russia	Institute of Earth Physics	kleimen@ifz.ru
Kozliner	Lev	Armenia	Alikhanyan Physics Institute	lev@crdlx5.yerphi.am
Kozyreva	Olga	Russia	Institute of Earth Physics	kozyreva@ifz.ru
Krivolutsky	Alexei	Russia	Central Aerological Observatory	alkriv@lenta.ru
Kudela	Karel	Slovakia	Institute of Experimental Physics, Slovak Academy of Sciences	kkudela@upjs.sk
Kuzin	Sergey	Russia	Lebedev Physical Institute	kuzin@mail1.lebedev.ru
Kuznetsov	Vladimir	Russia	IZMIRAN	kvd@izmiran.ru
Lazutin	Leonid	Russia	SINP MSU	lazutin@srd.sinp.msu.ru
Lucas	Caro	Iran	University of Tehran	lucas@ipm.ir
Maricic	Darije	Croatia	Astronomical Observatory Zagreb	darije.maricic@zg.htnet.hr
Marjin	Boris	Russia	SINP MSU	marjin@taspd.sinp.msu
Martirosyan	Hamlet	Armenia	Alikhanyan Physics Institute	hmart@crdlx5.yerphi.am
Melkumyan	Laura	Armenia	Alikhanyan Physics Institute	laura@crdlx5.yerpphi.am

Mirzoyan	Razmick	Germany	Max-Planck-Institute for Physics	razmik@mppmu.mpg.de
Mishin	Vladimir	Russia	Institute of Solar-Terrestrial Physics, SB RAS	vladm@iszf.irk.ru
Mnatsakanyan	Eduard	Armenia	Alikhanyan Physics Institute	vanmnats@yahoo.com
Mnatskanyan	Edik	Armenia	Alikhanyan Physics Institute	edom@mail.yerphi.am
Moiseenko	Veronika	Armenia	Alikhanyan Physics Institute	moiseenko@crdlx5.yerphi.am
Muraki	Yasushi	Japan	Solar-Terrestrial Environment Laboratory, University of Nagoya	muraki@stelab.nagoya-u.ac.jp
Nymmik	Rikho	Russia	SINP MSU	nymmik@sinp.msu.ru
Odian	Allen	USA	Stanford University	odian@pacbell.net
Oganesyan	Andranik	Armenia	Alikhanyan Physics Institute	designer@crdlx5.yerphi.am
Olson	Timothy	Italy	Aerospace Defence	tolson@aditaly.com
Panasyuk	Mikhail	Russia	SINP MSU	panasyuk@sinp.msu.ru
Peroomian	Vahe	USA	UCLA	vahe@igpp.ucla.edu
Petrosyan	Vahe	USA	Stanford University	vahe@astronomy.stanford.edu
Potapov	Alexander	Russia	Institute of Solar-Terrestrial Physics, SB RAS	potapov@iszf.irk.ru
Reimers	Artur	Armenia	Alikhanyan Physics Institute	arthur@crdlx5.yerphi.am
Rosa	Dragan	Croatia	Astronomical Observatory Zagreb	drosa@hpd.botanic.hr
Rshtuni	Hasmik	Armenia	Alikhanyan Physics Institute	hasmik@crdlx5.yerphi.am
Rushanyan	Geym	Armenia	Alikhanyan Physics Institute	geym@freenet.am
Sdobnov	Valery	Russia	Institute of Solar-Terrestrial Physics, SB RAS	sdobnov@iszf.irk.ru
Sheiner	Olga	Russia	Radiophysical Research Institute, Nizhny Novgorod	rfj@nirfi.sci-nnov.ru
Stepanova	Marina	Russia	SINP MSU	marinastepanova@vtr.net
Stoeva	Penka	Bulgaria	Solar Terrestrial Influences Laboratory, Acad. D. Mishev" – Bulgarian Academy of Sciences	penm@abv.bg
Stozhkov	Yuri	Russia	Lebedev Physical Institute	stozhkov@ian.fiandns.mipt.ru
Struminsky	Alexei	Russia	Space Research Institute	astrum@iki.rssi.ru
Timofeev	Vladislav	Russia	Yu.G.Shafer Institute of Cosmophysical Research and Aeronomy	vetimofeev@ikfia.ysn.ru
Tserunyan	Sargis	Armenia	Alikhanyan Physics Institute	sargis@crdlx5.yerphi.am
Tverskaya	Lyudmila	Russia	SINP MSU	tverskaya@taspd.sinp.msu.ru
Veselovsky	Igor	Russia	SINP MSU	veselov@dec1.sinp.msu.ru
Yermolaev	Yuri	Russia	Space Research Institute	Yermol@iki.rssi.ru
Zazyan	Mary	Armenia	Alikhanyan Physics Institute	mary@mail.yerphi.am